

INFORMATION TO USERS

This manuscript has been reproduced from the microfilm master. UMI films the text directly from the original or copy submitted. Thus, some thesis and dissertation copies are in typewriter face, while others may be from any type of computer printer.

The quality of this reproduction is dependent upon the quality of the copy submitted. Broken or indistinct print, colored or poor quality illustrations and photographs, print bleedthrough, substandard margins, and improper alignment can adversely affect reproduction.

In the unlikely event that the author did not send UMI a complete manuscript and there are missing pages, these will be noted. Also, if unauthorized copyright material had to be removed, a note will indicate the deletion.

Oversize materials (e.g., maps, drawings, charts) are reproduced by sectioning the original, beginning at the upper left-hand corner and continuing from left to right in equal sections with small overlaps.

ProQuest Information and Learning
300 North Zeeb Road, Ann Arbor, MI 48106-1346 USA
800-521-0600

UMI[®]

University of Alberta

Prediction and Measurement of the Combined Torsional and Axial
Loading of Pseudoelastic NiTi Shape Memory Alloy Wire

by

David J. Lario



A thesis submitted to the Faculty of Graduate Studies and Research in partial
fulfillment of the requirements for the degree of Master of Science.

Department of Mechanical Engineering

Edmonton, Alberta

Spring 2005



Library and
Archives Canada

Bibliothèque et
Archives Canada

0-494-08106-6

Published Heritage
Branch

Direction du
Patrimoine de l'édition

395 Wellington Street
Ottawa ON K1A 0N4
Canada

395, rue Wellington
Ottawa ON K1A 0N4
Canada

Your file *Votre référence*

ISBN:

Our file *Notre référence*

ISBN:

NOTICE:

The author has granted a non-exclusive license allowing Library and Archives Canada to reproduce, publish, archive, preserve, conserve, communicate to the public by telecommunication or on the Internet, loan, distribute and sell theses worldwide, for commercial or non-commercial purposes, in microform, paper, electronic and/or any other formats.

The author retains copyright ownership and moral rights in this thesis. Neither the thesis nor substantial extracts from it may be printed or otherwise reproduced without the author's permission.

AVIS:

L'auteur a accordé une licence non exclusive permettant à la Bibliothèque et Archives Canada de reproduire, publier, archiver, sauvegarder, conserver, transmettre au public par télécommunication ou par l'Internet, prêter, distribuer et vendre des thèses partout dans le monde, à des fins commerciales ou autres, sur support microforme, papier, électronique et/ou autres formats.

L'auteur conserve la propriété du droit d'auteur et des droits moraux qui protègent cette thèse. Ni la thèse ni des extraits substantiels de celle-ci ne doivent être imprimés ou autrement reproduits sans son autorisation.

In compliance with the Canadian Privacy Act some supporting forms may have been removed from this thesis.

Conformément à la loi canadienne sur la protection de la vie privée, quelques formulaires secondaires ont été enlevés de cette thèse.

While these forms may be included in the document page count, their removal does not represent any loss of content from the thesis.

Bien que ces formulaires aient inclus dans la pagination, il n'y aura aucun contenu manquant.


Canada

"Imagination is more important than knowledge."

-Albert Einstein

*To my late mother, Sandra Jean Lario (1949-1996) I know that she would of been
proud of me.*

ABSTRACT

In this research project the experimental and theoretical combined axial and torsional load response for a pseudoelastic SMA wire was explored. The experimental tests were conducted to observe the combined loading case where an axial load was first applied to the SMA wire followed with torsional loading until the martensite phase transformation was induced. The theoretical component of the research consisted of using the bilinear stress response assumption for both the axial and shear loading. Based on this assumption the axial and torsional load responses were modeled and compared with the experimental tests.

ACKNOWLEDGEMENTS

My acknowledgment list is pretty well endless, but I will try to fit everybody in. I would like to start by thanking my family, my mother Sandra, father Garry, brother Mark and my ever supportive wife, Alison.

The second most important people I would like to thank are all the teachers that have helped me along the way. From Grande Prairie Regional College there was Dr. Som Pillay, Dr. Jaime Santiago (1949 - 2004), Dr. Bert Hunt and Tom Kaip. These people were the ones that forged me into a determined student. Here at the University, almost every professor has given me inspiration of one form or another. On top of the list is my supervisor Dr. Don Raboud, then there is Mark Ackerman, Dr. Bhattacharyya, Dr. Faulkner, Dr. Yokota, Dr. Mahaar Quaraan and Dr. Fyfe.

Special thanks to all the machinist and technicians: Don Fuhr, Albert Yuen, Dave Pape, Terry Nord and Bernie Faulkner whose knowledge and abilities helped me a great deal.

I would finally like to thank all my fellow graduate students who have helped me along the way. I am greatly appreciative of the guidance that you have given me.

CONTENTS

1	Introduction	1
1.1	Introduction	1
1.2	SMA Background	1
1.2.1	Modeling of SMA Behaviour	3
1.2.2	SMA Geometry	7
1.2.3	Thermal Elastic Response	7
1.2.4	Thesis Outline	8
2	Experimental Combined Loading Testing	10
2.1	Introduction	10
2.2	MTS Testing Machine	10
2.3	Torsional Adapter	12
2.3.1	Load Cell	13
2.3.2	Environmental Chamber	17
2.3.3	Data Acquisition (DAQ)	18
2.3.4	Measuring the Wire Twist Angle	19
2.3.5	Evaluation of the Torsional Adapter	20
2.4	Preliminary SMA Testing	24
2.4.1	Wire Properties	25
2.4.2	Evaluating the SMA Load Response as a Function of Temperature	26
2.4.3	Comparing Strain Measurements from Extensometer and LVDT of an Axially Loaded SMA Wire	27
2.4.4	Training the Wire in Axial Loading	29
2.4.5	Training the Wire in Torsional Loading	33
2.5	Experimental Tests	35

3	Axial and Torsional Load Response Models	48
3.1	Axial Load Response Model	48
3.2	Torsional Load Response Model	50
3.2.1	Linear Elastic Region ($\gamma < \gamma_{TY}$)	53
3.2.2	Phase Transformation Region ($\gamma \geq \gamma_{TY}$)	54
3.3	Methods used to Determine Axial Material Properties from the Axial Load Response	55
3.3.1	Axial Transformation Yield Stress (σ_{TY})	56
3.3.2	Measuring the Axial Elastic Modulus (E_E) and Transformation Modulus (E_{TR})	59
3.4	Methods used to Determine Shear Material Properties from the Torsional Load Response	61
4	Combined Axial Torsional Loading	71
4.1	Transformation Yield Stress (σ_{TY}) and Transformation Yield Shear Stress (τ_{TY})	72
4.2	Elastic Shear Modulus (G_E) and Transformation Shear Modulus (G_{TR})	77
4.3	Combined Axial Torsional Load Response Prediction Comparison with Experimental Tests	78
5	Axial Load Response	92
6	Conclusions and Further Research	98
6.1	Torsional Adapter	98
6.2	Axial and Torsional Load Response Model	99
6.2.1	Axial Load Response Model	99
6.2.2	Torsional Load Response Model	100
6.2.3	Combined Load Response	100
6.3	Further Research	101
	Bibliography	104
A	Supplemental Information	108
A.1	Chapter 1	108
A.1.1	General Equations for Stress State ([Boresi et al., 1993]) . . .	108
A.1.2	Drucker-Prager Yield Criterion	109

A.1.3	Gillets Derivation	111
A.2	Chapter 2	112
A.2.1	Continuous Rotating Potentiometer	112
A.2.2	Design Loads of Torsional Adapter	113
A.2.3	Selecting Proper Wire Size for Testing	114
A.3	Chapter 3	115
A.3.1	Torsional Load Response Derivation	115
A.3.2	Other Methods used to Determine the Transformation Yield Point	116
A.3.3	Number of Data Points to be used with Tangent Modulus Method	117
A.3.4	Error in Yield Tangent Modulus Method for Determining the Transformation Yield Stress	120
A.3.5	Error in Yield Tangent Modulus Method for Determining the Transformation Yield Shear Stress	122
A.3.6	Quadratic Relation of the Standard Deviation of the Residual	124
A.3.7	How Noise Affects the PLSLR Method	125
A.4	Chapter 5	127
B	Experimental Procedure	128
B.1	Loading a Specimen	128
B.2	Calibration	130
B.2.1	MTS Calibration	130
B.2.2	Torsional Adapter Calibration	130
B.3	Addition Equipment Used	131
B.3.1	Differential Scanning Calorimeter, DSC	131
C	Experimental Combined Load Tests	132
C.0.2	Training	132
C.0.3	Sample 1 Testing	142
C.1	Sample Testing Summary	156

LIST OF TABLES

1.1	Comparing Properties of NiTi SMA with Steel [Funakubo, 1984]	4
4.1	Specimen 1: Material Properties	84
4.2	Specimen 2: Material Properties	85
4.3	Specimen 3: Material Properties	85

LIST OF FIGURES

1.1	Phase Interaction	2
1.2	Comparing SMA to Steel	3
1.3	Symmetrical and NonSymmetrical Transformation Stress Criterion . .	5
1.4	Effects of Temperature on Loading	9
2.1	Experimental Setup	11
2.2	Extensometer Setup	12
2.3	Extensometer Grip Modification	13
2.4	Torsional Adapter	14
2.5	Torsional-Axial Load Cell	15
2.6	Load Cell Calibration Setup	15
2.7	Torsional-Axial Load Cell: Torsional Calibration	16
2.8	Layout of the Torsional Adapter	17
2.9	Brass Wire Clamps	17
2.10	Data Acquisition System	19
2.11	Cyclic Axial Loading of Metal Wire	21
2.12	LVDT-Extensometer Comparison	22
2.13	Cyclic Torsional Loading of Steel	23
2.14	Torsional Cross Talk During Axial Loading	24
2.15	Axial Cross Talk During Torsional Loading	25
2.16	Differential Scanning Calorimeter (DSC)	27
2.17	Temperature-Stress-Strain Response for Pure Axial Loading	28
2.18	Temperature-Torque-Rotation Response for Pure Torsional Loading .	29
2.19	Comparing Extensometer and LVDT	30
2.20	Training SMA Wire Under Strain Control	34
2.21	Axial Load Response Under Strain Control Loading	35
2.22	Stress Controlled Training after Strain Controlled training	36

2.23	Train Axial Load Response	37
2.24	Torsional Training	38
2.25	Trained Torsional Load Response	39
2.26	Pure Torsional Loading	40
2.27	60 MPa Axial Preload and Phase Transformation Initiation by Torsional Loading	41
2.28	120 MPa Axial Preload and Phase Transformation Initiation by Torsional Loading	42
2.29	240 MPa Axial Preload and Phase Transformation Initiation by Torsional Loading	43
2.30	360 MPa Axial Preload and Phase Transformation Initiation by Torsional Loading	44
2.31	480 MPa Axial Preload and Phase Transformation Initiation by Torsional Loading	45
2.32	Pure Axial Loading	46
2.33	Axial Elongation due to Torsional Loading	47
3.1	Axial Load Response	49
3.2	Bilinear Material Load Response for Axial and Torsional Loading . .	51
3.3	Shear Stress Load Response Assumption and Corresponding Torsional Load Response	52
3.4	Axial Load Response Test Function	56
3.5	Tangential Modulus Method	57
3.6	Elastic Modulus as a Function of the Axial Strain	58
3.7	Young's Modulus, Tangent Modulus and Chord Modulus	60
3.8	Comparing the experimental axial load response with the axial test function and the axial load response model	62
3.9	Torsional Load Response Test Function	63
3.10	Modulus Method for Determining Transformation Yield Point	65
3.11	Piecewise Smooth Least Squares Regression Method	67
3.12	Error in the Transformation Yield Stress	69
3.13	Error in the Transformation Yield Tangent Modulus	70
4.1	Prediction of the Transformation Yield Surface	76

4.2	The Predicted and Experimental Transformation Yield Surface - Sample 1	78
4.3	The Predicted and Experimental Transformation Yield Surface - Sample 2	79
4.4	The Predicted and Experimental Transformation Yield Surface - Sample 3	80
4.5	Sample 1: Elastic and Transformation Shear Modulus Determined for Various Degrees of Axial Preload	81
4.6	Sample 2: Elastic and Transformation Shear Modulus Determined for Various Degrees of Axial Preload	82
4.7	Sample 3: Elastic and Transformation Shear Modulus Determined for Various Degrees of Axial Preload	83
4.8	Torsional Load Response Prediction Comparison for Zero Axial Preload.	86
4.9	Torsional Load Response Prediction Comparison for Axial Preload of 60 MPa.	87
4.10	Torsional Load Response Prediction Comparison for Axial Preload of 120 MPa.	88
4.11	Torsional Load Response Prediction Comparison for Axial Preload of 240 MPa.	89
4.12	Torsional Load Response Prediction Comparison for Axial Preload of 360 N.	90
4.13	Torsional Load Response Prediction Comparison for Axial Preload of 480 N.	91
5.1	Axial Elongation due to the Torsional Loading Induced Transformation	94
5.2	Torsionally Induced Phase Transformation with Consequence Axial Elongation	95
5.3	Composite Cylinder Model	96
A.1	Continuous Rotating Potentiometer Signal	113
A.2	Torsional Load Cell Noise Evaluation	114
A.3	Methods to Determine the Transformation Yield Point	116
A.4	Comparison of the Axial Tangent Modulus using Different Amount of Data Points	117

A.5	Comparison of the Torsional Tangent Modulus using Different Amount of Data Points	118
A.6	Maximum, Minimum and Average Values of the Tangent Modulus for the Torsional Load Response	119
A.7	Error in Yield Tangent Modulus Method for Axial Load Response . .	121
A.8	Error in Yield Tangent Modulus Method for Torsional Load Response	123
A.9	Quadratic Relation Between the Standard Deviation of the Residual and the Ratio of the Shear Modulus.	124
A.10	Error in the Transformation Yield Stress as a Function of Noise for PLSLR Method	125
A.11	Error in the Elastic Shear Modulus as a Function of Noise for the PLSLR method	126
A.12	Error in the Transformation Shear Modulus as a Function of Noise for the PLSLR method	126
C.1	Strain Controlled Axial Training of Sample 1	133
C.2	Load Controlled Axial Training of Sample 1	134
C.3	Torsional Load Training of Sample 1	135
C.4	Strain Controlled Axial Training of Sample 2	136
C.5	Load Controlled Axial Training of Sample 2	137
C.6	Torsional Load Training of Sample 2	138
C.7	Strain Controlled Axial Training of Sample 3	139
C.8	Load Controlled Axial Training of Sample 3	140
C.9	Torsional Load Training of Sample 3	141
C.10	Sample 1, Test 1: Pure Torsional Load Response with Theoretical Prediction	142
C.11	Sample 1, Test 1: Pure Torsional Load Response - Experimental Axial Strain and Torsional Rotation	143
C.12	Sample 1, Test 1: Pure Torsional Load Response - Experimental Axial Stress and Torque	144
C.13	Sample 1, Test 1: Pure Axial Load Response - Experimental Axial Strain and Torsional Rotation	145
C.14	Sample 1, Test 1: Pure Axial Load Response - Experimental Axial Stress and Torque	146

C.15 Sample 1, Test 1: Combined Axial-Torsional Loading (115 MPa Axial Preload) with Theoretical Prediction	147
C.16 Sample 1, Test 1: Combined Axial-Torsional Loading (115 MPa Axial Preload) - Experimental Axial Strain and Torsional Rotation	148
C.17 Sample 1, Test 1: Combined Axial-Torsional Loading (115 MPa Axial Preload) - Experimental Axial Stress and Torque	149
C.18 Sample 1, Test 1: Combined Axial-Torsional Loading (350 MPa Axial Preload) with Theoretical Prediction	150
C.19 Sample 1, Test 1: Combined Axial-Torsional Loading (350 MPa Axial Preload) - Experimental Axial Strain and Torsional Rotation	151
C.20 Sample 1, Test 1: Combined Axial-Torsional Loading (350 MPa Axial Preload) - Experimental Axial Stress and Torque	152
C.21 Sample 1, Test 1: Combined Axial-Torsional Loading (470 MPa Axial Preload) with Theoretical Prediction	153
C.22 Sample 1, Test 1: Combined Axial-Torsional Loading (470 MPa Axial Preload) - Experimental Axial Strain and Torsional Rotation	154
C.23 Sample 1, Test 1: Combined Axial-Torsional Loading (470 MPa Axial Preload) - Experimental Axial Stress and Torque	155

NOMENCLATURE

T	Torque
σ	Axial Stress
σ_{TY}	Combined Loading Transformation Yield Stress (Martensite Start)
σ_{MF}	Axial Yield Stress (Martensite Finish)
σ_0	Pure Axial Loading Transformation Yield Stress
ϵ	Strain in the Axial Direction
ϵ_0	Pure Axial Loading Transformation Yield Strain
ϵ_{ext}	Strain in the Axial Direction Measured by Extensometer
ϵ_{LVDT}	Strain in the Axial Direction Deter- mined from LVDT
τ	Shear Stress
τ_{TY}	Combined Loading Transformation Yield Shear Stress
τ_0	Pure Torsional Loading Transforma- tion Yield Shear Stress
τ_{inv}	Energy Equivalent Shear Stress
γ	Shear Strain

\mathfrak{R}	Proportionality Coefficient
γ_{TY}	Combined Loading Transformation Yield Shear Strain
γ_0	Pure Torsional Loading Transforma- tion Yield Shear Strain
γ_{inv}	Energetically Equivalent Shear Strain
ρ	Independent spatial variable (Wire ra- dius)
L	Length of the Wire
c	Outside Radius of the Wire
θ	Twist Angle
E_E	Axial Elastic Modulus (Young's Mod- ulus)
E_{TR}	Axial Transformation Modulus
G	Shear Modulus
G_E	Elastic Shear Modulus
G_{TR}	Transformation Shear Modulus
M_S	Martensite start temperature under given applied stress
M_F	Martensite finish temperature under given applied stress
A_S	Austenite start temperature under given applied stress
A_F	Austenite finish temperature under given applied stress

M_S^0	Martensite start temperature under zero stress
M_F^0	Martensite finish temperature under zero stress
A_S^0	Austenite start temperature under zero stress
A_F^0	Austenite finish temperature under zero stress
C^s	Experimental Energetically Equivalent Value
ξ	Martensite volume fraction
DAQ	Data Acquisition System
LVDT	Linear Variable Displacement Transducer
MT	Martensite Transformation
YTM	Yield Tangent Modulus
PSLSR	Piecewise Smooth Least Squares Regression

CHAPTER 1

INTRODUCTION

1.1 Introduction

The department of Mechanical Engineering at the University of Alberta has been involved in various areas in biomechanical engineering research including the design and application of Shape Memory Alloy (SMA) springs. The objective of this research was to develop a method to predict the combined axial and torsional load response of pseudoelastic SMA wires. As an introduction this chapter outlines the key properties of a SMA and information relative to the previous work of other authors.

1.2 SMA Background

In the 1960's a new alloy made from nickel and titanium (NiTi) was discovered which was able to recover its original shape after deformation [Andreasen and Morrow, 1978]. This type of material was characterized as a "Shape Memory Alloy" (SMA). The Shape Memory phenomena is the result of an alloy having a microstructure that consisted of two similar crystallographic phases that coexisted [Duerig et al., 1990]. This phase interaction as illustrated in Figure 1.1, has the original phase, known as austenite, transforming into a stress induced metastable phase called martensite.

The austenite phase is a B2 structure which is quite similar to the Body Center Cubic atomic structure. As depicted in Figure 1.1 the two dimensional representation of the austenite BCC structure is a square. The martensite phase structure forms from the austenite phase has a monoclinic shape. The martensite structure is typically known as the twinned structure. This twinned structure is quite mobile in the fact that its twinning direction can occur in as many as 12 different directions [Funakubo, 1984]. The direction of the twinning can change if the loading direction changes. For a pseudoelastic SMA, the martensite reverts back to the austenite phase

automatically upon unloading. The Shape Memory effect (different from the pseudoelastic effect) requires the SMA to be heated to revert back to the austenite phase. Whether the SMA experiences the pseudoelastic or shape memory effect is mainly determined by the composition ratio of nickel to titanium and the operation temperature but is also affected by other factors such as cold working and heat treatment [Gupta and Sczerzenie, 1997].

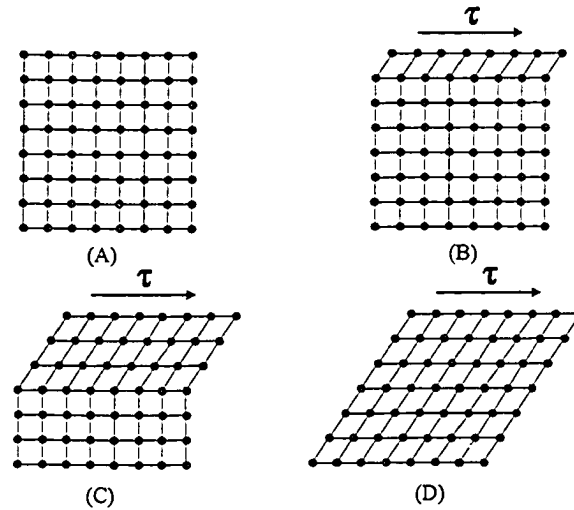


Figure 1.1: Atomic Configuration of the austenite and martensite phase. As crystal experience the shear load (τ) the austenite phase (square) begins to form into the martensite phase (parallelogram) (A) 100% austenite, (B) One Layer of martensite, (C) 50% martensite, (D) 100% martensite [Duerig et al., 1990]

Comparing the tensile load response of steel with the typical pseudoelastic SMA is illustrated in Figure 1.2. The steel load response has three distinct regions; an elastic loading/unloading region, a plastic loading region and a plastic unloading region. In the elastic region steel has the identical loading and unloading path. Once the steel specimen reaches the plastic region the unloading load response shifts right and there will be an associated residual strain when the loading is completely removed. The pseudoelastic shape memory alloy load response could be classified into six distinct regions. The initial load response is elastic, similar to the load response for steel. Loading a SMA past its elastic region begins to initiate the stress induced phase transformation from the austenite phase to the martensite phase. To distinguish this type of yielding from plastic yielding, the point where the phase transformation initiates is termed as the “Transformation Yield Point” [Perkins and Hodgson, 1990].

The load response of the phase transformation has a low modulus and at the end of the loading plateau the SMA consists of 100% martensite. If the SMA is loaded past this region, it experiences elastic loading of the transformed martensite phase. Further loading results in the SMA undergoing permanent deformation. Unloading the SMA specimen prior to the martensite plastic region results in the specimen being capable of recovering all of its deformation (No residual deformation). The initial unloading modulus is similar to the loading modulus and is followed by a low modulus unloading response as the martensite reverted back to the austenite phase. Once the reverse phase transformation from martensite back to austenite is complete, the SMA experiences linear elastic unloading of the austenite phase. A comparison of some of the material properties between steel and SMA material are summarized in Table 1.1.

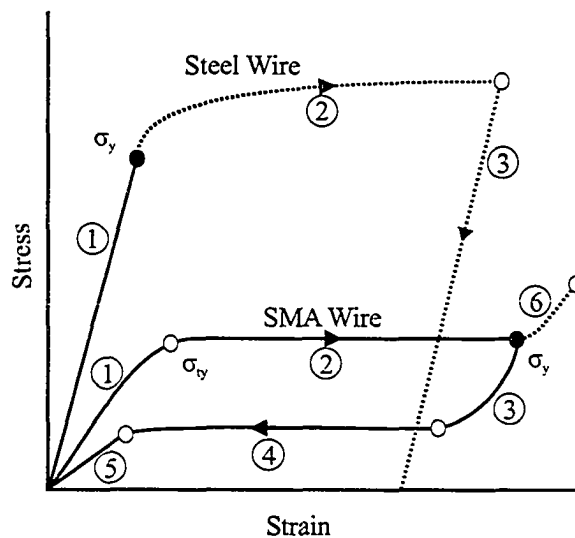


Figure 1.2: Comparing SMA to Steel: Steel has three distinct loading regions, 1) Elastic Loading/Unloading 2) Plastic Loading 3) Plastic Unloading. The SMA has 6 distinct regions, 1) Elastic loading/unloading, 2) Austenite - Martensite transformation loading 3) Initial elastic unloading of pseudoelastic response. 4) Martensite to Austenite transformation unloading. 5) Elastic unloading of pseudoelastic load response. 6) Elastic loading of martensite phase.

1.2.1 Modeling of SMA Behaviour

Some of the most prominent load response models used to predict the SMA load response were the Tanaka-Based Model, Ivshin-Pence Model and the Boyd Lagoudas

Table 1.1: Comparing Properties of NiTi SMA with Steel [Funakubo, 1984]

Shape Memory Alloys and Steel	SMA	Steel
Yield Stress	195 - 600MPa	260 - 520 MPa
Max Recoverable Strain	8%	.26%
Linear Elastic Modulus (estimated)	80 GPa	200GPa
Density	6500 $\frac{kg}{m^3}$	7920 $\frac{kg}{m^3}$

Model [Brinson, 1993], [Boyd and Lagoudas, 1996]. In these models the SMA load response were composed of a mechanical law governing the load response and a kinetic law to govern the transformation behavior. It was noted by Gillet [Gillet et al., 1998] who studied the axial and torsional loading of an SMA that “(Constitutive Modeling) lacked predictive capacity, strong assumptions needed in the calculation of the macroscopic thermodynamical potential that leads to determination of unstable behavior, and the need of an *a priori* kinetics rule.”

Gillet based his SMA load response model using the framework from plasticity. The behavior on loading was developed using the infinitesimal strain theory with uniform linear thermoelastic behavior of the austenite and martensite phase. The total strain was assumed to be the contributions from the elastic, thermal and transformation strain components where the elastic and thermal strain were similar for typical linear elastic materials while the transformation strain, $d\epsilon_{ij}^{pt}$ was assumed to follow the normality rule,

$$d\epsilon_{ij}^{pt} = d\lambda \frac{\partial F}{\partial \sigma_{ij}}, \quad (1.1)$$

where $d\lambda$ is the transformation plasticity multiplier and F denotes the transformation yield stress function. The von Mises criterion had been used as the transformation yield stress function, [Patoor et al., 1995], [Bondaryev and Wayman, 1988] but it was not accurate when considering compressive loading. It was found that the transformation yield stress function for NiTi SMA, [Duerig et al., 1990], [Gillet et al., 1998] was asymmetric as shown in Figure 1.3.

Assuming that the material was isotropic and that the volume change was negligible, Gillet chose to use the Prager equation [Gillet et al., 1998],

$$F(J_2, J_3, T, \epsilon^{pt}) = J_2 \left(1 + \frac{bJ_3}{J_2^{3/2}} \right) - K^2(\epsilon^{pt}, T) = 0 \quad (1.2)$$

which is the simplest phenomenological criterion that could be used to predict the

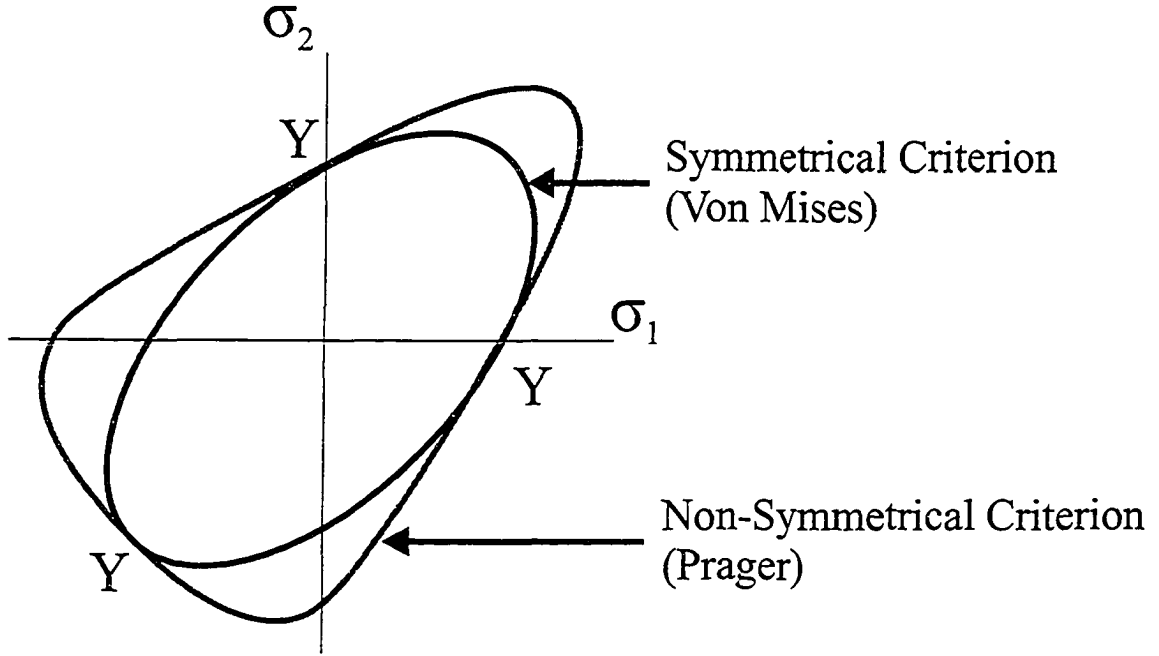


Figure 1.3: Symmetrical and NonSymmetrical Transformation Stress Criterion. σ_1 and σ_2 were the first and second principle stresses.

transformation yield stress for combined loading. In this equation, J_2 and J_3 are the second and third scalar invariant of the deviatoric part of the stress tensor and T is the temperature of the specimen. The function $K(\epsilon^{pt}, t)$ and the coefficient b are determined from experimental tests.

Gillet modeled the axial load response as a parabolic function,

$$\sigma_t = \sigma_0(T) + K_0(\epsilon)^{n_0}, \quad (1.3)$$

where it only considered the range up to the completion of the stress induced phase transformation. The parameters K_0 and n_0 are fitted from experimental tests. This equation considered the axial loading up to the completion of the phase transformation. The critical transformation stress, σ_0 was assumed to follow the linear Clausius-Clapeyron relation denoted as

$$\sigma_0(T) = \mathfrak{R}_0(T - M_s) \quad (1.4)$$

where \mathfrak{R}_0 is the proportionality coefficient between stress and temperature for axial loading. Using these relationships and the framework from plasticity, a constitutive

equation was defined that could be applied to structural calculations.

In the application to structural calculations, Gillet used the bilinear approximation (for simplicity), but noted that this did neglect the strongly non-linear first transformation stage (elastic region). This bilinear approximation was used to derive the torsional load response assuming that the assumptions of Saint-Venant and Navier-Bernoulli are valid. The torsional load response was derived as,

$$T = \frac{SR^2 G_{TR} \psi_s}{2} \left(\frac{G_{TR}}{G_E} \left(\frac{\psi}{\psi_s} - \frac{\psi^3}{\psi_s^3} \right) + \frac{4}{3} \left(1 - \frac{G_{TR}}{G_E} - \frac{\psi_s^3}{\psi^3} + \frac{G_{TR} \psi_s^3}{G_E \psi^3} \right) + \frac{\psi_s^3}{\psi^3} \right), \quad (1.5)$$

where

$$\psi_s = \frac{\tau_y}{cG_E} \quad (1.6)$$

and

$$\psi = \frac{\tau}{\rho G_E}. \quad (1.7)$$

The bilinear shear stress assumption was also used to study SMA rods in torsion by Davidson [Davidson and Liang, 1996]. The details of this derivation are shown in Appendix A.

Regarding the transformation yield surface, to this author's knowledge there have been other theories put forth with the description of the transformation yield surface. Sittner et al. studied the combined torsional axial load response and predicted the combined loading transformation stress on CuZnAl SMA tube specimens [Sittner et al., 1994b]. The torsional load response and the axial load response were directly compared by using experimentally derived coefficients to convert the values of τ and γ to invariant values which corresponded to the idea that the deformation energy density required to initiate a martensite transformation was equal in tension and torsion. Based on the transformation yield stress, σ_0 , and transformation yield strain, ϵ_0 for axial loading, the invariant values for torsional loading were given as

$$\tau_{inv} = \frac{\sigma_0}{\tau_0} \tau \quad (1.8)$$

and

$$\tau_{inv} = \frac{\epsilon_0}{\gamma_0} \gamma. \quad (1.9)$$

Similar to the von Mises criterion, the Sittner transformation yield criterion was defined using the Generalized Elliptical Yield Criterion with invariant values in place

for the torsional stress term. The stress yield function was

$$\frac{\sigma^2}{\sigma_0} + \frac{\tau_{inv}^2}{\sigma_0} = 1 \quad (1.10)$$

and the yield strain function was

$$\frac{\epsilon^2}{\epsilon_0} + \frac{\gamma_{inv}^2}{\epsilon_0} = 1. \quad (1.11)$$

Through their experimental research, Sittner studied the load path dependency in combined torsional and axial loading. It was concluded that the pseudoelastic deformation in continuous forward martensite transformation was characterized as slightly path dependent. That is, the order in which combined torsional and axial is applied will have a slightly different resulting shear and axial strain. Sittner identified that the martensite transformation was a stress controlled phenomena not strain controlled.

1.2.2 SMA Geometry

The two most common SMA geometries that have been studied were the cylinder and the flat sheet. The information from this research could be used to develop a method to predict the combined load response of wire springs. Cylindrical specimens are ideal for axial and torsional experimentation because the stresses across the cross section of the specimen can be assumed to be axis symmetrical and thus be determined as a function of the cross section radius. The combined torsional and axial load response of SMA cylinders is commonly modeled as thin wall cylinders because its ease to machine into proper test specimens, mounting strain gauges and thermocouples and theoretical simplicity where the shear stress across the thin wall cross section could be assumed to be constant [Sittner et al., 1994b], [Tokuda et al., 1999]. It was chosen to research the combined load response of a solid SMA wire because this research would be a valuable tool for spring design in areas such as orthodontics. The information from this research could also be used for future studies as a way to compare the torsional load response of SMA tubes with wires.

1.2.3 Thermal Elastic Response

The load response of a SMA was also dependent on the material temperature as illustrated in Figure 1.4. Although it is not illustrated, a similar relationship occurs for pure torsional loading. At lower temperatures the SMA load response would be simi-

lar to curve “C” where the SMA would remained deformed until it was heated to above its transformation temperature. Deforming the alloy while above its transformation temperature results in the alloy returning to its undeformed state upon unloading [Duerig et al., 1990], [Funakubo, 1984]. This response is known as the pseudoelastic response or superelasticity. There was an upper temperature limit where the SMA experienced permanent deformation with little or no pseudoelasticity. For the samples that were tested this upper thermal limit could not be determined as the testing apparatus was limited to 50°C. In general with increasing temperature there will be a corresponding increase in the transformation yield stress for the forward and reverse transformation. With increasing transformation with increasing temperature the elastic region becomes larger. The maximum pseudoelastic strain does not change with temperature which would result in the transformation plateau decreasing with increasing temperature. The transformation temperature also changes based on material composition, heat treatment and cold working [Gupta and Sczerzenie, 1997]. The manufacturing of a SMA material required controlling all these aspects to generate the preferred type of SMA response for its respective application. For this experimental research the NiTi SMA was tested at a temperature that would produce a pseudoelastic response.

1.2.4 Thesis Outline

This thesis is presented in six chapters. The first chapter is an introductory chapter in which the objective and background to this thesis research is discussed. In chapter two, the equipment that was made specifically for the experimental tests is described in detail. There is also an evaluation of the experimental apparatus and some preliminary tests performed on SMA wire. In the third chapter the axial and torsional load response models are introduced along with the evaluation of the techniques used to determine the material properties from these load responses. The fourth chapter is the study on the combined load response prediction of the SMA wire. In the fifth chapter the model for predicting the axial elongation due to the transformation induced by torsional loading while under a constant axial preload was developed. The final chapter is where the conclusions and the possible direction of this research for future projects are discussed.

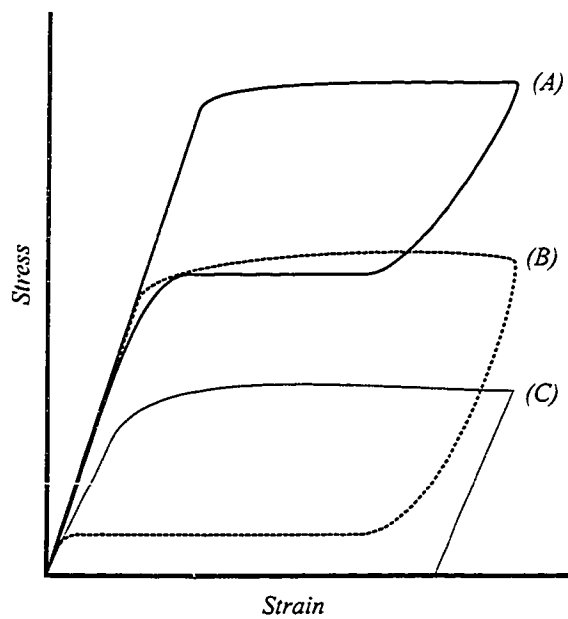


Figure 1.4: Effects of Temperature on Loading: Temperature $A > \text{Temperature } B > \text{Temperature } C$. Load response A and B were pseudoelastic while load response C had the shape memory effect where the sample was to be heated in order to recover its deformation.

CHAPTER 2

EXPERIMENTAL COMBINED LOADING TESTING

2.1 Introduction

Experimental combined axial and torsional load response tests were performed on pseudoelastic SMA wires to compare with the prediction models which will be introduced in the following chapters. The experimental testing is done to gather information on how the axial and torsional load response changes based on the load path. The load path is defined as the order and magnitude of the applied torsional and axial loading. Since this was the premier undertaking of combined load response testing of NiTi SMA wire for the Department of Mechanical Engineering at the University of Alberta, it was required that a combined loading testing apparatus be designed and built. The entire testing apparatus, as shown in Figure 2.1, consisted of an MTS testing machine, a torsional adapter and the Data Acquisition System (DAQ). The torsional adapter itself consisted of a torsional and axial load cell, an electric motor, worm gear drive, and a data acquisition system. An environmental chamber was used to control the temperature of the test specimen. In this chapter the experimental testing apparatus is discussed in detail along with the combined axial and torsional load response tests that were performed with this testing apparatus.

2.2 MTS Testing Machine

The MTS (Mechanical Testing and Simulation) machine was used to apply the axial load to an SMA wire specimen. This machine is equipped with an axial load cell, extensometer (strain measurements), and a “Linear Variable Displacement Transformer” (LVDT) to measure the ram stroke which could be used to calculate the axial strain. The MTS testing machine is capable of both load control and displacement control which can be applied either under manual control, automatic control

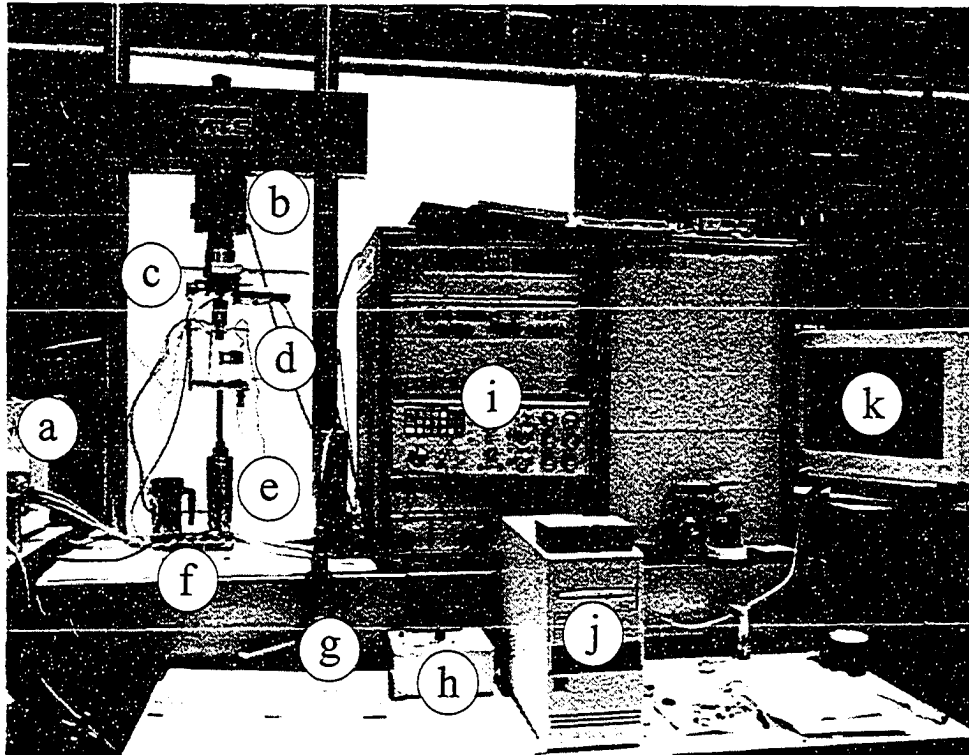


Figure 2.1: Experimental Setup: (a) A/D Converter, (b) MTS Load Cell, (c) Torsional Adapter, (d) Environmental Chamber, (e) MTS Hydraulic Ram, (f) Data Acquisition Terminal Board, (g) Heat Gun, (h) Motor Controller, (i) MTS Control Console, (j) PC Computer, (k) PC Monitor

with the sinusoidal loading or using the time ramp function. The MTS machine has a maximum capacity of 45000 N and its load cell was determined to have an accuracy of ± 7.7 N.

The axial strain of the SMA wire specimen was measured using the MTS extensometer. This extensometer uses a two bladed grip to attach itself to the specimen with a 25.4 mm (1") gauge length separation as shown in Figure 2.2. The extensometer was calibrated at room temperature (approximately 15°C) prior to the testing to be 1% strain per volt with an accuracy of $\pm 0.005\%$ strain. As per manufacturer's specifications the limiting range of the extensometer is 14% strain. During testing the extensometer was inside the environmental chamber and was taking measurements at a higher temperature than the calibration temperature. The test temperature

was at 45°C which was 30°C above the calibration temperature. The component of the extensometer that is affected by the change in temperature is the extensometer's strain gauge located within the extensometer. Changing the temperature of strain gauge changes its resistance and was corrected during experimental testing by zeroing the extensometer at the test temperature [OMEGA 1995].

The extensometer grips were modified, as illustrated in Figure 2.3, from the original flat blade to a notched blade to improve installation and alignment of the extensometer on the wire specimen. Without notching the blade grips it was possible for the extensometer to move from its original position while the specimen rotated under torsional loading. In one tested case with the notched grips, as the SMA wire rotated up to 180° five times and recording a drift in the extensometer of 0.0108 mm (0.000425in) or 0.0425% strain.

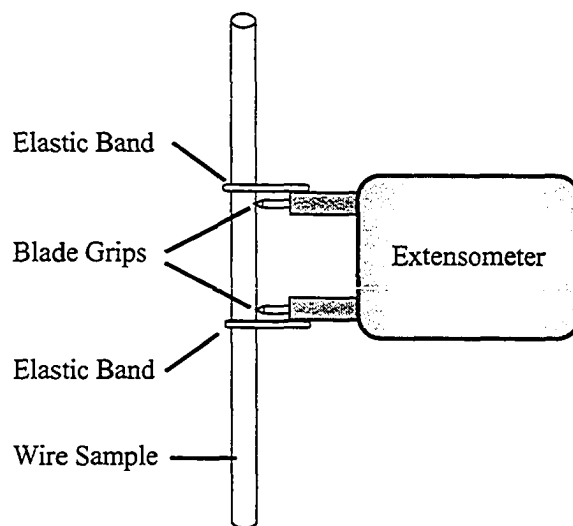


Figure 2.2: Extensometer Setup. The extensometer is used to measure the elongation of the test specimen by directly attaching to the wire specimen by using blade grips and elastic bands.

2.3 Torsional Adapter

The torsional adapter was designed and built in the Department of Mechanical Engineering at the University of Alberta. As shown in Figure 2.4, the torsional adapter was a device that applied torsional loading to a specimen while the MTS applied the axial loading. In the following sections the key components of the torsional adapter



Figure 2.3: Extensometer Grip Modification (a) The original blade geometry (b) Modified blade geometry by filing a notch in the center of the blade. This modification improved the ease of installation and reduced the drift in the extensometer as the specimen rotated under torsional loading.

are explained in detail. These components include the load cell, environmental chamber and the data acquisition system.

2.3.1 Load Cell

The combined torsional-axial load cell that was provided by the Vibrations Laboratory from the Department of Mechanical Engineering is shown in Figure 2.5. This load cell which was previously used in similar applications is made from a 6061 aluminum tube with an outside diameter of 15.450 mm, a wall thickness of 0.770 mm and is 114.3 mm long. The strain gauges on the torsional-axial cell were hard wired to the data acquisition system which restricted the mobility of the load cell to $\pm 360^\circ$. Since the MTS machine was already equipped with a calibrated axial load cell and there was not enough calibration weight available for the combined load cell for axial calibration, it was decided to use only the stress values measured using the MTS load cell.

The torsional calibration involved using an apparatus as illustrated in Figure 2.6 to apply a pure torque to the torsional load cell. The calibration of the torsional load cell is shown in Figure 2.7. The torsional load cell was calibrated to be -1.351 mV/Nmm in the clockwise direction and 1.401 mV/Nmm in the counterclockwise direction. The uncertainty of the torsional load cell was determined to be ± 7.5 Nmm. The apparatus used to perform the calibration was attached to the hydraulic ram of the MTS so that it could be positioned. With this setup it was not possible to calibrate in combined loading.

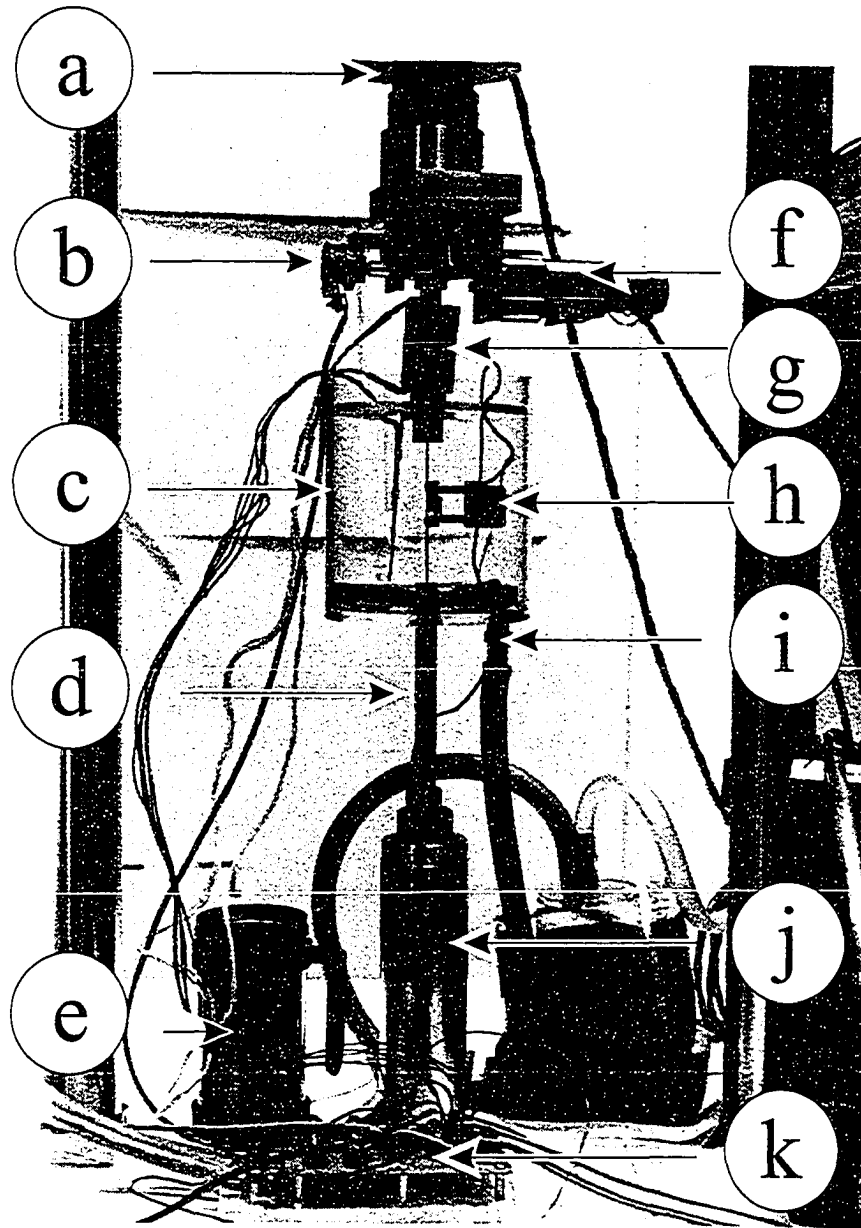


Figure 2.4: Torsional Adapter: (a) MTS Load Cell, (b) Continuous Rotating Potentiometer (c) Environmental Chamber, (d) Lower Grip Assembly, (E) Ice Bath, (f) Electric Motor (Torsion) (g) Load Cell, (h) Extensometer, (i) Air Intake, (j) MTS hydraulic Ram, (k) Data Acquisition Terminal Board

As shown in Figure 2.8, the torsional adapter uses an electric servo motor and a worm gear drive to rotate the load cell that was directly connected to the wire specimen. By mounting the load cell on a thrust bearing it allows the MTS to apply

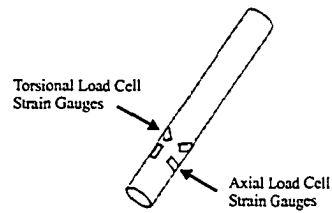


Figure 2.5: Torsional-Axial Load Cell: This load cell was made from 6061 aluminum and had strain gauges mounted to measure both torsional and axial loading.

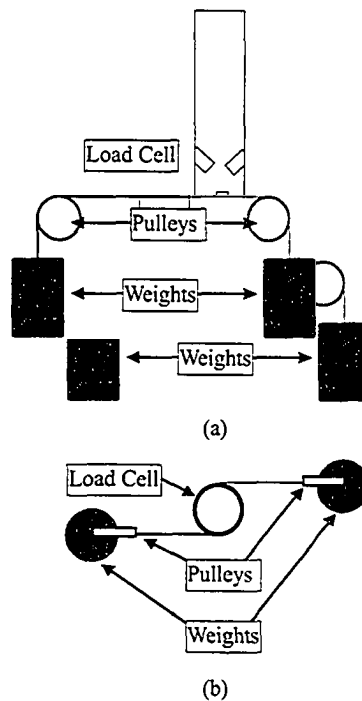


Figure 2.6: Load Cell Calibration Setup (a) side view (b) top view. The weight produced a pure torsional loading on the load cell with no bending moment or axial load.

the axial load simultaneously while the worm gear drive applied the torsional loading. The advantage of using the worm gear drive to apply the torsional loading is that it allows for fine control of the position of the load cell plus it locks the load cell in place when the motor is not in motion. The disadvantage of this system is that if a constant torque was to be applied, it would have to be manually controlled. The

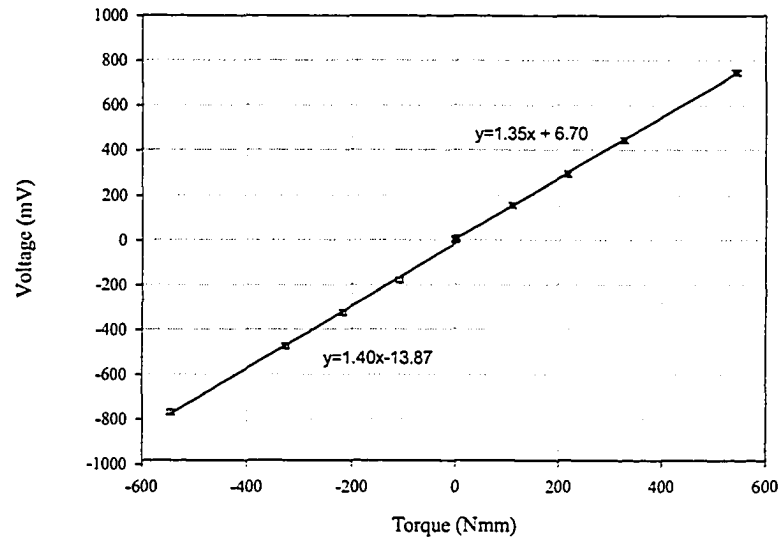


Figure 2.7: Torsional-Axial Load Cell: Torsional Dead Weight Calibration. The torsional load cell was calibrated to a ± 545 Nmm

torque is amplified through the worm gear drive with with a 60 tooth driven gear and a single pitch worm gear (60:1). The worm gear is driven with a manual control servo motor with a 19.5:1 gear reduction. The worm gear drive and gear reduction provided adequate rotation speed and power required for applying torsional loading to the wire specimen. With this gear reduction the servo motor can apply more torque, but it is at the expense of rotational speed. This limitation does affect the torsional adapters ability to apply a constant torque during the phase transformation using manual control.

The specimen is secured to the torsional adapter using brass clamps as shown in Figure 2.9. The upper clamp is attached directly to the load cell and the lower clamp is part of a brass shaft that connects to the hydraulic ram of the MTS. The clamping surfaces are grooved to increase the contact area which in turn increase the gripping force. This design for a clamping mechanism was chosen for its ease of use and cost. A concern with the grips is that the wire may reduce its cross sectional area while elongating in the axial direction enough to cause the specimen to slip. This issue is further addressed in Section 2.3.5.

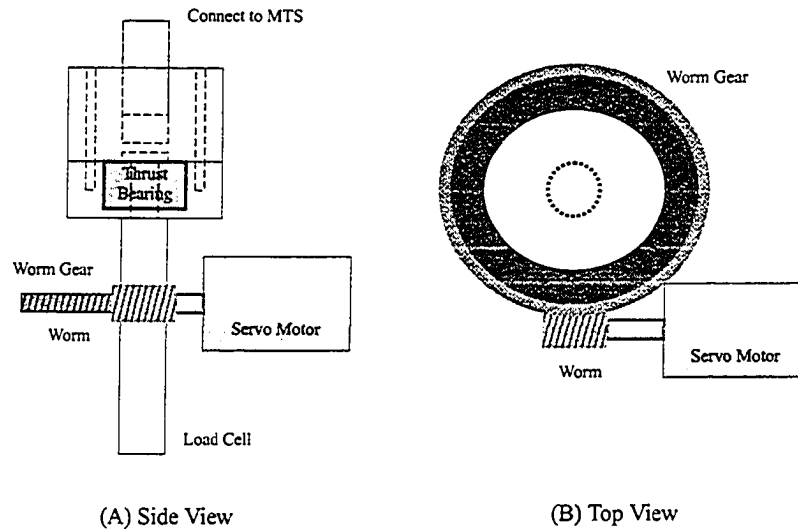


Figure 2.8: Layout of the Torsional Adapter. An electric motor and a worm gear drive powers the torsional loading of the load cell.

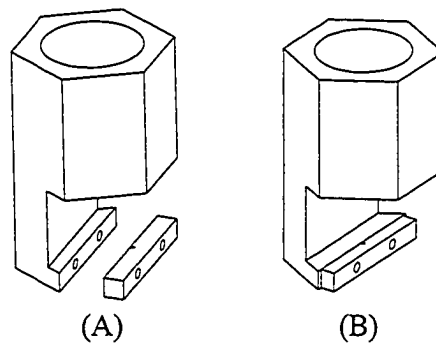


Figure 2.9: Brass clamps used to secure the specimen to the torsional adapter. (a) disassembled view, (b) assembled view

2.3.2 Environmental Chamber

The specimen test temperature was controlled using an environmental chamber. A suitable test temperature is required in the environmental chamber in order for the SMA to have a suitable pseudoelastic load response. The environmental chamber is made from a polycarbonate plastic cylinder that encased the entire specimen as shown in Figure 2.4. The main body of the chamber attaches to the lower grip assembly and is able to slide down in order to provide access to the test section. The main chamber moves with the hydraulic ram of the MTS tester and the top cover rotates

with the load cell. This configuration allows for the large deformations in the torsional and axial axis while maintaining an environmental barrier from the room. The lid has a 1/4" radial clearance from the main chamber body to eliminate the frictional resistance while they move relative to one another. This clearance also acts as a vent for the circulation of air in the cylinder. To maintain a constant air temperature in the environmental chamber a variable speed heat gun was used which created a constant flow of warm air into the chamber. During the experimental loading of the SMA wire specimen it was expected that there would be a small amount of heat generated as a result of the martensite transformation [Funakubo, 1984] [Tobushi et al., 1998]. Although it was not expected to affect the material behavior significantly, the flow of air through the environmental chamber would aid the dissipation of the heat energy and maintain a constant specimen temperature.

The temperature inside the environmental chamber was monitored using type "T" thermocouples with an ice bath reference. The temperature of the test specimen was estimated by using a separate SMA wire instrumented with thermocouples and was placed close to the test specimen. The thermocouples were not attached directly to the tested sample in order to avoid any adverse effects such as insulating the heat that was released/absorb during the phase transformation and affecting phase composition and material properties. In total, there were three thermocouples mounted on the dummy sample and one used to monitor the air temperature of the environmental chamber. The experiments proceeded when the chamber air temperature and the thermocouple on the dummy wire achieved a steady state. Using the thermocouples to monitor the temperature of the environmental chamber with the heat gun running, the temperature during the experimental tests was maintained within $\pm 1.5^{\circ}\text{C}$.

2.3.3 Data Acquisition (DAQ)

A Hewlett Packard Analog to Digital Converter collected the measured information from the MTS and the Torsional Adapter, potentiometer, thermocouples, extensometer and the data was stored digitally on a computer as shown in the schematic in Figure 2.10. The data acquisition system is composed of a Command Module (HP 8210) and a Strain Gauge Signal Conditioning unit(HP 1413A). This command module provides an excitation voltage of 3.9 Volts to the wheatstone bridges of the torsional and axial load cell and the rotating potentiometer. The HP data acquisition system was also used to record temperatures measured using the thermocouples.

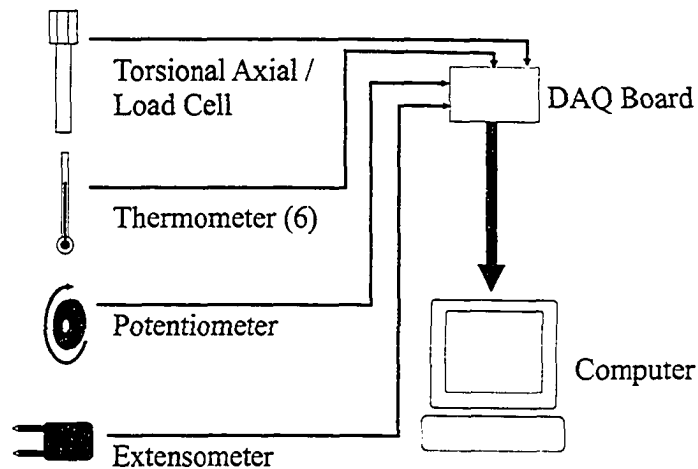


Figure 2.10: Data Acquisition System System. The torsional/ axial load cell, thermometer, potentiometer and extensometer measurements were all recorded digitally using the HP1820 Data Acquisition unit and a PC computer.

2.3.4 Measuring the Wire Twist Angle

For the torsional test the wire sample was twisted by having the lower wire grip stationary while the upper grip rotated with the combined torsional load cell. A rotating potentiometer was used to determine the angle of wire twist by measuring the angle of rotation of the torsional load cell. This potentiometer was a continuous potentiometer where the output voltage signal was a direct function of the rotational angle from 0 to 360°. At 0° the output voltage was zero and at 359° the voltage was the same as the input voltage. This potentiometer was powered from the data acquisition board which supplied a voltage of 3.9 Volts. Once past 360° the output voltage would drop to 0 Volts. Thus for each rotation of the potentiometer a sawtooth signal would be generated. Ideally the potentiometer was to be installed so that it directly measured the angle of rotation of the load cell. Since this could not be done without using additional gears or pulleys it was decided to attach it directly to the drive shaft of the electric motor that drove the load cell. With this it was required to convert from the measured angle of rotation of the electric motor to the angle of rotation of the load cell. More information on how this was done is shown in Appendix 1, Section A.2.1.

2.3.5 Evaluation of the Torsional Adapter

Upon the completion of the construction and calibration of the torsional adapter, the next step was to evaluate the pure axial, pure torsional and a combined axial and torsional loading of a metal wire sample. This was done to ensure that the torsional adapter was working as expected for a linear elastic material. This was followed with the preliminary tests that were performed on SMA wire samples to evaluate the limitations for testing the SMA wire with the given testing apparatus. The metal wire sample had a diameter of 1.57 mm and a test section length of 100 mm. This length was chosen based on the smallest wire length that could be tested where the extensometer could be attached to the specimen with ease.

The first test performed on the metal sample was to cyclicly axial load the specimen in the linear elastic region. Figure 2.11 illustrates three load controlled loading cycles which have a maximum stress of 365 MPa. The cyclic axial loading of the steel wire in the elastic region was repeatable with some initial deviation from linearity occurring up to 0.03% strain. It is noted in ASTM E111-97 that factors such as specimen curvature and initial grip alignment may introduce significant errors in strain determined by the extensometer for small loads applied to the specimen. These items were noted to be present in the experimental tests.

The elastic modulus of the metal wire specimen was determined using the MTS machine with and without the torsional adapter to identify if there was any difference with the addition of the torsional adapter. Performing an axial load test using the MTS machine without the torsional adapter, it was found that the modulus of the metal wire was 157 GPa. Having the torsional adapter mounted the elastic modulus of the steel wire was determined to be 165 GPa. The difference between the modulus measured using the torsional adapter and the MTS machine was only 13 MPa which corresponds to a 7.6% difference. Since there was only a single sample tested with the MTS machine and with the torsional adapter it is uncertain if the difference is a result of the variance in the material properties between the two samples.

With the brass clamps it was questioned whether the sample would be slipping in the grips during testing. It can be reasoned that whether the specimen slips in the grips or not, the loading and strain measurements in the test section would remain the same.

Comparing the strain determined from the LVDT and the extensometer is another way to determined if there are any abnormal deformations in the measured load re-

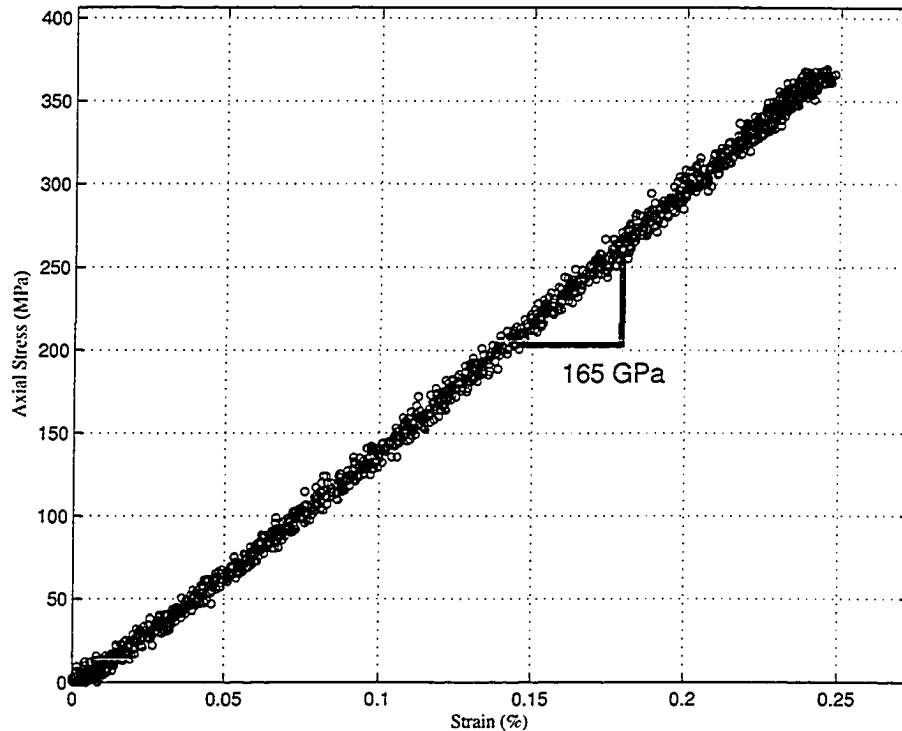


Figure 2.11: Cyclic Axial Loading of Metal Wire. The three loading cycles shown here were linear and repeatable which was expected for a linear elastic material. There was some deviation from linearity up to 0.05% strain which is noted by ASTM E111-97 is a result of misalignment of the specimen along the loading axis and possible curvature in the specimen.

sponse as a result of using the torsional adapter. The LVDT measures the deformation of the entire testing apparatus including the MTS machine torsional adapter and the specimen. Comparing the strain of the specimen from the LVDT with that of the extensometer serves as an indication of deformation of the specimen is relative to the deformation of the entire testing apparatus. The testing apparatus was designed so that the torsional load cell was the weakest component by at least a factor of 1.5 and would yield at a load of 8500 N. The loading capacities of the other components are listed in the Appendix 1 Section A.2.2. Comparing the extensometer and the LVDT strain as done in Figure 2.12 the ratio of the strain measured using the LVDT and the extensometer (Strain Ratio) is 1.21 which indicates that the LVDT measured strain is higher than the strain measured by the extensometer. The difference can be mainly attributed to the calibrated error of the LVDT. The LVDT was calibrated to

an accuracy of ± 0.1 mm and the test section length of the specimen was also known to within ± 0.1 mm. The extensometer was calibrated to an accuracy of ± 0.00125 mm with a set gauge length of 25.4 mm.

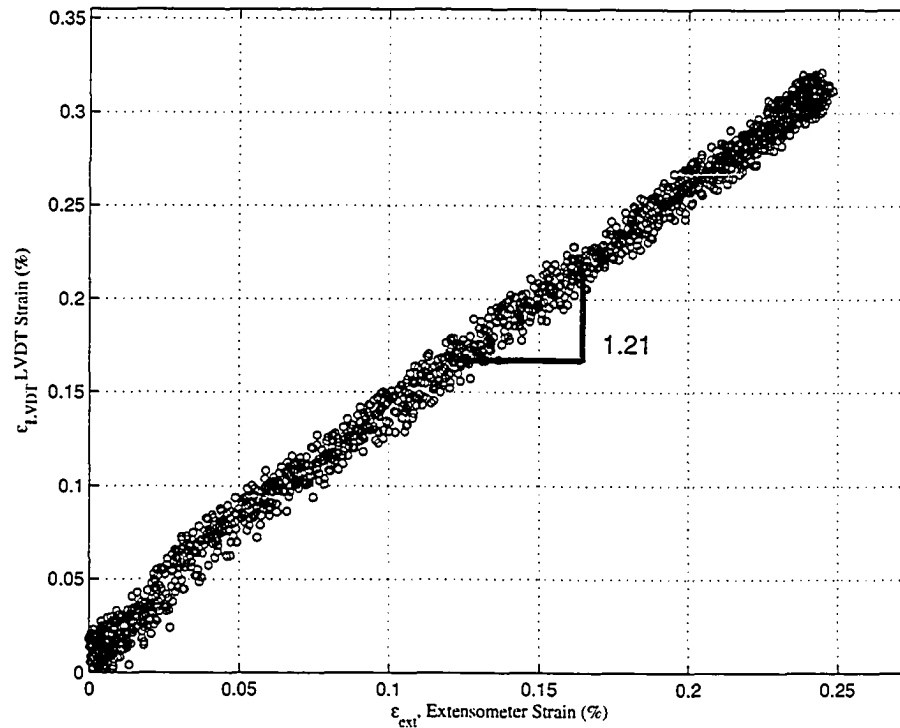


Figure 2.12: LVDT-Extensometer Comparison. The comparison showed the strain determined from the LVDT than the strain measured by the extensometer.

Torsional loading testing of the steel specimen involved cyclic elastic loading as shown in Figure 2.13. In the three successive cycles the maximum applied torque experienced was 400 Nmm with each cycle being linear, repeatable and having no residual strain. The slope of the torsional load response was found to be $7.0 \text{ Nmm}/^\circ$ (67.6 GPa).

It was found during the testing that the load cell used had some degree of cross talk in combined loading. When cross talk occurs with the torsional and axial load cell this means that in pure torsional loading the axial load cell is sensing a load even though there is no axial load present. The cross talk can occur for pure axial loading as well. This occurs mainly due to the alignment of the strain gauges in the axial and torsional load cells. The orientation of the strain gauges in the torsional and axial load cells as show in 2.5 do minimize cross talk but during preliminary testing it was

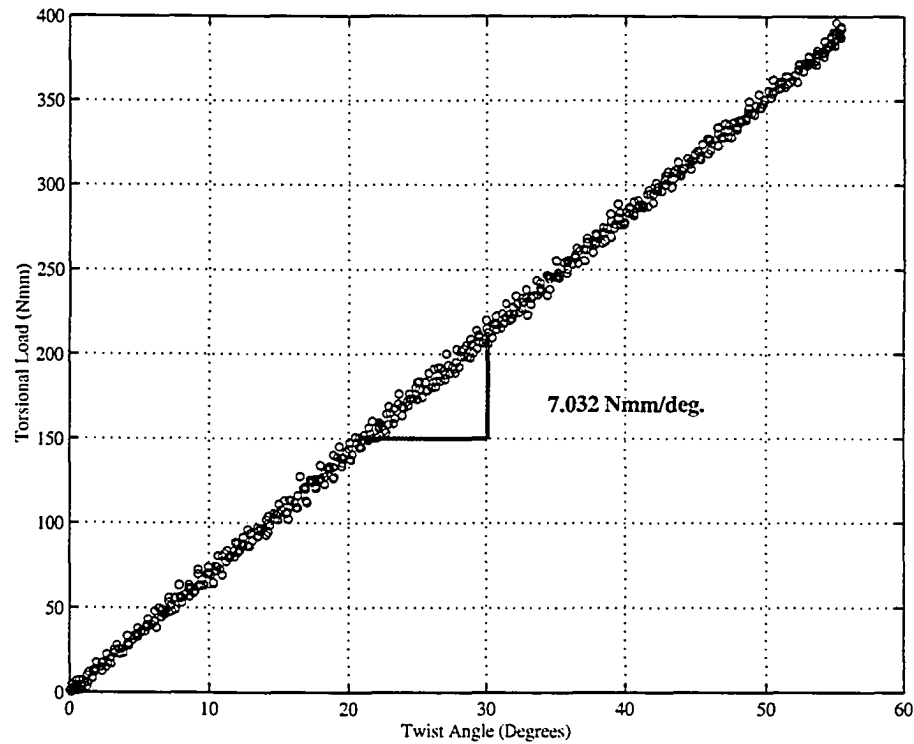


Figure 2.13: Three torsional load cycles of the metal wire sample. Each cycle was linear and repeatable, which is expected for a linear elastic material. The slope of the load response was determined to be $7.0 \text{ Nmm}/^\circ$ (67.6 GPa)

found that cross talk was present. Shown in Figures 2.14 and 2.15, are the cross talk relationships between the torsional and axial load cell for the pure axial and torsional loading cases, respectively. In Figure 2.14 is a single load test where the torsional cross talk experienced with pure axial loading. As the axial loading increased there was a corresponding decrease in the torque as measured by the torsional load cell. At the maximum axial load of 1400 N the torsional load cell cross talk -35 Nmm and for a torsional load of 900 Nmm the axial cross talk was less than the noise of the axial load cell. Because there was a higher magnitude of axial stress on the load cell compared to the torsional stress during experimental testing, the torsional measurements experienced a considerable amount of cross talk from axial loading while the axial loading experienced a negligible amount of cross talk from torsional loading. It was decided to confine the testing to first applying the axial preload, then zero the cross talk error, then apply the torsional loading. From the results of the metal sample tested in the elastic region, it was concluded that the torsional adapter

was operating adequately for testing a SMA with torsional loading up to 400 Nmm, torsional rotation up to 360°, axial loading up to 1400 N and axial strain up to 14% strain.

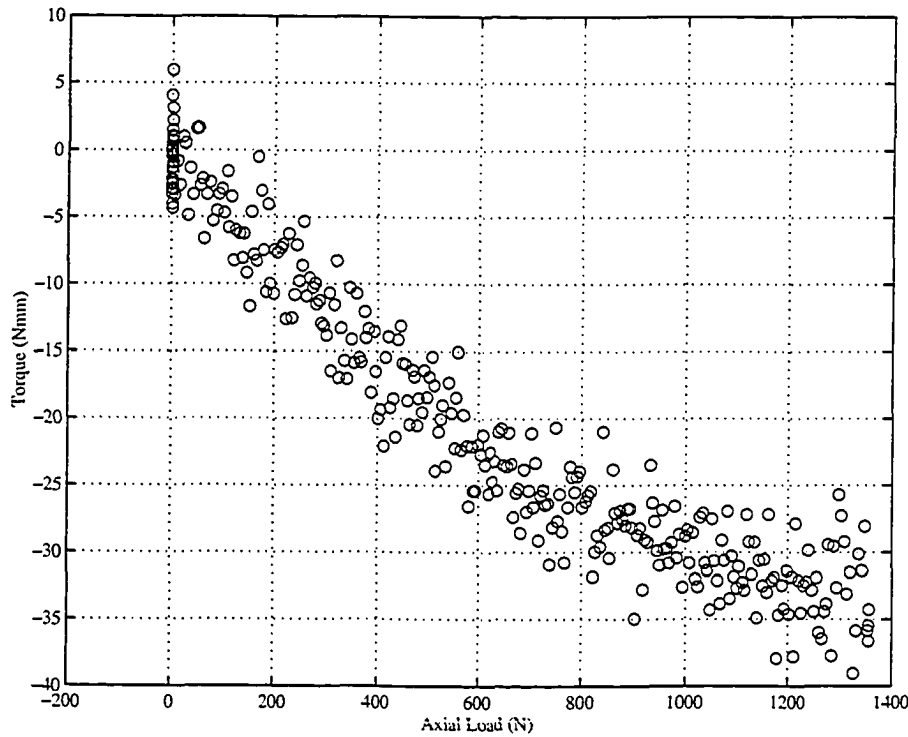


Figure 2.14: Torsional Cross Talk During Axial Loading. In one test as shown here, with an axial load of 1400 N there was a corresponding cross talk in the torsional load cell of $-35 \text{ Nmm} \pm 7.5 \text{ Nmm}$

2.4 Preliminary SMA Testing

The preliminary SMA testing was performed to assess the limitations of the experimental apparatus and to further understand the pseudoelastic load response of the material. The SMA was tested at a variety of temperatures and various degrees of combined loading to evaluate the SMA load response. The extensometer and LVDT measurements were compared to determine if the phase transformation occurred uniformly along the entire SMA specimen. Also in this section the issue of training the SMA wire prior to testing was addressed.

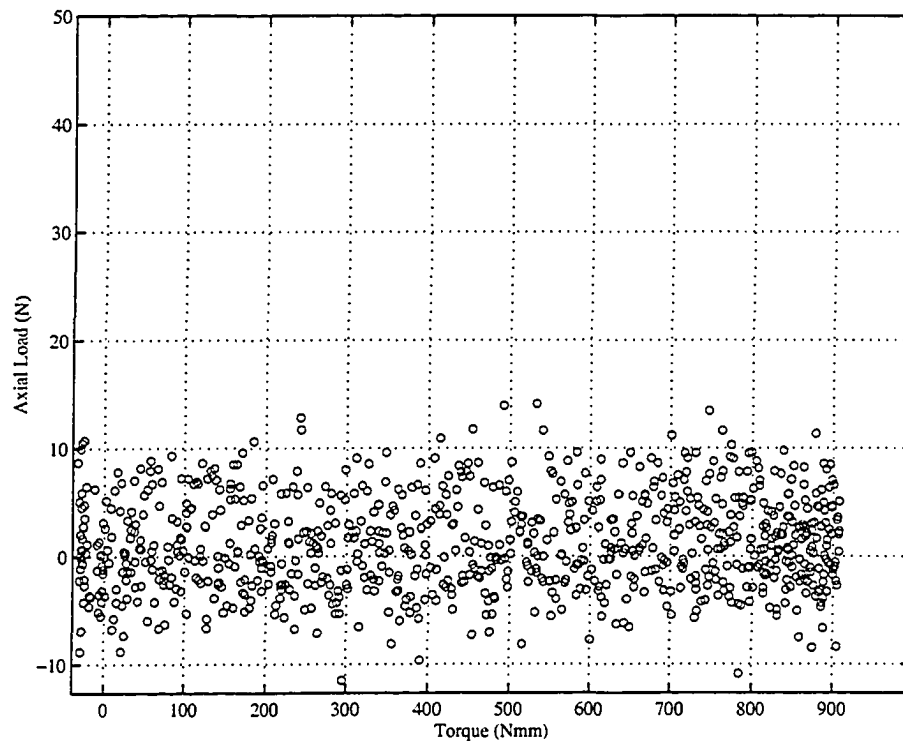


Figure 2.15: Axial Cross Talk During Torsional Loading. In one test shown here, with torsional loading there appeared to be no cross talk to the MTS axial load cell

2.4.1 Wire Properties

The SMA wire for this experimental research was donated by Special Metals Corporation in Utica, New York. This wire had an average diameter of 1.56 mm (± 0.005) and the test section length was 100 mm long. The 1.564 mm wire was the smallest size of wire that could be tested because of the noise in the torsional load cell as detailed in section A.2.3. With preliminary testing using NiTi SMA wire, it was estimated that the maximum torsional load will be 300 Nmm to test the initial pseudoelastic response of a 1.564 mm wire and with the load cell having ± 7.5 Nmm uncertainty this translates to a minimum 2.5% error at its maximum load and would be even higher error for lower loads. Ideally the preferred wire length would be as small as possible to have the most samples tested with the provided wire and so that the twist angle could be minimized during testing. The test section was chosen to be 100 mm because it was the smallest test length that could be used and still be able to install the extensometer with ease.

For optimum pseudoelastic properties the NiTi be cold worked 30% and heat treated at 400°C for 15 minutes followed by cooling in air for optimal pseudoelastic properties [Gupta and Sczerzenie, 1997]. Although the exact details of processing the sample NiTi alloys as received from the Manufacturer is proprietary, it is assumed that the samples were prepared to similar specifications. Further heat treatment would only soften the material requiring more strain deformation to achieve the same pseudoelastic state, which could cause a nonuniform cross section diameter along the length of the test section. Because of this, the wire samples were tested in the “as received” state.

Using X-ray diffraction from the electron microscope at the Department of Chemical and Materials Engineering, the specimens were determined to have a composition of 52.8% Ni and 47.2% Ti (atomic weight). Using a Differential Scanning Calorimeter (DSC) from the Smart Materials Laboratory in the Department of Mechanical Engineering at the University of Alberta the transformation temperatures of this wire were measured to be: $M_s = -13^\circ\text{C}$, $M_f = -22^\circ\text{C}$, $A_s = 4^\circ\text{C}$, and $A_f = 13^\circ\text{C}$. The results of the DSC analysis are shown in Figure 2.16. For this wire sample to have a pseudoelastic response the test temperature would have to be above 13°C. Typically it is preferred to have the test temperature higher than this value, but if the temperature is too high then the wire will begin to experience plastic deformation rather than pseudoelastic deformation. How the test temperature was chosen is detailed in the next section.

2.4.2 Evaluating the SMA Load Response as a Function of Temperature

To determine the optimum temperature for testing the SMA pseudoelastic response there were pure axial and torsional tests performed over a range of temperatures from 30°C to 50°C. The temperatures tested in axial loading are shown in Figure 2.17 and the torsional load response are shown in Figure 2.18. The upper thermal limit of the environmental chamber is 50°C and the lowest temperature that could be tested using only air cooling is 20°C. Any of the temperatures between 20 and 50°C would produce a suitable pseudoelastic response for testing. Based on the preliminary analysis a suitable temperature used to test the pseudoelastic response for experimental testing was chosen to be 45°C. This value was slightly higher than what was recommended by Sittner which was 38°C ($25^\circ\text{C} + A_f$) [Sittner et al., 1997]. The samples that were tested were to be loaded repeatedly and it was not desired to

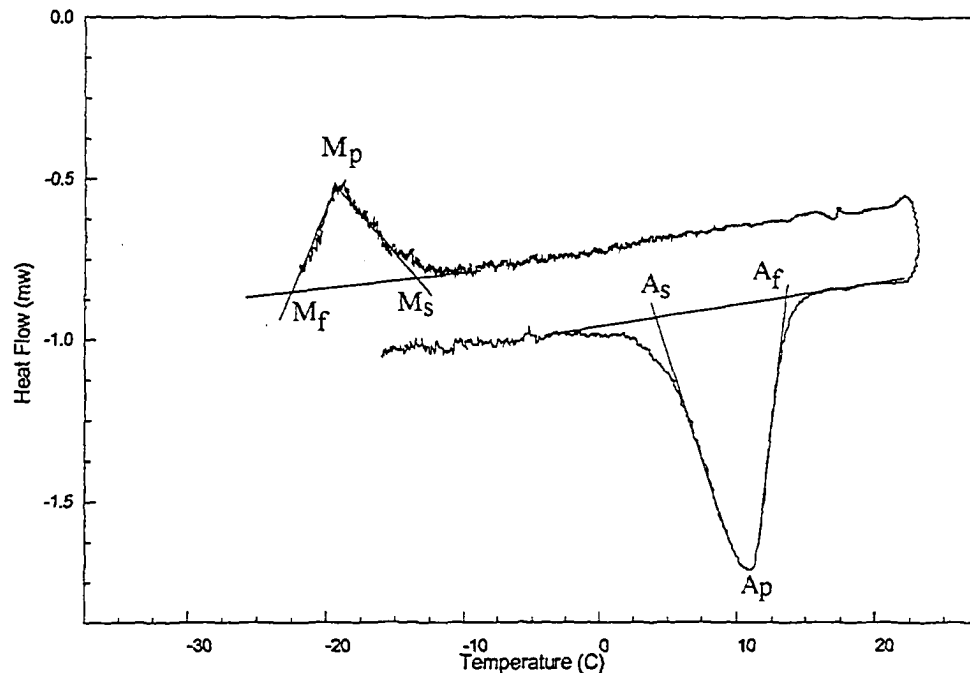


Figure 2.16: Differential Scanning Calorimeter (DSC). The DCS was used to determine the transformation temperatures by slowly heating and cooling the specimen and measuring the heat flow through the specimen.

have the unloading response experience the shape memory effect (Experience residual strain until the specimen is heated). If this would to occur the specimen would have to be heated then cooled again to the test temperature between each cycle.

2.4.3 Comparing Strain Measurements from Extensometer and LVDT of an Axially Loaded SMA Wire

The comparison between the axial strain measured by the Extensometer and LVDT was performed to primarily determine if the specimens were slipping within the grips and if the martensite transformation was initiated as a result of the compressive loading of the grips. These samples were also compared with the metal sample strain ratio as shown in Figure 2.12. If the initial transformation occurred outside the gauge section of the extensometer the associated elongation would be detected by the LVDT measuring the ram stroke, but not by the extensometer. If the extensometer and the LVDT measurement were in agreement the strain ratio would be 1. As shown

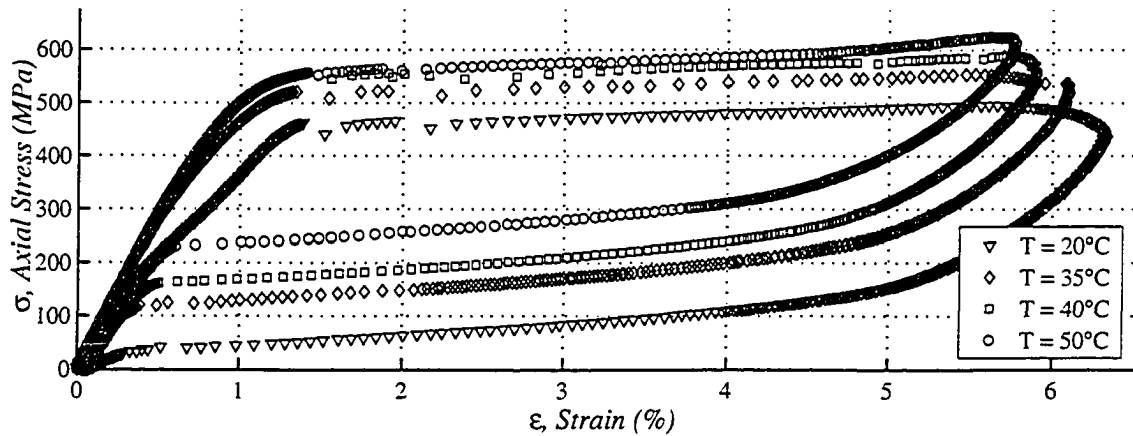


Figure 2.17: Temperature-Stress-Strain Response for Pure Axial Loading. As temperature increased the load response increased.

with the metal sample the strain ratio was found to be 1.21 for the majority of the evaluated load response. For the regular SMA sample the strain ratio was 1.24 up to an extensometer strain of 0.6% after which a sharp rise in the LVDT strain occurred then at 1% strain the ratio returned back to 1.24. This jump was assumed to be a result of the compressive loading of the grips causing the transformation to be induced at the grip locations. This would cause the extensometer to still be registering a linear elastic load response while the LVDT would be registering the transformation load response. The extensometer and LVDT strain measurements were compared with a regular SMA sample and a notched SMA sample as shown in Figure 2.19. The notched SMA was a wire that had a small notch ground into the wire at mid length to reduce the wire diameter in the test section from 1.564mm to 1.312mm. In doing this the initiation of the phase transformation would be more likely to first occur at this location rather than at the grips. With the notched specimen the strain ratio did maintain a constant value of 1.24 up to 0.8% strain which was an improvement of 0.2% from the un-notched specimen. This improvement only corresponds to the increased strain that would accompany the reduction in cross section area. The deviation from the strain determined from the LVDT and measured by the extensometer occurred at the same stress as the un-notched sample. Thus the notch test did not further confirm nor deny the possibility that the transformation occurs non-uniformly along the specimen cross section. Further research in this area would be required to confirm that this is occurring and how to minimize this effect for testing wire samples. At this

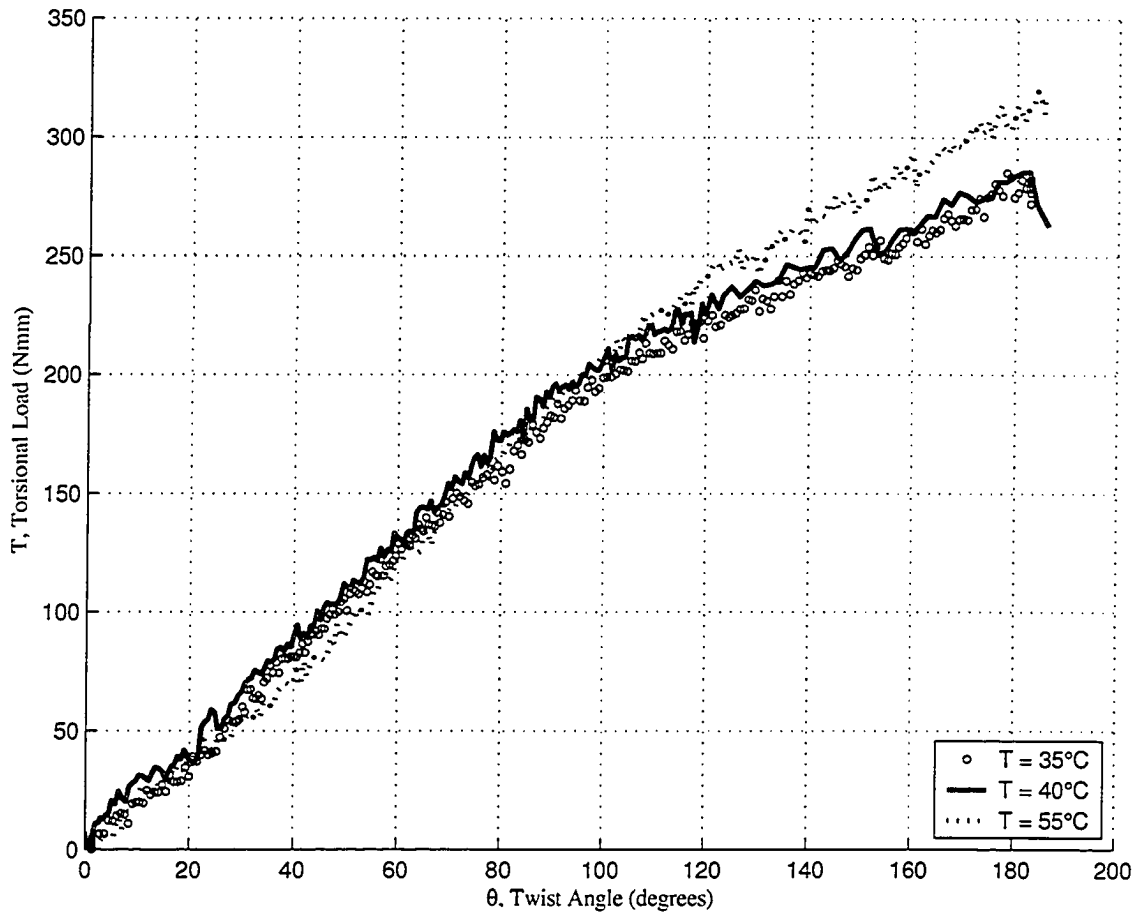


Figure 2.18: Temperature-Torque-Rotation Response for Pure Torsional Loading. As temperature increased there was general corresponding increase in the transformation yield stress.

point it can only be assumed that the phase transformation does initiate at the grips. As a result the use of the extensometer with the MTS load cell would still measure the load response that is characteristic of the material load response, but there will be some error associated with the non uniform phase transformation along the length of the SMA specimen. The load response would be lower in stress values than if the transformation was to occur uniformly along the entire length of the SMA.

2.4.4 Training the Wire in Axial Loading

The preliminary testing of the wire established that the load response for the virgin SMA wire samples were unpredictable and changed with each successive loading cy-

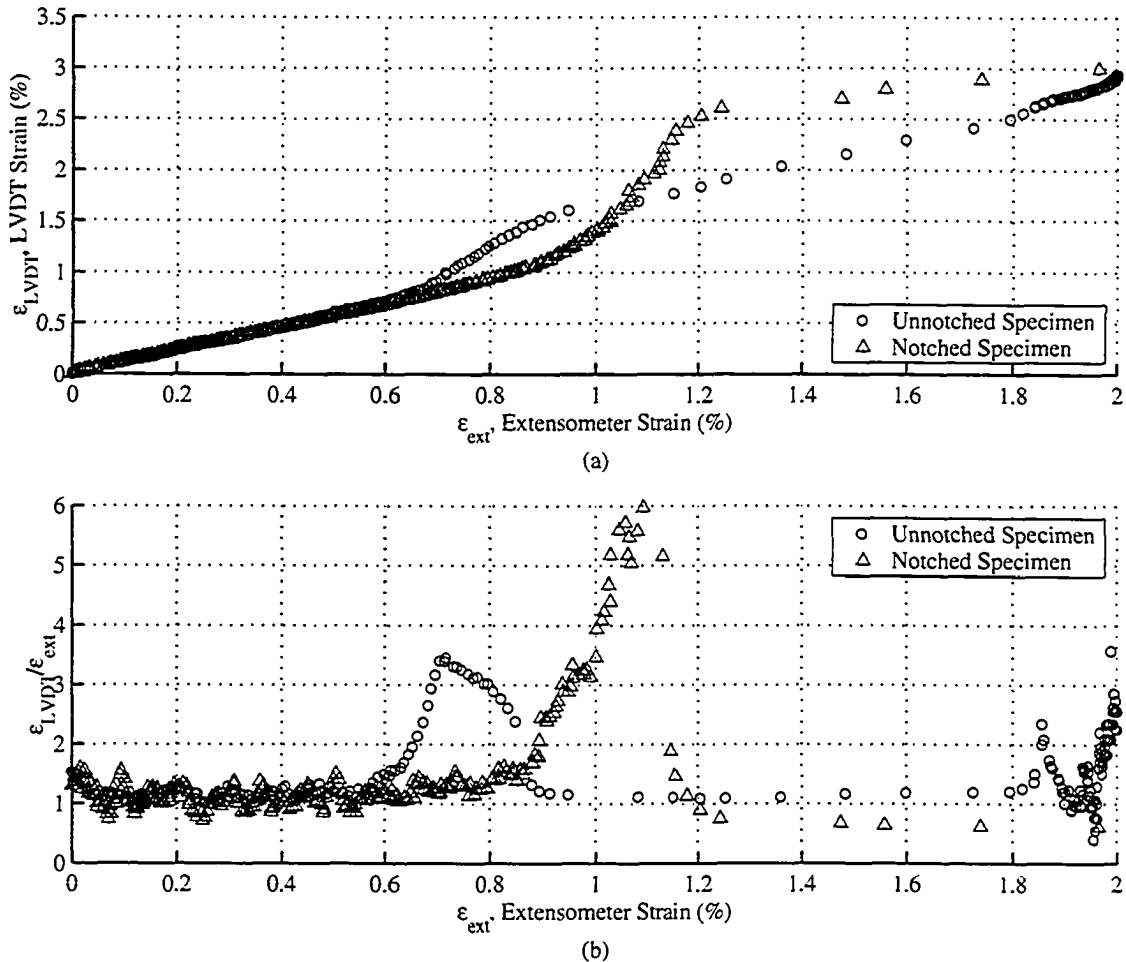


Figure 2.19: Comparing the strain measured with extensometer and the LVDT. a) The comparison between the strain measured by extensometer and LVDT for a notched and unnotched specimen. b) The tangent slope of (a). Note the deviation from constant slope changes from 0.6 to 0.8% strain for the unnotched to the notched case.

cle. With previous research it was shown that the loading response did become more predictable and the residual strain during a loading cycle was minimized by training the wire [Davidson and Liang, 1996] [Sittner et al., 1994a] [Sittner et al., 1995] [Tobushi et al., 1998]. The residual strain is the plastic deformation that occurs after a specimen has been loaded and unloaded. For typical materials such as steel this occurs due to mechanisms such as slip deformation. For SMA materials the residual deformation occurs for a different reason which can be explained how dislocations within a grain move around. A virgin SMA consists of many crystal grains

(polycrystal) and within each grain there are missing atoms, impurities and precipitates. There are also defects in the crystal structure in the grains in the form of grain boundaries, edge dislocations, screw dislocations and precipitates of other phases [Reed-Hill and Abbaschian, 1994]. Dislocations were line imperfections in the grain due to the beginning or ending of a plane of atoms within the crystal lattice. The nucleation of the martensite phase from the austenite phase requires a shape change in the atomic structure. In a grain of randomly orientated dislocations and defects, the energy required for the martensite transformation would be the same in any direction the shape change was to take place. During cyclic loading as experienced during training the dislocations and defects become mobile and move around within the grain of the SMA. While moving around in the crystal grain dislocations cannot move through one another or any other crystal defects such as a grain boundary. These dislocation pile-ups tend to have residual energy stored within them. During the initial cycles of training a virgin SMA wire, the dislocations that were once spread randomly throughout begin to pile-up. This was seen as the residual deformation with each training cycle. Since the bulk of the dislocations pile-up at the obstacles within the first few cycles the plastic deformation that occurred in each cycle decreased. [Sittner et al., 1994b] [Davidson and Liang, 1996] [Tobushi et al., 1998]. The second thing that occurred as a result of dislocation pile-up was the localized energy build up which prevented the complete transformation back to austenite upon unloading. This creates sites where the martensite phase is already nucleated under zero external stress. On the next loading cycle the energy required for creating a martensite nucleus was not needed; thus, the stress at the martensite transformation decreases. The dislocation pile-up also tended to be orientated in such a manner to aid the martensite transformation in the direction that it is trained. Changing the loading from that which the specimen was trained in would cause the martensite transformation to occur in a different direction and thus would have to go through the dislocation pile-ups that were formed from the original training. As a result, the stress would be higher than that of the trained loaded direction for the first cycle but would also decrease with successive repeated loading cycles. Thus training was required to condition the dislocations within the SMA specimen to minimize the plastic deformation associated with each loading cycle and to make the load response more consistent. Based on previous research the training of the SMA sample consisted of cyclic loading the SMA 20 times in the anticipated loading direction to establish a stable load response

[Sittner et al., 1994b] [Davidson and Liang, 1996] [Tobushi et al., 1998].

Depending on whether the loading was under strain control or stress control and on the rates that the loads were applied affects the load response immediately after the initiation of the martensite transformation. Applying the load under strain control at a slow strain rate the energy required to drive the phase transformation goes down immediately after the transformation yield point. To maintain a constant strain rate this decrease in energy had a corresponding decrease in stress. It was explained by Tobushi that for a small strain rate there was enough time for the martensite transformation to move after the creation of the martensite nucleus and therefore there was a corresponding relaxation in the stress [Tobushi et al., 1998]. Under stress control loading of a virgin wire the energy does not decrease after the transformation yield point to maintain a constant stress rate therefore the energy after the nucleation of the martensite phase contributes to the progression of the martensite transformation. As consequence there would be a sharp increase in the corresponding strain. It was preferred to model the load response under stress control because its load response was simpler than the load response under strain controlled loading, but it was required to initially train the SMA specimen under strain control to stabilize the load path for loading up to 2% strain. If training was done under only load control the loading would overshoot the 2% strain mark.

How training affects the load response for a SMA can be explained by considering the dislocations in the SMA which occur at an atomic level.

In the preliminary tests it was difficult to achieve a 2% strain accurately using the stress controlled loading of a virgin wire. The strain controlled training was performed before load control training to obtain a stabilized load response to a specific strain. As shown in Figure 2.20, the first 10 cycles of the training were performed using strain control up to approximately 2% strain. This value of strain was chosen to be consistent with the work of Sitter, who performed similar testing on CuZnAl tube specimens [Sittner et al., 1994b]. The last cycle of the strain controlled training is shown in Figure 2.21. The remaining training cycles were applied under stress control until a stable load cycle developed as shown in Figure 2.22. The first ten loading cycles were applied with a strain amplitude of 2% strain and at a rate of 120 seconds per cycle. The maximum strain rate experienced by the SMA wire under axial training was 0.05 %strain/s. During the first two cycles of the strain controlled training there was an audible cracking noise that occurred at the same instance that the wire initiated the

phase transformation. The noise could be attributed to the energy release associated with nucleation of the martensite phase.

While training the wire under strain control it was noted that the SMA wire experienced permanent deformation with each training cycle. This permanent deformation pertains to the dislocation piles-ups as described earlier. With the initial load cycles the majority of the dislocation movement would occur which acts to block the reverse transformation. As a result, the wire would buckle when the strain of the load cycle returned to zero for the initial loading cycles. This was shown in the load response plot as the stress was negative at the origin. This was not believed to be a result of the grips slipping because the residual strain per cycle reduced as the yield stress became more consistent. It was not desired to have the wire under compressive loading during strain controlled training as it would buckle causing excessive deformation in the wire at the grips which could possibly damage the specimen. To avoid this, the extensometer was zeroed at the end of each load cycle to avoid the compressive loading. The strain controlled training was complete when there was no more apparent permanent deformation and the load response was repeatable.

After the first 10 cycles of strain control training the wire was then trained under load control. When stress controlled tests were performed after strain controlled training, the yield strength and load required to achieve the desired strain would be known from the strain controlled training. Load control training was performed because the combined loading testing was also performed under axial load control. As shown in Figure 2.22, the load controlled training consisted of five loading cycles after which the load response did not change significantly in successive cycles. One of the advantages of load controlled training was that the specimen does not buckle upon unloading when there is any residual deformation. The load response of the SMA, trained under stress controlled axial loading, is shown in Figure 2.23.

2.4.5 Training the Wire in Torsional Loading

The final training stage involved the cyclic loading of the NiTi sample in pure torsion. Due to the limitations of the equipment used, the training and testing in torsion was restricted to manual rotational control. As shown in Figure 2.24 the first training cycle had a nonlinear elastic load response and about 13° of residual deformation. After the first cycle the load response changed minimally which indicated that the torsional load response was sufficiently trained. The trained torsional load response

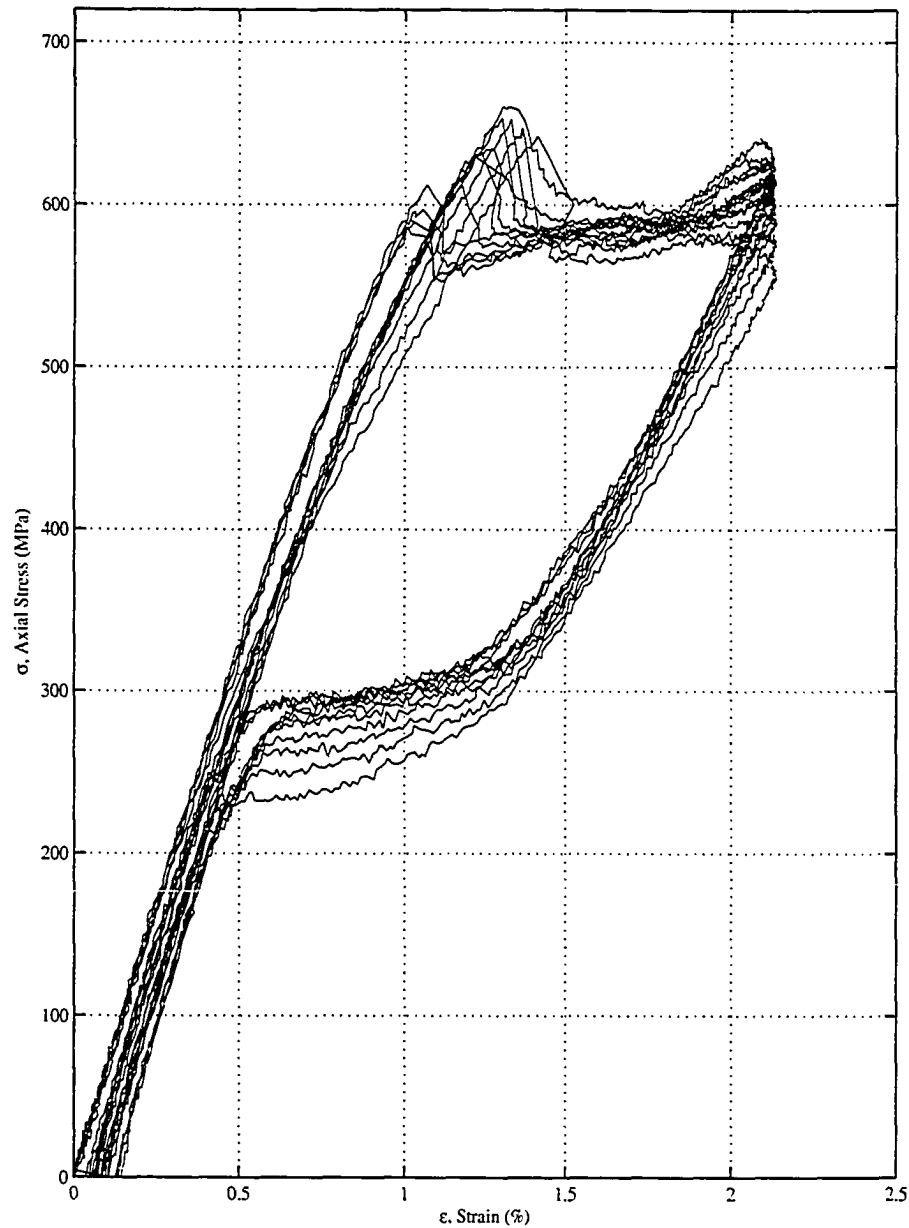


Figure 2.20: Training the SMA Wire Under Strain Control. In this figure shows the first ten cycles of the axial training. During the training the SMA experience residual deformation with each loading cycle. At the end of each loading cycle the SMA experience some plastic deformation and it was required to manually reset the zero strain value in order to avoid buckling of the SMA sample. This is shown on this figure as the load response does not always begin at the origin. The amount of residual deformation decreased with each loading cycle as part of the training process. The SMA wire behaved perfectly plastically from 1% strain to 1.75% strain as the wire extended with minimal increase in force. After 1.75% strain the slope of the stress-strain plot increased to 35 GPa.

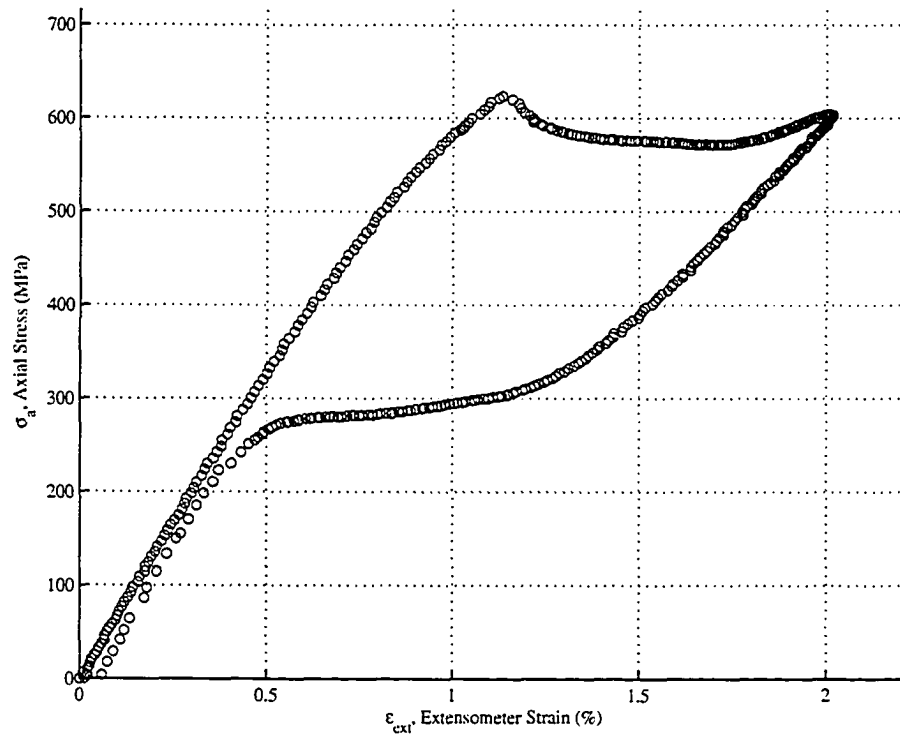


Figure 2.21: The axial load response for strain controlled loading. This load response had a local stress peak at the transformation yield point followed by a decreasing then increasing load response.

is illustrated in Figure 2.25 After both the axial and torsional training the wire was considered ready for combined load testing as explained in the next section.

2.5 Experimental Tests

With the SMA wire samples trained for both axial and torsional loading, the combined axial and torsional loading tests could be performed. The goal of the testing was to see how the torsional load response changed as a function of the applied axial preload. The amount of axial preload that was tested was 0, 60 MPa, 120 MPa, 240 MPa, 350 MPa and 480 MPa. At 550 MPa the phase transformation was induced by axial loading. With these experimental tests it was hoped to develop a model that could be used to predict the load response for combined axial and torsional loading for this particular loading path.

The test that were performed on a single wire specimen are shown in Figures 2.26

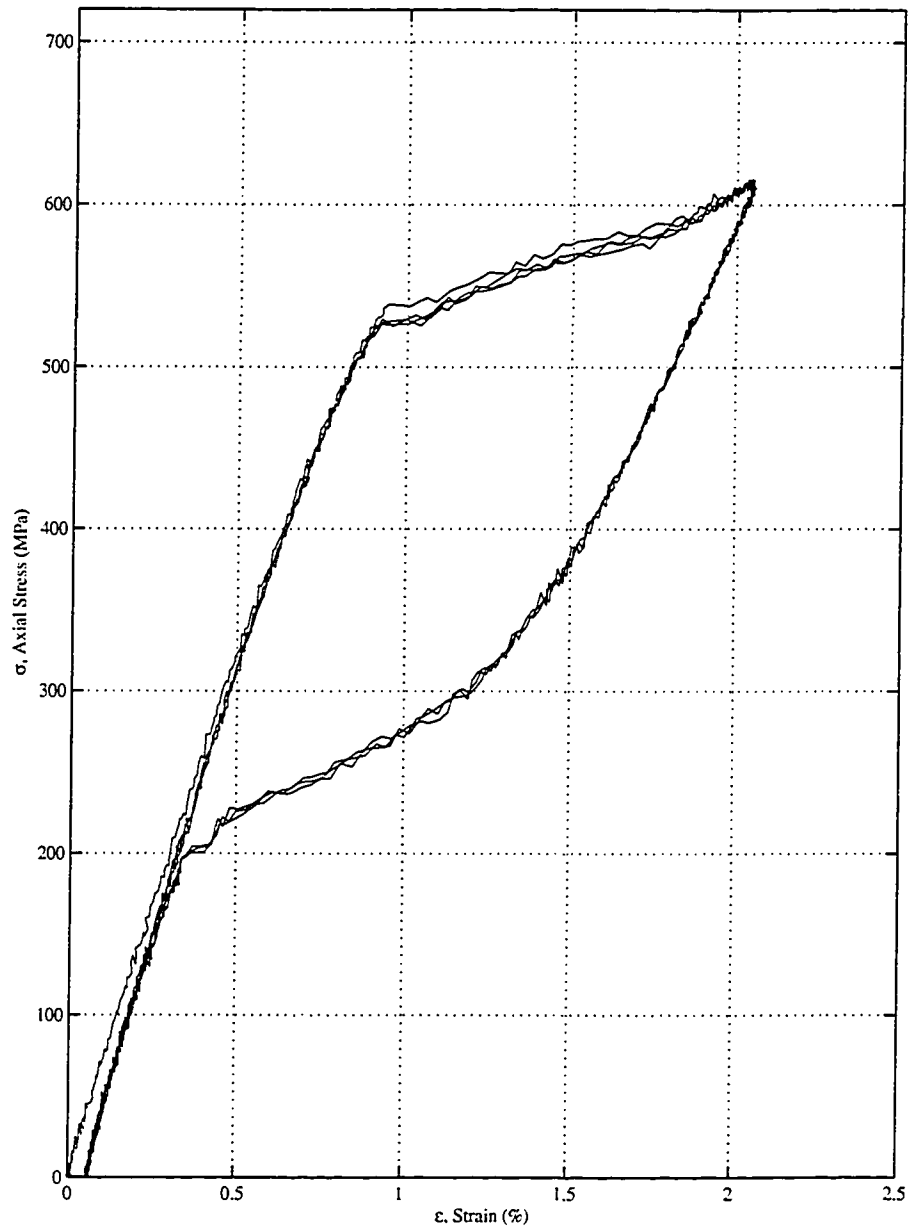


Figure 2.22: Stress Controlled Training after Strain Controlled training. There was some residual deformation with the first loading cycle. After this there was no apparent residual deformation with each loading cycle.

to 2.32. These figures show the complete load response for one particular specimen. When comparing the theoretical models with the experimental data for the axial and torsional load response in Chapter 3 only the loading component of the response was considered but for illustration purposes the entire load response is shown here. The

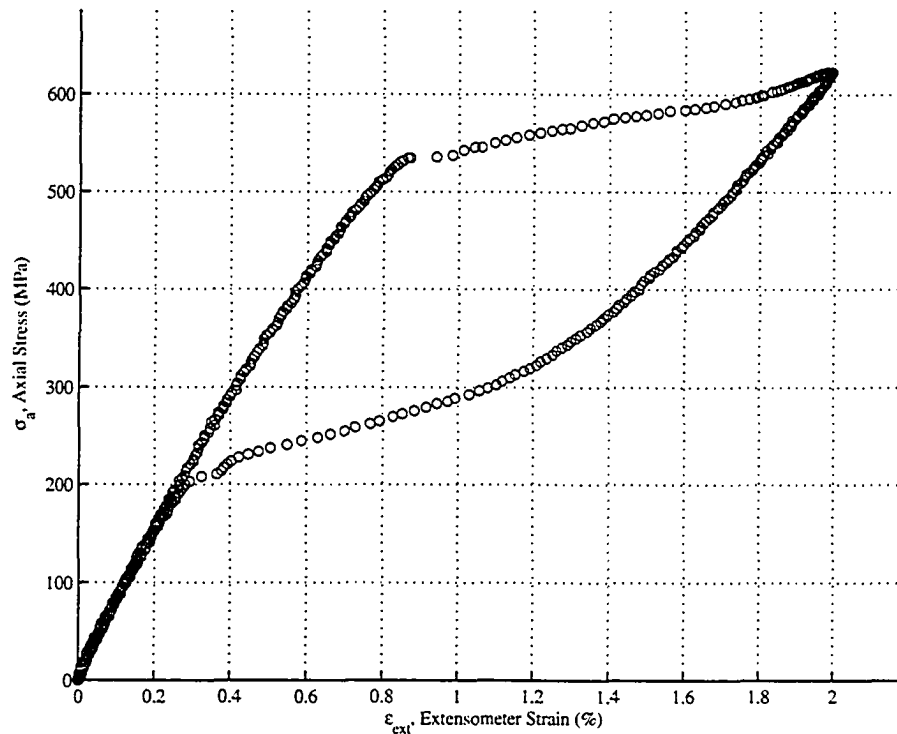


Figure 2.23: Trained axial load response. Shown here was the complete pseudoelastic load response for a axially trained SMA tested under load control. Compared with the strain controlled loading response in Figure 2.21, the stress controlled response has a small peak stress at the transformation yield point and a more linear transformation load response.

unloading of a SMA under torsional loading has been considered by Gillet and is a more complex model than the loading model [Gillet et al., 1998]. It was decided for this initial experimental and theoretical analysis of NiTi SMA combined axial and torsional load response research to limit the model to the loading process only.

With the combined load response tests it could be seen that for axial preloads higher than 360 MPa there was a significant change in the torsional load response as it deviates from linearity at a lower stress (transformation yield point) and there appears to be some residual deformation that occurred upon torsional unloading. It was not until the axial preload was removed that this apparent residual deformation disappeared. This residual deformation is not discussed in this research, but illustrates the coupling between the torsional and axial loading for pseudoelastic deformation. This coupling was also seen with one sample when it was tested at 420 MPa and

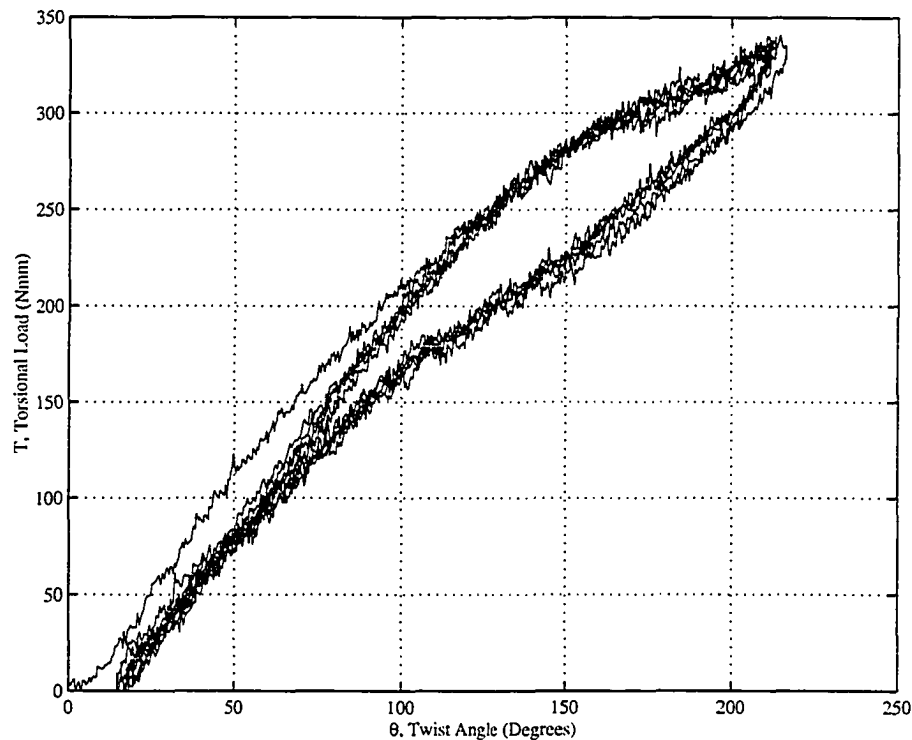


Figure 2.24: Torsional Training Load Cycles. The first cycle has a permanent deformation but the remaining cycles did not.

the specimen began to have an abnormal axial elongation during torsional loading as shown in Figure 2.33. In the subsequent chapters it was determined if the material properties that define the torsional load response model change as a function of the applied axial preload. This study is limited to applying axial preloads that are lower than that would initiate the martensite phase transformation. The additional axial elongation that occurred during the application of torsional loading for high axial preload is also considered.

Although not shown here, there were some tests performed where the specimen had an torsional preload and had an axial load that was applied to the specimen to induce the phase transformation. The torsional load was controlled by using a servo motor with gear reduction and a worm gear drive. The advantage of this setup was that there was ample torque that could be applied to the test specimen and that the worm gear drive could hold the specimen in place when the motor was stopped. The disadvantage to this setup was that there was only manual rotational control and no load control capabilities. Once the axial load initiated the martensite transformation,

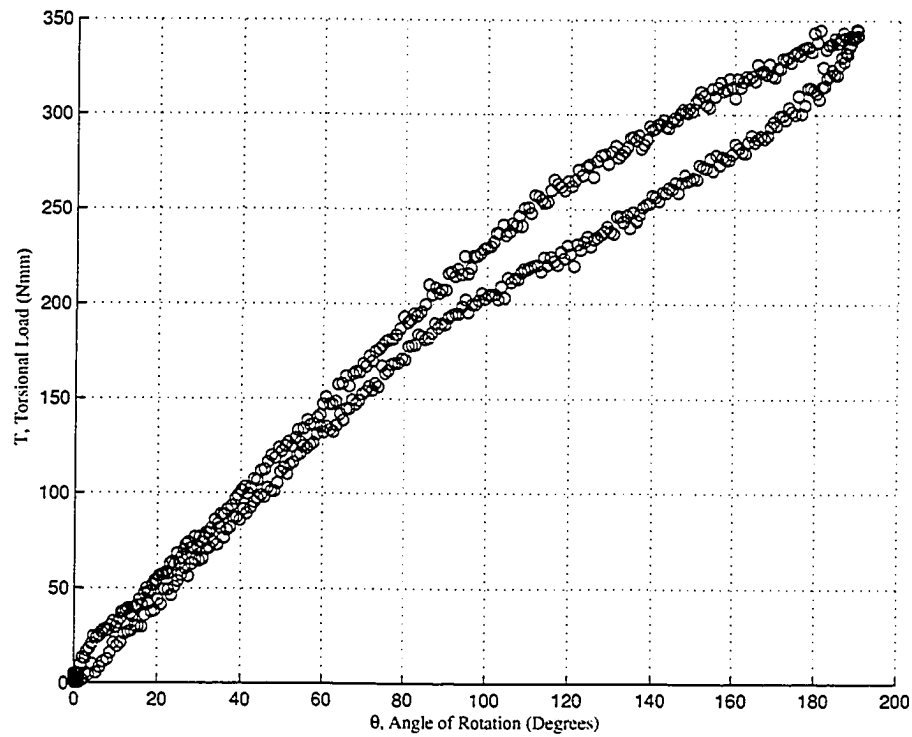


Figure 2.25: Trained Torsional Load Response. This is the full pseudoelastic torsional load response for a trained SMA wire.

the torque in the specimen would decrease at a rate that could not be compensated by manual control of the servo motor. The torsional adapter can apply rotational control torsional loading but can not apply load control loading which limits the load path to first applying the axial load then applying the torsional loading for load controlled testing.

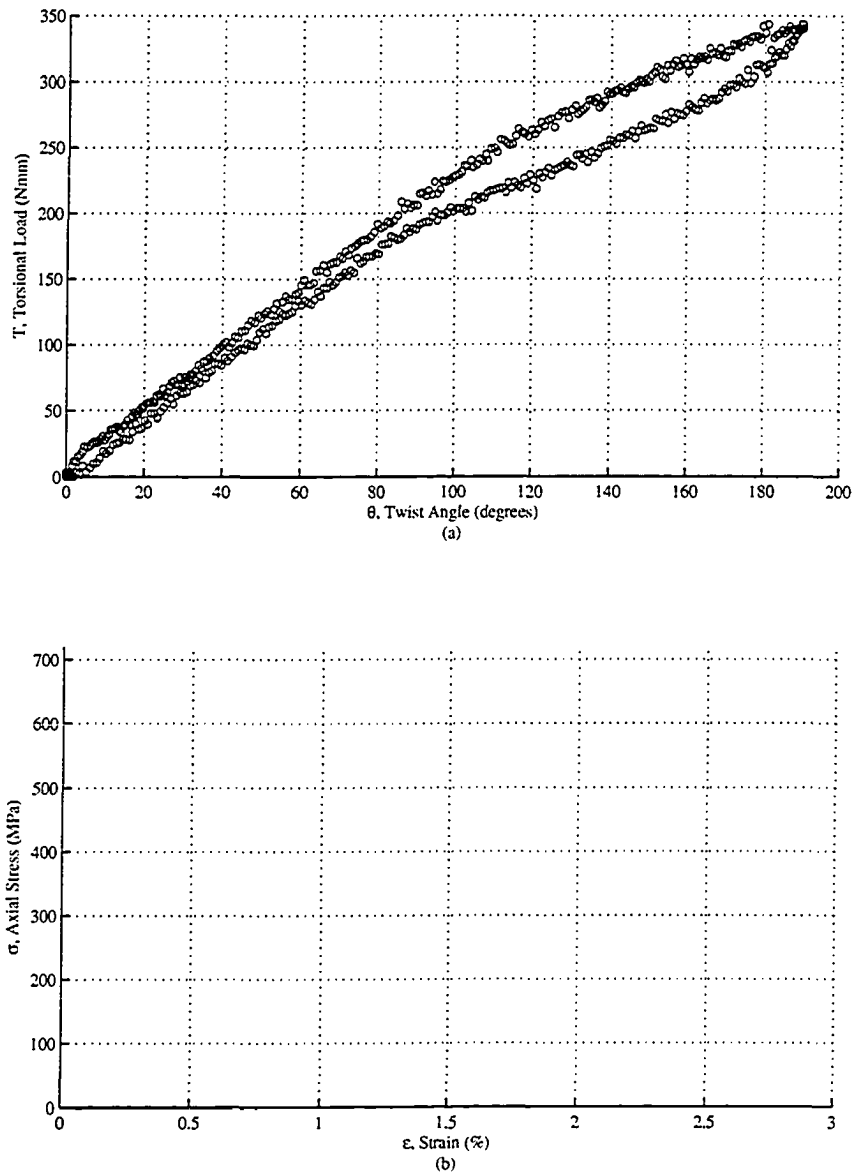


Figure 2.26: Pure Torsional Loading. With pure torsional loading the load response was identical to the trained torsional pseudoelastic load response.

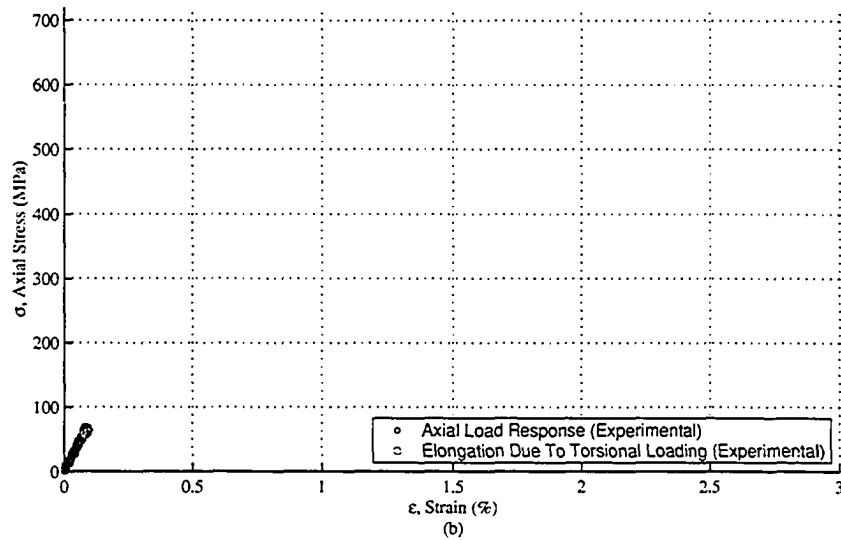
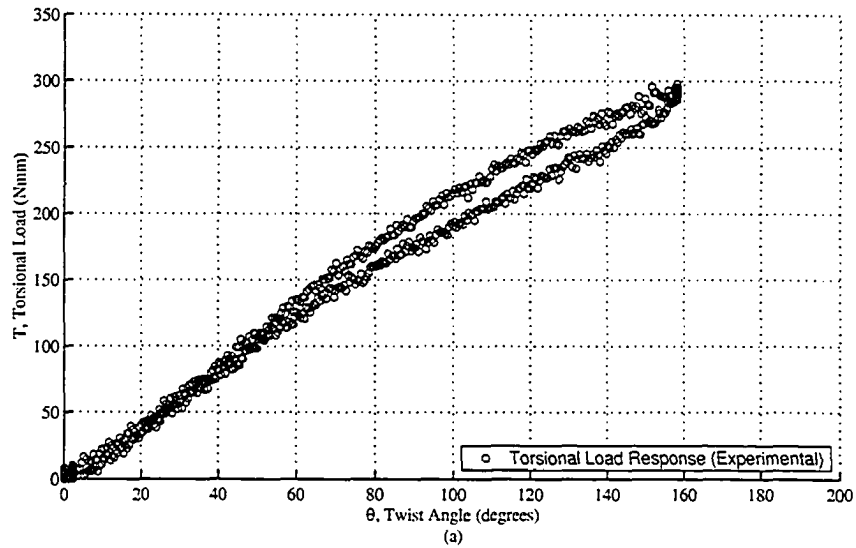


Figure 2.27: 60 MPa Axial Preload and Phase Transformation Initiation by Torsional Loading. The there is no significant change in the torsional load response from the pure torsional loading case as a result of the axial preload.

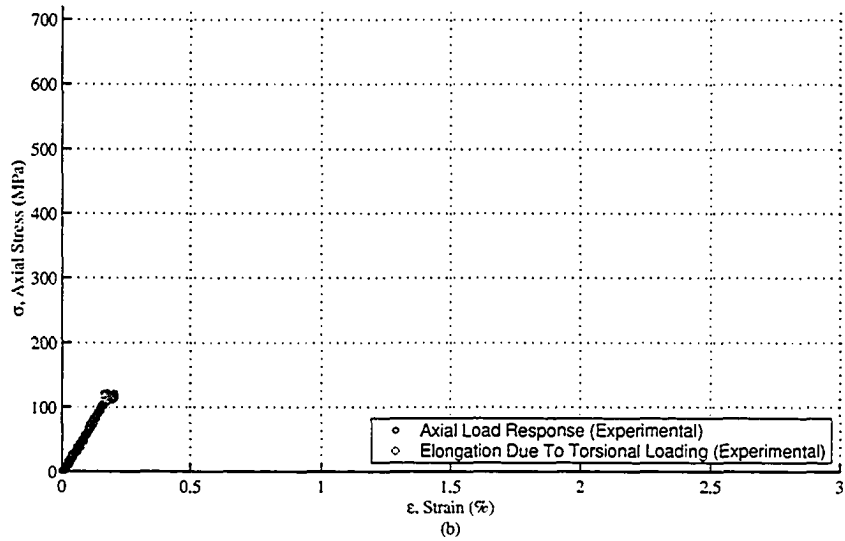
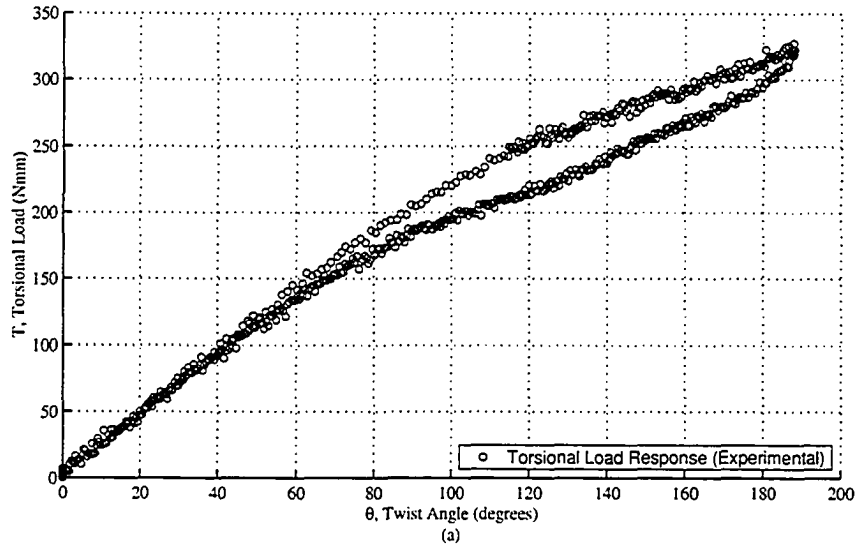


Figure 2.28: 120 MPa Axial Preload and Phase Transformation Initiation by Torsional Loading. There is no significant change in the torsional load response from the pure torsional loading case as a result of the axial preload. There appears to be a small increase in axial strain as a result of the torsional loading.

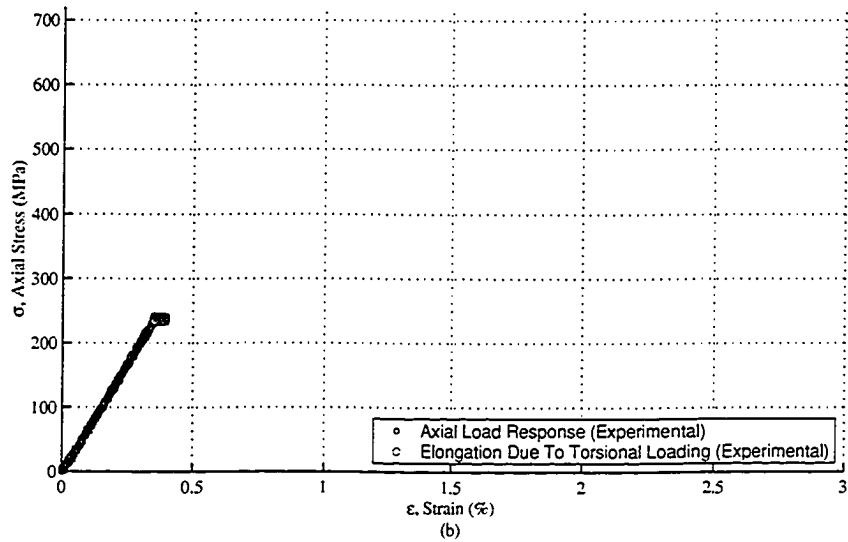
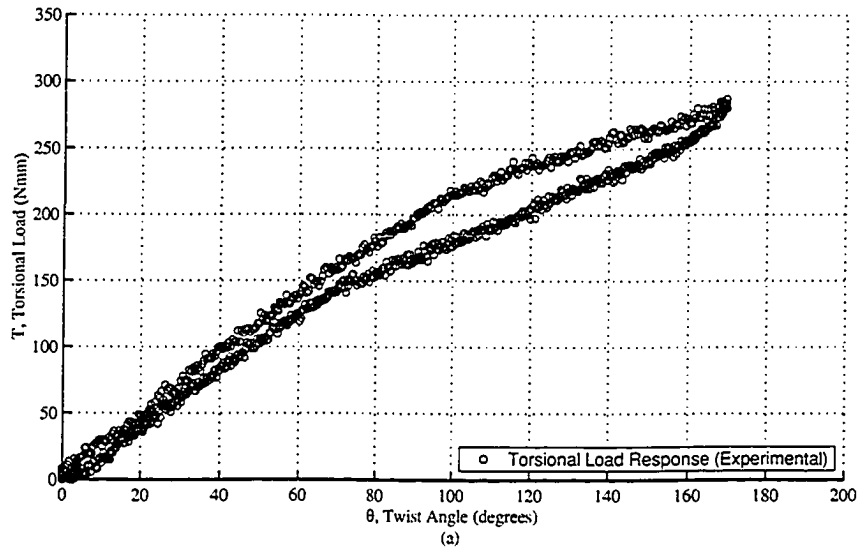


Figure 2.29: 240 MPa Axial Preload and Phase Transformation Initiation by Torsional Loading. There is no significant change in the torsional load response from the pure torsional loading case as a result of the axial preload. There appears to be a slightly higher increase in axial strain than with the 120 MPa axial preload as a result of the torsional loading.

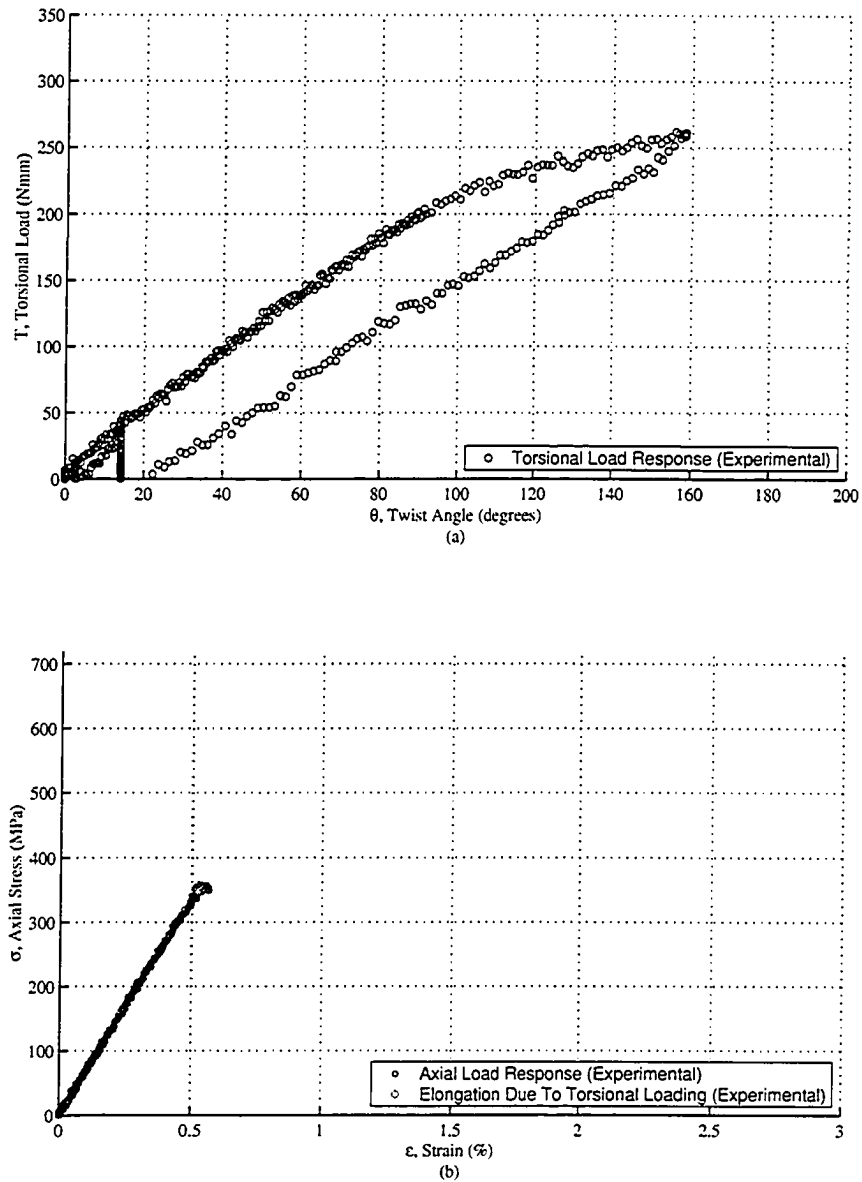


Figure 2.30: 360 MPa Axial Preload and Phase Transformation Initiation by Torsional Loading. The torsional load response was significantly different from the tests with lower axial preloads in which there appeared to have a lower load where the torsional load response deviates from linearity and the appearance of residual deformation upon unloading the torsional load while the axial load was still applied. Once the axial load was removed the residual torsional loading disappeared.

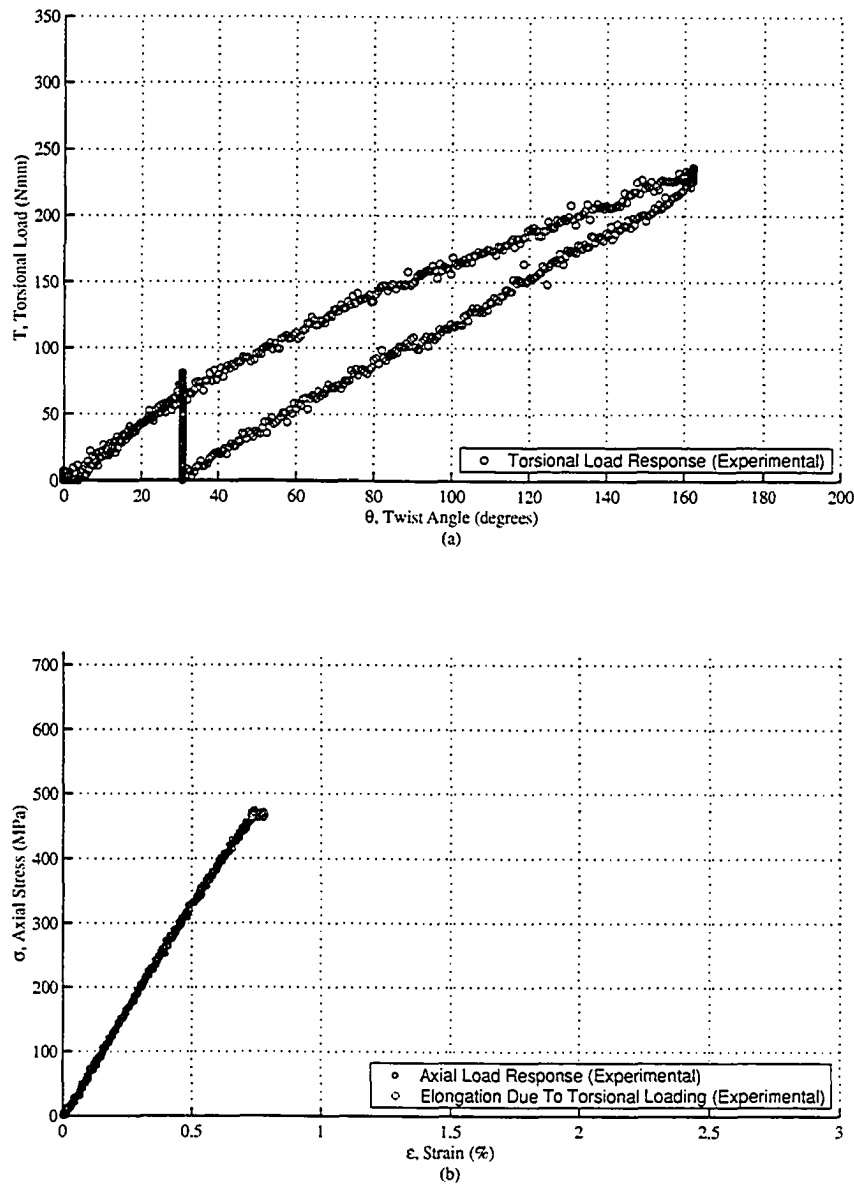


Figure 2.31: 480 MPa Axial Preload and Phase Transformation Initiation by Torsional Loading. The torsional load response was similar to the 360 MPa load case but load response seem to deviate from linearity around 75 MPa and the apparent residual angular rotation was 30°. The axial load response is similar to the previous cases with a notable but still relatively small (compared with the overall strain) increase in strain due to torsional loading.

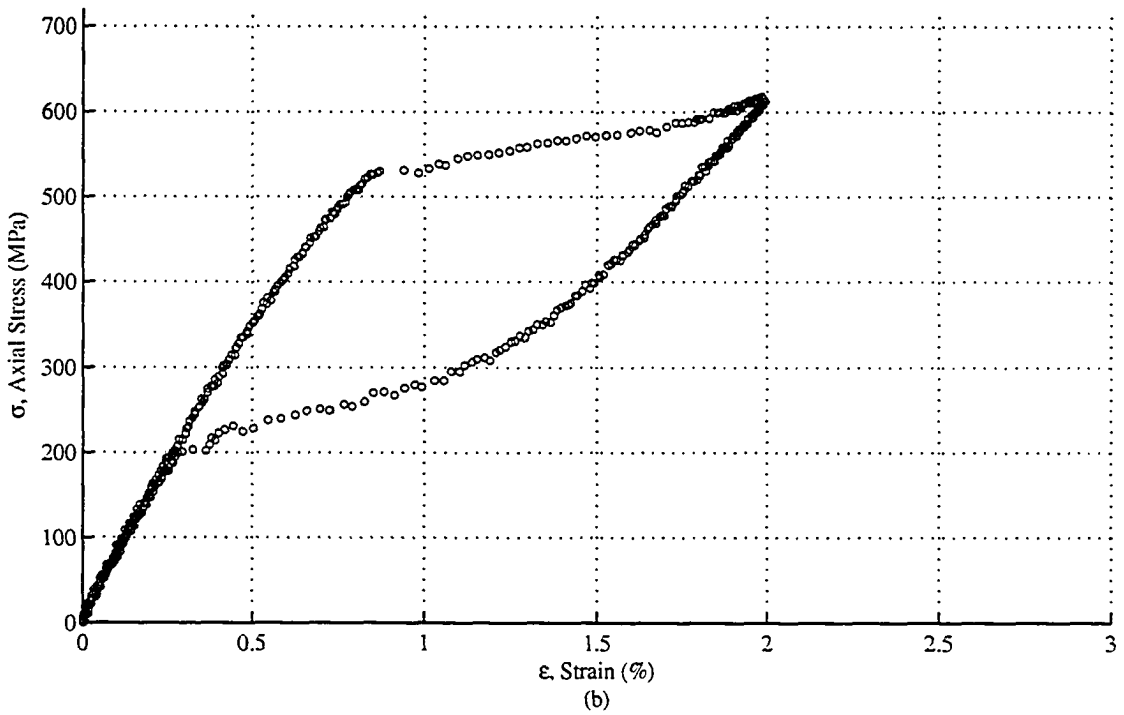
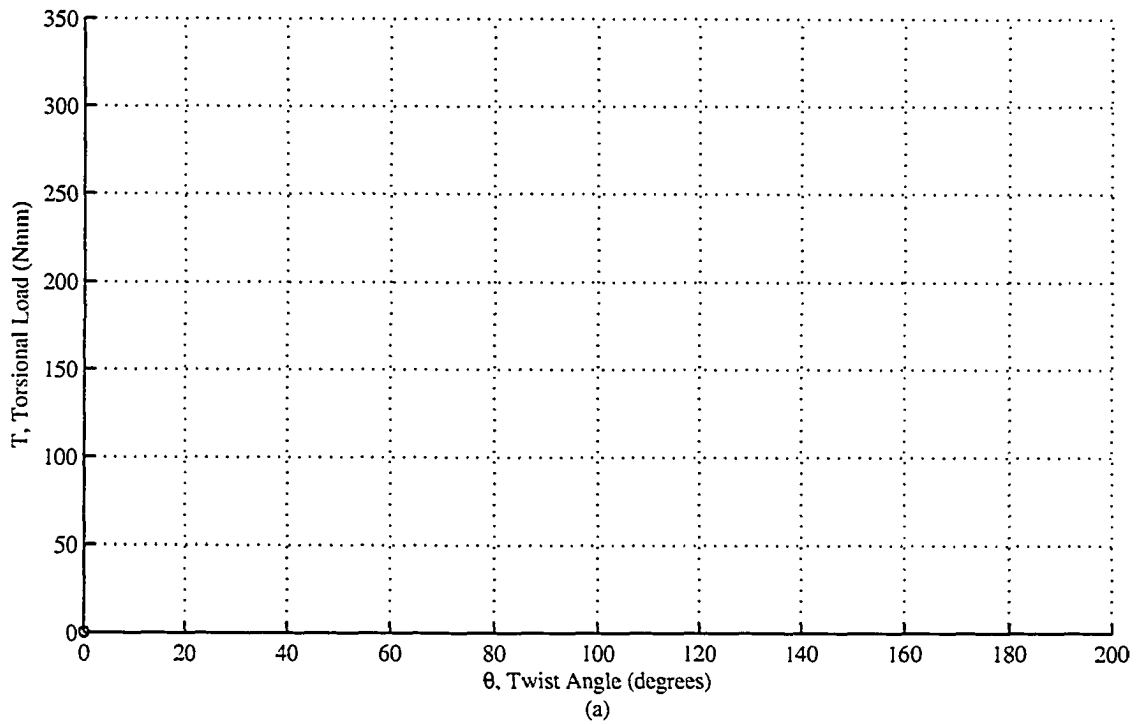


Figure 2.32: Pure Axial Loading. The pure axial loading case is the same as the trained axial load response.

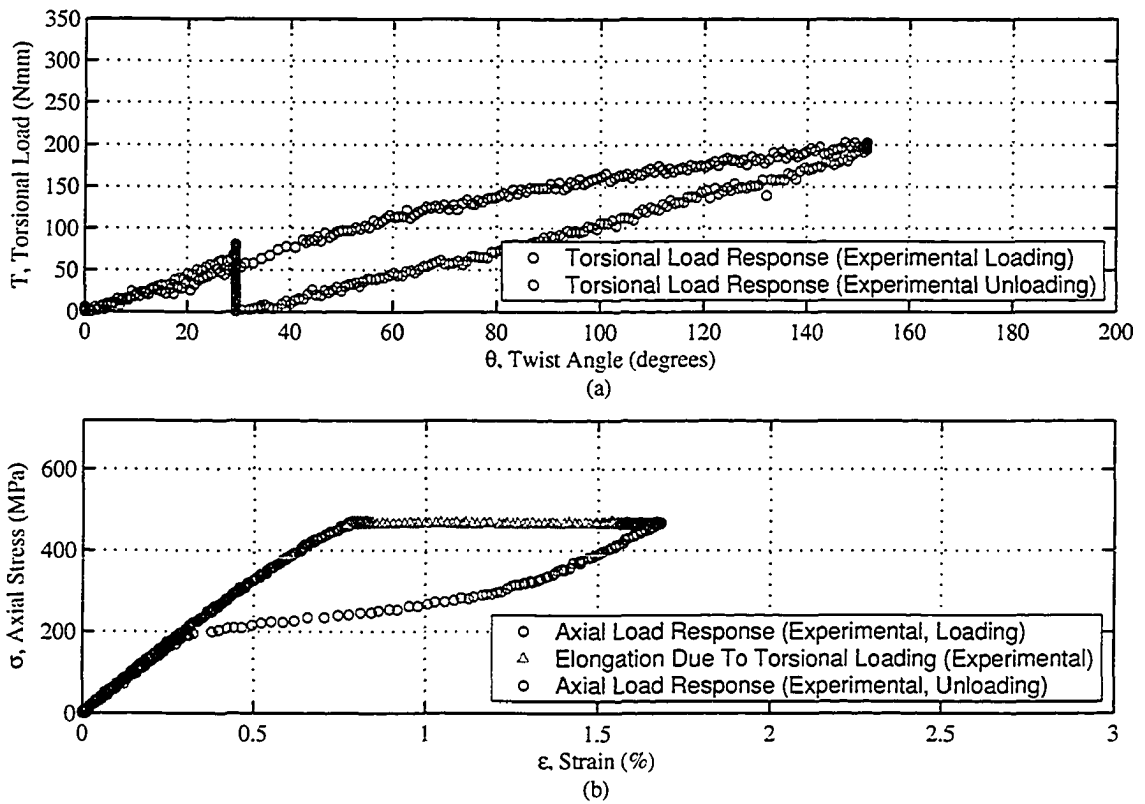


Figure 2.33: Axial elongation due to torsional loading. For the second sample that was tested it was found that the specimen had an abnormal elongation during torsional loading.

CHAPTER 3

AXIAL AND TORSIONAL LOAD RESPONSE MODELS

In this chapter the axial and torsional load response models are introduced along with a study on how the material properties are determined from the experimental load tests. The axial and torsional load response models are compared with the experimental tests that were presented in Section 2.5.

3.1 Axial Load Response Model

With pseudoelastic pure axial load response for a SMA wire as shown in Figure 3.1 there are three main key regions which make up this load response: Linear Region, Transformation Region and the Transformation Yield Point. The simplest model that can be used to capture these three components of the axial load response is the bilinear load response model. The bilinear load response model has been used by previous authors to model the SMA axial load response [Kafka, 1994] [Vokoun and Kafka, 1996] [Boyd and Lagoudas, 1996]. The bilinear axial load response model as illustrated in Figure 3.1 is defined as

$$\sigma = \begin{cases} E_E \epsilon, & 0 < \epsilon \leq \epsilon_{TY} \\ E_{TR} \epsilon + \sigma_{TY} \left(1 - \frac{E_{TR}}{E_E}\right), & \epsilon_{TY} < \epsilon \leq \epsilon_{MF} \end{cases} \quad (3.1)$$

where E_E is the elastic modulus and E_{TR} is the transformation modulus. At the transformation yield point there was a corresponding transformation yield stress, σ_{TY} , and transformation yield strain, ϵ_{TY} . In using the bilinear load response model the following assumptions are made:

- the elastic load response is linear (thus the elastic modulus, E_E , is a constant);
- the transformation load response is linear (thus the transformation modulus,

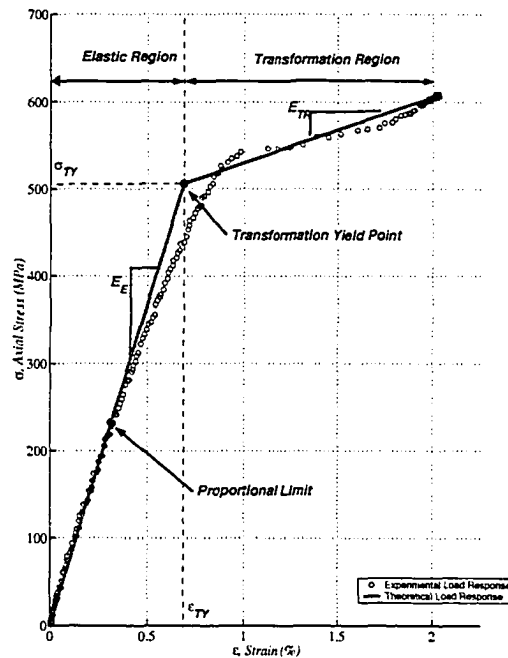


Figure 3.1: Axial Load Response. The experimental pure axial load response (shown as the circles) is modeled as a bilinear function. This material properties used to define the axial load response model are the elastic modulus, transformation modulus and the transformation yield point. The transformation yield point can be defined by either the transformation yield shear stress or transformation yield shear strain. The elastic region pertains to the load response as defined by the elastic modulus and prior to the transformation yield point. The transformation region pertains to the load response defined by the transformation modulus and after the transformation yield point. Also shown in this figure is the proportional limit where the experimental load response deviates from linearity.

E_{TR} , is a constant);

- the temperature of the specimen is constant; and;
- the martensite phase transformation is assumed to occur uniformly throughout the entire specimen length

From Figure 3.1 it can be seen the elastic load response is linear for only part of the linear elastic region and the load response in the transformation region is not linear, but for simplicity they are both assumed to be linear. As a consequence the experimental yield stress and strain will be higher than that of the modeled load response. Other assumptions that are made with the load response model is that

the temperature and phase transformation are uniform along the length of the wire specimen. These factors rely on the experimental testing and can only be considered as sources of error when comparing the theoretical model with the experimental data.

The transformation modulus, E_{TR} , as shown in Figure 3.1 as the load response after the transformation yield point, is a combination of the austenite modulus, martensite modulus and the modulus to transform the austenite phase to the martensite phase. The modulus of the load response in the transformation region is lower than that of the pure austenite and martensite phase [Brinson, 1995]. The austenite and martensite phase contribution to the transformation modulus is insignificant in comparison to the modulus of the transformation from the austenite phase to the martensite phase. Assuming that the transformation modulus is constant it is deduced that the austenite to martensite phase transformation is a linear function of the applied load. For a SMA crystal the transformation load response occurs with a extremely low modulus and could be considered perfectly plastic deformation. In this case the SMA wire is composed of a multitude of randomly orientated crystals and the stress required to initiated the MT in each crystal is based on the angle between the transformation direction and the applied load. Thus it is reasoned that the transformation modulus is a linear function of the applied load as the preferred crystals transforms first then as the load is increased the less optimally lined up crystals will transform.

3.2 Torsional Load Response Model

In deriving the torsional load response it was assumed that the shear material load response was a bilinear function which is the same type of function used to model the axial load response. The bilinear load response model for the axial and torsional load response is illustrated in Figure 3.2. How the bilinear shear response function corresponds to the torsional load response is shown in Figure 3.3. This torsional load response model has been derived by Gillet in terms of the elastic shear modulus, G_E , transformation shear modulus, G_{TR} , and a term $\psi = \tau/cG_L$ (More information on this derivation in Section A.1.3). In the derivation here it is desired to have the torsional load response model in terms of the elastic shear modulus, the transformation shear modulus and the transformation yield stress, τ_{TY} , which are the three material properties that define the pseudoelastic shear response.

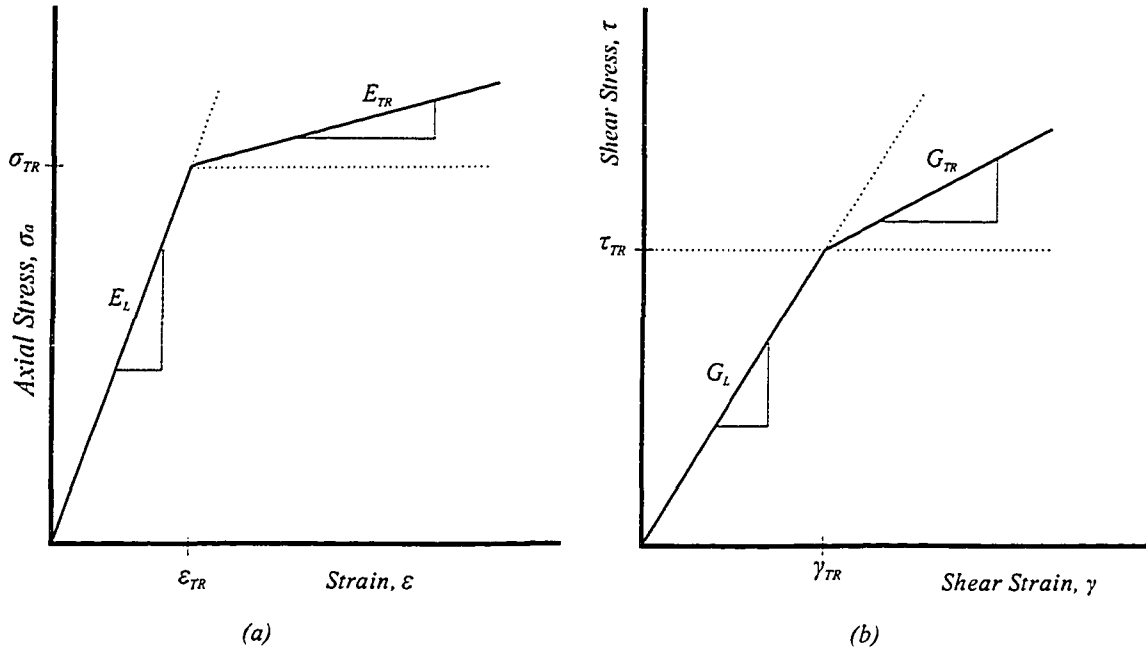


Figure 3.2: Bilinear Material Load Response: (a) Axial bilinear loading: The common simplified axial load response model consisting of three material properties, elastic modulus, E_E , transformation yield stress, σ_{TR} and the transformation modulus, E_{TR} . (b) Bilinear shear load response: this model used in this research had three shear material properties, elastic shear modulus, G_E , transformation yield shear stress, τ_{TY} and the transformation shear modulus, G_{TR} .

The bilinear shear stress response model as shown in Figure 3.2(b) is

$$\tau = \begin{cases} G_E \gamma, & \gamma < \gamma_{TY} \\ G_{TR} \gamma + \tau_{TY} \left(1 - \frac{G_{TR}}{G_E}\right), & \gamma \geq \gamma_{TY} \end{cases} \quad (3.2)$$

where G_E is the elastic shear modulus and G_{TR} is the transformation shear modulus. At the transformation yield point there is a corresponding transformation yield shear stress, τ_{TY} , and transformation yield shear strain, γ_{TY} . Similar to axial loading, the assumptions for the torsional load response model are

- the elastic load response is linear (Thus the elastic shear modulus, G_E , is constant);
- the transformation load response is linear (Thus the transformation shear modulus, G_{TR} , is constant);

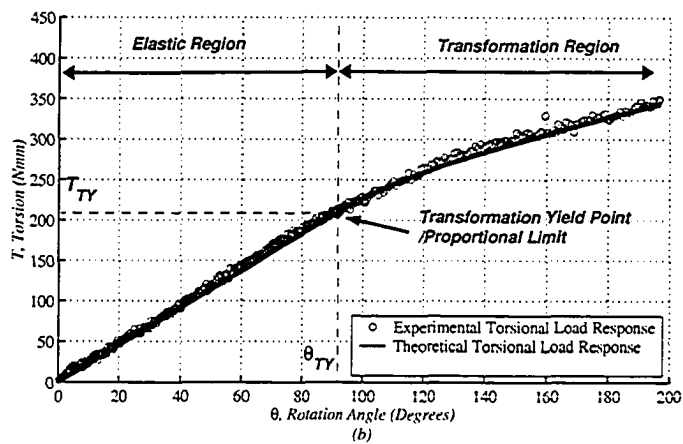
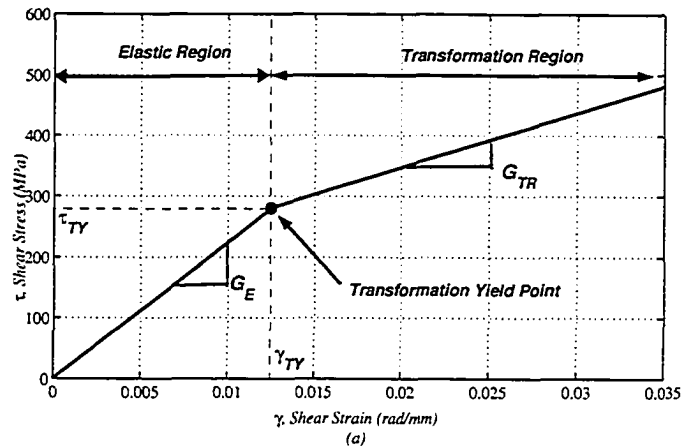


Figure 3.3: Shear Stress Load Response Assumption and Corresponding Torsional Load Response. (a) Shear stress load response was assumed to be a bilinear function that has a linear elastic modulus, G_E , transformation modulus, G_{TR} and a transformation yield point, which defines the boundary between the elastic and transformation region. At the transformation yield point there is a corresponding transformation yield shear strain and transformation yield shear stress. (b) The torsional load response for a wire specimen appears to have a linear elastic and a nonlinear transformation load response with the transformation yield point defining the boundary between the two regions. The transformation yield point for the torsional load response has a corresponding yield torque and yield angle of rotation.

- the temperature of the specimen is constant; and,
- the martensite phase transformation is assumed to occur uniformly throughout the entire specimen length

The general expression for the torque applied to a given cross section is

$$T = 2\pi \int_0^c \rho^2 \tau d\rho \quad (3.3)$$

where T is the torque, τ is the shear stress acting on an element located at a distance, ρ , from the center of the wire and c , is the wire diameter. The shear strain, γ , for a wire specimen is

$$\gamma = \frac{\rho\theta}{L} \quad (3.4)$$

where θ is the twist angle of the wire and L is the wire length and is expressed in terms of radians when used in the equation.

3.2.1 Linear Elastic Region ($\gamma < \gamma_{TY}$)

For the linear torsional load response the shear stress, τ is defined as

$$\tau = G_E \gamma \quad 0 < \gamma < \gamma_{TY} \quad (3.5)$$

where G_E is the elastic shear modulus. The relationship is only valid up to the point where the shear strain equals the transformation shear strain, γ_{TY} , where the transformation shear strain is defined from equation (3.4) to be

$$\gamma_{TY} = \frac{c\theta_{TY}}{L} \quad (3.6)$$

where θ_{TY} is the twist angle when the martensite phase transformation initiates. Since the martensite phase transformation occurs at the point with the highest stress, it will occur at the circumference of the wire where $\rho = c$. From equations (3.3), (3.5) and (3.6) the linear elastic torsion load response as a function of the twist angle is derived to be

$$T_L = \frac{\pi c^4 G_E \theta}{2L} \quad 0 < \theta < \theta_{TY}. \quad (3.7)$$

As seen by this equation, using the bilinear shear stress response assumption the linear torque response will be a linear function which is a characteristic of the load response that is seen in Figure 3.3. In the next section the torsional load response is considered after which the martensite phase transformation initiates in the wire is discussed.

3.2.2 Phase Transformation Region ($\gamma \geq \gamma_{TY}$)

Once the wire specimen has undergone the martensite phase transformation from pure torsional loading the shear stress response is modeled as in equation (3.2) using the case where $\gamma \geq \gamma_{TY}$. Rearranging equation (3.2) and using equation (3.6), the shear stress is defined as a function of the twist angle and distance from the center of the wire and is given as

$$\tau = \begin{cases} \frac{G_E \rho \theta}{L}, & \theta < \theta_{TY}, \quad 0 < \rho < \rho_{TY} \\ \frac{G_{TR} \theta}{L} \left(\rho - \frac{\tau_{TY} L}{G_E \theta} \right) + \tau_{TY}, & \theta < \theta_{TY}, \quad \rho_{TY} \leq \rho \leq c \end{cases} \quad (3.8)$$

The radial distance that located the boundary between the two regions was called the transformation yield radius which was defined from the linear elastic component of equation (3.8) to be

$$\rho_{TY} = \frac{\tau_{TY} L}{G_E \theta}. \quad (3.9)$$

The torsional load response defined for loading past the transformation yield point by equation (3.3) will have the linear elastic component ($0 < \rho < \rho_{TY}$) and the phase transformation component ($\rho_{TY} \leq \rho \leq c$) where the shear stress is defined by equation (3.8) and the torsional load response is given as

$$T = 2\pi \int_0^{\rho_{TY}} \frac{G_E \rho^3 \theta}{L} d\rho + 2\pi \int_{\rho_{TY}}^c \left(\frac{G_{TR} \rho^2 \theta}{L} \left(\rho - \frac{\tau_{TY} L}{G_E \theta} \right) + \tau_{TY} \right) d\rho. \quad (3.10)$$

The first term of this equation is the linear component of the torque and its solution is given by equation (3.7) with its domain defined from $0 \leq \rho \leq \rho_{TY}$. Solving the second component of the integral and simplifying the results the torsional load response becomes

$$T_{TR} = \frac{\pi c^4 G_{TR} \theta}{2L} + \frac{\pi G_{TR} \tau_{TY}^4 L^3}{6G_E^4 \theta^3} - \frac{2\pi c^3 G_{TR} \tau_{TY}}{3G_E} + \frac{2\pi c^3 \tau_{TY}}{3} - \frac{2\pi \tau_{TY}^4 L^3}{3G_E^3 \theta^3}. \quad (3.11)$$

The integrated torsional load response from equation (3.10) is

$$T = \begin{cases} \frac{\pi \rho_{TY}^4 G_E \theta}{2L}, & \tau < \tau_{TY} \\ \frac{2\pi \rho_{TY}^4 G_E \theta}{4L} + \frac{\pi c^4 G_{TR} \theta}{2L} + \frac{\pi G_{TR} \tau_{TY}^4 L^3}{6G_E^4 \theta^3} - \frac{2\pi c^3 G_{TR} \tau_{TY}}{3G_E} + \frac{2\pi c^3 \tau_{TY}}{3} - \frac{2\pi \tau_{TY}^4 L^3}{3G_E^3 \theta^3}, & \tau \geq \tau_{TY} \end{cases} \quad (3.12)$$

(for more details on the intermediate steps of this derivation see Appendix 1, Section A.3.1). The three unknowns from this equation are the linear elastic shear modulus,

G_E , transformation shear modulus, G_{TR} , and transformation shear stress, τ_{TY} .

With the axial load response model given as equation (3.1) and the torsional load response model given as equation (3.12), the axial and torsional load response can be predicted using only six material properties. As done here the material properties are typically determined from experimental tests. In the next section the procedures used to determine the material properties from the experimental tests are evaluated.

3.3 Methods used to Determine Axial Material Properties from the Axial Load Response

For the pure axial load response model as defined by equation (3.1) and shown in Figure 3.1 there are three material properties that are required by the model which are the linear elastic modulus, E_E , transformation modulus, E_{TR} , and the transformation yield point (Can be either determined from the transformation yield shear stress, τ_{TY} , or the transformation shear strain, γ_{TY}). The material properties can be determined from the pure torsional and axial load response using methods such as least squares to determine the modulus and the strain offset method to determine the transformation yield point. As the method used to determine the material properties from the load response will have an error associated with the method it was decided to develop a method to assess these errors. Since there is no axial load response available with known material properties the techniques used to determine these values was assessed by creating a test function which was a load response with known material properties. The test function as shown in Figure 3.4, which similar to the experimental load response, has an elastic modulus that decreases from 73 GPa to 22 GPa, a transformation yield stress of 545 MPa and a transformation modulus of 7.5 GPa. Comparing the test function with an experimental load response as shown in Figure 3.4, the test function uses a 3rd degree polynomial function defined as,

$$\sigma = -175810\epsilon^3 - 297\epsilon^2 + 76\epsilon + 0.0057, \quad (3.13)$$

that fitted the nonlinear elastic load response reasonably well. The test function captures the most important characteristics of the experimental load response which is the gradual decrease in modulus and the abrupt change in modulus at the transformation yield point. Both of these characteristics of the axial load response affects the value determined for the elastic modulus and the transformation yield point. The

transformation load response for the test function does not have good fit with the experimental data but the intent of the test function was to evaluate the methods used to determine the transformation yield point.

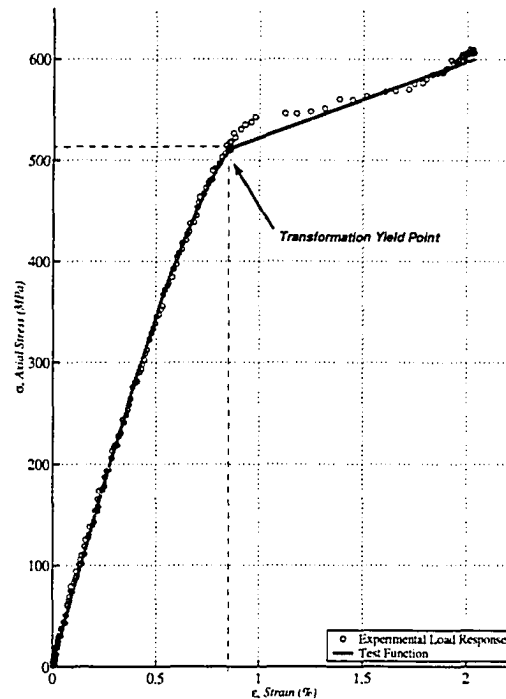


Figure 3.4: Axial Load Response Test Function: The experimental axial loading cycle was reproduced for evaluating the methods to determine the material properties. This function used a 3rd degree polynomial for the elastic loading with its elastic modulus decreased from 80 GPa to 22 GPa and the transformation modulus was constant at 7 GPa. The transformation yield stress of the spline model was 545 MPa. The unloading path was not modeled.

3.3.1 Axial Transformation Yield Stress (σ_{TY})

Comparing the experimental load response with the modeled load response as done in Figure 3.1 it is difficult to determine a transformation yield point that would be appropriate for the axial load response model. A method suggested by Haythornthwaite [Haythornthwaite, 1968] was to use the intersection of the linear elastic slope and the transformation slope as done with the axial load response model to determine the transformation yield stress (Also see Appendix A.3.2). It is required that the elastic and transformation modulus be known; this would then require that the pro-

portional limit and/or transformation yield stress of the experimental load response be determined in order to calculate the elastic and transformation modulus. The transformation yield point is determined by using the yield tangent modulus method. The yield tangent modulus method was used to determine the transformation yield point as the point when the slope of the load response (Modulus) equals a given fraction of the initial slope.

For determining the transformation yield point using the yield tangent modulus method, the tangent modulus is to be determined for the entire load response. The tangent modulus is calculated at each point in the load response using linear regression of 10 data points before and after the point in question as illustrated in Figure 3.5. More information regarding how the number of data points used in the tangent modulus method is in Appendix ???. As a consequence of using a total of 21 data points, the tangent modulus at transition between the elastic and transformation region is not as sharp as the actual tangent modulus. Since there is a dramatic change in the tangent modulus between the elastic region and the transformation region as shown in Figure 3.6, the error in the tangent modulus as a result of using 21 data points will have little impact on determining the transformation yield point.

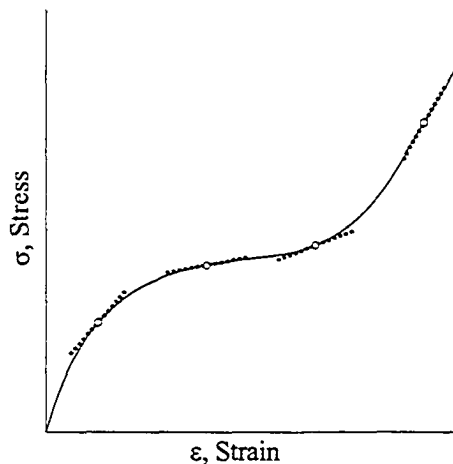


Figure 3.5: Tangent Modulus Method. As shown here is the tangent modulus method shown at four locations. For calculating the tangent modulus it is required that a number of data points be used before and after the point of interest as illustrated here as the dotted lined at each point.

As part of the yield tangent modulus method the transformation yield point would be defined as the point where the modulus is a given fraction lower than the initial

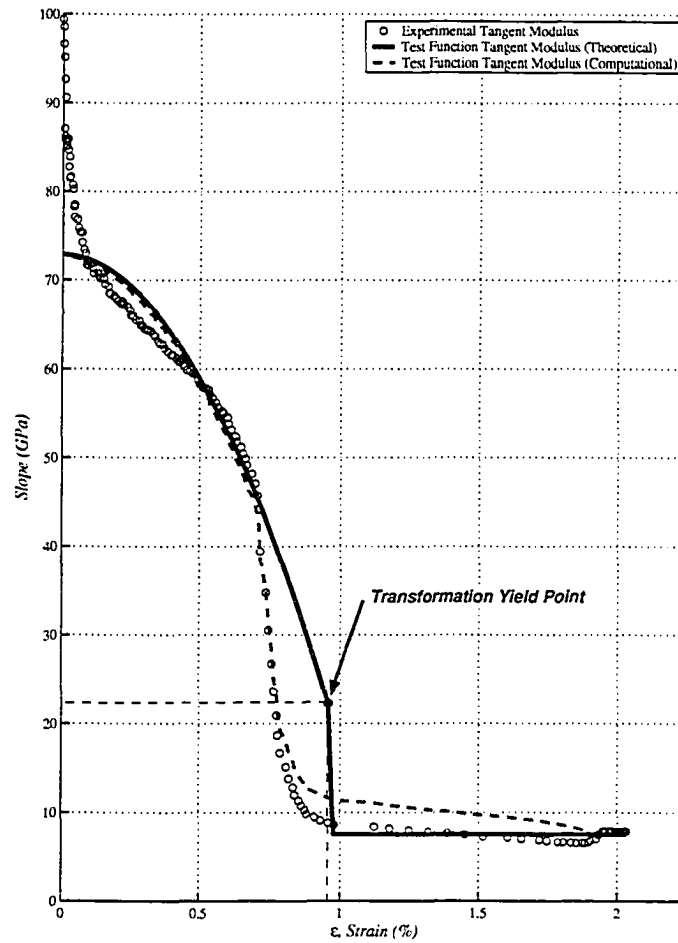


Figure 3.6: The Elastic modulus as a Function of the Axial Strain. In this figure is the local modulus determined as a function of the axial strain. There is the elastic modulus for the test function and the elastic modulus for the experimental and theoretical load response as determined using the tangent modulus method. It can be seen that the elastic modulus determined using the tangent modulus method was similar for both the experimental and theoretical load response.

modulus. This value, termed as the “Critical Yield Tangent Modulus”, does not have an explicit value; therefore, it is required to examine how accurate would a given critical yield tangent modulus be to determine the transformation yield point from the test function. Choosing a critical yield tangent modulus within the range between 40 GPa and 10 GPa it was determined that the transformation yield point differed from the test function by 28% (max). (See Appendix A.3.4 for details on how this is determined) Having a transformation yield tangent modulus between 11 and 20

GPa would reduce the difference to a maximum of 20%. Picking a value in between revealed that the best critical yield tangent modulus for the test function was 12.5 GPa or 17% of the initial tangential modulus of the elastic region. When specifying the transformation yield point determined by a particular method, it is customary by ASTM standards to state how it is determined. In this case, the transformation yield point of the test function as determined by the yield tangent modulus method would be 547 MPa (YTM 17%) [ASTM, 2004].

3.3.2 Measuring the Axial Elastic Modulus (E_E) and Transformation Modulus (E_{TR})

The axial elastic and transformation modulus are both assumed to be constant values as defined by the axial load response model. The American Society for Testing Materials recognize three methods to determine the modulus for structural materials. As illustrated in Figure 3.7, these methods are the Young's modulus, tangent modulus and the chord modulus [ASTM, 2003] [ASTM, 2004]. The Young's modulus method is defined by ASTM E111-97 as "the ratio of tensile (or compressive) stress to corresponding strain below the proportional limit of the material." As shown in Figure 3.7 it is recommended to use the data points to determine the Young's Modulus not from the origin but from a given preload value because of the experimental problems that are associated with applying the initial axial loading. Such problems noted by ASTM E111-97 are specimen curvature and initial grip alignment which may introduce significant errors in strain determined by the extensometer. These problems are noted in the axial load response for the steel wire specimen as discussed in Section 2.3.5. The tangent modulus as introduced in the previous section is defined from ASTM E111-97 as "the slope of the stress-strain curve at a specified value of stress or strain". It is recommended by ASTM that the tangent modulus method be used for materials that have a nonlinear elastic stress-strain load response. The chord modulus is defined by the ASTM as "the slope of the chord drawn between any two specified points on the stress strain curve below the elastic limit of the material". This method is also recommended by ASTM to be used to determine the modulus for a nonlinear elastic load response.

Young's Modulus method is preferred over the other methods to determine the elastic modulus because this method determines a single constant value which can be used in the axial load response model. Since the elastic modulus was determined

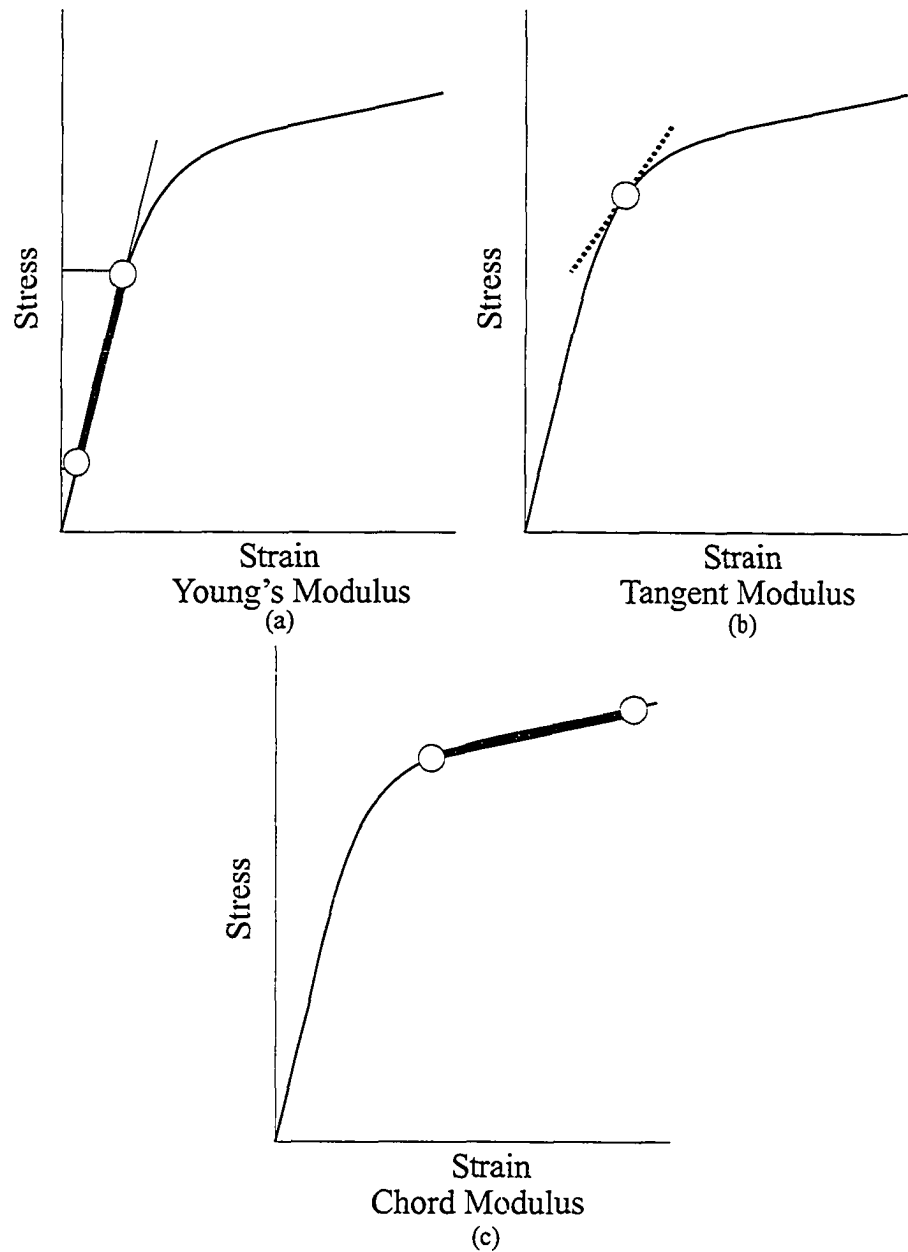


Figure 3.7: (a) Young's Modulus. The ratio of the tensile stress and strain above a given stress and below the proportional limit. (b) Tangent Modulus. The slope of the stress-strain response at a specified value of stress or strain (c) Chord Modulus. The slope of the chord drawn between any two specified points on the stress-strain load response. [ASTM E111-97]

using computational methods, it was chosen to use linear regression of the data points from a stress of 5 MPa to 50% of the estimated yield stress. The lower limit of 5 MPa

was chosen to avoid the problems associated with applying the initial axial loading as mentioned earlier. As shown in Figure 3.1, 50% of the estimated yield stress is approximately the proportional limit of the axial elastic load response. After this point the modulus decreases up to the transformation yield point thus the elastic modulus as determined by the Young's Modulus method will be higher than the actual value from proportional limit up to the transformation yield point.

The axial load response in the transformation region was approximately linear thus it is modeled with this assumption. It is preferred to use linear regression from the transformation yield point to the upper limit of the load response to determine the transformation modulus so that the difference between the experimental results and the theoretical model could be as closely matched as possible over using the chord method from the transformation yield point to the end of the loading component of the load response.

From the elastic modulus and transformation modulus determined from the experimental data, the transformation yield point for the load response model can be determined. As detailed in Section 3.1 the transformation yield point is defined as the intersection between the elastic load response and the transformation load response. The elastic load response is defined by the elastic modulus and has zero stress at zero strain. The transformation load response is defined with the transformation modulus and that this function passes through the modeled transformation yield point. The modeled transformation yield point was determined to be the intersection of these two load responses and is determined with the test function to be at 506 MPa and 0.68% strain. The resulting axial load response model that was determined from the test function is shown in Figure 3.8. As compared with the experimentally determined value of 545 MPa, the modeled transformation yield point occurs at a lower stress and strain than the actual experimental test.

3.4 Methods used to Determine Shear Material Properties from the Torsional Load Response

The torsional load response as shown in Figure 3.9a is modeled using equation (3.12) which only requires three material properties: the elastic shear modulus, G_E , transformation yield shear stress, τ_{TY} , and the transformation shear modulus, G_{TR} . In determining the elastic shear modulus from the experimental load response it can be seen that the slope of the elastic torsional load response is linear. The result is that

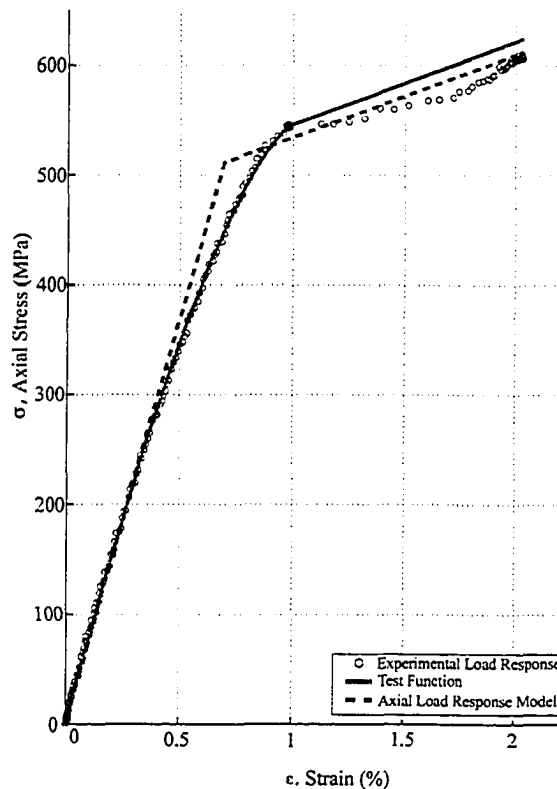


Figure 3.8: Comparing the experimental axial load response with the axial test function and the axial load response model.

the constant elastic shear modulus assumption is valid for the entire elastic region. The transformation yield stress is difficult to determine because only the circumference of the wire begins to transform from martensite to austenite while the bulk of the wire still behaves elastically. As shown in Figure 3.9 the elastic and transformation load response are apparent, but the transformation yield point is not. This characteristic in the torsional load response affects the way that the transformation yield point is determined and is addressed later in this chapter. The second complication with the nonlinear transformation load response is that the transformation shear modulus could not be determined explicitly from the load response. When the torsional load response model is first generated using Matlab and compared with experimental data it was found that the shear material properties could be determined by fitting the torsional load response to the experimental data. Using techniques from least squares regression it was found that the material properties could be determined in

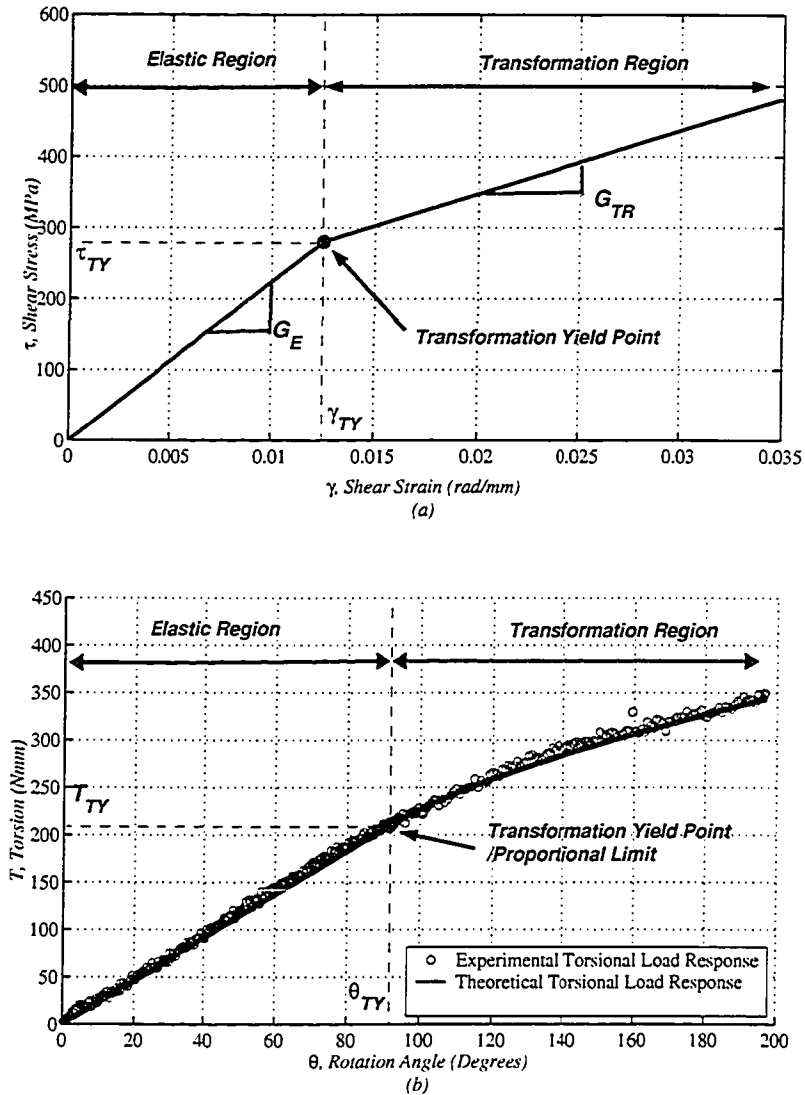


Figure 3.9: Torsional load response test function. Using the bilinear shear stress response assumption, a theoretical test curve was generated with known material properties which was used to evaluate the methods used to determine the material properties from experimental data. Noise of $\pm 8\text{MPa}$ was added to the theoretical curve to replicate the conditions of the experimental curve.

such a way that the torsional load response model would reproduce the experimental load response. This method was termed as the “Piecewise Smooth Least Squares Regression” method (PSLSR).

It is impossible to evaluate the accuracy of the PSLSR method using the test function because both the PSLSR and the test function are base on equation (3.12).

Instead, noise is introduced in the test function that is similar to that of the torsional load response to see how noise affects the PLSLR method. The theoretical torsional load response as shown in Figure 3.9b has a linear elastic shear modulus of 22.4 GPa ($2.285 \text{ Nmm}/\theta$), transformation yield shear stress of 280.2 MPa (257.6 Nmm) and a transformation shear modulus of 9.0 GPa. Noise of $\pm 8 \text{ MPa}$ ($\pm 6 \text{ Nmm}$) is added to the theoretical curve to simulate the noise from the torsional load cell. As shown in this figure, the test function is identical to the experimental load response throughout the entire range in consideration.

How the PLSLR method determines the material properties from the torsional load response is done by first determining the elastic modulus using linear regression. The yield tangent modulus method is used to determine the proportional limit so that the elastic shear modulus could be calculated. This method is the same one used in Section 3.3.1 for determining the axial transformation yield point. The tangent modulus of the linear region of the test function was determined to be on average 22.6 GPa with an uncertainty of $\pm 5.8 \text{ GPa}$. This uncertainty is mainly due to the noise in the torsional load response. Because of this high uncertainty it is preferred to find the critical yield tangent modulus with the search starting at the end of the data set and the transformation yield tangent modulus would be the point where the load response slope is higher than the critical yield tangent modulus as illustrated in Figure 3.10. Performing the yield tangent modulus method in the reverse direction, the expected difference between the actual transformation yield strain and the value determined from the yield tangent modulus method reduces to 7% using a critical tangent modulus between 19.5 and 22 GPa. (See A.3.5 for more details on how this is determined.) The reverse search method is not susceptible to the uncertainty of the elastic modulus as with the forward search as it did not use data points from that region. Also with using the reverse method the search begins with the highest stress and works towards the transformation yield point. Thus working with higher stress values the noise in the load cell will have a lesser impact on the accuracy of the method. Based on these results the best method to determine the transformation yield point for torsional loading is to use the yield tangent modulus method with the reverse search and a critical tangent modulus of 20 GPa. The 20 GPa critical tangent yield slope corresponds to 88% of the elastic shear modulus for the test function. The transformation yield torque determined using the yield tangent modulus method was 226 Nmm (296 MPa) in this case it was determined within a 5.6% difference from the

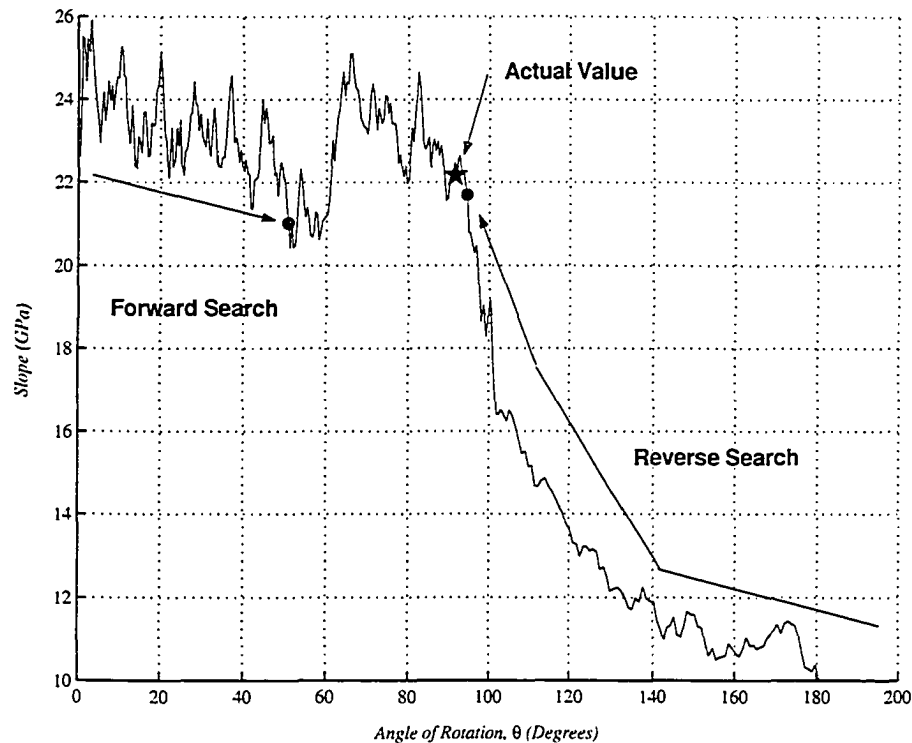


Figure 3.10: Modulus Method for Determining Transformation Yield Point. Unlike the axial load response the torsional load response had more noise and not as great a change in modulus from the linear elastic region and the transformation region. This greatly affected the yield tangent modulus method in forward and reverse searching.

values used to define the test function. With the transformation yield point estimated, the elastic shear modulus is determined using linear regression. Only the first half of the data in the linear elastic region is used to determine the elastic shear modulus in order to avoid including data points from the transformation region. The elastic shear modulus determined using least squares linear regression using the first half of the linear region, is determined to be 22.4 GPa (2.28 Nmm/deg) which corresponds to a 2.2% difference from the values used to define the test function.

With the elastic shear modulus determined, the PLSLR method is only required to find the transformation yield stress and transformation shear modulus. These two remaining material properties are determined using least squares regression to fit the torsional load response model to the experimental data.

In the least squares regression analysis the residual, e_i , between the experimental data and the proposed fitted curve as the value to determined at each data point, i ,

by

$$e_i = (T_i - T^*) \quad (3.14)$$

where T_i was the torque of the experimental load response and T^* was the torque of the theoretical load response as defined by equation (3.12). A measure of the quality of the curve fit that was used was the sum of the square of the residual,

$$S_r = \sum_{i=1}^n e_i^2 = \sum_{i=1}^n (T_i - T^*)^2. \quad (3.15)$$

The optimum curve fit corresponds with the material parameters that produce the smallest sum of squares of the residuals. Using MatLab to find optimal curve fit requires establishing a range of values of the transformation shear yield stress and transformation shear modulus in which the solution would fall and a method to search for the solution within this domain. It is reasoned that the range of values for the transformation yield shear stress would be $\tau_{TY_{est}} \pm 134MPa$ ($T_{TY_{est}} \pm 100Nmm$) where $\tau_{TY_{est}}$ is the estimated transformation yield shear stress which was determined earlier with the yield tangent modulus method ($T_{TY_{est}}$ is the estimated torque). Using this range of values the actual transformation yield point would have to be within 50% difference from the value determined using the yield tangent method. The range of values for the transformation modulus is bounded from $G_{TR} = 0$ to $G_{TR} = G_E$ which corresponds to the perfectly plastic and elastic cases, respectively, and is shown in Figure 3.9. It is chosen to search for the values that would produce the lowest residual and is done by splitting the ranges for the transformation yield stress and modulus into intervals as illustrated in Figure 3.11(a). The combination of transformation yield shear stress and transformation modulus with the lowest square of the residual would be the material properties for the torsional load response as determined from the PLSLR method. The solution could be further refined by setting the new search domain as one interval above and below from the solution of the previous interval.

The search process is optimized by noting that for a given transformation yield stress the sum of the square of the residual is a quadratic function of the transformation shear modulus. As illustrated in Figure 3.11(b), the minimum sum of the residual at each transformation yield shear stress interval could be calculated using three data points. Four data points were shown in this figure to illustrate that the function was indeed a quadratic relation. To further confirm that this is the case an additional run is illustrated in Section A.3.6 where 10 data points were used.

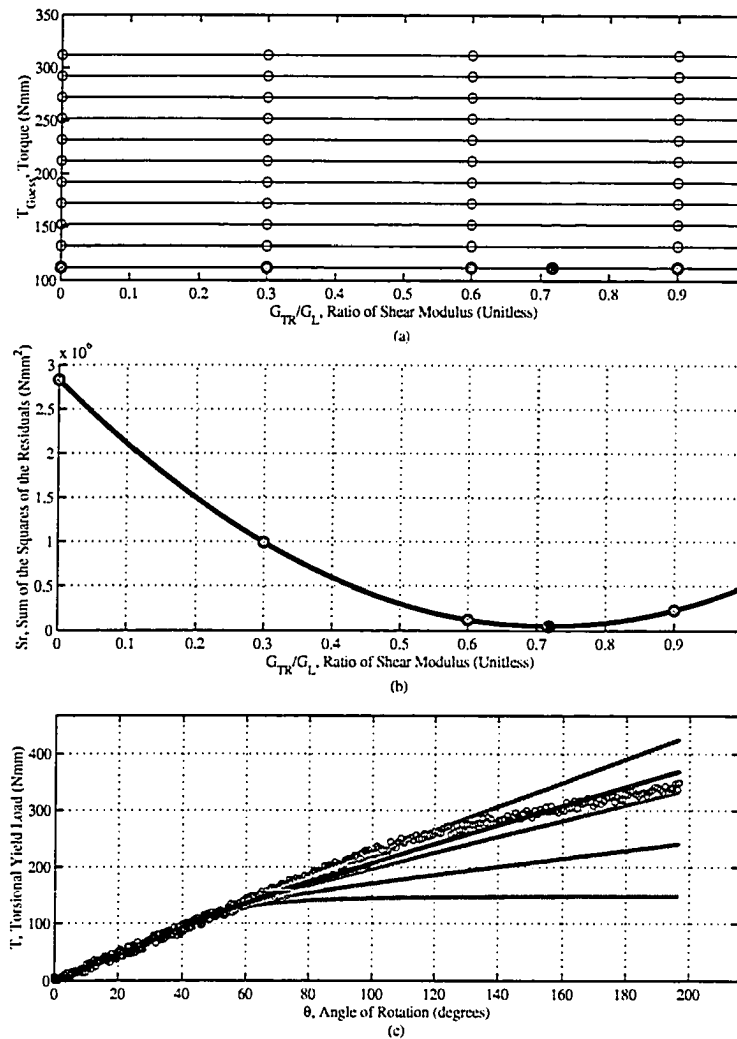


Figure 3.11: Piecewise Smooth Least Squares Regression Method. a) The range of values searched. Each circle represents the combination of parameters that were evaluated. The bottom row represents the parameters that were evaluated in this illustration. The horizontal lines through each set of points corresponded to the quadratic function as shown in (b) with the black dot representing the minima of this function. b) The sum of the squares of the residual as a function of the transformation to elastic shear modulus ratio. It was noted that this was a quadratic function and a minima could be calculated with only using three data points. c) Torsional load response functions that corresponded to the values that were shown in (a) and (b). For the the given torque, a torsional load response function was determined with the lowest square residual as shown by the black line.

It was found that the noise in the torsional load response does not greatly affect the PLSLR method (More detail on this is given in Appendix A.3.7). Since this method determined the best fit curve for all the data points, the effects of random error are minimized.

Determining the transformation yield stress of the test function using the PLSLR method from the test function predicted the transformation yield stress to be 279.8 MPa (209.4 Nmm) which had a maximum difference from the test function value of 2.5%. The transformation shear modulus determined with the transformation yield stress is 9.01 GPa which had a maximum difference from the test function value of 5.3%.

The effect of the error on the torsional load response is shown in Figure 3.12. As seen here the load response with a 5% error in determining the transformation yield point begins to have a predicted load response that is greater than the experimental load response with noise. It is concluded that noise in the torsional load response did not significantly affect the accuracy of the PLSLR method. The effect of error in the transformation shear modulus is shown in Figure 3.13. The load response does have a significant deviation from the test function with a 10% error in the transformation shear modulus.

In this chapter the pure axial and torsional load response is introduced along with the techniques used to determine the material properties from the experimental load response. In the next sections the combined axial and torsional load response is considered. It is determined if the torsional load response material properties are affected by axial loading.

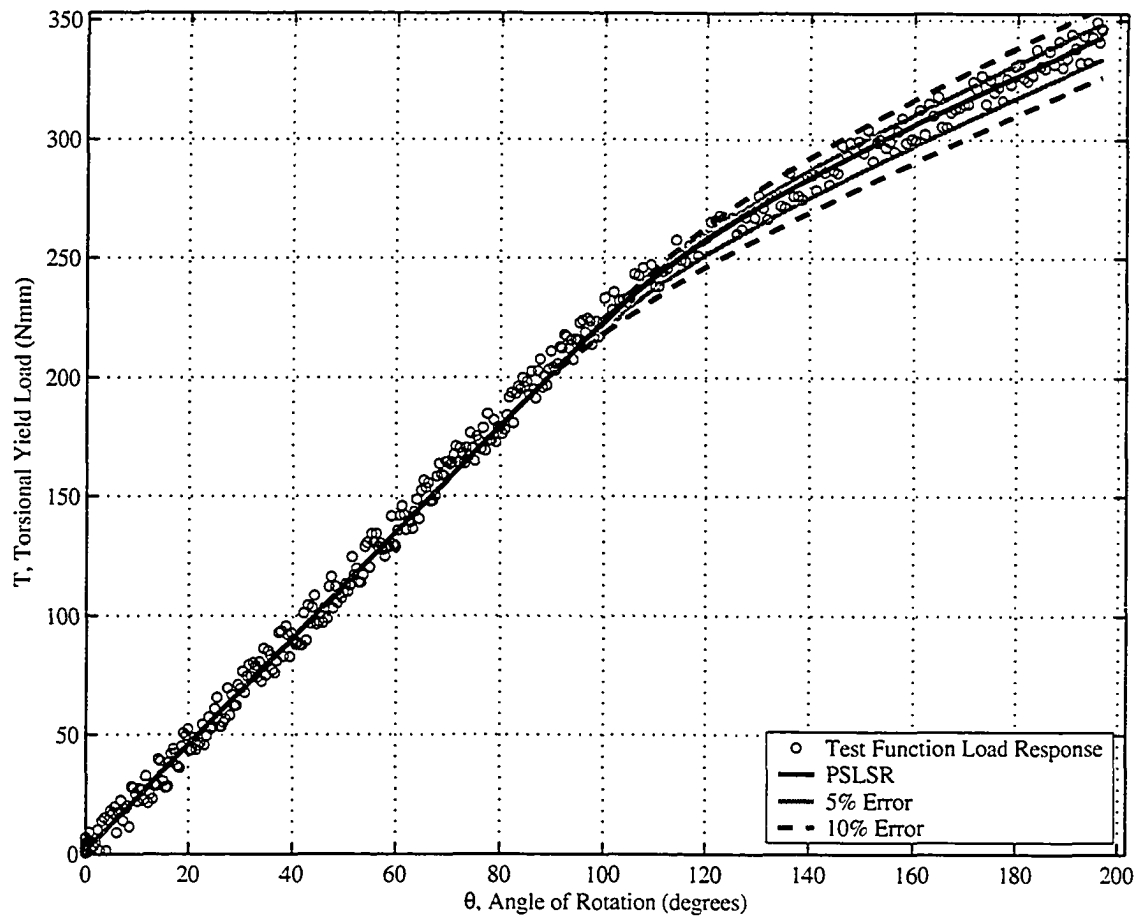


Figure 3.12: Error in the Transformation Yield Stress. Up to 5% error in the transformation yield point the predicted torsional load response varies as much as the noise in the experimental load response.

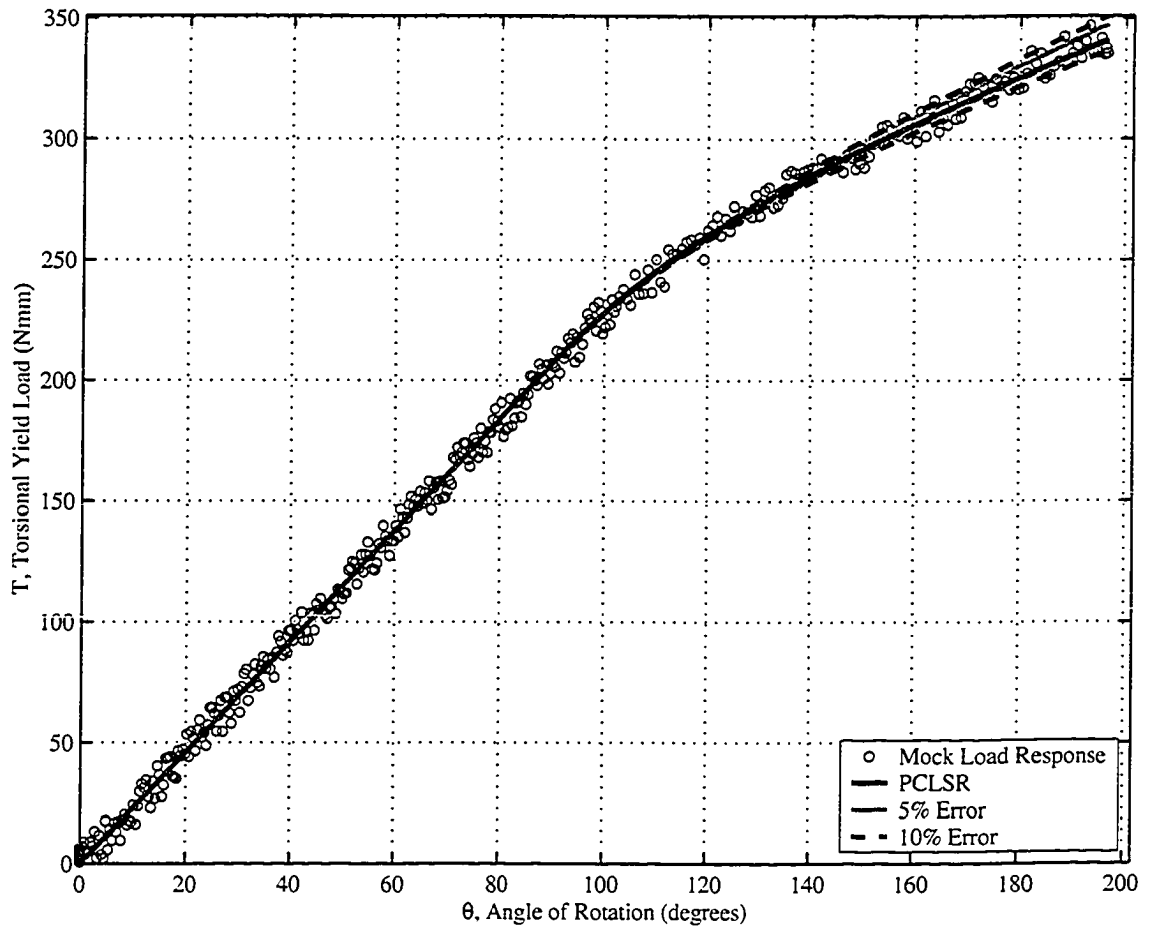


Figure 3.13: Error in the transformation yield tangent modulus. Up to 10% error in the transformation modulus was found not to significantly alter the theoretical load response.

CHAPTER 4

COMBINED AXIAL TORSIONAL LOADING

In this research the combined axial and torsional load response is an extension of the pure torsional and axial load response models discussed in Chapter 3. In combined loading it is assumed that the torsional and axial loading components are not coupled while the material behaves linear elastically. To determine the general stress state, the axial and torsional stress exerted on the wire can be simply superimposed. Based on this assumption the elastic modulus and the elastic shear modulus are assumed to be independent of the applied axial and torsional loading for linear elastic deformation. It is also assumed that the transformation yield stress and the transformation yield shear stress are indeed related and are coupled using a yield criterion as done for linear elastic materials. There are various different types of criterion that can be used but it was decided to only compare three yield criterions. These yield criterions are the von Mises Criterion, Drucker-Prager Criterion and the Generalized Elliptical Yield Criterion (GEYC). The last assumption was that the elastic and transformation shear modulus was independent of the axial preload. Using the Piecewise Smooth Least Squares Regression method the elastic and transformation shear modulus can be determined from the experimental torsional load response. Thus it can be seen if the elastic and transformation shear modulus is dependent on the applied axial loading. After each of these items are discussed and the assumptions are evaluated, the combined torsional and axial loading response model is compared with the experimental tests.

4.1 Transformation Yield Stress (σ_{TY}) and Transformation Yield Shear Stress (τ_{TY})

For linear elastic loading it is assumed that the axial and torsional load response is uncoupled. The axial and torsional load response are independent of one another, which means the material properties are independent. The second assumption with linear elastic loading is that the stresses on the wire are composed of the superposition of the torsional and axial stress. In other words, the stress required to initiate the martensite phase transformation has contributions from the applied torsional and axial loading. This relationship between the applied loads and when the material will yield is predicted by using a yielding criterion. In this section the use of yielding criterions to predict the torsional yield shear stress is detailed.

The axial and torsional stress at the yield point has been a topic that research for elastic-plastic type deformations and can be seen in various text books on material behavior [Boresi et al., 1993] [Zyczkowski, 1981] [Chen and Han, 1988]. The yielding of a material in a multiaxial stress state occurs when the effective stress reaches a limiting value which is defined by a yield function, $f(\sigma_e, Y)$ where σ_e is the effective stress and Y is the yield strength of a given test. Typically the yield function is presented in such a way that the function is negative for elastic loading and zero when the material yields in the multiaxial stress state. When the material yields in the multiaxial stress state the yield function is equal to zero. The effective stress is a function used to combine the multiaxial stress state into a single term that can be compared with the yield strength determined from a given test(s). Typically the material yield strength is determined from a uniaxial test or a compression test because these types of tests are easy to perform and yield strength can be directly determined from the load response. In this research the yield strength can also be determined from the pure torsional load response using the PSLSR method for determining the combined loading yield point. The yield criterions that were evaluated were the von Mises Criterion, Drucker-Prager and a Generalized Elliptical Yield Criteria (GEYC). These criteria are introduced in terms used in elasticity and plasticity where the name “yield stress” is used in context with linear elastic plastic deformation as the “transformation yield stress” as used in pseudoelastic deformation. The reasons why these criterions were selected to be evaluated were because the von Mises criterion is a generally accepted criterion for elasticity and plasticity analysis, the Drucker-Prager criterion was used in previous SMA research by Gillet [Gillet et al., 1998] and the

GEYC was used by Sittner for the study of the combined loading of a CuZnAlMn SMA tube specimen [Sittner et al., 1994c].

The von Mises Criterion is also known as the distortional energy density criterion and is based on the assumption that the amount of distortional strain energy required to initiate yielding would be the same for a uniaxial test as with a multistress state [Boresi et al., 1993]. The distortional energy for an isotropic elastic material is determined from the strain energy density, U_D , to be

$$U_D = \frac{(\sigma_1 - \sigma_2)^2 + (\sigma_2 - \sigma_3)^2 + (\sigma_3 - \sigma_1)^2}{12G_E} = \frac{1}{2G_E} J_2 \quad (4.1)$$

where σ_1 , σ_2 and σ_3 are the principle stresses of the multiaxial stress state, G_E is the elastic shear modulus and J_2 is the second deviator stress invariant (see appendix A.1.1 for more details) given as

$$J_2 = \frac{1}{6} [(\sigma_1 - \sigma_2)^2 + (\sigma_2 - \sigma_3)^2 + (\sigma_3 - \sigma_1)^2]. \quad (4.2)$$

The distortional strain energy density at yielding for a uniaxial test where $\sigma_1 = \sigma$, $\sigma_2 = 0$ and $\sigma_3 = 0$ is

$$U_{DY} = \frac{Y^2}{6G}. \quad (4.3)$$

The yield function for the von Mises criterion is defined as the general multiaxial stress state distortion energy (given by equation (4.1)) minus the pure axial loading distortional energy for yielding (given by equation (4.3)) which is

$$f(\sigma_e, Y) = U_D - U_{DY} = \frac{1}{6} [(\sigma_1 - \sigma_2)^2 + (\sigma_2 - \sigma_3)^2 + (\sigma_3 - \sigma_1)^2] - \frac{1}{3} Y^2 = 0, \quad (4.4)$$

which could be alternatively written as

$$f(\sigma_e, Y) = 3J_2 - Y^2 = \sigma_e^2 - Y^2 = 0; \quad (4.5)$$

where

$$\sigma_e = \sqrt{\frac{1}{3} [(\sigma_1 - \sigma_2)^2 + (\sigma_2 - \sigma_3)^2 + (\sigma_3 - \sigma_1)^2]} = \sqrt{3J_2}. \quad (4.6)$$

Since the material yield strength could be determined either from the pure axial load test or the pure torsional load test, the von Mises Criterion is evaluated with both of these cases. For materials that follow the von Mises criterion the axial yield

stress could be related to the torsional yield stress from equation (4.4) to be

$$\sigma_0 = \sqrt{3}\tau_0 \quad (4.7)$$

[Boresi et al., 1993]. The advantage that the von Mises Criterion has over the other methods is that only one material test is required.

For the combined axial and torsional loading of the SMA wire the stresses across the cross section of the bar can be defined in terms of the axial stress, σ_x and the torsional stress, τ_{xy} . With this biaxial stress state, the von Mises relation simplifies to

$$\sigma_x^2 + 3\tau_{xy}^2 = \sigma_0^2 \quad (4.8)$$

with yield strength determined from the axial load test or

$$\sigma_x^2 + 3\tau_{xy}^2 = 3\tau_0^2 \quad (4.9)$$

if the yield strength was determined from the torsional test. Equation (4.8) and (4.9) are used to determine when the combination of the axial and torsional stress required to initiate the phase transformation.

The Drucker Prager criterion is a variation from the von Mises Criterion where the influence of a hydrostatic stress component is included in the yield function and is given as

$$f(\sigma_e, Y) = \alpha I_1 + \sqrt{J_2} - K = 0. \quad (4.10)$$

This yield function requires two experimental tests to determine α and K parameters. The two tests that are usually performed to determine these parameters are the axial test and a compressive test, but since experimental tests performed here did not involve compressive loading the torsion test is substituted for the compressive test. In the case for pure torsional loading $\sigma_x = 0$ and $\tau_{xy} = \tau_0$. K is determined to be

$$K = \tau_0 \quad (4.11)$$

For a pure axial loading condition where $\sigma_x = \sigma_0$ and $\tau_{xy} = 0$, α is determined to be

$$\alpha = \left(\tau_0 - \sqrt{\frac{\sigma_0^2}{3}} \right) \frac{1}{\sigma_0} \quad (4.12)$$

Including these terms in the yield function given by equation (4.10)

$$f = \left(\tau_0 - \sqrt{\frac{\sigma_0^2}{3}} \right) \frac{\sigma}{\sigma_0} + \sqrt{\frac{\sigma^2}{3} + \tau^2} - \tau_0 = 0 \quad (4.13)$$

where the effective stress and yield strength are implicitly defined in this equation.

The generalized elliptical yield criteria (GEYC) is used in most practically oriented engineering manuals and in general plasticity for the case of combined loading of bars [Zyczkowski, 1981] [Hohenemser, 1932] [Zhukov, 1966] [Ohashi and Tokuda, 1973]. The GEYC is used by Sittner in the research of combined loading of a CuZnAlMn SMA thin tube specimen [Sittner et al., 1994c], [Sittner et al., 1994b], [Sittner et al., 1994a], [Sittner et al., 1997]. The generalized elliptical yield criteria is given by the elliptical function

$$\left(\frac{\sigma}{\sigma_0} \right)^2 + \left(\frac{\tau}{\tau_0} \right)^2 = 1. \quad (4.14)$$

or alternatively

$$\sigma^2 + c\tau^2 = \sigma_0^2 \quad (4.15)$$

where $c = \frac{\sigma_0^2}{\tau_0^2}$. For the CuZnAlMn tube specimens that Sittner tested, it was experimentally determined that $c = 1.51$. Comparatively, the von Mises elliptical yield function given by equation (4.7) corresponded to the case where $c = 3$.

The yield surfaces of the von Mises, Drucker-Prager, von Mises and the GEYC are illustrated in Figure 4.1. The GEYC criterion matches the von Mises Criterion for the torsional test at zero axial preload and matches the von Mises Criterion using the axial test at the higher axial preloads. The von Mises criterion using the axial test predicts the highest yield surface while using the same criterion with the torsional test predicts the lowest yield surface of the four criteria evaluated. Yield surface for the GEYC and the Drucker-Prager criterion match for the pure torsional and axial case while for the rest of the combined load response the Drucker-Prager criterion is slightly higher.

Using the PLSR method to determine the transformation yield shear stress from the torsional load response in combined loading the values can be used to compare with the yield criteria when plotted against the axial preload. This comparison is shown for all three samples tested in Figures 4.2 to 4.4. It was required to plot these yield surfaces on different plots because the transformation yield stress and transformation yield shear stress which are used to define the theoretical yield stress

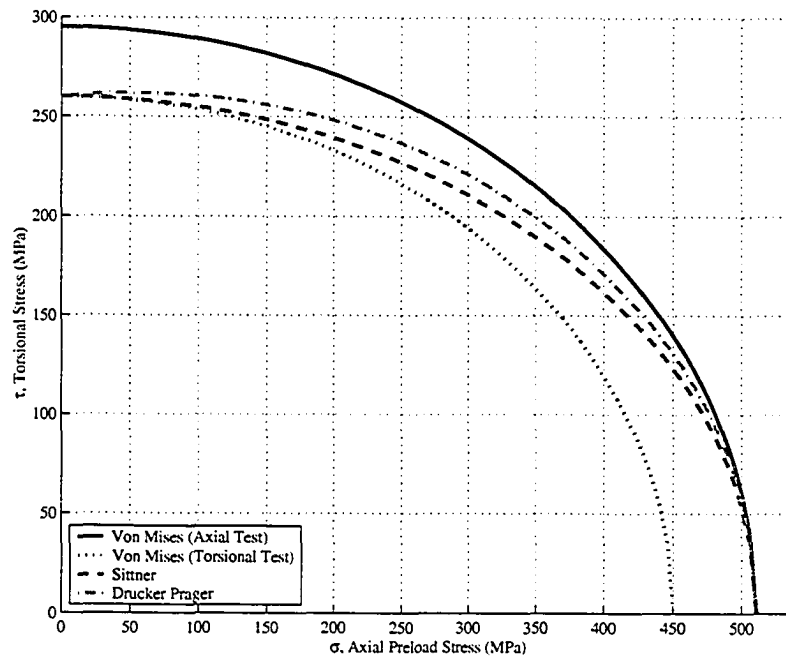


Figure 4.1: Prediction of the Transformation Yield Surface. Four transformation yield surfaces were compared, the Generalized Elliptical Yield criterion, von Mises criterion using the axial test and the von Mises criterion using the torsional test and the Drucker-Prager criterion.

are slightly different for each sample. In each figure the experimental values does have a noticeable variance of about $\pm 25 \text{MPa}$, but it also follows the same trend as the yield criterions. There are many other factors that affect the transformation yield stress such as temperature, composition, cold working, heat treatment and previous load history which all contribute to the variance that is seen in the figures and between samples.

As shown in the Figures 4.2 to 4.4 the von Mises transformation yield criterion based on the axial test generally predicted a higher transformation yield stress than determined by PLSLR. Using the torsional test with the von Mises Criterion under predicted the transformation yield stress. The GEYC and the Drucker Prager criterion are the most consistent criterions when compared with experimental values. The Drucker Prager criterion does extend slightly more outward than the GEYC giving slightly higher transformation yield stresses which is more consistent with the experimentally determined values. Based on this the Drucker Prager is overall the best criterion of the ones evaluated here to predict the transformation yield surface for the case where an axial preload is first applied and followed with torsional loading to induce the phase transformation.

4.2 Elastic Shear Modulus (G_E) and Transformation Shear Modulus (G_{TR})

Typically the elastic shear modulus and the transformation shear modulus are assumed to be independent to the applied axial load and in this section this assumption is confirmed. Using the PLSLR method, the elastic shear modulus and transformation shear modulus are determined from the experimental combined loading tests. They are plotted as a function of the applied axial load in Figures 4.5 to 4.7. The elastic shear modulus is constant up to 350 MPa but at 480 MPa the elastic shear modulus decreases by about 5 GPa. It is assumed that at the higher axial preload the phase transformation initiates at the specimen grips and the applied torsional loading is twisting this area more at the grips than the rest of the wire. This would be analogous to twisting a metal rod that was red hot and easily deformable at the ends and seeing that the weaker section would twist more than in the middle where the material was colder and stronger. It can be reasoned that the determined elastic shear modulus would be a value that was closer to that of the transformation shear modulus which is noted in Figure 4.5. Assuming that this is the case, the elastic and transformation shear modulus can be assumed to be independent of the applied axial

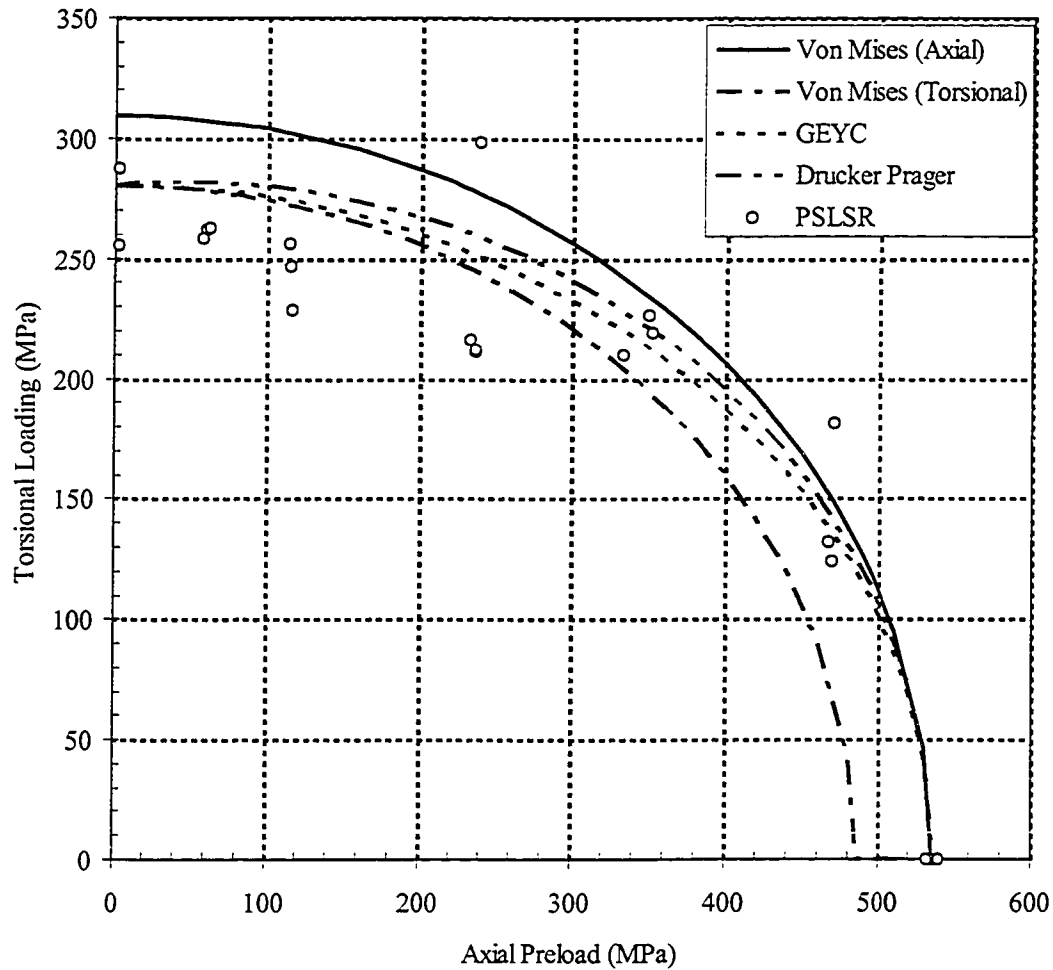


Figure 4.2: The Predicted and Experimental Transformation Yield Surface - Sample 1.

load. From Figure 4.5 the elastic modulus is $G_E = 23.1 \pm 5 \text{ GPa}$ and transformation modulus is $G_{TR} = 7.8 \pm 5 \text{ GPa}$.

4.3 Combined Axial Torsional Load Response Prediction Comparison with Experimental Tests

The predicted combined axial and torsional load response was compared with the experimental load response using the material properties from the pure axial and torsional load response. For the predicted transformation yield shear its value is

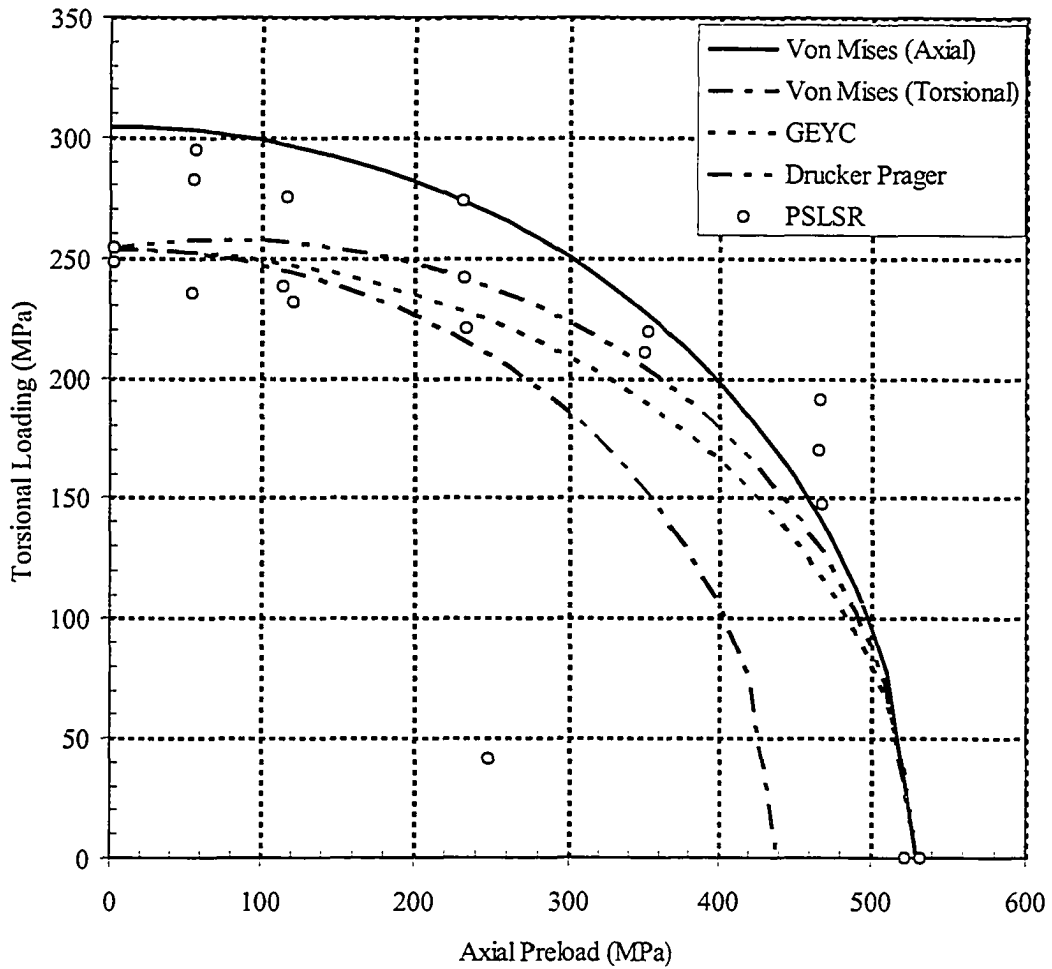


Figure 4.3: The Predicted and Experimental Transformation Yield Surface - Sample 2.

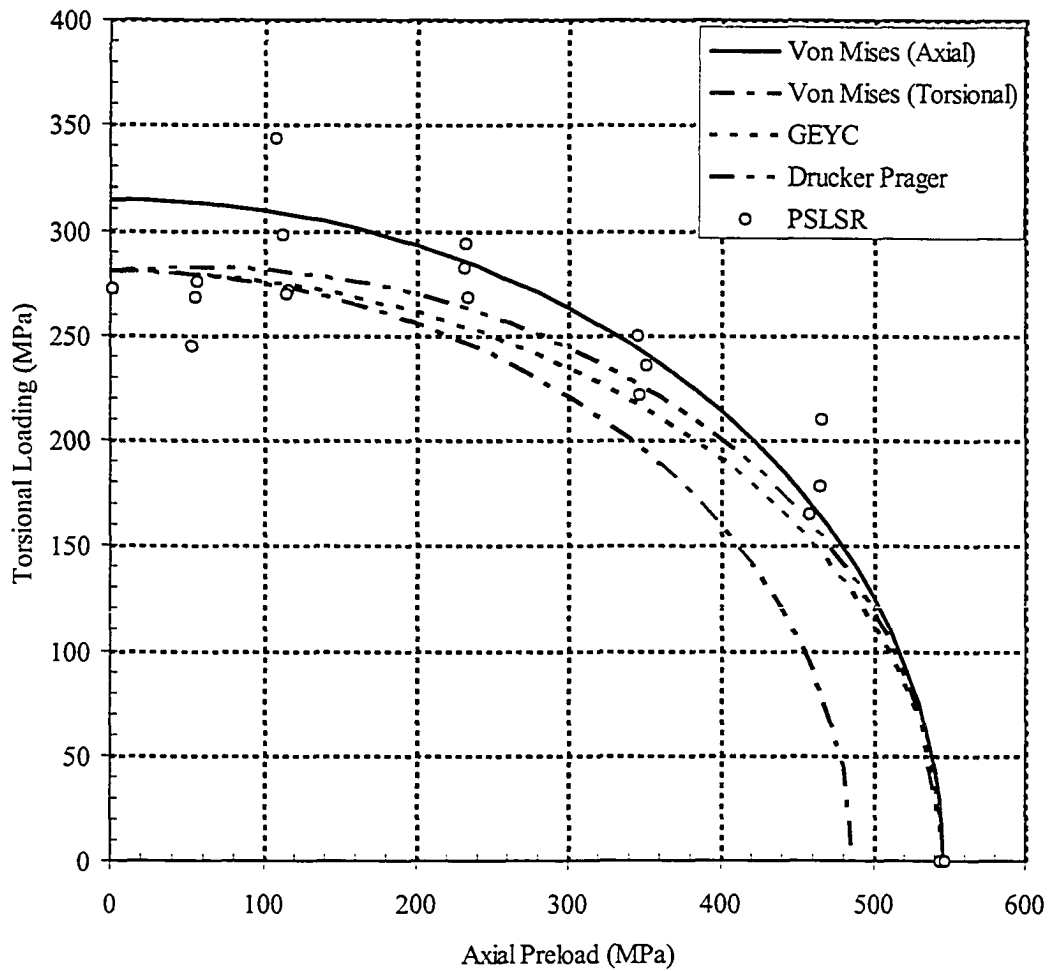


Figure 4.4: The Predicted and Experimental Transformation Yield Surface - Sample 3.

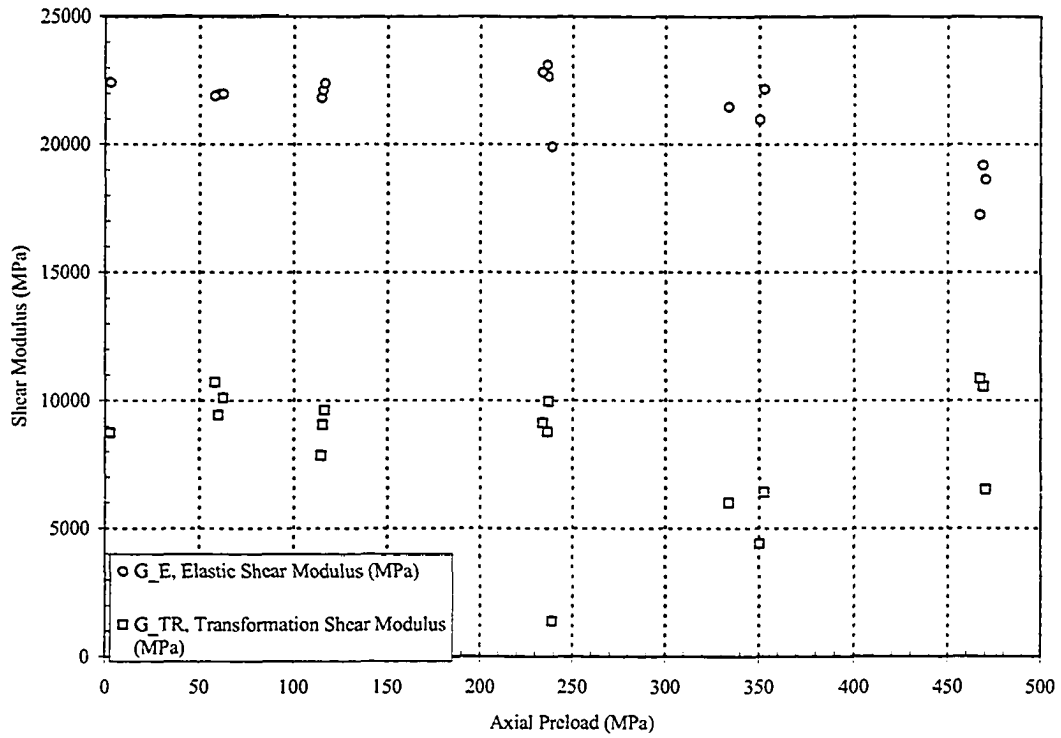


Figure 4.5: Sample 1: Elastic and Transformation Shear Modulus determined for various degrees of axial preload

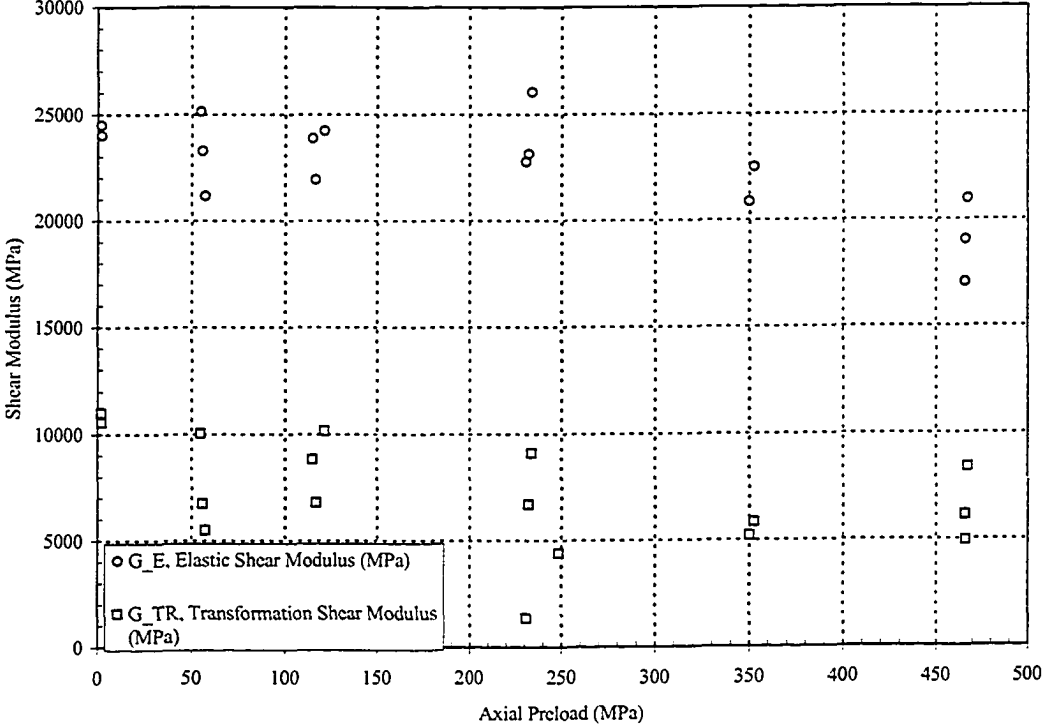


Figure 4.6: Sample 2: Elastic and Transformation Shear Modulus determined for various degrees of axial preload

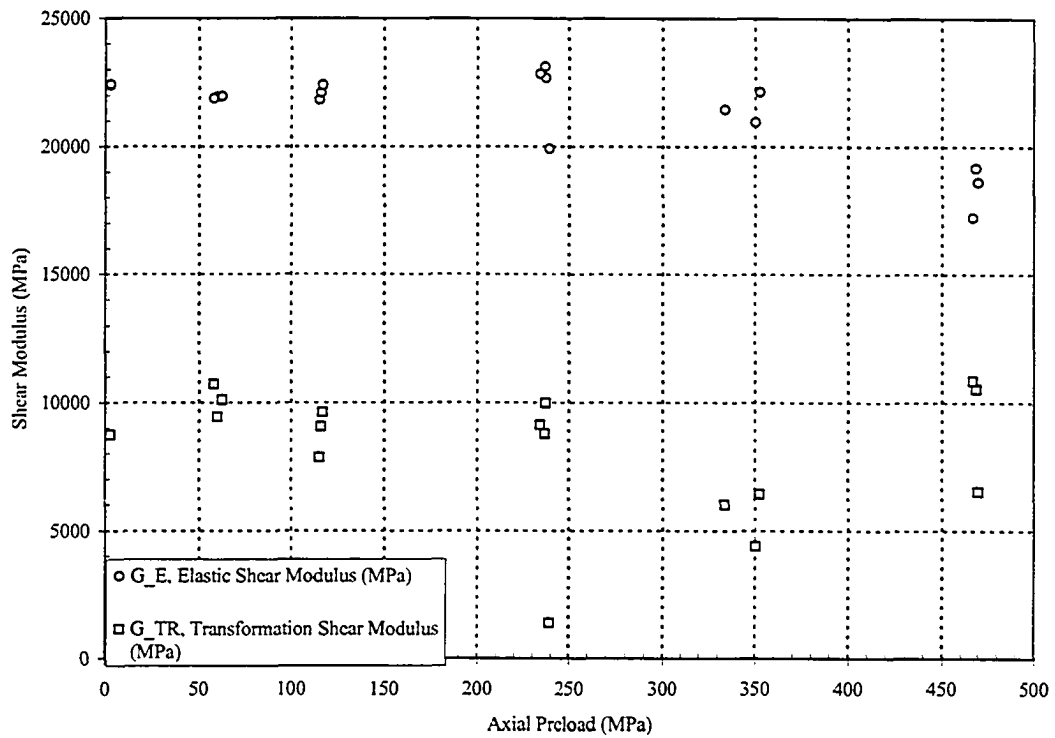


Figure 4.7: Sample 3: Elastic and Transformation Shear Modulus determined for various degrees of axial preload

Table 4.1: Specimen 1: Material Properties

Material Property	Value	Method
G_L , Elastic Shear Modulus	22.3 GPa	Least Squares
τ_{TY} , Transformation Yield Shear Stress	280.6 MPa	PSLSR
G_{TR} , Transformation Shear Modulus	10.3 GPa	PSLSR
E_L , Elastic Modulus	74.3 GPa	Least Squares
σ_{TY} , Transformation Yield Stress	532.1 MPa	Yield YTM Modulus (17%)
E_{TR} , Transformation Modulus	7.9 GPa	Least Squares

dependent on the applied axial preload and is required to be determined using a yield criterion. The possible yield criterions that could be used are the von Mises, Drucker Prager and the GEYC. The material properties determined from the pure axial and torsional tests are shown for each sample in Tables 4.1 to 4.3. The theoretical prediction using each of these criterions with the experimental tests are compared in Figures 4.8 to 4.13. The axial preload is also shown in these figures to illustrate the magnitude of axial loading and to show any axial elongation that may occur as the torsional loading is applied. This phenomena is further discussed in the next chapter. The yield criterions were used to predict the transformation yield shear stress for a given axial preload. With the elastic and transformation modulus determined in the previous section to be not a function of the axial preload, the transformation yield shear stress was the only material properties used in the torsional load response model that was a function of the axial preload. Because of this, when comparing the torsional load response with the transformation yield shear stress determined by the various transformation yield criterions it is expect the result to be the same as when comparing the yield surfaces.

With the criteria that were evaluated, the Drucker-Prager criterion is the most consistent with the experimental load response. It is noted that for an axial preload of 480N (The experimental elastic shear modulus is lower than the predicted modulus). As discussed in section 4.2 this occurred probably due to the specimen grips causing the wire to act softer locally at the grips thus making the entire wire appear softer. The torsional load response prediction using the von Mises criterion determined from the torsion test predicted that the wire sample yields at 480 MPa causing a discrepancy between the theoretical and experimental load response.

Table 4.2: Specimen 2: Material Properties

Material Property	Value	Method
G_L , Elastic Shear Modulus	24.2 GPa	Least Squares
τ_{TY} , Transformation Yield Shear Stress	253.7 MPa	PSLSR
G_{TR} , Transformation Shear Modulus	10.8 GPa	PSLSR
E_L , Elastic Modulus	74.0 GPa	Least Squares
σ_{TY} , Transformation Yield Stress	531.0 MPa	Yield YTM Modulus (17%)
E_{TR} , Transformation Modulus	8.3 GPa	Least Squares

Table 4.3: Specimen 3: Material Properties

Material Property	Value	Method
G_L , Elastic Shear Modulus	23.8 GPa	Least Squares
τ_{TY} , Transformation Yield Shear Stress	280.6 MPa	PSLSR
G_{TR} , Transformation Shear Modulus	8.0 GPa	PSLSR
E_L , Elastic Modulus	73.6 GPa	Least Squares
σ_{TY} , Transformation Yield Stress	528.6 MPa	Yield YTM Modulus (17%)
E_{TR} , Transformation Modulus	7.0 GPa	Least Squares

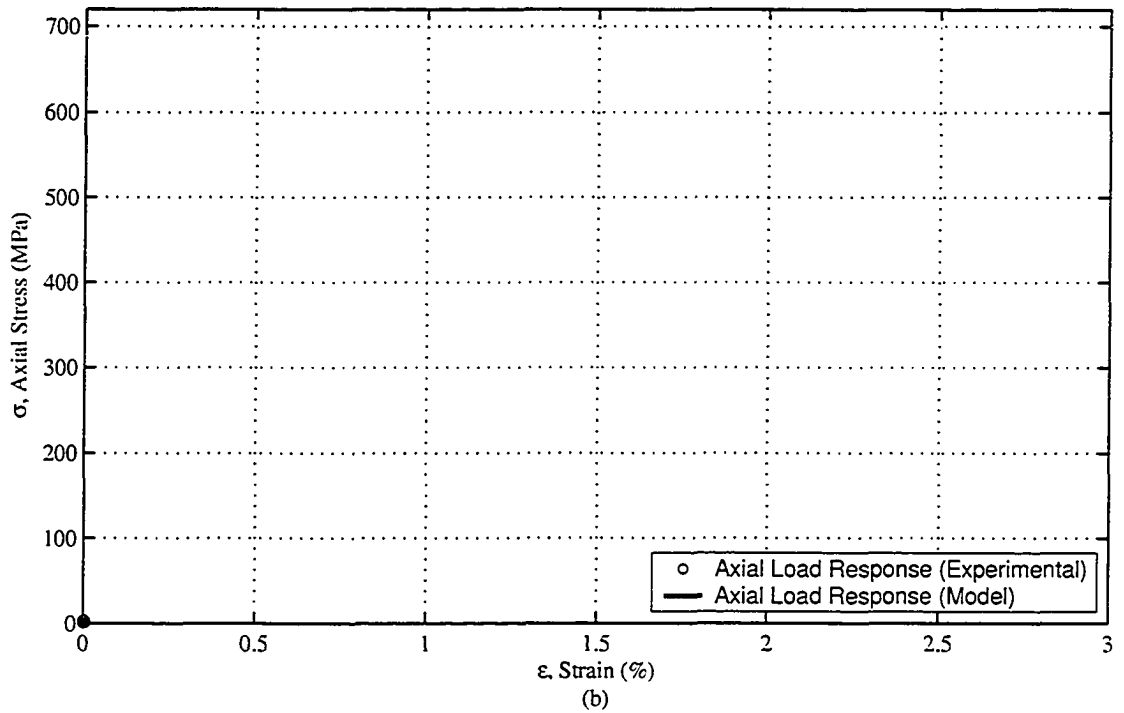
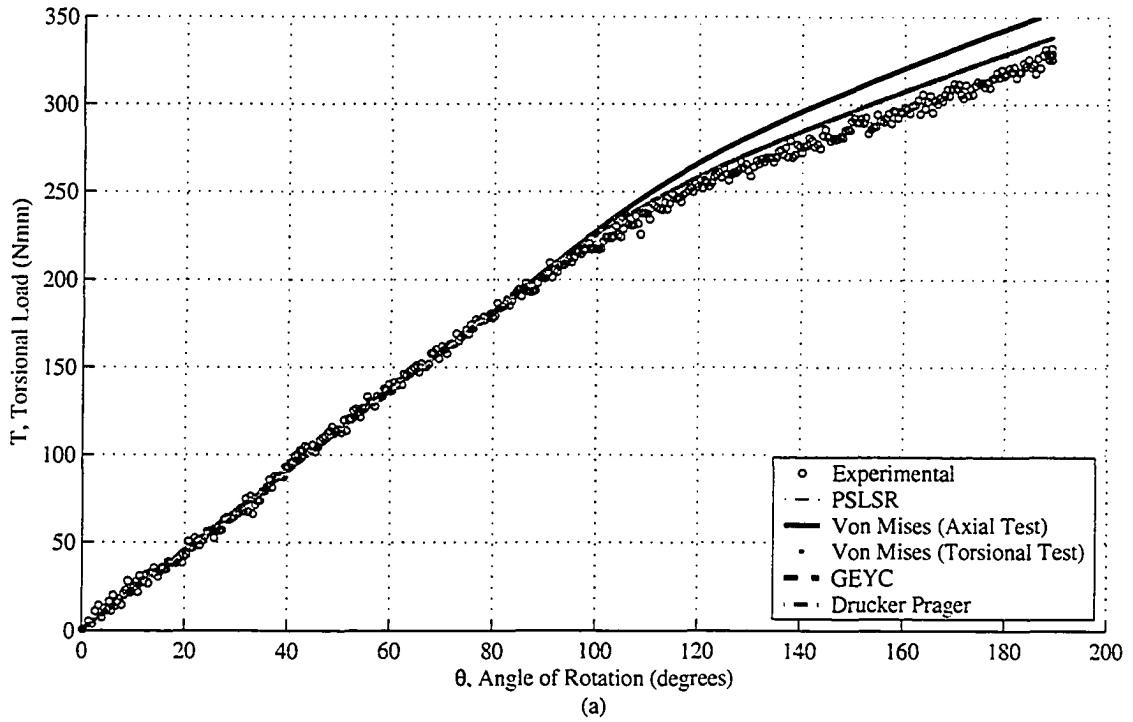


Figure 4.8: Torsional load response prediction comparison for zero axial preload.

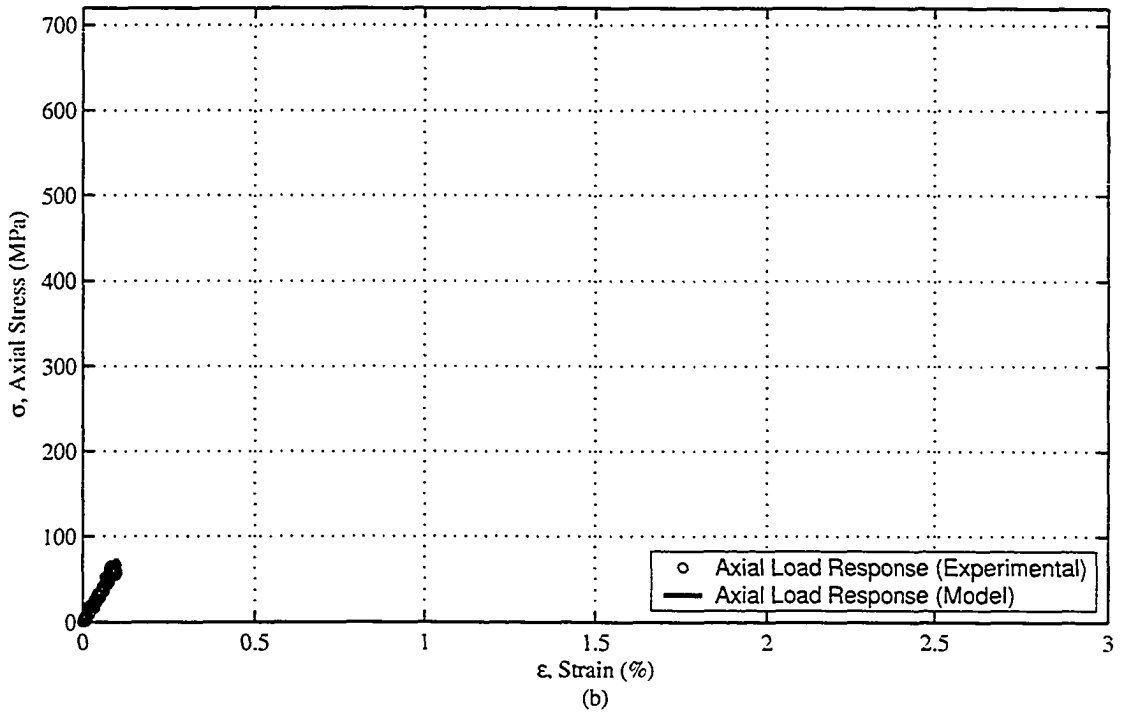
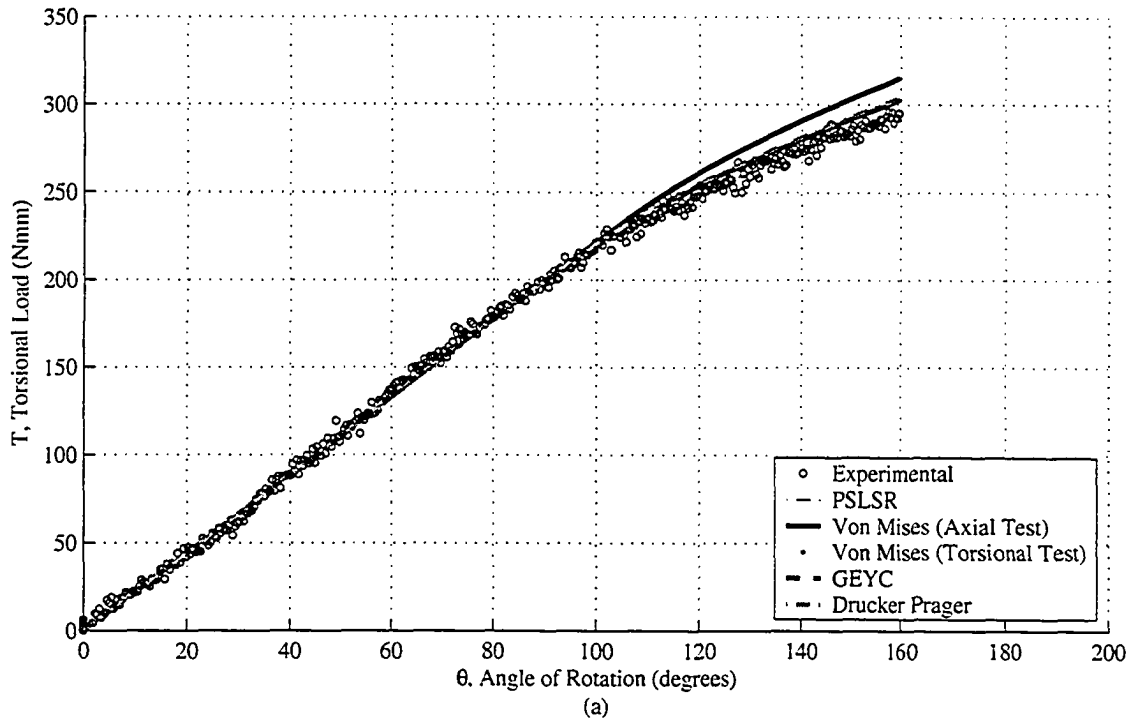


Figure 4.9: Torsional load response prediction comparison for axial preload of 60 MPa.

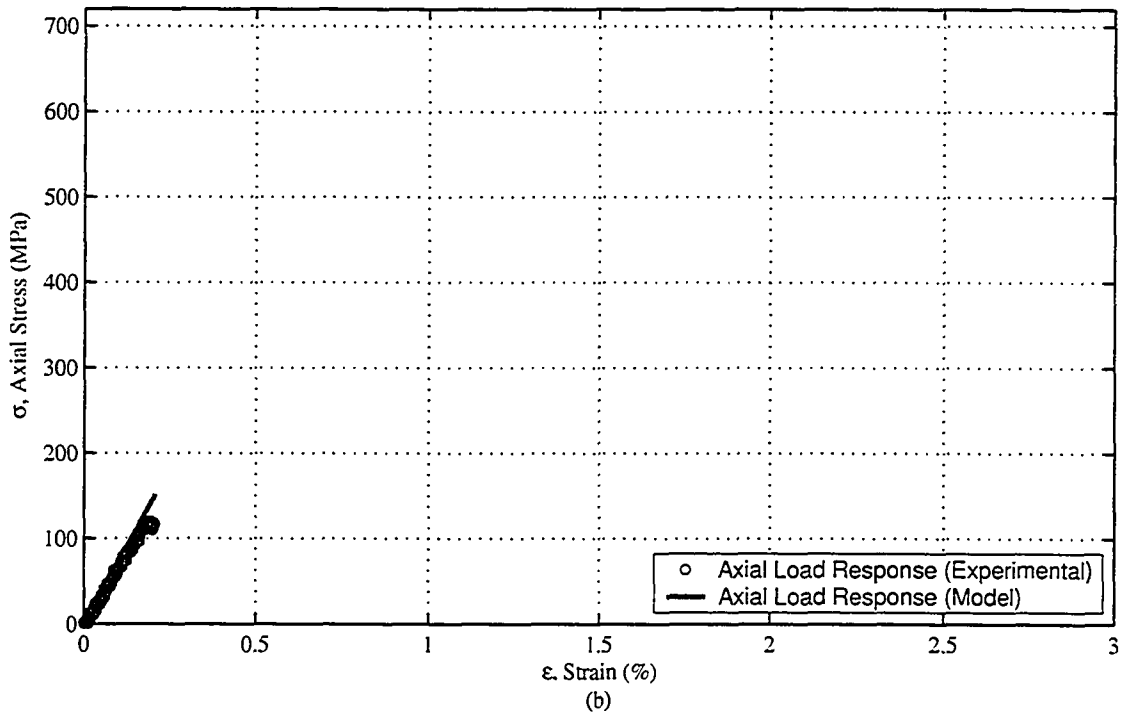
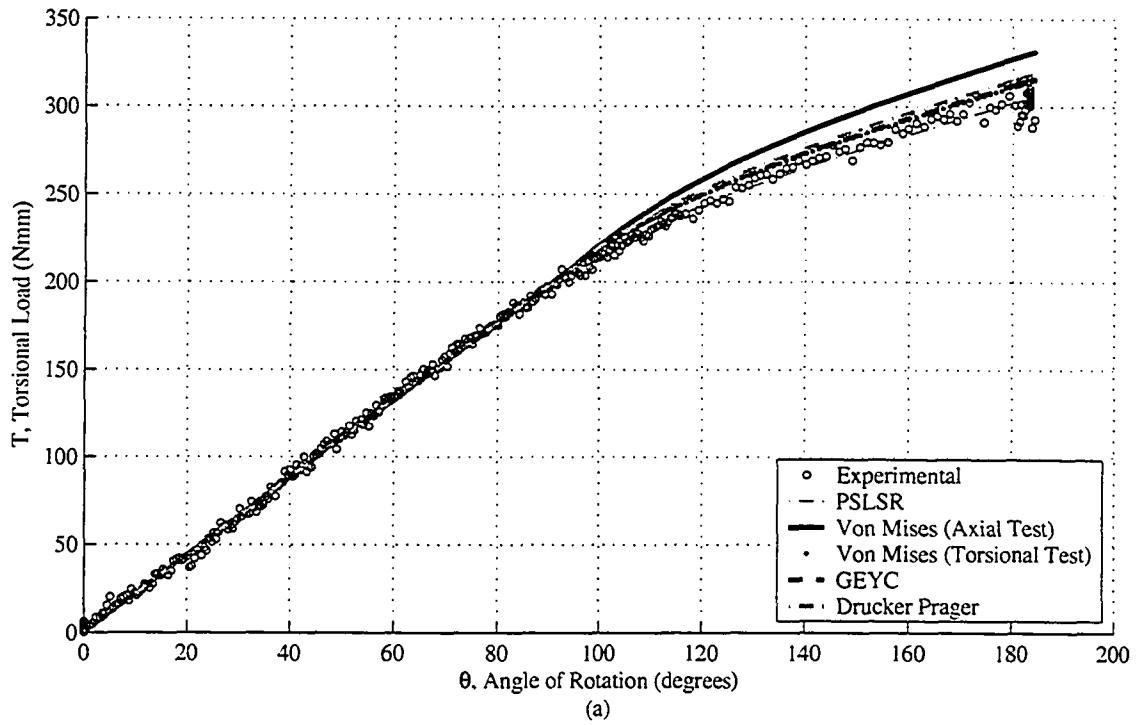


Figure 4.10: Torsional load response prediction comparison for axial preload of 120 MPa.

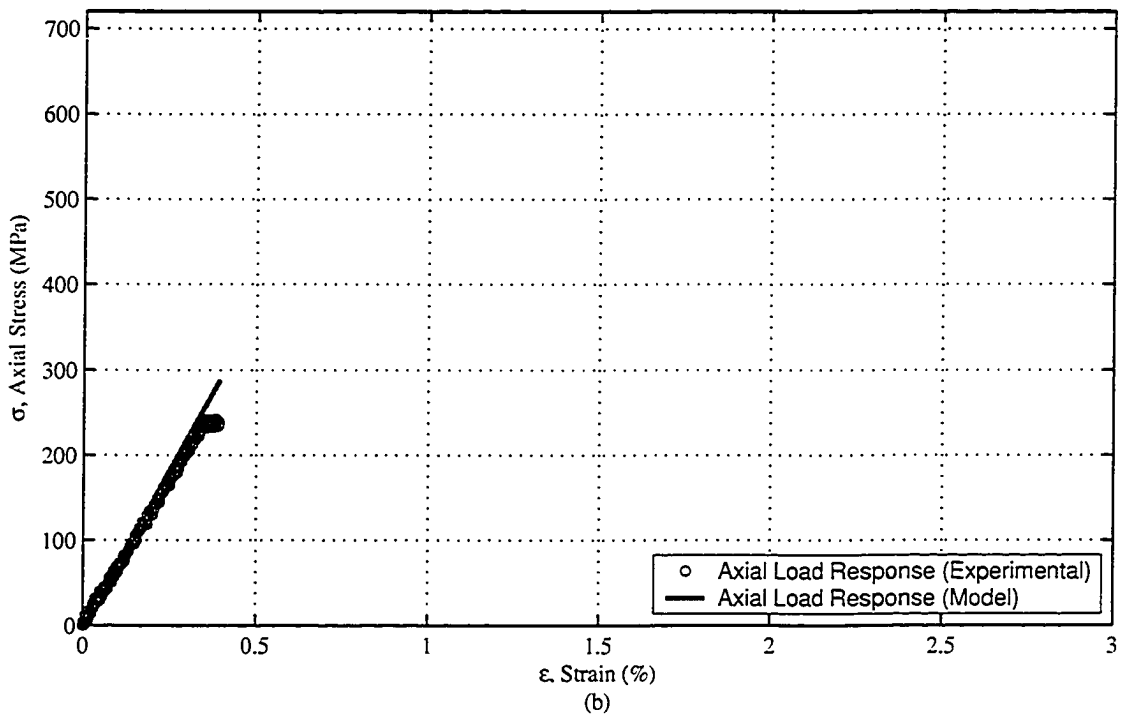
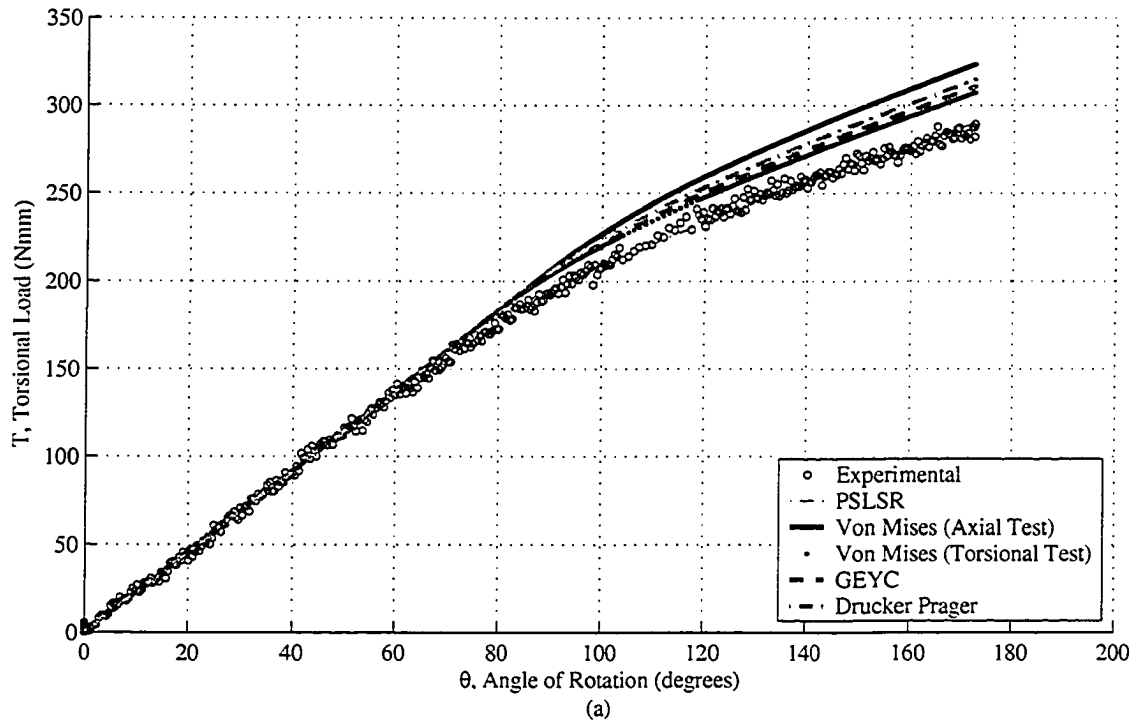


Figure 4.11: Torsional load response prediction comparison for axial preload of 240 MPa.

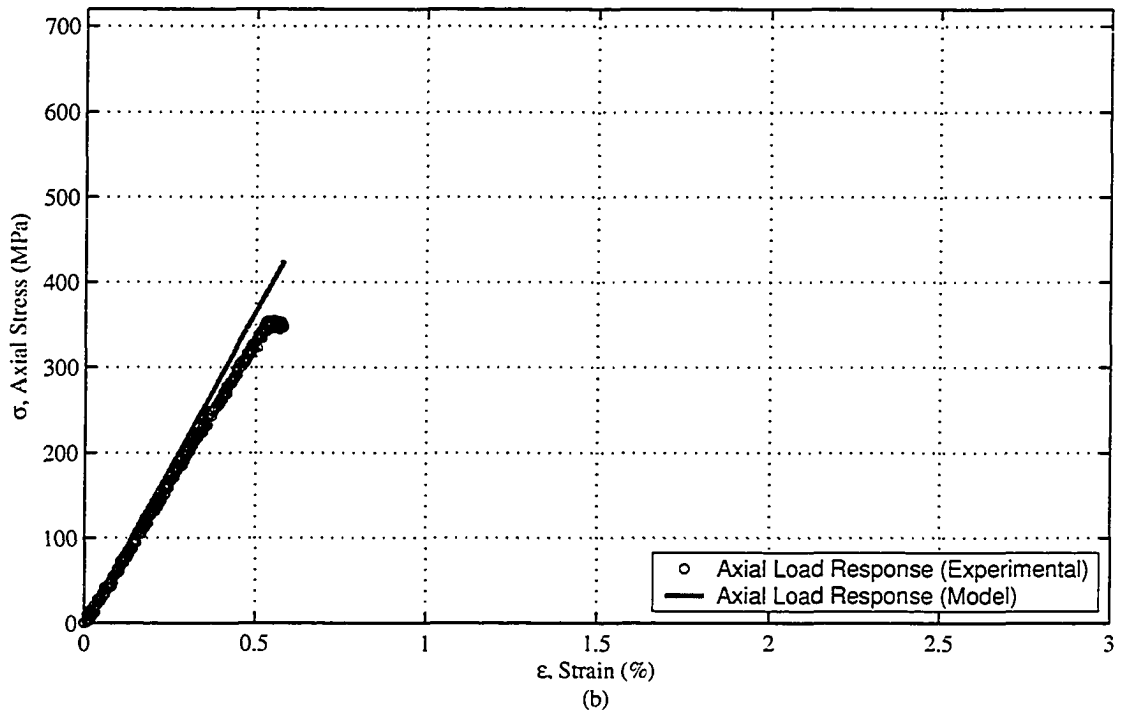
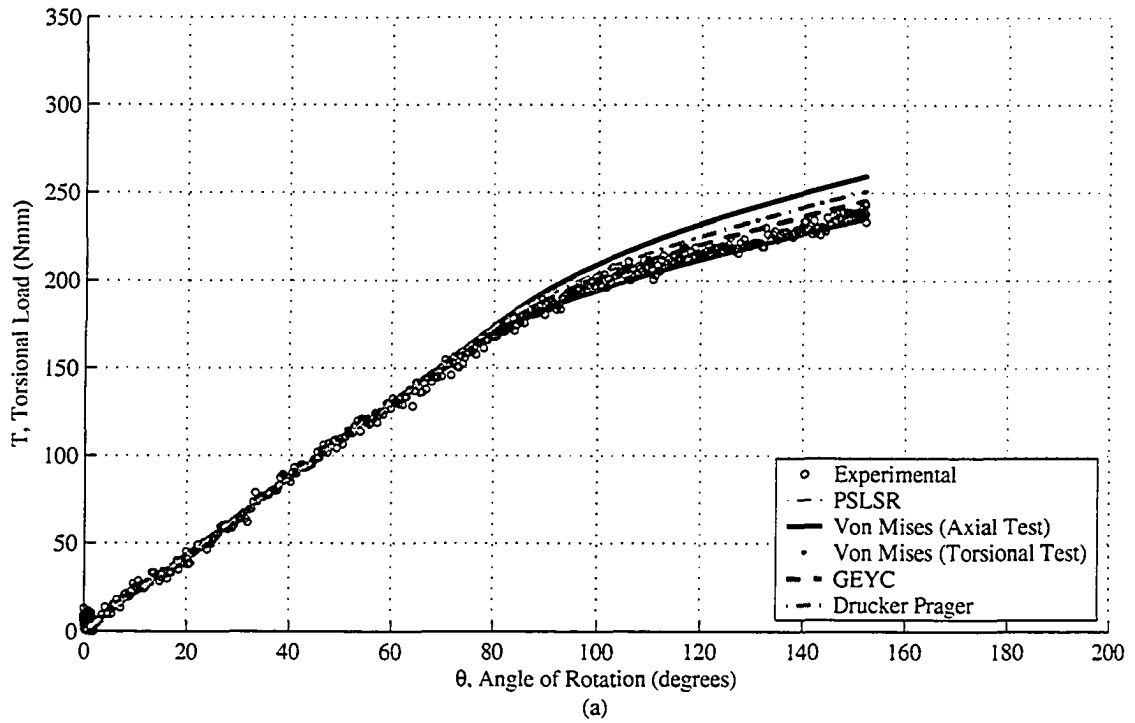


Figure 4.12: Torsional load response prediction comparison for axial preload of 360 N.

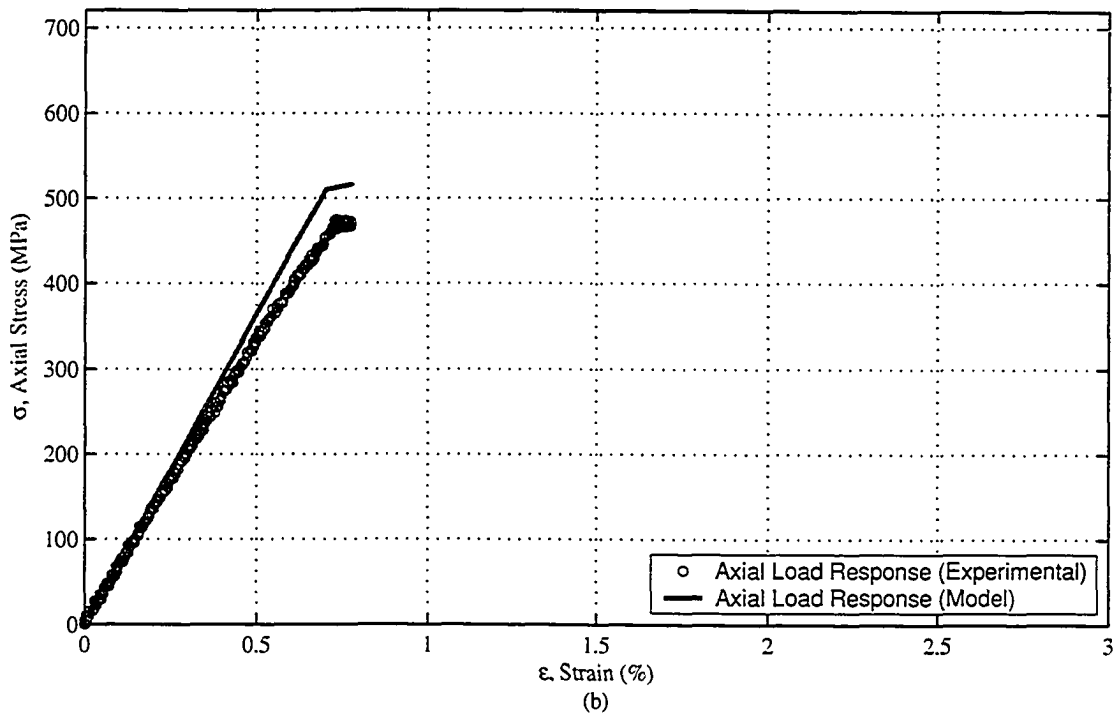
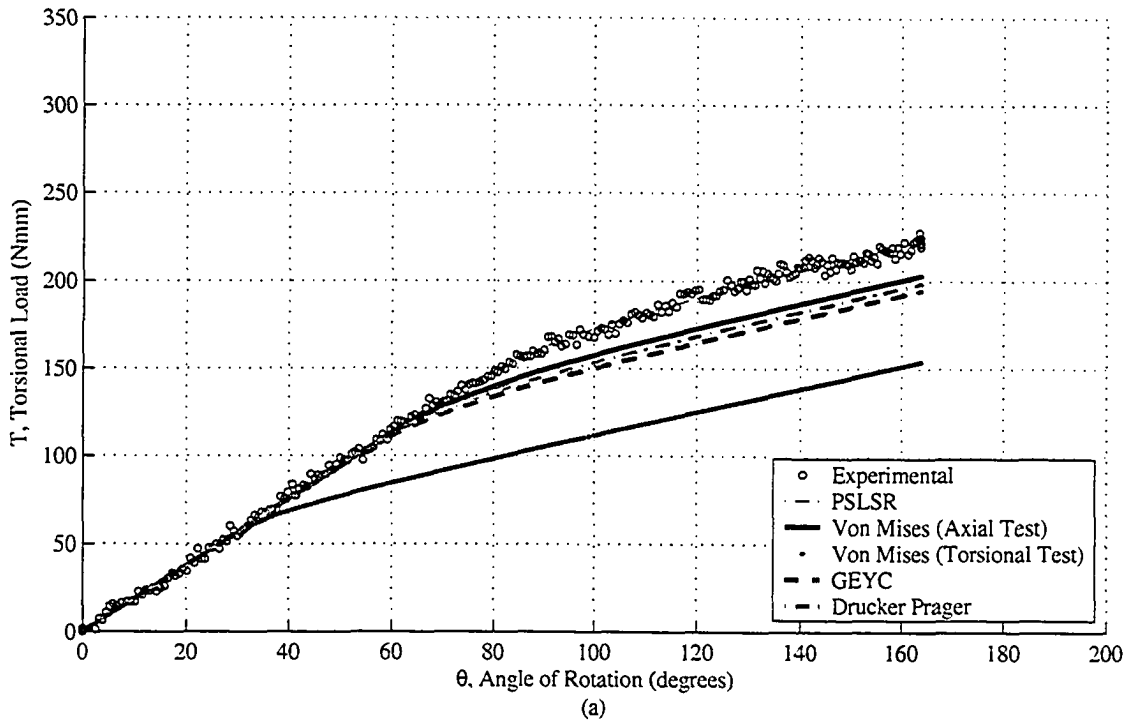


Figure 4.13: Torsional load response prediction comparison for axial preload of 480 N.

CHAPTER 5

AXIAL LOAD RESPONSE

It has been noted in the previous chapters that for the experimental combined axial and torsional tests with an axial preload of 480MPa there was an additional axial elongation that occurred as a result of weakening of the SMA wire due to the phase transformation induced by torsional loading. This coupled load response between the axial and torsional loading occurred only with one of the three samples tested. Due to the significance of this load response coupling this phenomenon is discussed in detail in this chapter. Also in this chapter a simple model is introduced to explain and perhaps be used in future research to predict this phenomenon.

The experimental test data for the second SMA sample was shown in Figure 5.1, during the combined torsional and axial experimental testing of the SMA wire once the axial preload was applied to the wire the axial strain did not change significantly while the torsional loading was applied for the bulk of the tests. As shown in Figure 5.1 there were four tests illustrated with axial preloads ranging from 63 MPa to 475 MPa. The vertical lines on this plot represent the axial loading and unloading of the SMA specimen. The axial loading of the specimen would be the vertical lines on the left hand side of the plot and are more or less coincident with the vertical axis. Since this research only considered the combined axial and torsional loading, the procedures for unloading the test specimen was not consistent thus there were some samples that were not completely unloaded to zero rotational angle. One of the biggest reasons why this did not occur was because the location of the rotational potentiometer used to measure the angle of wire twist was put in a location where the specimen angle could not be easily determined during experimental testing (see Section 2.3.4). What is of particular interest in Figure 5.1 is axial strain response to torsional loading while the specimen is under constant axial loading. In the experimental tests that

were performed with the axial preload ranging from 63 to 360 MPa the axial strain remained relatively constant while the torsional loading was applied. For the 475 MPa axial preload case the axial strain begins to change as a function of the angle of rotation plus the unloading response does not follow the loading response as seen in the cases with a lower axial preload. As shown in Figure 5.2a, this SMA was loaded three times to the same axial preload force and in two of these tests the angle where the axial strain become dependent on the torsional rotational angle was at about 100 degrees and for the other test it was 130 degrees. After this point the axial strain seems to be a linear function of the twist angle with a slope of about 0.018%/°. Although there is not a significant amount of experimental data on this, the next section is the initial development of a model used to explain this torsional and axial load response coupling.

Using the torsional load response model as detailed in Chapters 3 and 4 the additional elongation due to the transformation induced by torsional loading can be explained. From the torsional load response model as detailed in Section 3.2 when the martensite phase transformation initiates in torsional loading, the boundary between the elastic and transformation region is defined as yield radius and is determined by equation (3.9). The axial load response model can be modified to consider the axial loading of the wire as though it was a composite cylinder consisting of a pure austenite (core) region and a transforming martensite (shell) region. It should be clarified that during the axial preload the wire sample is assumed to be pure austenite. It is during the torsional loading that the martensite phase transformation initiates and thus having the austenite and martensite regions. These distinct regions, as illustrated in Figure 5.3, are assumed to behave as a composite cylinder and the axial loading would be modeled such that the core and shell components have the same strain but because they have different stiffness the loading in each component will be different. The fraction of loading on each component can be determined by assuming each component behaves like a linear elastic spring and both ends of the springs are fixed.

The load response for a single spring is given as

$$P = K\Delta x, \quad (5.1)$$

where P is the applied force on the spring, K is the spring stiffness of that component and Δx is the axial elongation. For springs in parallel the elongation in each spring is identical and the forces in each spring add up to the total force. Considering the

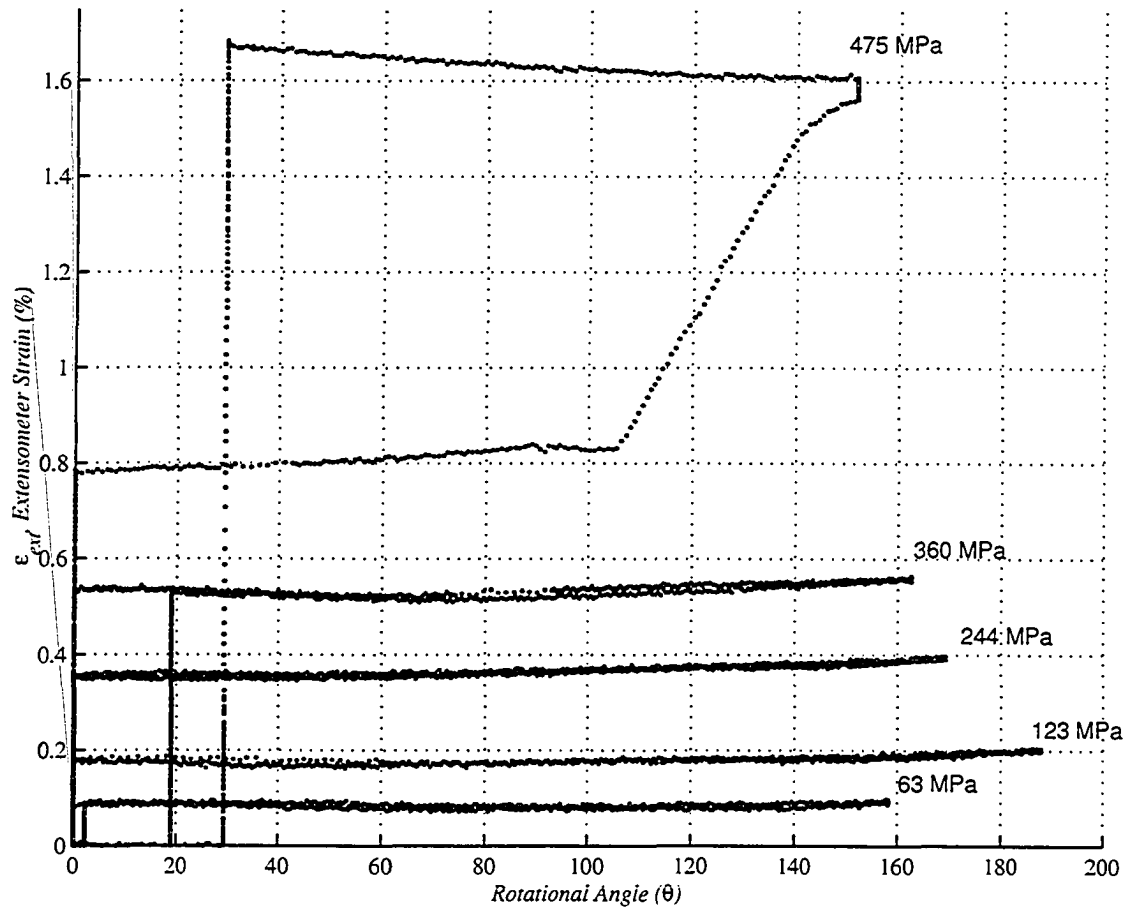


Figure 5.1: Axial elongation due to the torsional loading: The stroke and extensometer measurements of the increased strain due to the transformation induced by torsional loading at various degrees of axial loading. This effect was more pronounced with higher axial preload. There was also a corresponding residual torsional rotation associated with axial elongation due to torsional loading induced transformation

austenite core alone, the stress in the core is given as

$$\sigma = E_E \epsilon \quad (5.2)$$

where E_E is the elastic modulus and ϵ is the strain of the core defined as

$$\epsilon = \frac{\Delta x}{L} \quad (5.3)$$

where L is the length of the wire. From equations (5.1) to (5.3) the stiffness of the

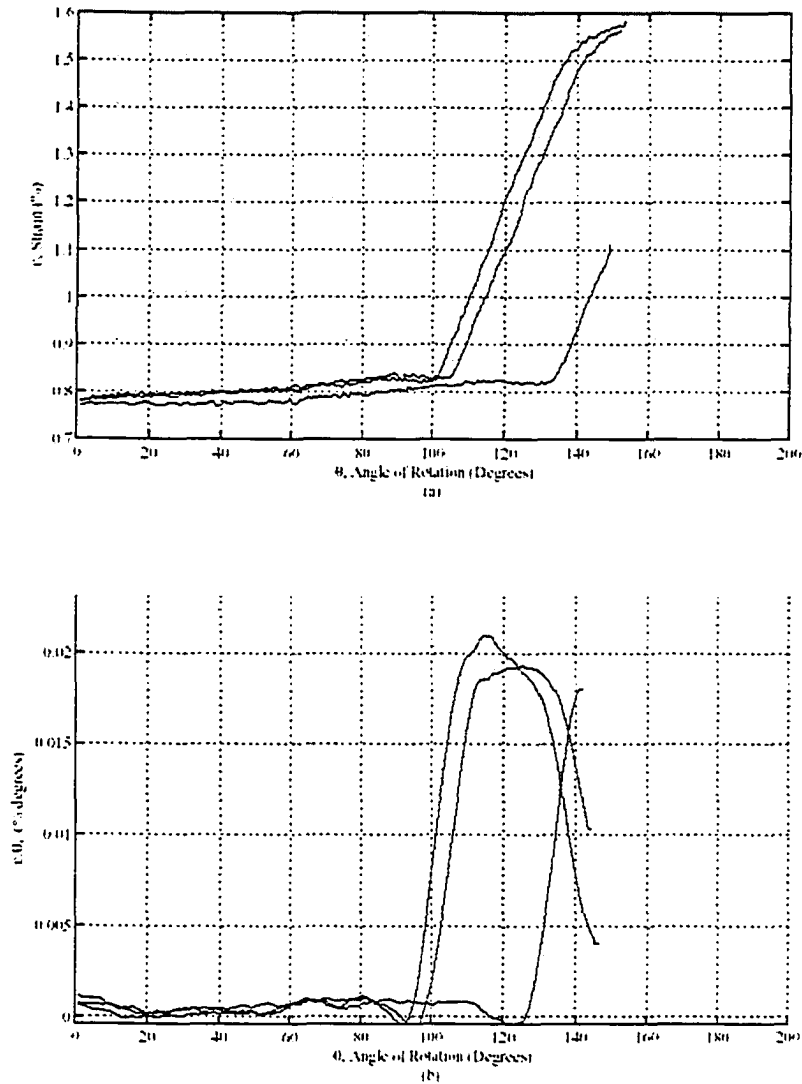


Figure 5.2: Torsionally induced phase transformation with consequence axial elongation. One sample that was tested three times with an axial preload of 475 MPa had experienced the axial elongation during torsional loading. In Figure (a) is the load response and in Figure (b) is the slope of the load response.

austenite core, K_L , can be determined to be

$$K_L = \frac{E_E \pi \rho_{TR}^2}{L} \quad (5.4)$$

where ρ_{TR} is the transformation yield radius as defined from the torsional load response model and given by equation (3.9). As with the loading modeled in Fig-

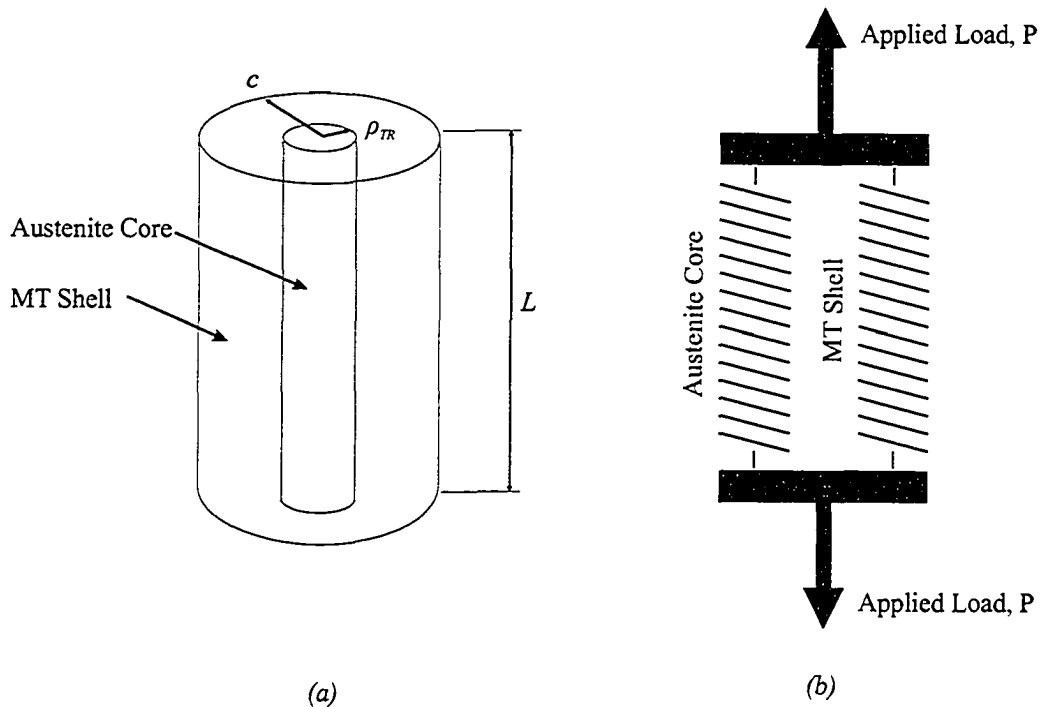


Figure 5.3: Composite Cylinder Model. Modeling the axial elongation due to the transformation induced by torsional loading was developed using the composite cylinder model. a) The composite cylinder model assumed that the SMA consisted of a Austenite core and a transforming martensite shell. b) Loading the composite cylinder axially, each component of the composite cylinder was treated as a spring in parallel.

ure 5.3(b) both the austenite core and transforming martensite shell will have the same strain, the critical axial transformation yield point occurs when the axial strain reaches the transformation yield strain given by

$$\epsilon_{TR} = \sigma_{TR}/EE. \quad (5.5)$$

In short using the combined cylinder model for combined loading, axial transformation yield strain will be the same as the yield strain for the pure axial load case. The strain at the transformation yield point for the pure axial test was determined to be 1% (YTM 17%) although the slope of the axial load response begins to change at 0.8% strain while the axial strain at the axial transformation yield point in combined loading was 0.83, 0.82 and 0.83% strain. For the other samples tested, where the additional axial elongation due to the transformation induced by torsional loading did

not occur, the maximum axial strain was 0.81%, 0.81%, 0.8% for the first sample and 0.78%, 0.78% and 0.77% for the third sample. It seems that for the first and second sample the axial strain was not high enough to induce this phenomena. Further research is required to confirm that the axial strain required to initiate the phase transformation in the axial direction is the same for the pure axial load response as in the combined axial and torsional load response.

CHAPTER 6

CONCLUSIONS AND FURTHER RESEARCH

The goal of this research was to develop a combined axial and torsional load response model for a NiTi SMA wire and to compare it with experimental tests. The load response was restricted to applying an axial preload followed with a torsional loading that induced the martensite phase transformation. The results from the experimental tests and theoretical model were to be used in SMA spring design where the SMA exhibits the pseudoelastic load response. In this concluding chapter the summary of the results from the design of the torsional adapter, torsional and axial load response models and experimental tests are summarized. This is followed with some final remarks on the future direction of this research.

6.1 Torsional Adapter

The torsional adapter was developed at the Department of Mechanical Engineering to apply axial and torsional loading to a SMA wire. The design of the torsional adapter was based on incorporating torsional loading capabilities to the MTS machine. The key components of the torsional adapter were the axial-torsional load cell, electric servo motor and worm gear drive to rotate the torsional load cell, the environmental chamber to control the test temperature and the data acquisition system to collect the experimental measurement.

With the supplied torsional-axial load cell it was found that to have ± 7.5 Nmm of noise was a source of considerable error in the range of torque that was tested (0-350Nmm). This type of load cell was chosen because it could handle the axial loading that was applied to the wire specimen. Unfortunately with testing wire specimens the torsional load cell was slightly oversized for this application which resulted in the high noise in the torsional load response measurements. A second problem that was

found with this torsional axial load cell was that even though the strain gauges were orientated optimally for minimizing cross talk there was a considerable amount of cross talk while applying axial loading.

With the design of the torsional adapter one of the disadvantages the torsional loading was controlled manually and was to only rotational controlled loading. The experimental testing with the torsional adapter consisted of first applying an axial load first then applying a torsional load past the transformation yield point.

One of the major concerns with the design of the torsional adapter was that the grips used to hold the test specimen needed to have sufficient compressive loading to generate enough friction force to prevent the specimen from slipping out. As a consequence it was believed that the grips contributed to inducing the martensite phase transformation at the grip locations. It is assumed that the phase transformation would initiate at this location then progress toward the gauge section thus the elongation of the wire specimen was not uniform along the length of the wire. As part of future work it would be of interest to see how the specimen grips would affect the SMA wire load response and if a proper grip could be made that could hold the specimen securely and allow the specimen to elongate uniformly along the length of the wire. This area could also be further researched in the design of small SMA wire grips that are used in applications such as orthodontics.

6.2 Axial and Torsional Load Response Model

The combined load response model studied here consisted of the axial load response and the torsional load response with the transformation yield stress coupling the two responses through the transformation yield surface. The axial load response and the shear stress response are both assumed to follow a bilinear load response described by of a linear elastic and a linear transformation modulus. It was assumed for the load response model that the transformation was axis symmetric and occurred uniformly along the length of the wire.

6.2.1 Axial Load Response Model

The axial load response model was assumed to be a bilinear function with a constant elastic and transformation modulus. With the bilinear assumption the axial load response could be defined from elastic modulus, transformation yield stress and the

transformation modulus. For axial loading it was determined that the critical tangent modulus that defined the transformation yield point was 17% of the initial tangent modulus. The modeled transformation yield point is the intersection of the modeled elastic and transformation load response. As a result the modeled transformation yield point occurred at a lower stress and strain than the experimental value.

6.2.2 Torsional Load Response Model

Similar to the axial load response model, the torsional load response model was based on the bilinear shear response assumption. Using this assumption the torsional load response could be predict using only three material properties: the elastic shear modulus, transformation yield shear stress and the transformation shear modulus. In determining the material properties from the experimental torsional load response there was three difficulties encountered;

1. The transformation yield stress was not a distinct point which made it difficult to determine accurately;
2. The transformation modulus was not a material properties that could be explicitly determined from the torsional load response; and,
3. The noise in the torsional load cell made it difficult to determine the transformation yield shear stress and transformation shear modulus.

This authors contribution to research in this area was the development of the "Piecewise Smooth Least Squares Regression Method". This method was originally conceived to determine the transformation shear modulus from the torsion load response for a solid cylindrical specimen. This technique was found to be effective for determining the material properties for the torsional load response (assuming the bilinear shear load response) and the torsional load response model seem to fit the experimental data quite well. Since this method uses the entire data set to determine the best curve fit it does compensate for the noise that was experienced with the load cell.

6.2.3 Combined Load Response

Of the three material properties required for the axial and torsional load response, only the transformation yield stress and transformation yield shear stress were be

dependent on one another under combined loading circumstances. Since the experimental testing was limited to applying an axial preload then applying the torsional loading to initiate the martensite transformation only the assumption that the elastic and transformation shear modulus was independent of the applied axial preload for elastic loading of the SMA. From the experimental combined loading tests the elastic and transformation shear modulus were found to be independent of the axial loading for elastic loading of the SMA. As with linear elastic materials, the transformation yield shear stress was related to the axial preload which is consistent with yield criteria that are used with linear elastic materials. The von Mises, Drucker Prager and the General Elliptical Yield criteria were compared to determine which one was the most consistent with the experimental tests. It was found that the predicted load response using the Drucker Prager criterion was the more consistent with the experimental data. The General Elliptical Yield criterion marginally less consistent than the Drucker Prager criterion where its assumed transformation yield surface was slightly less. The von Mises criterion was the least consistent of the criteria that were tested. The only advantage for the von Mises criterion was that it only required a single test whereas the GEYC and the Drucker Prager criterion required two tests. For one sample that was tested it was found for higher axial preloads there was additional axial elongation that occurred when the applied torsional loading induced the phase transformation. This additional axial elongation was modeled as a composite cylinder where the core of the composite cylinder was the austenite phase and the shell component was considered to be the transforming martensite region. Using this model it was deduced that the phase transformation induced by axial loading occurred at the transformation yield strain which was determined from a pure axial load test. With the specimens that were tested the axial and torsional load response coupling occurred at 0.83% axial strain.

6.3 Further Research

If this research was to be done over again I would recommend that attention should be paid to how the specimen attaches to the grips and also to devise a method to ensure that the wire samples are perfectly aligned. The design of the torsional adapter could be improved with more automation of the torsional load response and temperature control. For the measurement of the load cell twist angle it is recommended to devise a method directly measures the angle of rotation of the load cell. When determining the

material properties for the SMA, a load test should be performed at a low temperature to determine the load response for the martensite phase. If possible an axial and/or torsional load response test should be carried out until failure for a given sample. This information would be beneficial for the further development of the combine load response models. If it was required to test at a temperature that was lower than room temperature an easy way to perform cold test that was not detailed in this research was to put a canister of dry ice inline with the air line used to circulate within the environmental chamber. Using this method it was possible to get -30°C . If the air supplied is from the room, the water condensing from the air would need to be dealt with. A final addition to this research would be to research methods to monitor the transformation during testing. Measuring the resistance of the wire would be a way to gauge how much of the wire was transformed during testing. This would also provide valuable information if incorporated with the pseudoelastic load test to failure and the low temperature (martensite phase) test to failure. For training it would be recommended to employ a strict training regime and try to develop a way to automate the whole training scheme.

The intended direction for future research was to perform similar testing with smaller diameter wires and to further expand the types of loading and wire geometry. In this particular topic of combined torsional and axial loading of SMA wires further research would be into testing various other load paths in combined loading to induce the phase transformation.

"If I have seen farther than others, it is because I was standing on the shoulders of giants."

-Isaac Newton

BIBLIOGRAPHY

- [Andreasen and Morrow, 1978] Andreasen, G. F. and Morrow, R. (1978). Laboratory and clinical analysis of nitinol wire. *Am. J. Orthod.*, 73(2):142–151.
- [ASTM, 2003] ASTM (2003). *Standard Test Method for Young's Modulus, Tangent Modulus, and Chord Modulus*, chapter E 111 - 97, pages 249–255. ASTM International.
- [ASTM, 2004] ASTM (2004). *Standard Terminology Relating to Methods of Mechanical Testing*, chapter E 6 - 02a, pages 21–30. ASTM.
- [Bondaryev and Wayman, 1988] Bondaryev, E. and Wayman, C. (1988). Some stress-strain-temperature relationships for shape memory alloys. *Metallurgical Transactions*, 19(10):2407–2413.
- [Boresi et al., 1993] Boresi, A., Schmidt, R., and Sidebottom, O. (1993). *Advance Mechanics of Materials*, volume 1. John Wiley and Sons Jr.
- [Boyd and Lagoudas, 1996] Boyd, J. and Lagoudas, D. (1996). A thermodynamical constitutive model for shape memory materials part i: The monolithic shape memory alloy. *Int. J. Plasticity*, 12:805–842.
- [Brinson, 1995] Brinson, C. (1995). A new look at shape memory alloy constitutive models - comparisons and micromechanics. *Adaptive Material Systems*, 206:129–140.
- [Brinson, 1993] Brinson, L. (1993). One dimensional constitutive behavior of shape memory alloys: Thermodynamical derivation with non-constant material functions. *J. Intelligent material systems and structures*, 4(2):229–242.
- [Chen and Han, 1988] Chen, W. and Han, D. (1988). *Plasticity for Structural Engineers*. Springer-Verlag New York Inc.

- [Davidson and Liang, 1996] Davidson, F. and Liang, C. (1996). Investigation of torsional shape memory alloy actuators. volume 2717, pages 672–682, San Diego State University, San Diego, CA 92182. SPIE.
- [Duerig et al., 1990] Duerig, T. W., Melton, K., Stockel, D., and Wayman, C. (1990). *Engineering Aspects of Shape Memory Alloys*. Butterworth-Heinemann, London.
- [Funakubo, 1984] Funakubo, H., editor (1987 (Original in Japanese - 1984)). *Shape Memory Alloys*, volume 1 of *Precision Machinery and Robotics*. Gordon and Breach Science Publishers S.A., New York, New York 10276, USA.
- [Gillet et al., 1998] Gillet, V., Patoor, E., and Berveiller, M. (1998). Calculation of pseudoelastic elements using a non-symmetrical thermomechanical transformation criterion and associated rule. *Journal of Intelligent material systems and structures*, 9:366–378.
- [Gupta and Sczerzenie, 1997] Gupta, S. and Sczerzenie, F. (1997). Effect of cold work on mechanical properties and on TTR's of a nickel titanium shape memory alloy. Technical report, Special Metals Corporation, Special Metals Corporation, 4317 Middle Stttlement Rd., New Hartford, NY 13413, USA.
- [Haythornthwaite, 1968] Haythornthwaite, R. (1968). A more rational approach to strain hardening data. In Heyman, J. and Leckie, F., editors, *Engineering Plasticity*, pages 201–218. Cambridge U.P.
- [Hohenemser, 1932] Hohenemser (1932). W. prager, beitrage zur mechanik des bildsamen verhaltens von flubstahl,. *ZAMM*, 11:15–19.
- [Kafka, 1994] Kafka, V. (1994). Shape memory: A new concept of explanation and of mathematical modeling. part II: Mathematical modelling of the SM effect and of psuedoelasticity. *Journal of Intelligent Material Systems and Structures*, 5:815–824.
- [Ohashi and Tokuda, 1973] Ohashi, Y. and Tokuda, M. (1973). Precise measurment of plastic behaviour of mild steel tubular specimens subjected to combined torsion and axial force. *Journal of Mechanics and Physics of Solids*, 21(4):241–261.
- [Patoor et al., 1995] Patoor, E., Amrani, M. E., Eberhardt, A., and Berveiller, M. (1995). Determination of the origin for the dissymmetry observed between tensile

- and compression tests on shape memory alloys. In *Proceeding of ESOMAT '94*, pages C2-495. ESOMAT.
- [Perkins and Hodgson, 1990] Perkins, J. and Hodgson, D. (1990). *The Two-Way Shape Memory Effect*, pages 195-206. Butterworth-Heinemann Ltd.
- [Reed-Hill and Abbaschian, 1994] Reed-Hill, R. E. and Abbaschian, R. (1994). *Physical Metallurgy Principles*. PWS Publishing Company.
- [Sittner et al., 1994a] Sittner, P., Hara, Y., Takakura, M., and Tokuda, M. (1994a). On the general stress controlled thermoelastic martensitic transformation. *Res. Rep. Fac. Eng. Mie. Univ.*, 19:9-24.
- [Sittner et al., 1994b] Sittner, P., Hara, Y., and Tokuda, M. (1994b). Pseudoelastic deformation in combined tension and torsion. *Strength of materials*, pages 319-322.
- [Sittner et al., 1994c] Sittner, P., Hara, Y., and Tokuda, M. (1994c). SMA hysteresis under combined tension and torsion. pages 541-545.
- [Sittner et al., 1997] Sittner, P., M.Takakura, and Tokuda, M. (1997). Shape memory effects under combined forces. *Materials science and engineering*, A234-236:216-219.
- [Sittner et al., 1995] Sittner, P., Takakura, M., and Tokuda, M. (1995). The stabilization of transformation pathway in stress induced martensite. *Scripta Metallurgica et Materialia*, 32(12):2073-2079.
- [Tobushi et al., 1998] Tobushi, H., Shimeno, Y., Hachisuka, T., and Tanaka, K. (1998). Influence of strain rate on superelastic properties of TiNi shape memory alloy. *Mechanic of Materials*, (30):141-150.
- [Tokuda et al., 1999] Tokuda, M., Ye, M., Takakura, M., and Sittner, P. (1999). Thermomechanical behavior of shape memory alloy under complex loading conditions. *International Journal of Plasticity*, 15:223-239.
- [Vokoun and Kafka, 1996] Vokoun, D. and Kafka, V. (1996). On mathematical modelling of the incomplete transformation in pseudoelastic processing in binary alloys. pages 541-545, Prosecka 74, 190 00 Praha 9, Czech Republic. ICIM/ECSSM.

- [Zhukov, 1966] Zhukov, A. (1966). Plastic deformations of the alloy AKG in the case of simple and combined loadings. *VMU*, 12:260–289.
- [Zyczkowski, 1981] Zyczkowski, M. (1981). *Combined Loadings in Theory of Plasticity*. Polish Scientific Publishers.

APPENDIX A

SUPPLEMENTAL INFORMATION

A.1 Chapter 1

A.1.1 General Equations for Stress State ([Boresi et al., 1993])

The stress components also known as the stress tensor in the rectangular coordinate system is denoted as

$$\sigma_{ij} = \begin{bmatrix} \sigma_x & \tau_{xy} & \tau_{xz} \\ \tau_{yx} & \sigma_y & \tau_{yz} \\ \tau_{zx} & \tau_{yz} & \sigma_z \end{bmatrix}. \quad (\text{A.1})$$

In determining the principle values and directions of the stress vector from the stress tensor given equation A.1 there are three invariants that are defined which are I_1 , I_2 and I_3 and are given as

$$I_1 = \sigma_x + \sigma_y + \sigma_z, \quad (\text{A.2})$$

$$I_2 = \begin{vmatrix} \sigma_y & \tau_{yz} \\ \tau_{yz} & \sigma_z \end{vmatrix} + \begin{vmatrix} \sigma_x & \tau_{xz} \\ \tau_{zx} & \sigma_z \end{vmatrix} + \begin{vmatrix} \sigma_x & \tau_{xy} \\ \tau_{yx} & \sigma_y \end{vmatrix} \quad (\text{A.3})$$

and

$$I_3 = \begin{vmatrix} \sigma_x & \tau_{xy} & \tau_{xz} \\ \tau_{yx} & \sigma_y & \tau_{yz} \\ \tau_{zx} & \tau_{yz} & \sigma_z \end{vmatrix}. \quad (\text{A.4})$$

In neglecting the effects of the hydrostatic stress state in the stress tensor the hydrostatic component, p , defined as

$$p = \frac{1}{3}(\sigma_x + \sigma_y + \sigma_z) = \frac{1}{3}I_1 \quad (\text{A.5})$$

is subtracted from the stress tensor to give the deviator stress tensor which is

$$s_{ij} = \begin{bmatrix} s_x & s_{xy} & s_{xz} \\ s_{yx} & s_y & s_{yz} \\ s_{zx} & s_{yz} & s_z \end{bmatrix} = \sigma_{ij} = \begin{bmatrix} (\sigma_x - p) & \tau_{xy} & \tau_{xz} \\ \tau_{yx} & (\sigma_y - p) & \tau_{yz} \\ \tau_{zx} & \tau_{yz} & (\sigma_z - p) \end{bmatrix} \quad (\text{A.6})$$

Similarly to the stress invariants given for the stress tensor there are the deviator stress invariants which are defined as

$$J_1 = s_x + s_y + s_z = 0, \quad (\text{A.7})$$

$$J_2 = \begin{vmatrix} s_y & s_{yz} \\ s_{yz} & s_z \end{vmatrix} + \begin{vmatrix} s_x & s_{xz} \\ s_{zx} & s_z \end{vmatrix} + \begin{vmatrix} s_x & s_{xy} \\ s_{yx} & s_y \end{vmatrix} \quad (\text{A.8})$$

and

$$J_3 = \begin{vmatrix} s_x & s_{xy} & s_{xz} \\ s_{yx} & s_y & s_{yz} \\ s_{zx} & s_{yz} & s_z \end{vmatrix} = s_x s_y s_z \quad (\text{A.9})$$

If it is required to find the deviator stress invariant from the stress invariants

$$\begin{aligned} J_1 &= 0 \\ J_2 &= \frac{1}{3}(I_1^2 - 3I_2) \\ J_3 &= \frac{1}{27}(2I_1^3 - 9I_1I_2 + 27I_3) \end{aligned} \quad (\text{A.10})$$

is used.

A.1.2 Drucker-Prager Yield Criterion

The Drucker-Prager is similar to the von Mises criterion except for the fact that it considers the effects of the hydrostatic stress component. The Drucker Prager yield criterion is given as

$$\begin{aligned} f(I_1, J_2) &= \alpha I_1 + \sqrt{J_2} - k = 0 \\ k &= \tau_0 \end{aligned} \quad (\text{A.11})$$

For the combined tension and torsion loading of the wire the pure tension and torsion cases could be evaluated to determine the α and K coefficients. For the pure torsion

test the stress tensor is given as

$$\sigma_{ij} = \begin{bmatrix} 0 & \tau_{xy} & 0 \\ \tau_{yx} & 0 & 0 \\ 0 & 0 & 0 \end{bmatrix} \quad (\text{A.12})$$

and the yield criterion becomes

$$\begin{aligned} f(I_1, J_2) &= \sqrt{\tau_0^2} - k = 0 \\ k &= \tau_0 \end{aligned} \quad (\text{A.13})$$

For the pure axial load test the stress tensor is given as

$$\sigma_{ij} = \begin{bmatrix} \sigma_0 & 0 & 0 \\ 0 & 0 & 0 \\ 0 & 0 & 0 \end{bmatrix} \quad (\text{A.14})$$

and the yield function becomes

$$\begin{aligned} f(I_1, J_2) &= \alpha\sigma_0 + \sqrt{\frac{\sigma_0^2}{3}} - k = 0 \\ \alpha &= \left(\tau_0 - \sqrt{\frac{\sigma_0^2}{3}} \right) \frac{1}{\sigma_0} \end{aligned} \quad (\text{A.15})$$

In the general stress state for combined loading the stress tensor is given as

$$\sigma_{ij} = \begin{bmatrix} \sigma_x & \tau_{xy} & 0 \\ \tau_{yx} & 0 & 0 \\ 0 & 0 & 0 \end{bmatrix} \quad (\text{A.16})$$

and with the coefficients as determined from the pure axial and torsional load test the yield function is given as

$$\begin{aligned} f(I_1, J_2) &= \alpha\sigma_0 + \sqrt{\frac{\sigma_0^2}{3} + \tau_0^2} - k = 0 \\ \left(\tau_0 - \sqrt{\frac{\sigma_0^2}{3}} \right) \frac{\sigma}{\sigma_0} + \sqrt{\frac{\sigma^2}{3} + \tau^2} - \tau_0 &= 0 \end{aligned} \quad (\text{A.17})$$

[There are several interpretations of the stress invariants I_1 and J_2 . Namely $I_1/3$ is the octahedral normal stress, σ_{oct} while $\sqrt{\frac{2}{3}J_2}$ is the octahedral shear stress [Chen and Han, 1988].

Assuming that the material was isotropic and that the volume change was ne-

glectable, Gillet chose to use the Prager equation,

$$F(J_2, J_3, T, \epsilon^{pt}) = J_2 \left(1 + \frac{bJ_3}{J_2^{3/2}} \right) - K^2(\epsilon^{pt}, T) = 0 \quad (\text{A.18})$$

which was the simplest phenomenological criterion that could be used to predict the transformation yield stress for combined loading. In this equation, J_2 and J_3 were the second and third scalar invariant of the deviatoric part of the stress tensor and T was the temperature of the specimen. The function $K(\epsilon^{pt}, t)$ and the coefficient b were determined from experimental tests.

A.1.3 Gillets Derivation

Gillet derived the torsional load response from a bilinear shear stress response. From the equation that defines the torque from the shear stress distribution the torque is given as

$$T = 2\pi \int_0^c \rho^2 \tau d\rho = 2\pi \int_0^{\rho_{TR}} \rho^3 G_L \psi d\rho + 2\pi \int_{\rho_{TR}}^c \rho^3 G_{TR} \psi - \rho^2 \tau_{TR} \frac{G_{TR}}{G_L} + \rho^2 \tau_{TR} d\rho \quad (\text{A.19})$$

where

$$\psi = \frac{\tau}{G_L \rho} = \frac{\gamma}{\rho} = \frac{\theta}{L} \quad (\text{A.20})$$

and

$$\psi_s = \frac{\tau_{TR}}{G_L c} = \frac{\gamma_{TR}}{c} = \frac{\theta_{TR}}{L} \quad (\text{A.21})$$

Solving the integral given by equation A.19 the torsional load response is

$$T = \frac{\pi \rho_{TR}^4 G_L \psi}{2} + \frac{\pi c^4 G_{TR} \psi}{2} - \frac{\pi \rho_{TR}^4 G_{TR} \psi}{2} - \frac{4\pi c^4 G_{TR} \tau_{TR}}{6 G_L} + \frac{4\pi \rho_{TR}^3 G_{TR} \tau_{TR}}{6 G_L} + \frac{4\pi \rho_c^3 \tau_{TR}}{6} - \frac{4\pi \rho_{TR}^3 \tau_{TR}}{6} \quad (\text{A.22})$$

and simplifying

$$T = \frac{\pi c^4}{2} \left(\frac{\rho_{TR}^4 G_L \psi}{c^4} + G_{TR} \psi - \frac{\rho_{TR}^4 G_{TR} \psi}{c^4} - \frac{4 G_{TR} \tau_{TR}}{3 c G_L} + \frac{4 \rho_{TR}^3 G_{TR} \tau_{TR}}{3 c^4 G_L} + \frac{4 \tau_{TR}}{3 c} - \frac{4 \rho_{TR}^3 \tau_{TR}}{3 c^4} \right). \quad (\text{A.23})$$

Using the relationship

$$c = \rho_{TR} \frac{\psi}{\psi_s} \quad (\text{A.24})$$

the expression is further reduced to

$$T = \frac{\pi c^4}{2} \left(\frac{\psi_s^4 G_L}{\psi^3} + G_{TR} \psi - G_{TR} \frac{\psi_s^4}{\psi^3} - \frac{4G_{TR}\tau_{TR}}{3cG_L} + \frac{4\psi_s^3 G_{TR}\tau_{TR}}{3\psi^3 c G_L} + \frac{4\tau_{TR}}{3c} - \frac{4\psi_s^3 \tau_{TR}}{3\psi^3 c} \right). \quad (\text{A.25})$$

Using another relationship given as

$$\frac{\tau_{TR}}{c} = G_L \psi_s \quad (\text{A.26})$$

the torsion load response is reduced to the form that is presented by Gillet which is

$$T = \frac{\pi c^4}{2} G_L \psi_s \left(\frac{\psi_s^3}{\psi^3} + \frac{G_{TR} \psi}{G_L \psi_s} - \frac{G_{TR} \psi_s^3}{G_L \psi^3} - \frac{4G_{TR}}{3G_L} + \frac{4\psi_s^3 G_{TR}}{3\psi^3 G_L} + \frac{4}{3} - \frac{4\psi_s^3}{3\psi^3} \right). \quad (\text{A.27})$$

A.2 Chapter 2

A.2.1 Continuous Rotating Potentiometer

The angular rotation of the load cell measured using a continuous rotating potentiometer attached to the drive axial of the motor. This location amplifies the measurement by the number of teeth in the worm gear drive (60 times). The disadvantage of this setup was that the accuracy was dependent on the degree of backlash in the worm gear drive. The signal of the continuous rotating potentiometer could not be processed during testing using the existing software. The signal was post-processed from the sawtooth form to the actual angle of rotation using Matlab.

The continuous rotating potentiometer was calibrated by creating a marking on the potentiometer and a reference point. The potentiometer was then rotated 360° (line up the marks again). The excitation voltage across the potentiometer was drawn from the data acquisition board. [Include code tree in appendix, find calibration]

The following is the main Matlab function used to process the potentiometer signal:

```
function [angleout] = procangle2(anglein)
angleout(1) = 0; for i = 1 : length(anglein)
- 1; rateout(i) = anglein(i+1) - anglein(i); if rateout(i) > 100 rateout(i) = rateout(i) - 100
angleout(i+1) = rateout(i) + angleout(i); else angleout(i+1) = angleout(i) + rateout(i-1);
end end
```

In this function the initial angle is zero. Then the difference between the rotational angle of the first data point is compared with the second data point. If the change in rotational angle is higher than ± 100 then it is considered as either a full rotation in the

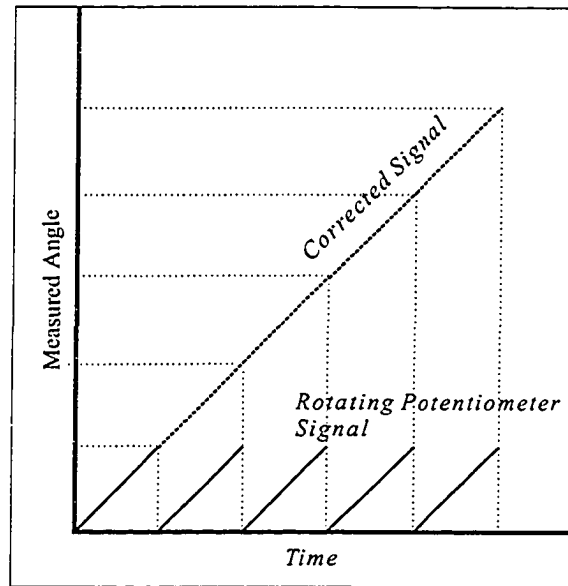


Figure A.1: Continuous rotating potentiometer signal.

potentiometer where the signal steps from 3.9 V to 0 Volts (or visa versa depending on the rotational direction). With this type of potentiometer there is always the possibility that there will be a momentary jump in voltage because of the way that the potentiometer is constructed. In any occurrence it there is a difference in angle determined from the potentiometer of less than 100 degrees it is perceived as a change in angle of the potentiometer as per normal operation. If this is not the difference in angle that was determined from the previous measurement is used as the incremental increase to determine the current value. After the entire data set has been analyzed it required to be checked again to remove any discontinuities in the data.

A.2.2 Design Loads of Torsional Adapter

Component	Material	Failure
1" Shaft	Steel	60800 N
Single #10 Hex Screw	Steel	20000 N
4 #10 Hex Screws	Steel	81000 N
Bearing	-	-
Brass Pin	Brass	50700 N
Load Cell	Aluminum	8500 N
Upper Wire Clamp	Brass	13600 N

A.2.3 Selecting Proper Wire Size for Testing

The wire size chosen for this test reflected the limitation of the load cell. The wire size was required was small enough that the load cell could be safely used in axial loading while having enough sensitivity to measure the torque applied to the wire. The expected error of the torsional load cell of ± 7.5 Nmm and the yield stress for a NiTi SMA wire was assumed to be 487 MPa [SMA Inc]. Based on this information the ratio of the noise to yield stress and axial yield load was plotted as a function of the wire diameter as shown in Figure A.2 in order to determine the optimum wire size to be selected for the experimental tests. The maximum wire size was limited to the safe operating limit of the combined axial and torsional load cell to be 2125 N (Safety Factor of 4) which would limit the wire diameter to more than 1.982 mm. For torsional loading as the wire size decreased, the yield torque also decreased which would make the uncertainty in the torsional load cell more prominent. Thus with this in mind it was required that the wire size be as close but not over 1.982 mm. The wire that was donated to this project by the Special Metals Cooperation in Utica, New York had a diameter of 1.564 mm.

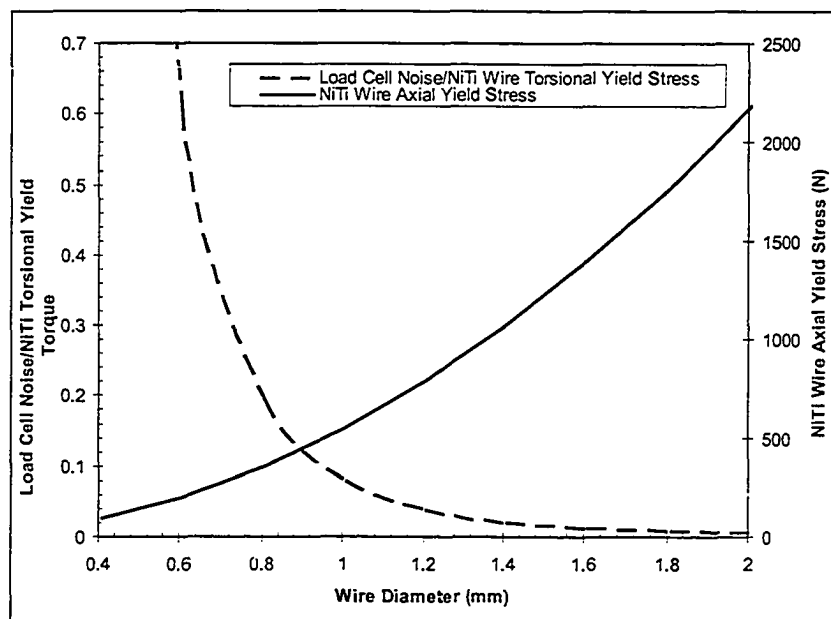


Figure A.2: Torsional load cell noise ratio to torsional yield load and axial yield load as a function of wire diameter.

A.3 Chapter 3

- Complete Torsional Derivation
- Quadratic Relation for shear modulus and LSR
- Effect of noise on the PLSLR Method
- MatLab Code
- Axial/Torsioal Load Response Prediction

A.3.1 Torsional Load Response Derivation

Solving the integral given by equation 3.10 the torsional load response becomes

$$T_{TR} = \frac{2\pi c^4 G_{TR} \theta}{4L} - \frac{2\pi \rho_y^4 G_T \theta}{4L} - \frac{2\pi c^3 G_{TR} \tau_{TR}}{3G_L} + \frac{2\pi \rho_{TR}^3 G_{TR} \tau_{TR}}{3G_L} + \frac{2\pi c^3 \tau_{TR}}{3} - \frac{2\pi \rho_{TR}^3 \tau_{TR}}{3}. \quad (\text{A.28})$$

From equation 3.10, ρ_y as defined by equation 3.9 is put in this equation to give

$$T_T = \frac{\pi c^4 G_{TR} \theta}{2L} - \frac{\pi G_{TR} \theta}{2L} \left(\frac{\tau_y L}{G_L \theta} \right)^4 - \frac{2\pi c^3 G_{TR} \tau_y}{3G_L} + \frac{2\pi G_{TR} \tau_y}{3G_L} \left(\frac{\tau_y L}{G_L \theta} \right)^3 + \frac{2\pi c^3 \tau_y}{3} - \frac{2\pi \tau_y}{3} \left(\frac{\tau_y L}{G_L \theta} \right)^3 \quad (\text{A.29})$$

which is simplified to

$$T_T = \frac{\pi c^4 G_{TR} \theta}{2L} - \frac{\pi G_{TR} \tau_y^4 L^3}{2G_L^4 \theta^3} - \frac{2\pi c^3 G_{TR} \tau_y}{3G_L} + \frac{2\pi G_{TR} \tau_y^4 L^3}{3G_L^4 \theta^3} + \frac{2\pi c^3 \tau_y}{3} - \frac{2\pi \tau_y^4 L^3}{3G_L^3 \theta^3} \quad (\text{A.30})$$

and can be further simplified to give equation 3.11.

A.3.2 Other Methods used to Determine the Transformation Yield Point

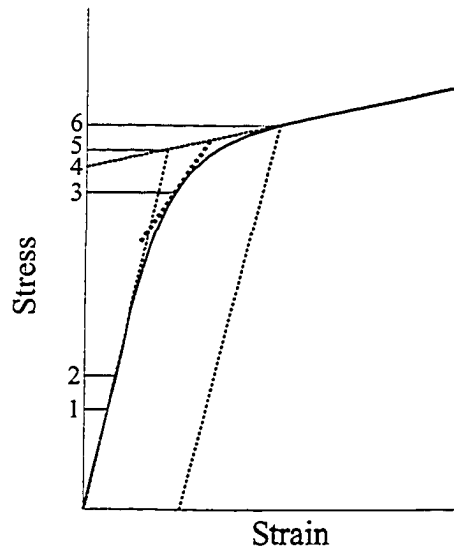


Figure A.3: Methods to Determine the Transformation Yield Point [Haythornthwaite, 1968]. (1) Departure from linearity, (2) Measurable plastic strain, (3) Slope of the diagram equal to a given fraction of the initial slope, (4) Intersection of the post-yield slope (transformation slope) with the stress axis, (5) Intersection of post-yield (transformation slope) and elastic slopes, (6) Offset elastic slope.[Haythornthwaite, 1968]

A.3.3 Number of Data Points to be used with Tangent Modulus Method

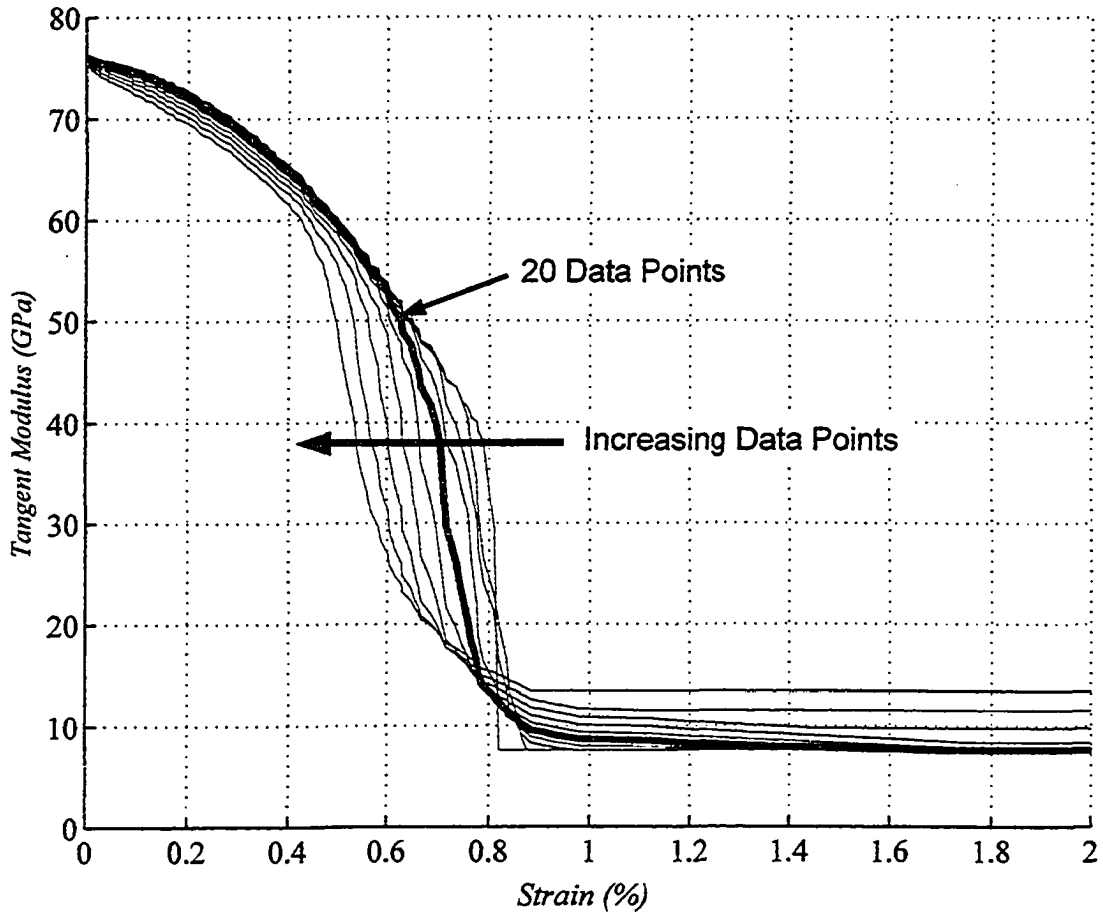


Figure A.4: Comparison of the axial tangent modulus using different amount of data points. The axial tangent modulus was determined from the axial load response test function. As the number of data points used in the Tangent Modulus Method the slope curve deviates to the left. All the curves for the different amount of data points appear to converge at around 0.8% strain and a tangent modulus of around 12 GPa. Using a critical modulus of around 12 GPa would have little error in the transformation yield point as determined using the yield tangent modulus method with any number of data points from 2 to 50.

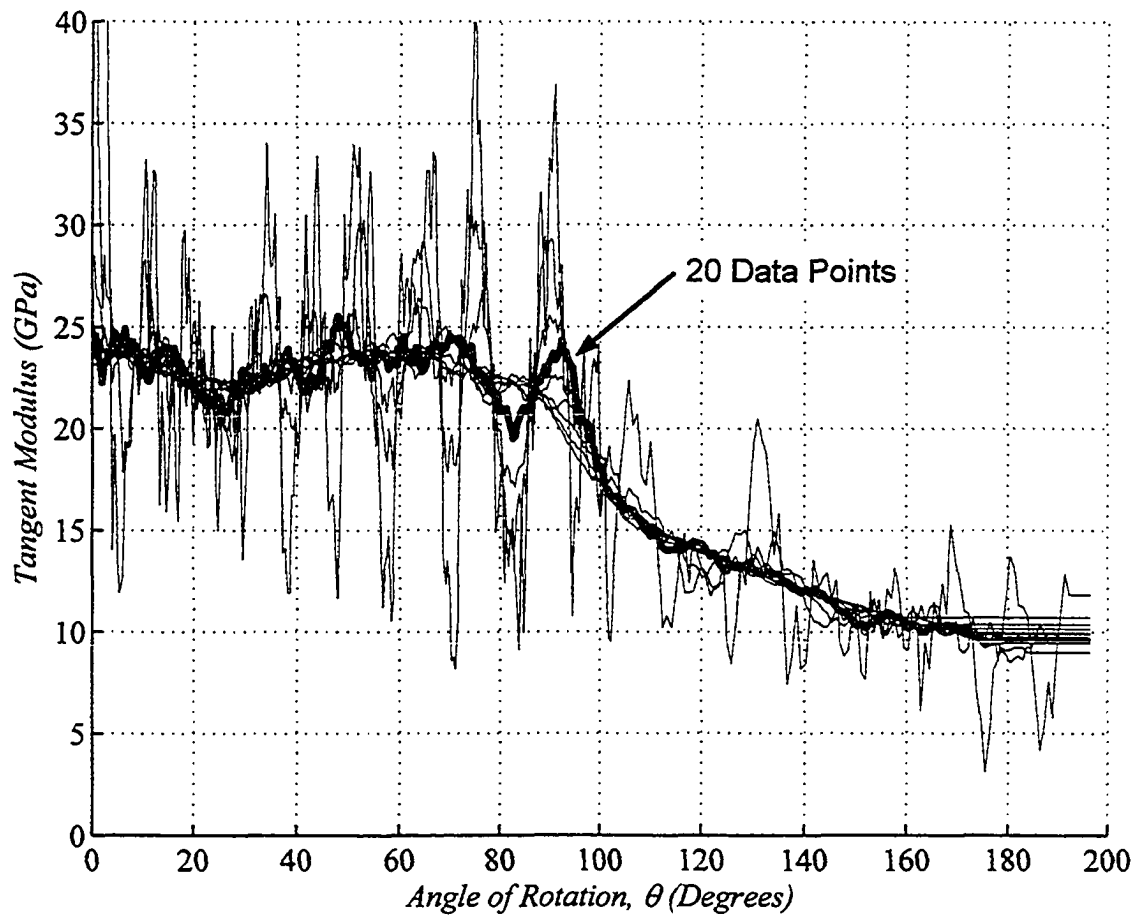


Figure A.5: Comparison of the torsional tangent modulus using different amount of data points. The torsional tangent modulus was determined from the torsional load response test function. Using more data points in the tangent modulus method decreased the fluctuations in the maximum and minimum tangent modulus in the linear elastic region.

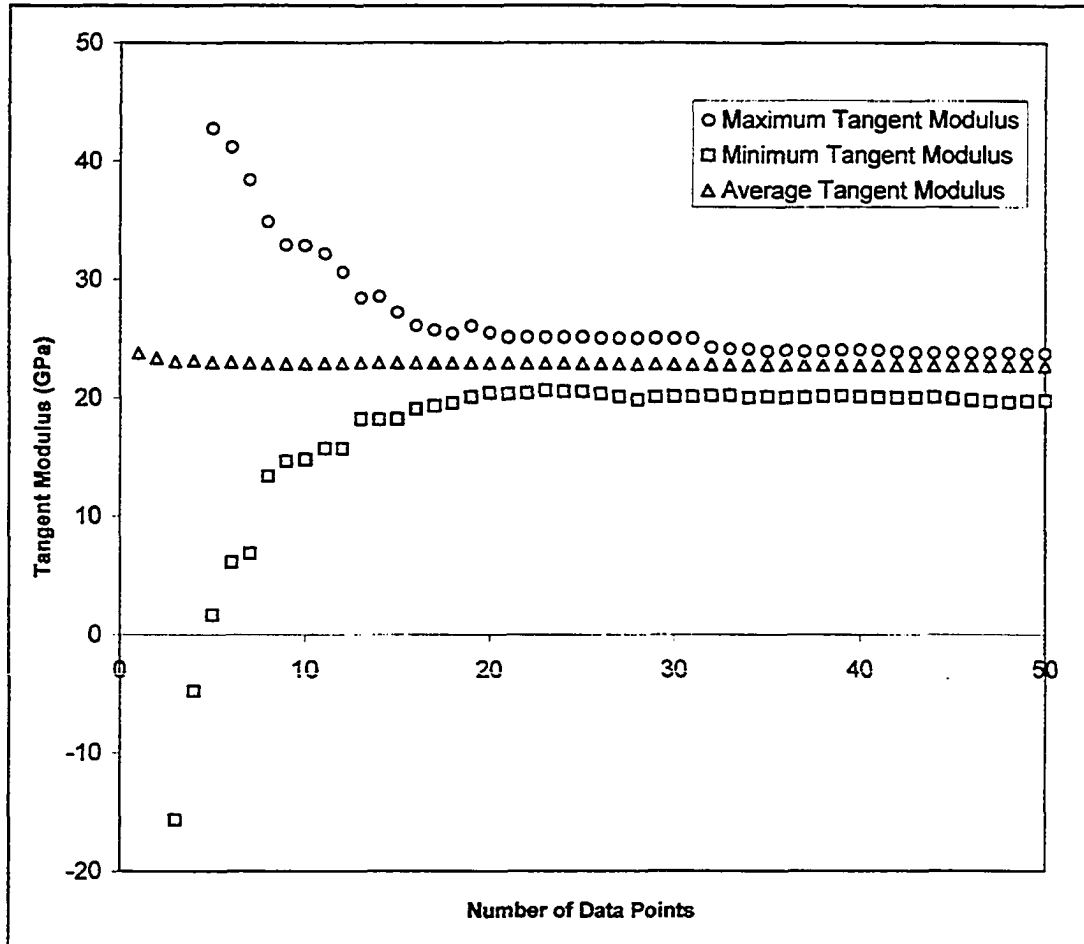


Figure A.6: Maximum, Minimum and Average Values of the Tangent Modulus for the Torsional Load Response. Using the torsional load response test function it was found that increasing the number of data points in the tangent modulus method decreased the uncertainty of the tangent modulus determined for the linear elastic region. As shown in this figure, using 20 data points or more there is a little increase in accuracy with increase of number of data points used.

A.3.4 Error in Yield Tangent Modulus Method for Determining the Transformation Yield Stress

The error in the yield tangent modulus methods for determining the transformation yield stress was determined for the test function given in Section 3.3. In this figure each critical yield modulus value was compared with the tangent modulus of the test function which is the slope of the axial load response. Using the forward search technique the tangent slope is compared with the Yield Modulus starting at the beginning of the data set. The transformation yield point is found when the tangent slope of the test function is lower than that of the yield modulus. From Figure A.7 the error in the determined transformation yield stress compared with the test function value is plotted versus the proposed value to use in the yield tangent modulus method for the critical yield modulus. Although at about 12 GPa it appears that this is zero error with using this value with the yield modulus method it is expected that the exact value may change with the experimental load response. For argument sake if the actual experimental curve was the same as the test function except it shifted right 1 GPa the error in the determined transformation yield point would increase by 20% and by 40% for a 2 GPa shift. On the other hand if the critical yield modulus value was chosen to be 15 GPa the worst case scenario for the difference between the experimental data and the test function would be a shift in the function to the right. If the experimental data was similar to the test function but shifted to the left 5 GPa the only change in error would be 2.5%.

In conclusion it would be safer to use a critical modulus higher than 12 GPa for the yield tangent modulus method.

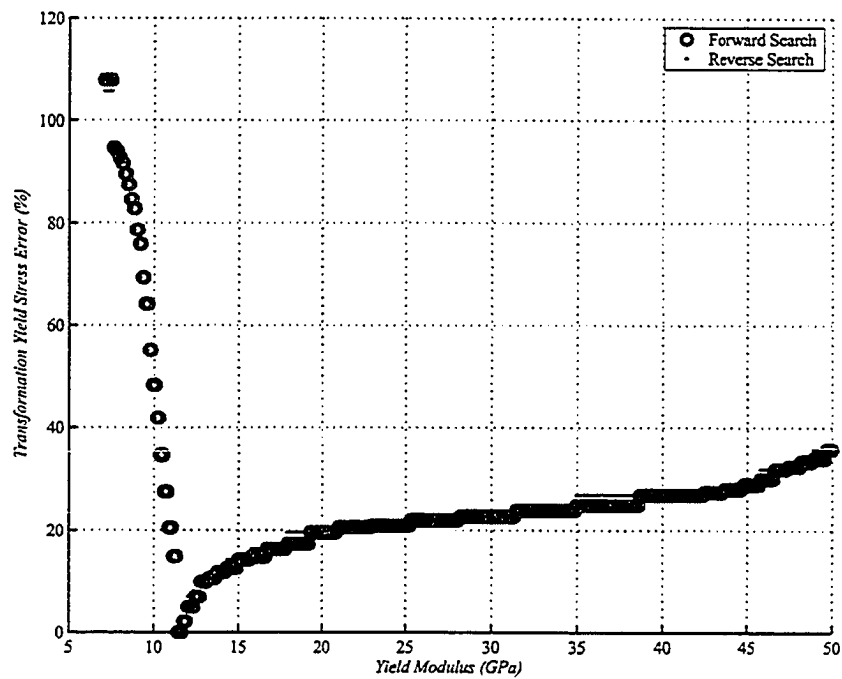


Figure A.7: Error in yield tangent modulus method for axial load response

A.3.5 Error in Yield Tangent Modulus Method for Determining the Transformation Yield Shear Stress

Determining the error with the yield tangent modulus method for torsional load response is performed in the same manner as the axial load response as described in Section A.3.4. The difference with the torsional load response is its shape and how it affects the yield tangent modulus method. By having an indistinct transformation yield point and high noise in the torsional load response it becomes difficult to use the yield tangent modulus method with a forward search (Beginning at the start of the data set and working forward.) Using the forward method it is possible to have a determined modulus that is lower than the modulus at the actual transformation yield point but is still well within the linear elastic region. This is shown in Figure A.8 as the sharp increase in the error when the critical yield modulus is higher than 21 GPa. By performing the search in the reverse direction (starting at the end of the data set and working reverse to find when the determine tangent modulus of the load response is higher than the critical yield modulus) the high uncertainty that is associated with the linear elastic region is avoided and there is no sharp change in error if the actual yield modulus in the experimental load response is slightly different than that of the test function that is shown here. Thus in conclusion it is preferred to use the reverse search when using the yield tangent modulus method for determining the transformation yield shear stress. The value to use as the critical modulus is 21 GPa.

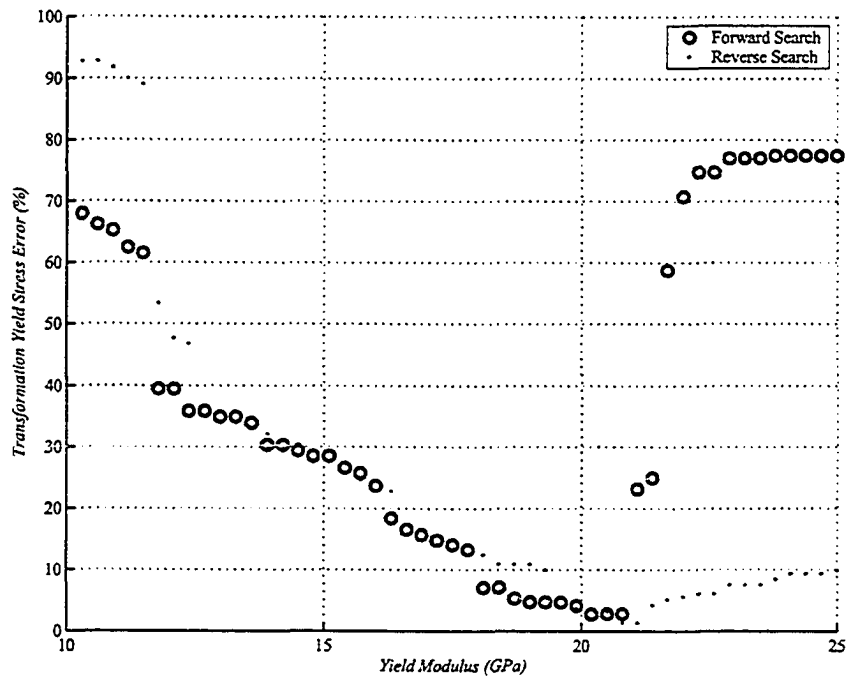


Figure A.8: Error in yield tangent modulus method for torsional load response

A.3.6 Quadratic Relation of the Standard Deviation of the Residual

In Figure A.9 is a sample run with the Piecewise Smooth Least Squares Regression method where the sum of the squares of the residuals is plotted for 11 points ranging from the ratio of the shear modulus from 0 to 1. As seen here the function follows a quadratic relationship perfectly allowing for only 3 points to be processed by the PLSR method and the minimum value be calculated from that.

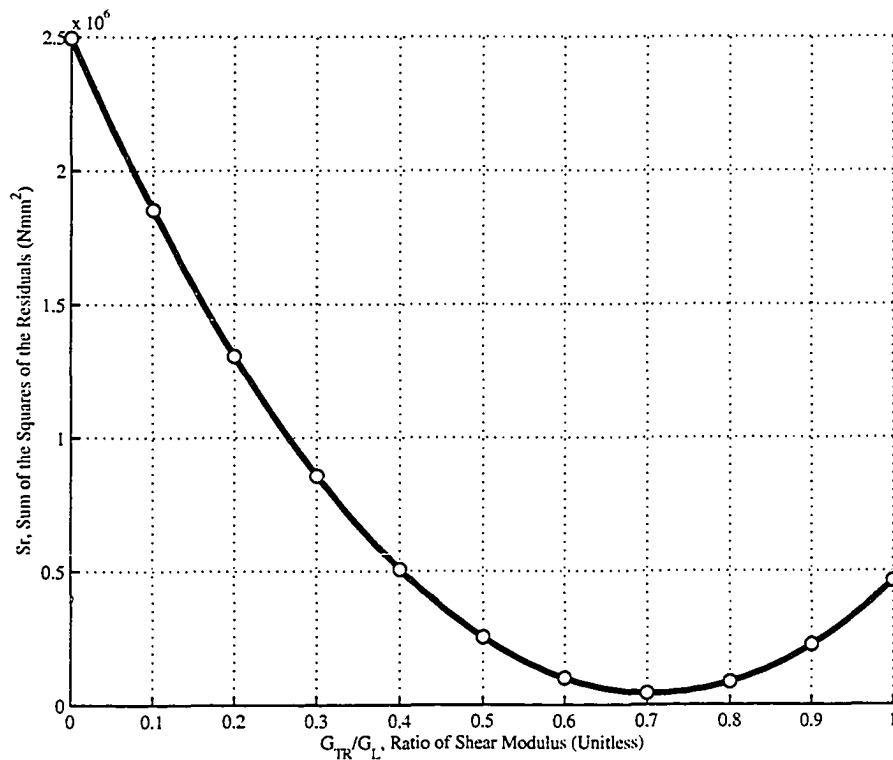


Figure A.9: Quadratic relation between the standard deviation of the residual and the ratio of the shear modulus.

A.3.7 How Noise Affects the PLSLR Method

The benefit of the PLSLR method is that it fits the torsional load response to the experimental data and determine the material properties as the values that give the best fit between the data and the function. This was a requirement for this research as there was excessive noise in the torsional load response (± 7.5 Nmm). In Figures A.10 to A.12 is an illustration of the expected error in the PLSLR method with a given amount of noise in the torsional load cell for different degrees of axial preloading ranging from 0 to 480 MPa.

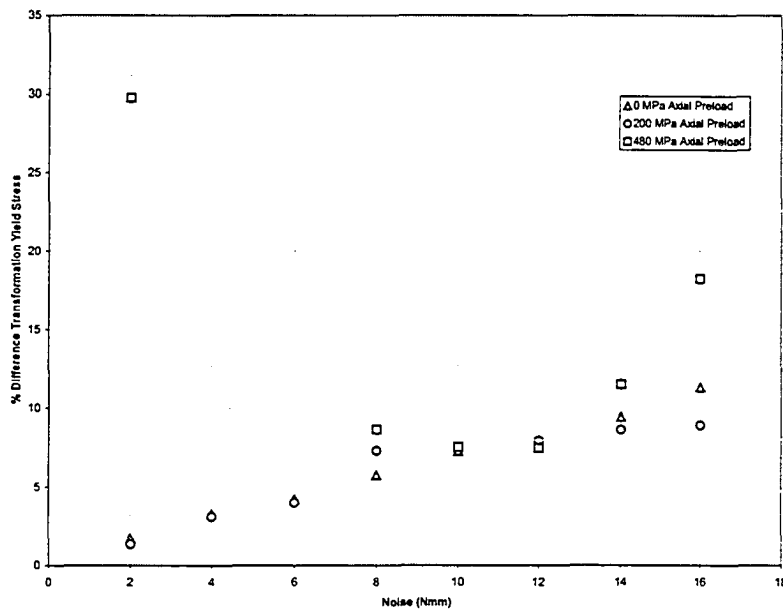


Figure A.10: Error in the transformation yield stress as a function of noise for the PLSLR method.

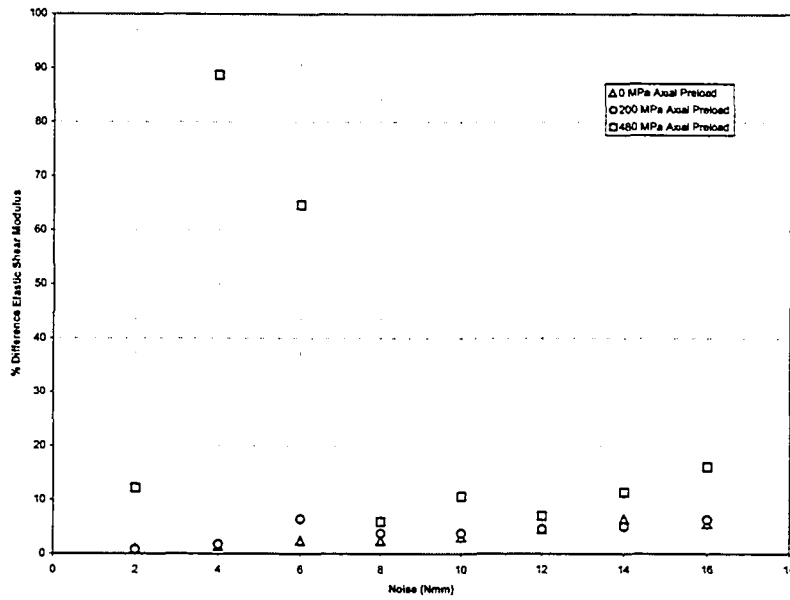


Figure A.11: Error in the elastic shear modulus as a function of noise for the PLSR method.

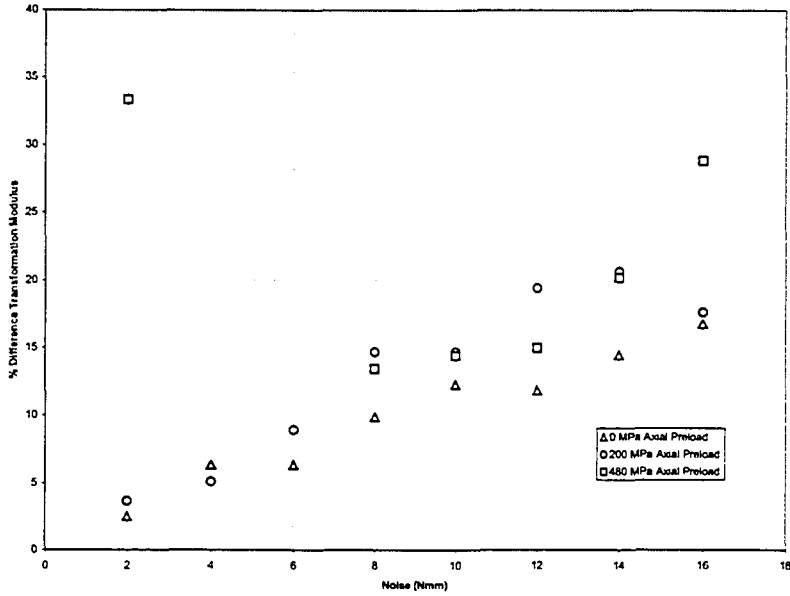


Figure A.12: Error in the transformation shear modulus as a function of noise for the PLSR method.

A.4 Chapter 5

The equation for spring stiffness is typically given as

$$P = K\Delta x, \quad (\text{A.31})$$

where P is the applied load, K is the spring constant and x is the elongation of the spring. The axial stress on a wire specimen is given as

$$\sigma = \frac{P}{A} \quad (\text{A.32})$$

where A is the cross section of the wire specimen. For a linear elastic material the relationship between the stress and the strain of the specimen is given as

$$\sigma = E\epsilon \quad (\text{A.33})$$

where E is the elastic modulus. The strain of the specimen given as ϵ can be defined as

$$\epsilon = \frac{\Delta x}{L} \quad (\text{A.34})$$

where L is the length of the wire specimen. The load on the wire can be defined from equations A.31 to A.34 to be

$$P = \sigma A = EA\epsilon = \frac{EA}{L}\Delta x = K\Delta x \quad (\text{A.35})$$

where the spring stiffness can be defined from this equation as

$$K = \frac{EA}{L}. \quad (\text{A.36})$$

APPENDIX B

EXPERIMENTAL PROCEDURE

The experimental procedure was required to be drawn up for the apparatus that was built at the University of Alberta Mechanical Engineering Department. The following sections are detailed instructions that were used to set up the equipment, perform the instrument calibration and perform the tests.

- The ram for the MTS tester is set 2' - 2" above the lower grip
- Disconnect the potentiometer
- Remove the motor
- Wrap Load Cell Cables Around Load Cell
- Screw in the MTS bolt into the upper MTS RAM
- Slide on the locking clamp onto the bolt and then screw on the torsional adapter (Face the the torsional adapter so that the worm drive is in plain view while testing)
- install the motor, and potentiometer connection.

B.1 Loading a Specimen

The most reliable method to load a specimen is to start the machine in stroke control. Make sure that the dial is turned counter clock wise (+10) so that the lower ram does not come up and contact the torsional adapter.

1. The most reliable method to load a specimen is to start the machine in stroke control. Make sure that the dial is turned counter clock wise (+10) so that the lower ram does not come up and contact the torsional adapter.

2. Rotate the displacement dial clock wise until the dial reads exactly on 5. You may have to adjust the stroke zero dial so that the lower ram does not contact the torsional adapter during this step.
3. Using a calibration block or a measuring device, adjust the stroke zero dial until the ram distance is set for the initial testing length.
4. Lower the ram by turning the stroke dial CCW, enough to mount the specimen in the lower grip.
5. Once the lower grip is secured, raise the ram (Stroke Dial) until the ram is at the initial position. The wire will have to be guided into the upper grips. Once in position the upper grips can be secured.
6. If the test requires the at the MTS strain extensometer is to be used, it would me now mounted on to the specimen. There are special knives for the extensometer that are notched which are used to test wire specimens.
7. If the test is to be stress controlled, the control is to be changed from stroke control to stress control. This is done by making sure that the strain and stress is zero. The stroke should already be at zero by the previous steps. This can be checked by the viewing knob. Hold down the stress button to switch to stress control. If it does not switch over, slowly turn the stroke knob back and forth till it switches.
8. Note: Whatever control that the machine is under (Stress, Strain and Stroke), the knobs values reflect that particular control. In other words, the knobs used in stroke motion are now used in stress control.
9. To control the rate of the motion of the MTS machine, the rate button beside the position button is set. The values on the know reflect the range setting of the MTS machine.
10. To start the rate controlled stress or displacement, hit the start button. To return to zero, press the return to zero button. For any reason if you would like to pause the rate stress/ displacement, press the hold button.

11. Once the test is completed, make sure that the controls are returned to zero loading and power down the testing machine. And the specimen can be removed from the grips.
12. When the machine is powered down, it can be switch to stroke control and a new specimen can be loaded.

One of the difficulties faced with testing SMA wire was that the wire was prone to slipping from the grips during the preliminary testing. Proper maintenance and cleaning of the brass clamps along with sanding the ends of the SMA specimen increase the load capacity of the brass grips.

B.2 Calibration

B.2.1 MTS Calibration

The load cell for the MTS machine was calibrated by the Mechanical Engineering Department and the extensometer was calibrated at the beginning of the project using an extensometer calibration device.

B.2.2 Torsional Adapter Calibration

In the table below is a summary of the failure of the components used to connect the load Cell to the MTS testing machine.

Component Failure	-
Load Cell	8500 N
Brass Pin	50670 N
4 - number 10 hex Screws	81480 N
1" Bolt	608000 N
Wire Clamp	13600 N

Load Cell is a 6160 Aluminum tube of a length 114.3mm and an outside diameter of 15.440mm. Based on Engineering Failure Calculations, the tube will yield at 8000N of Axial Load or 35000 Nmm of torsional loading. Both the axial and torsional strain gauge bridges are full wheatstone bridges. The axial load cell strain gauges are orientated to take advantage of the poisson effect.

B.3 Addition Equipment Used

B.3.1 Differential Scanning Calorimeter, DSC

Applications: The differential scanning calorimeter (DSC) measures temperatures and heat flow associated with thermal transitions in materials. These measurements can be utilized to determine the melting point and glass transition temperatures of materials, as well as heats of fusion, specific heat capacities, crystallinity, purity, degree of cure, and reaction kinetics.

Operation: The DSC uses a thermoelectric (constantan) disc to transfer heat to the sample material and an inert reference, both of which sit in pans on raised portions of the disc. Differential heat flow to the sample and reference is monitored by Chromel constantan thermocouples. The change in temperature of the sample and reference, when heated at a known rate in a controlled environment, will be similar (depending on specific heat differences) unless the sample undergoes heat-related changes. During these changes, the sample will either absorb or evolve heat. The temperature difference between sample and reference resulting from such a heat effect can be related to the differential heat flow to provide valuable material property information.

APPENDIX C

EXPERIMENTAL COMBINED LOAD TESTS

C.0.2 Training

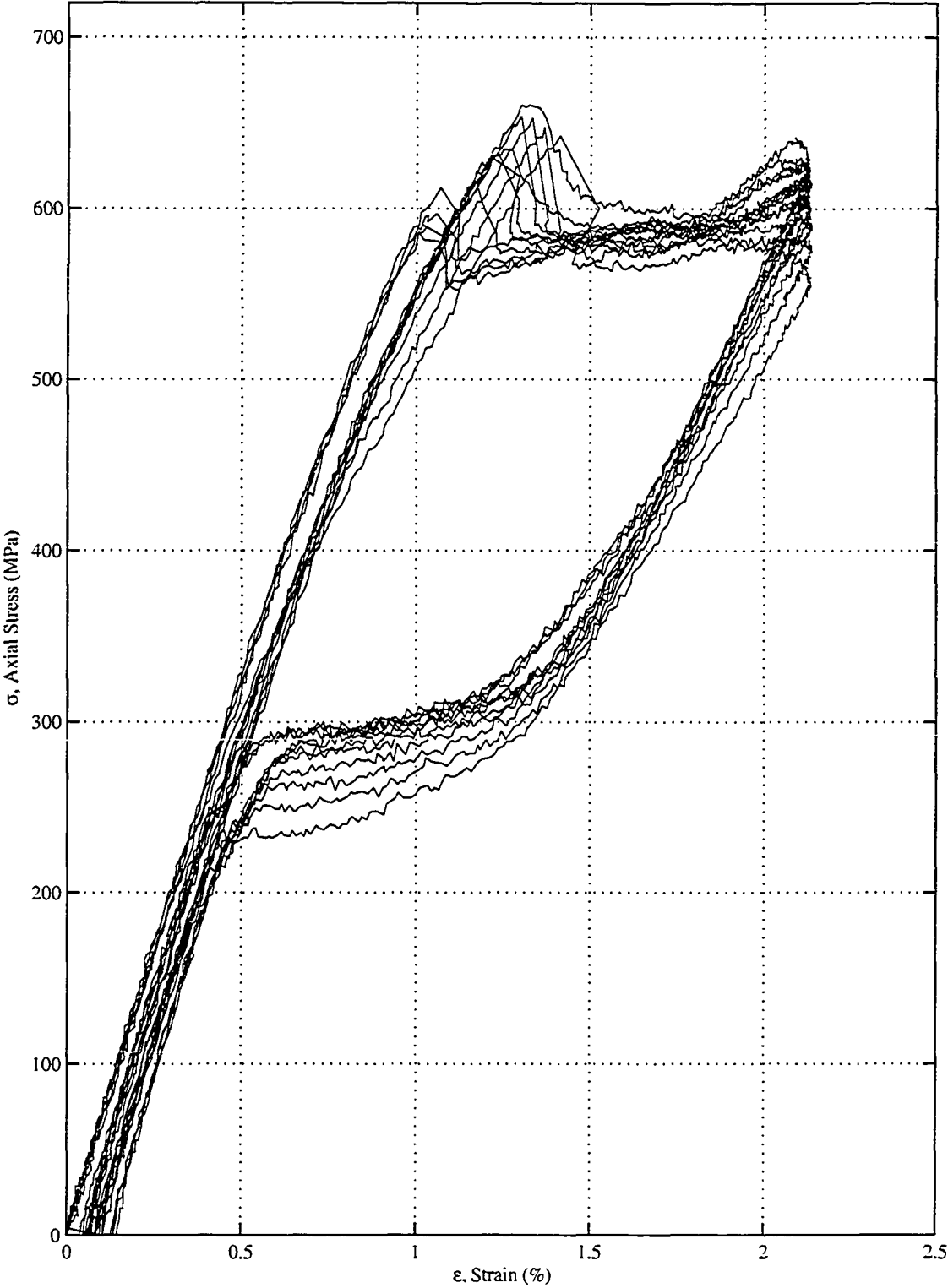


Figure C.1: Strain controlled axial training of sample 1

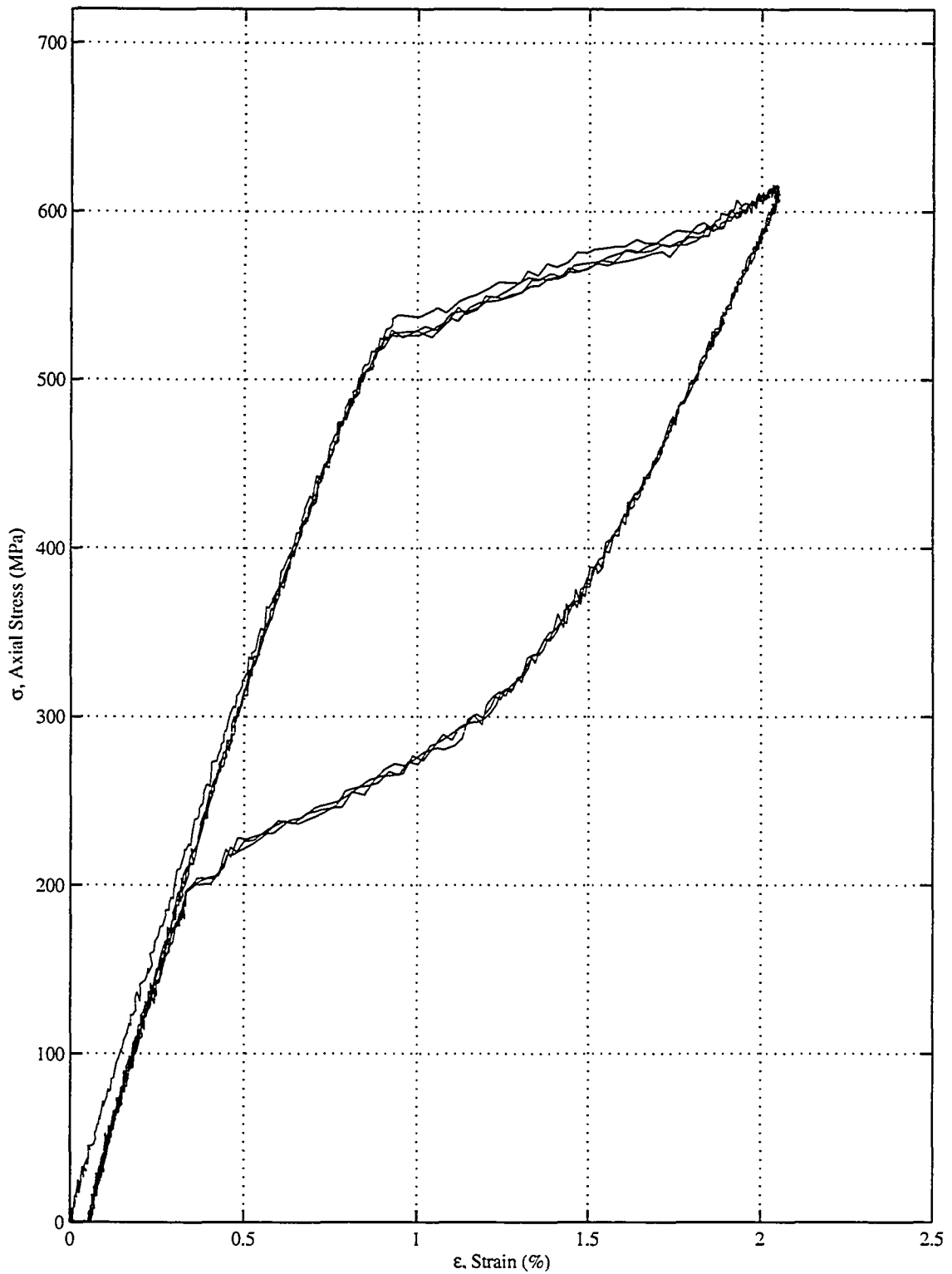


Figure C.2: Load controlled axial training of sample 1

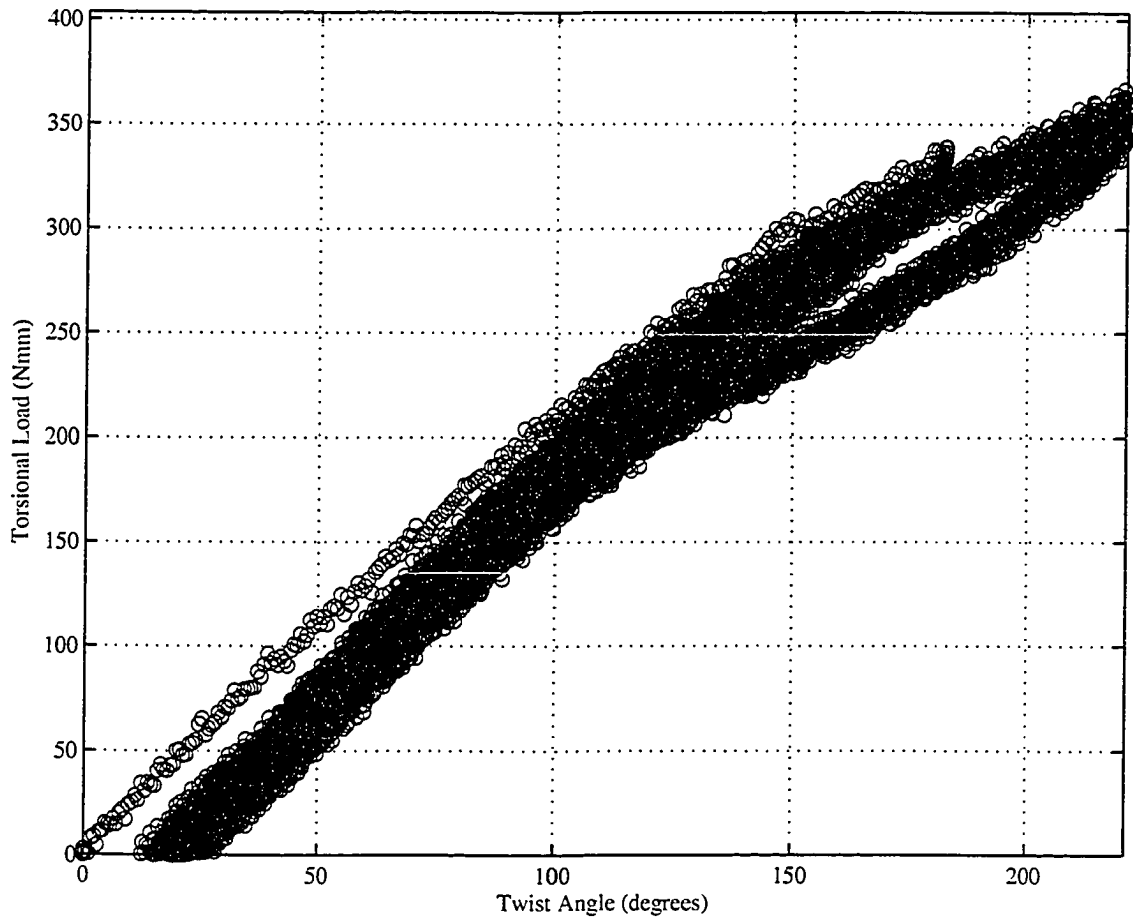


Figure C.3: Torsional Load Training of Sample 1

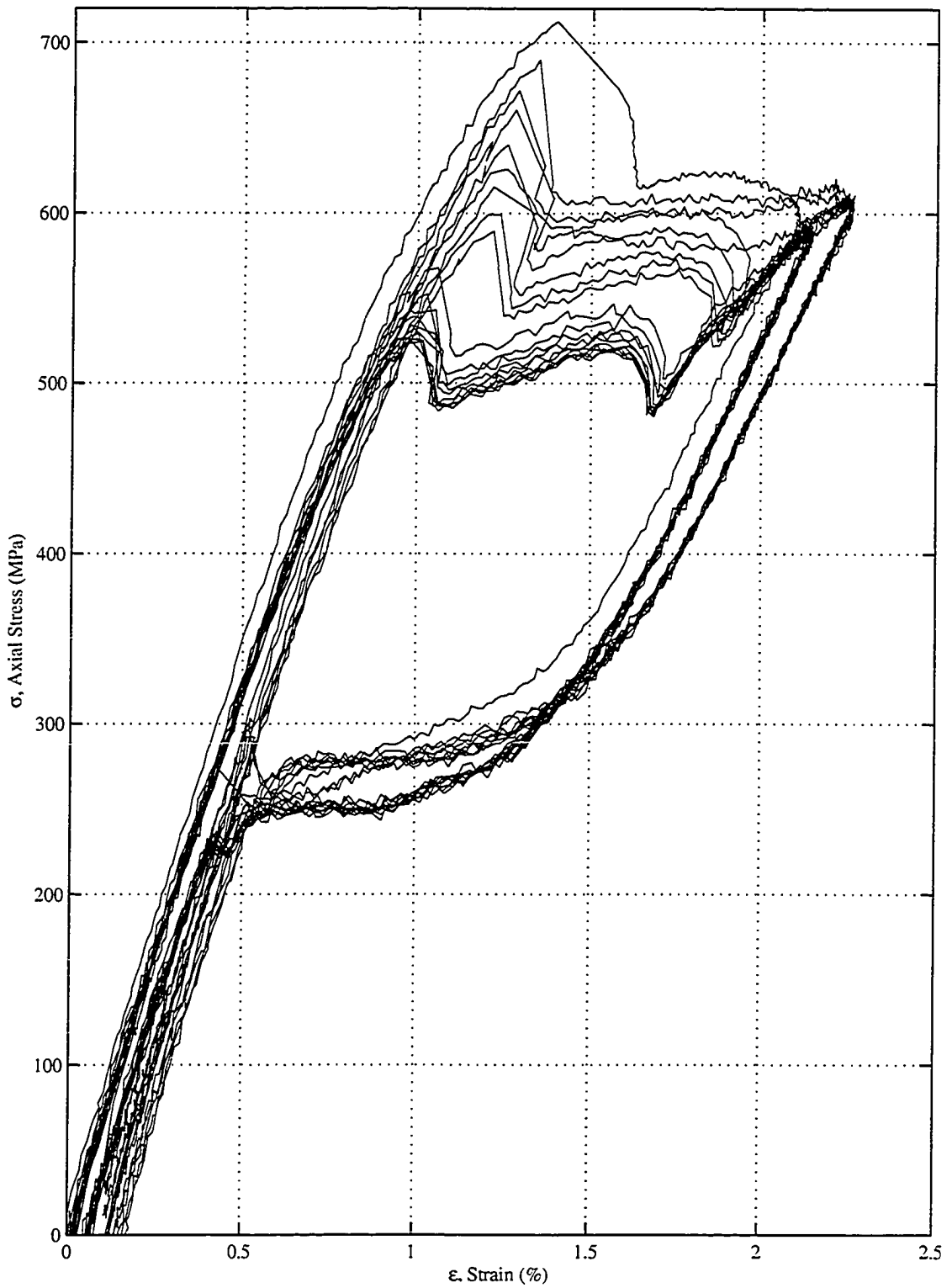


Figure C.4: Strain controlled axial training of sample 2

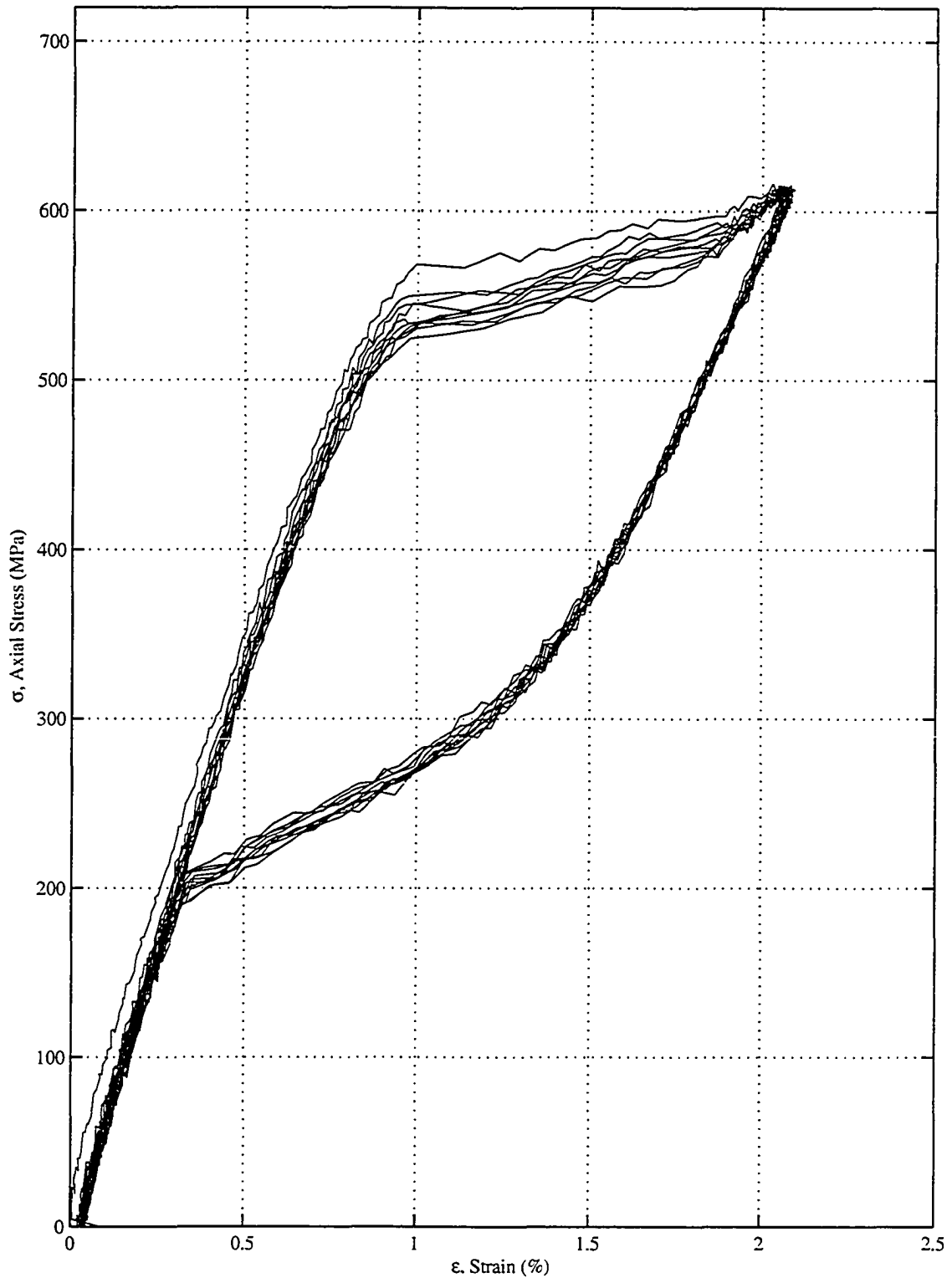


Figure C.5: Load controlled axial training of sample 2

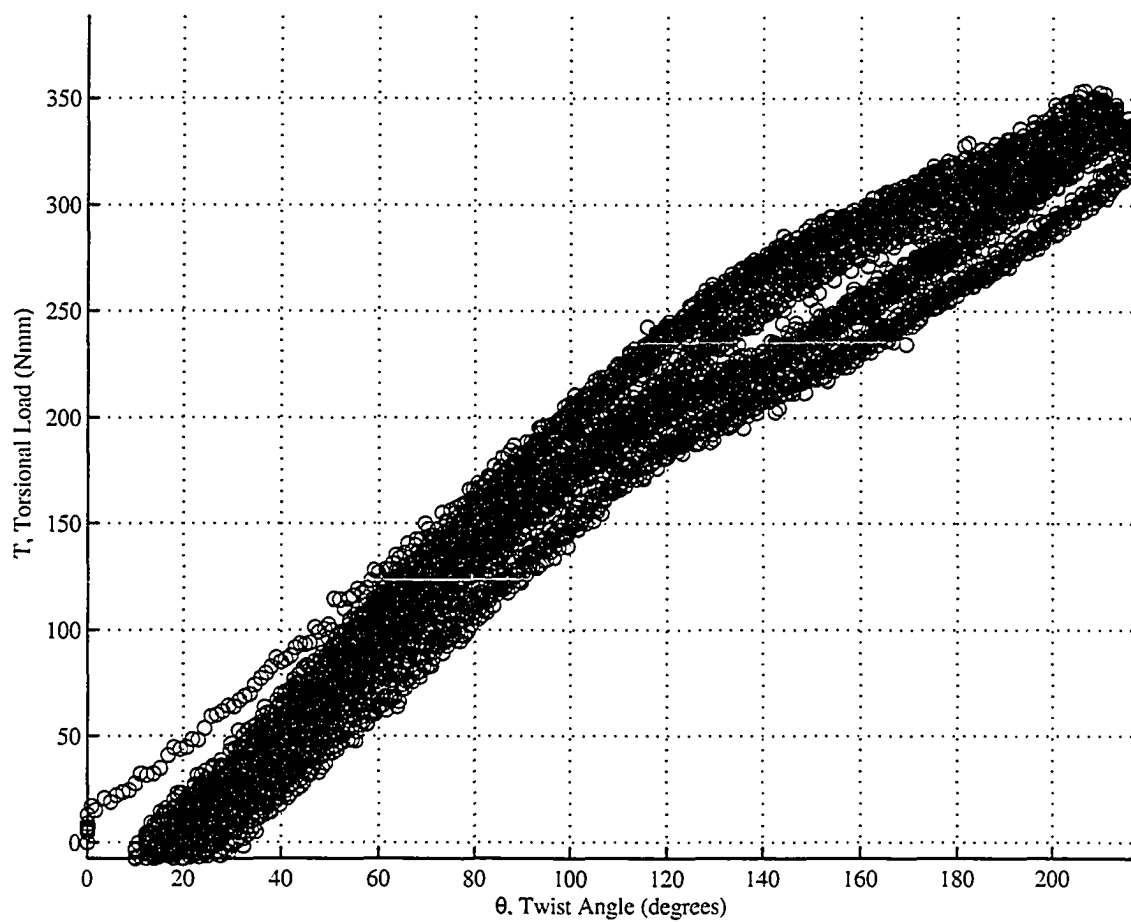


Figure C.6: Torsional Load Training of Sample 2

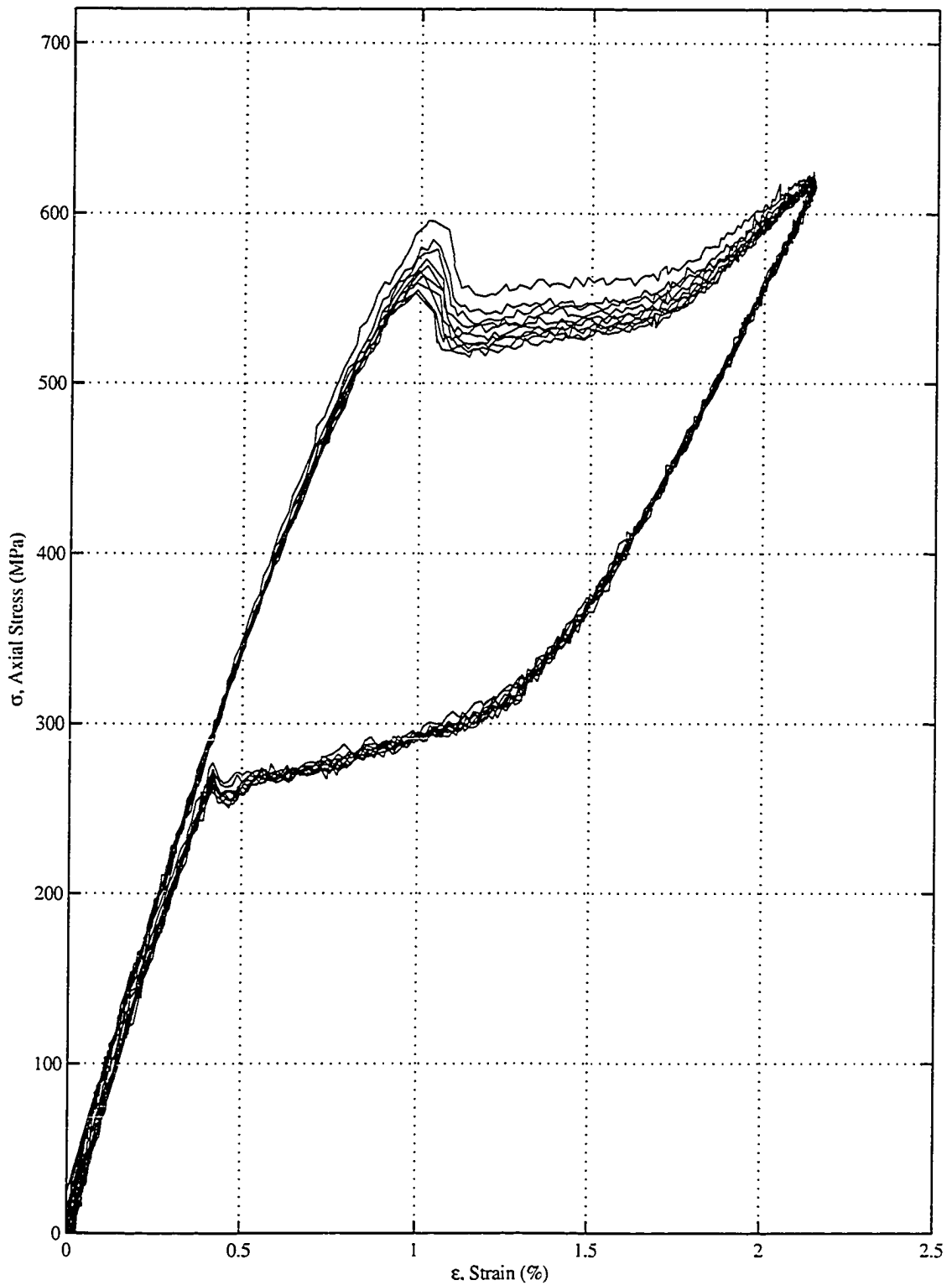


Figure C.7: Strain controlled axial training of sample 3

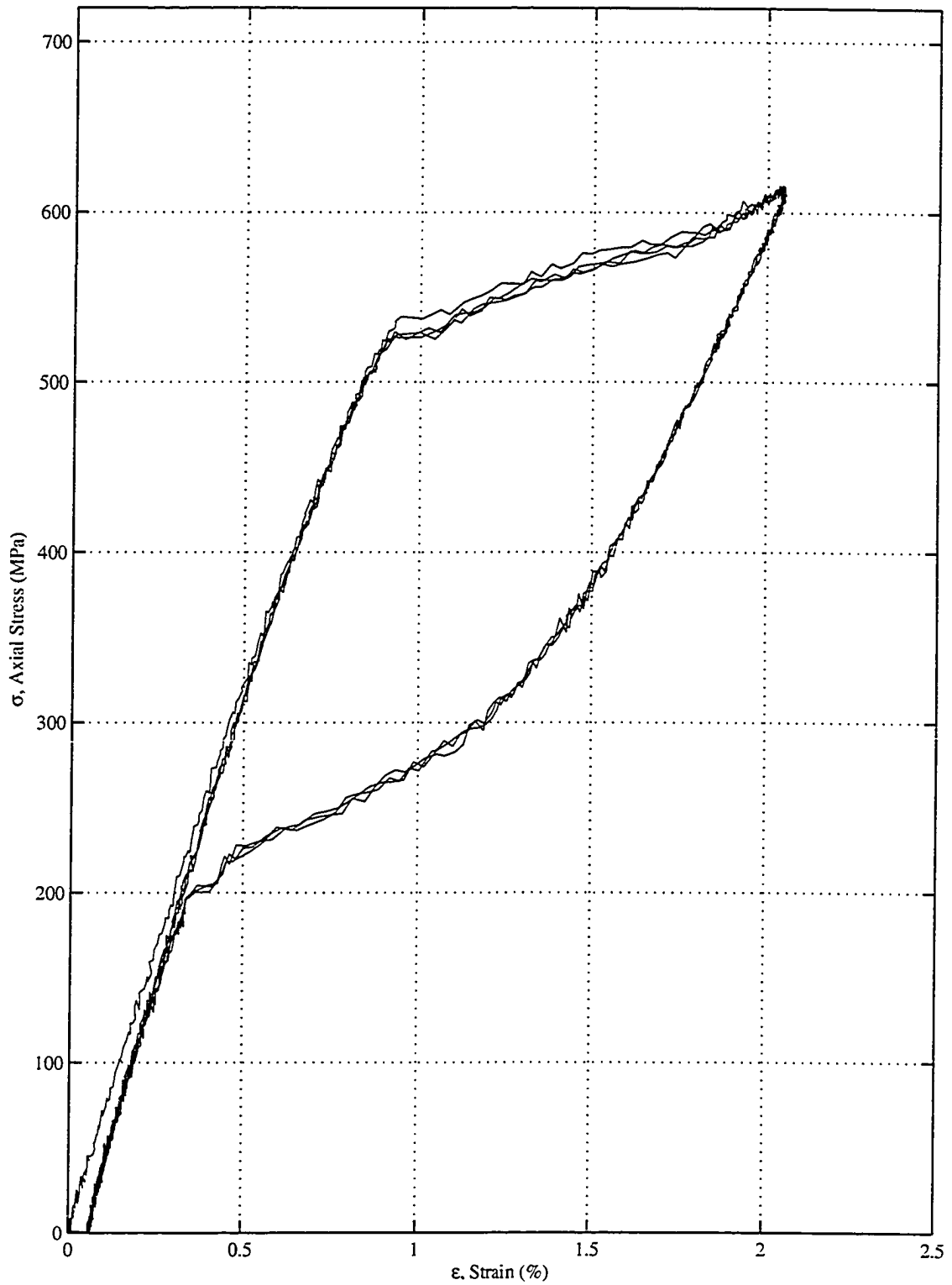


Figure C.8: Load controlled axial training of sample 3

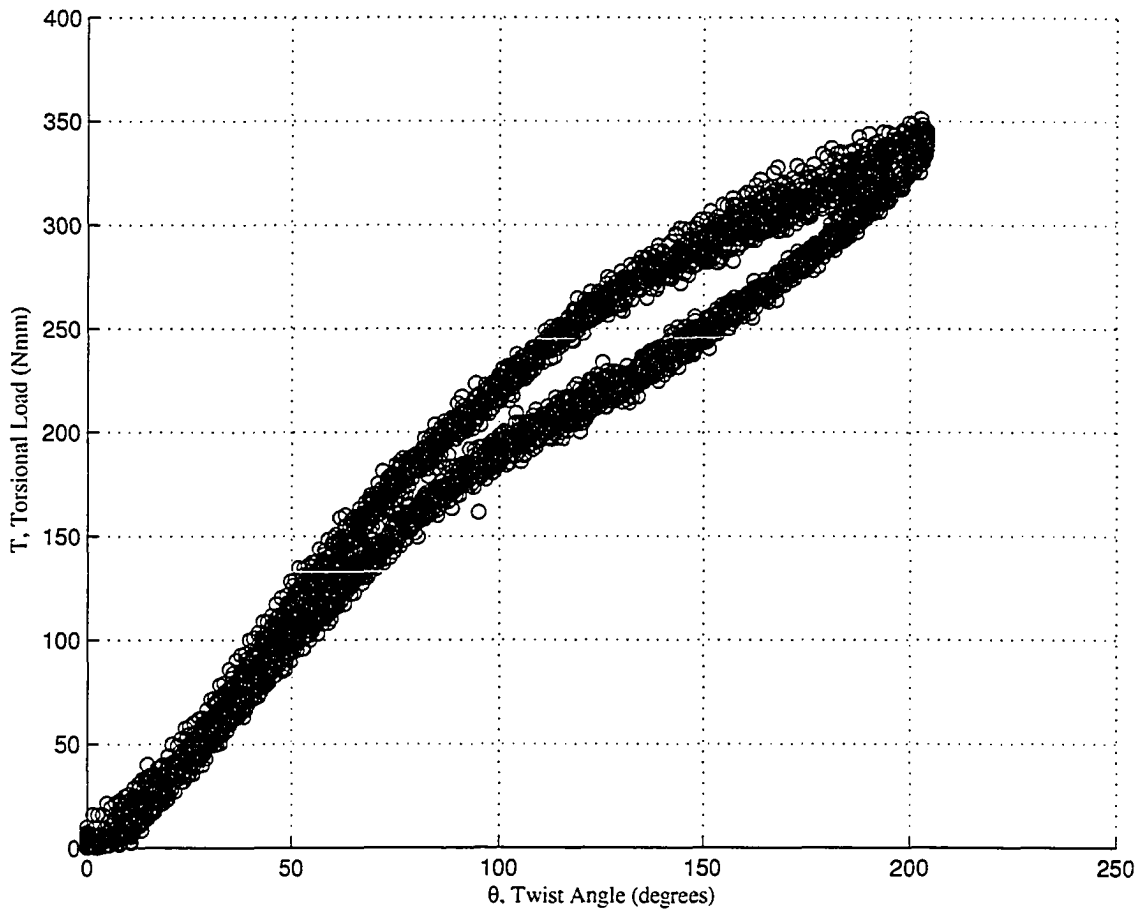


Figure C.9: Torsional Load Training of Sample 3

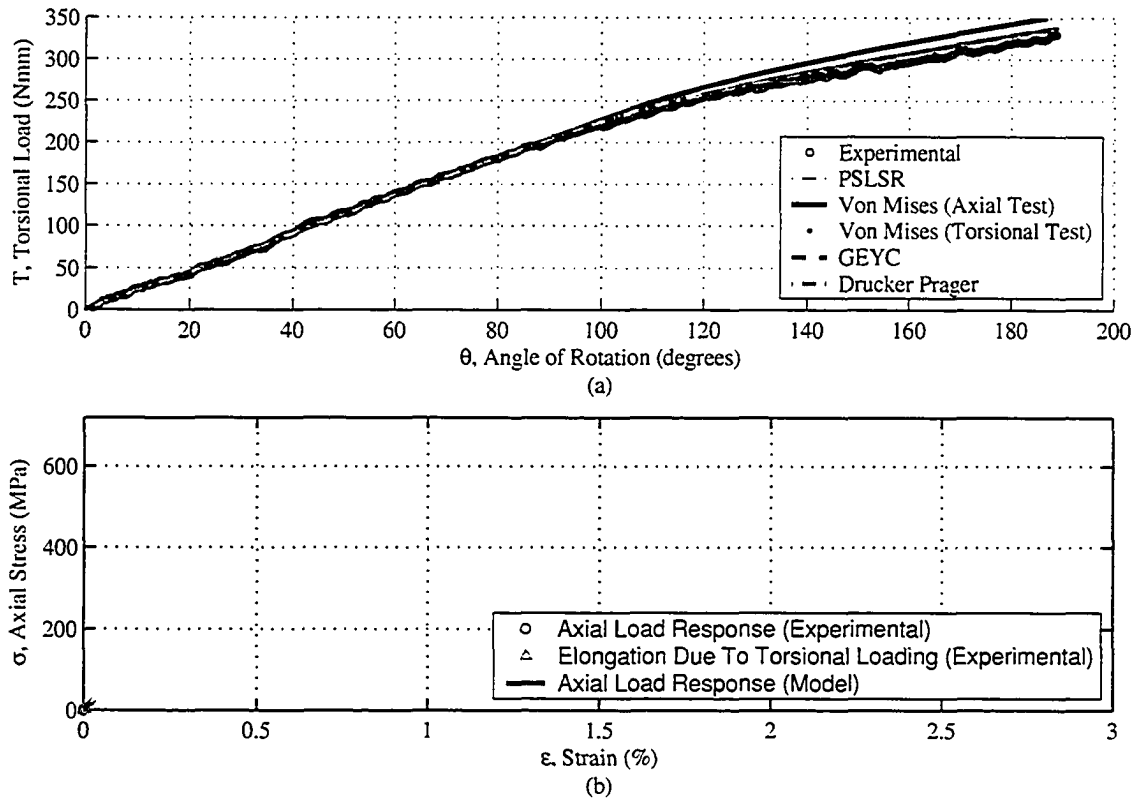


Figure C.10: Sample 1, Test 1: Pure torsional load response with Theoretical Prediction

C.0.3 Sample 1 Testing

To reduce the number of pages in the appendix, only a few of the cases for the first sample and first test are shown here. In total there were three samples and each sample was tested three times at 0, 60, 115, 233, 350, 470 N axial preload. There was three tests perform on each of the three samples with only axial loading. The summary of the material properties determined from these load responses are shown in Section C.1.

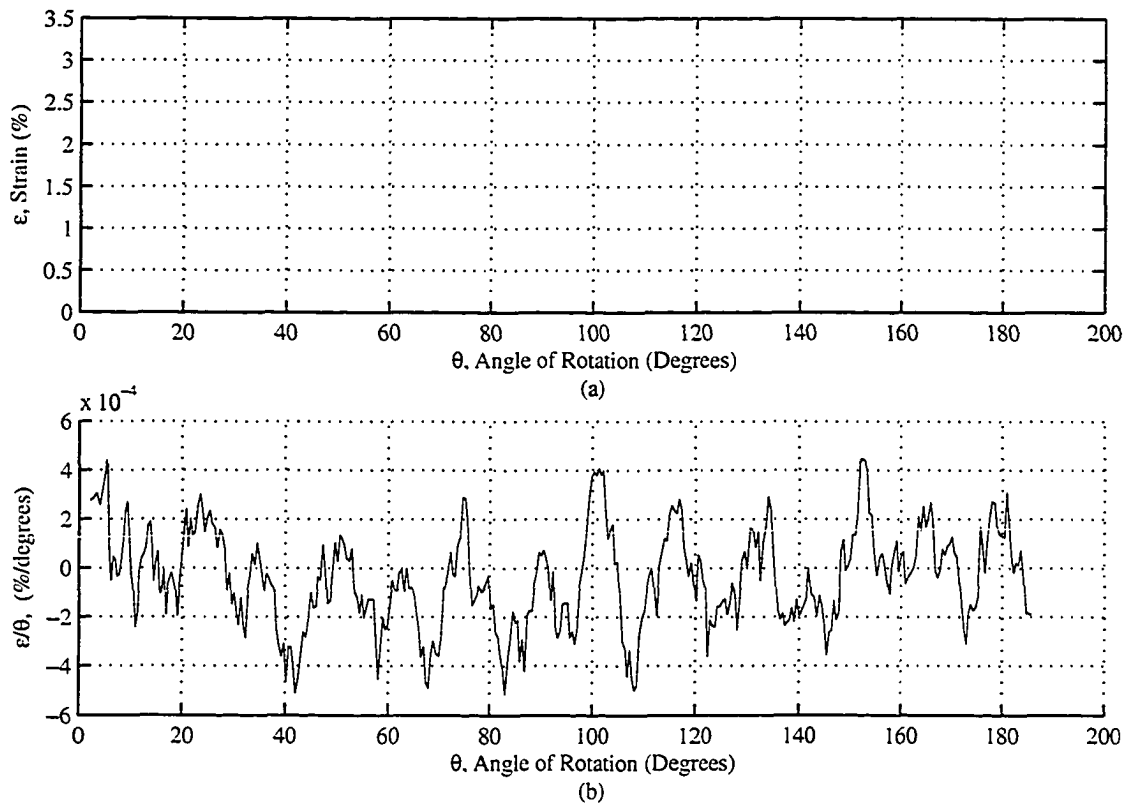


Figure C.11: Sample 1, Test 1: Pure torsional load response - Experimental axial strain and torsional rotation

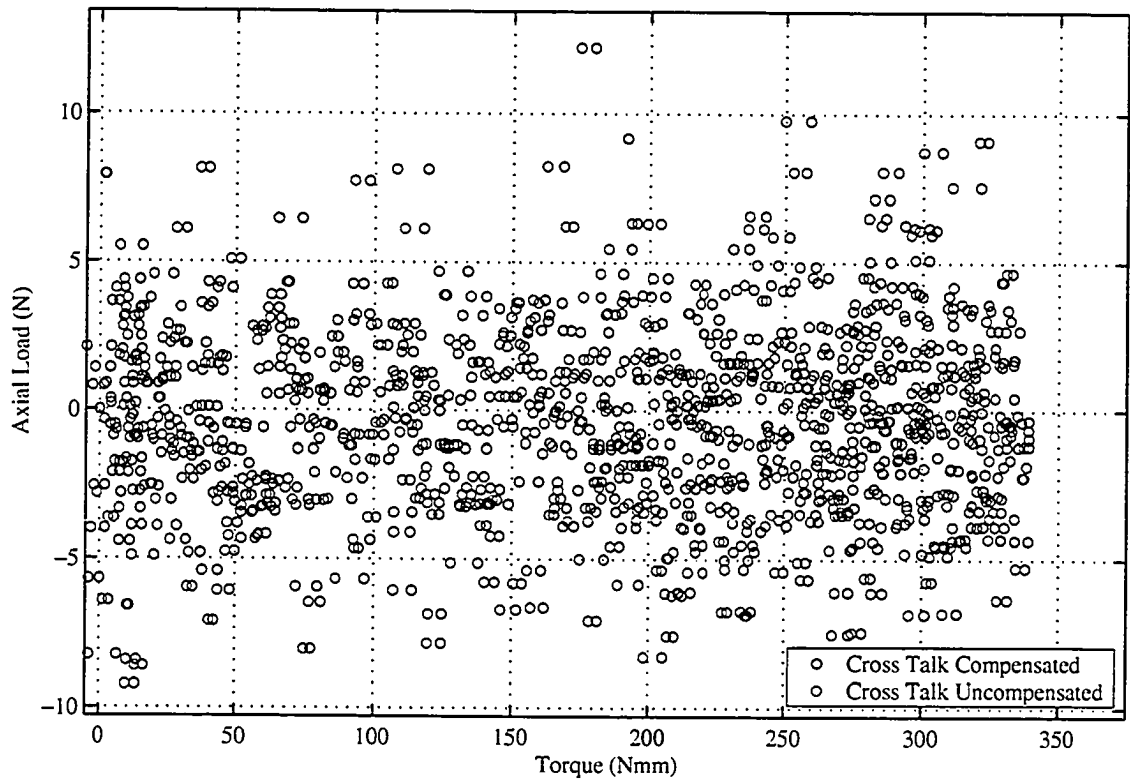


Figure C.12: Sample 1, Test 1: Pure torsional load response - Experimental axial stress and torque

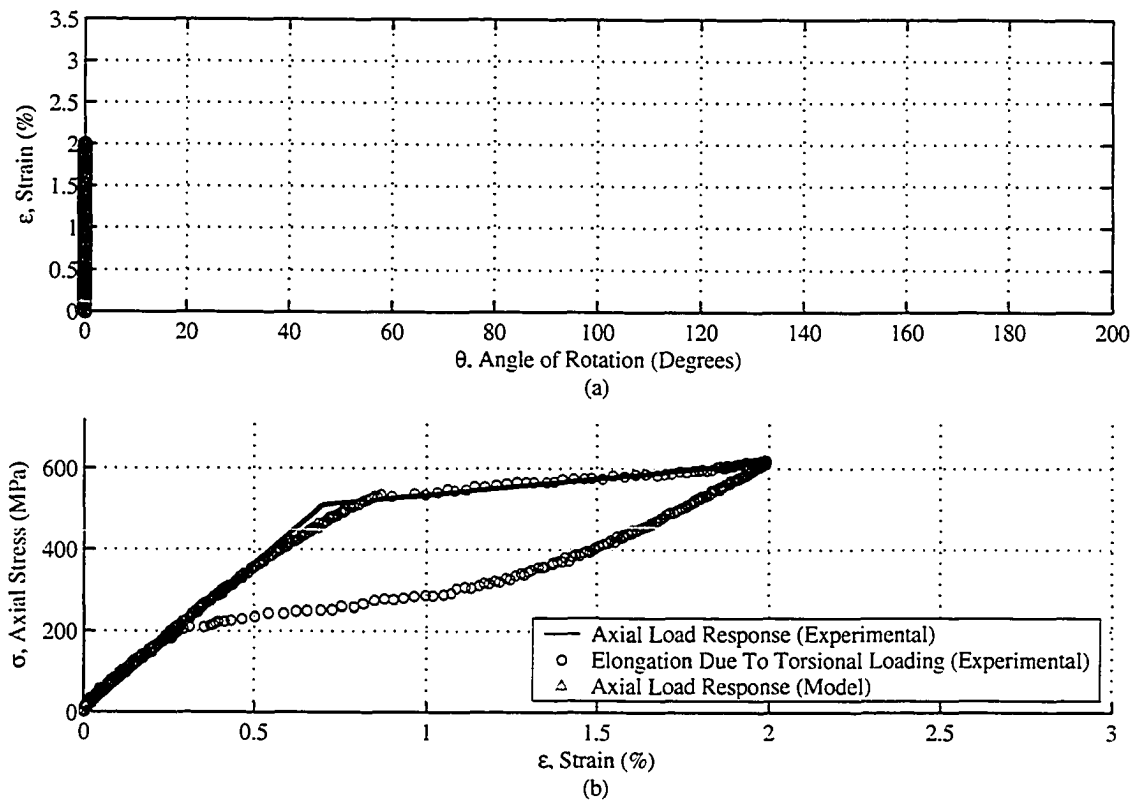


Figure C.13: Sample 1, Test 1: Pure axial response - Experimental axial strain and torsional rotation

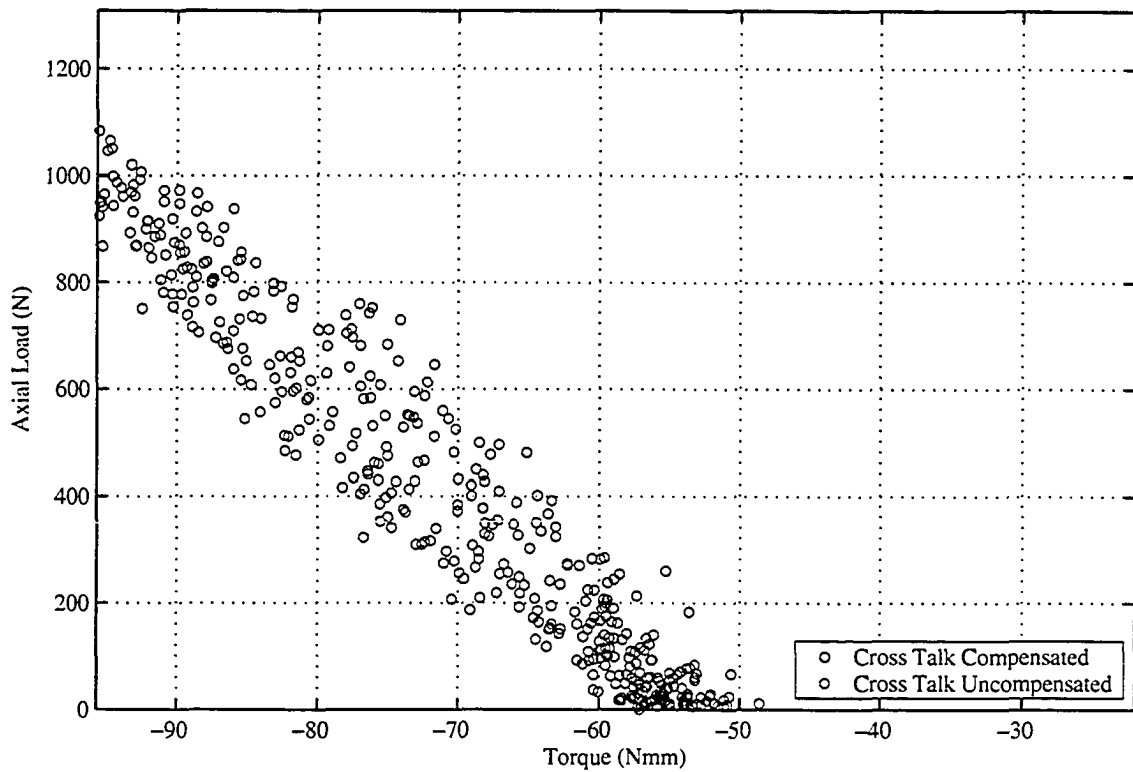


Figure C.14: Sample 1, Test 1: Pure axial load response - Experimental axial stress and torque

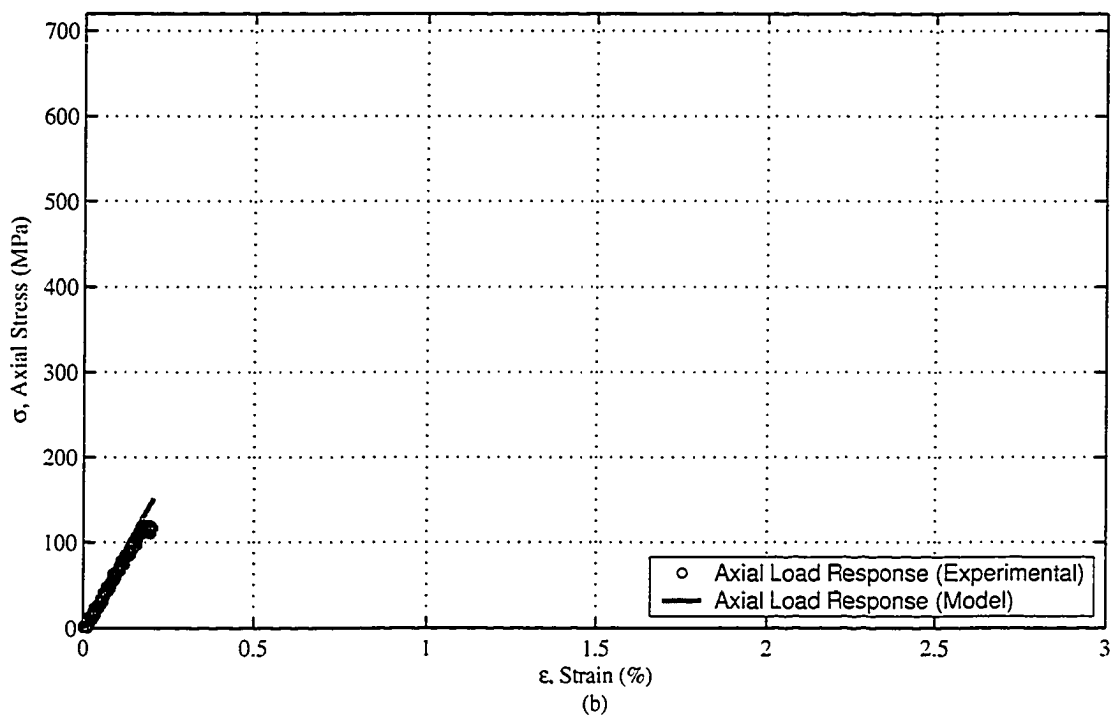
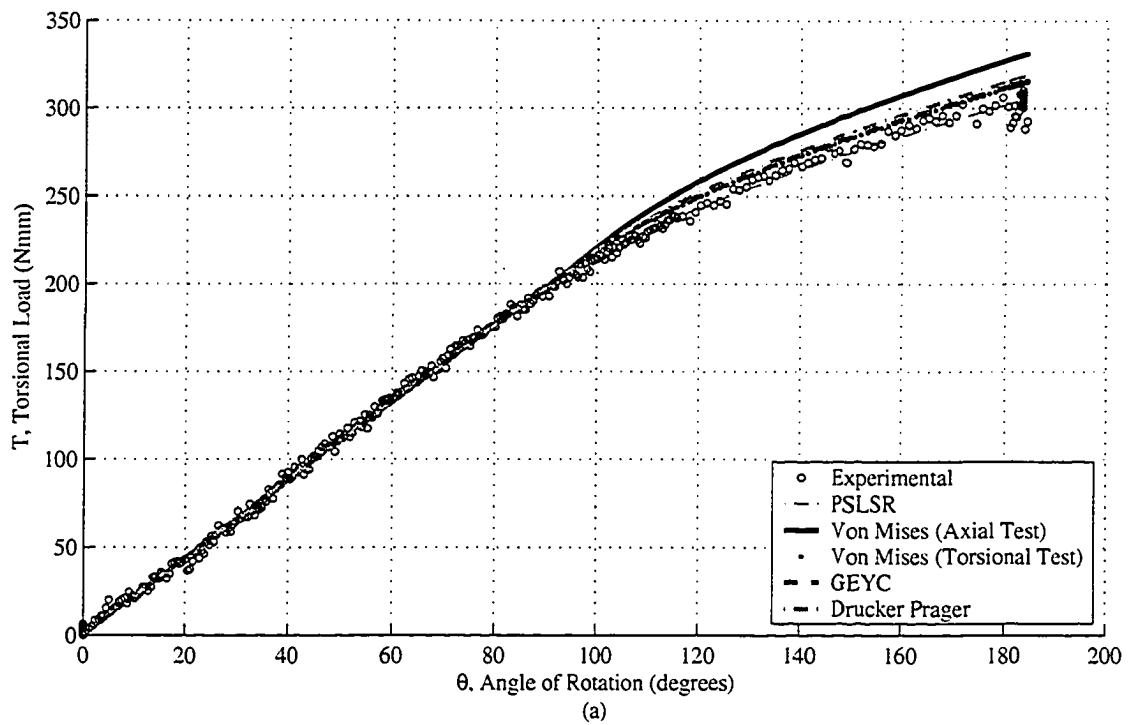


Figure C.15: Sample 1, Test 1: Combined Axial-Torsional Loading (115 MPa Axial Preload)Theoretical Prediction

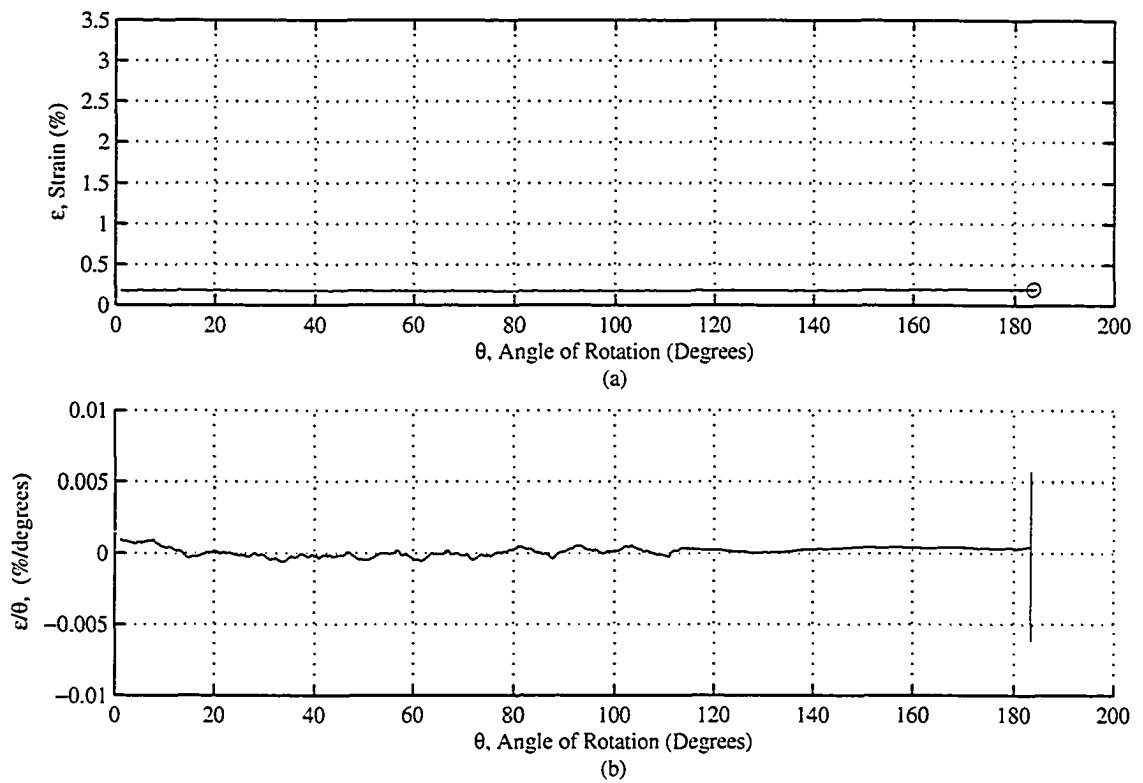


Figure C.16: Sample 1, Test 1: Combined Axial-Torsional Loading (115 MPa Axial Preload) - Experimental axial strain and torsional rotation

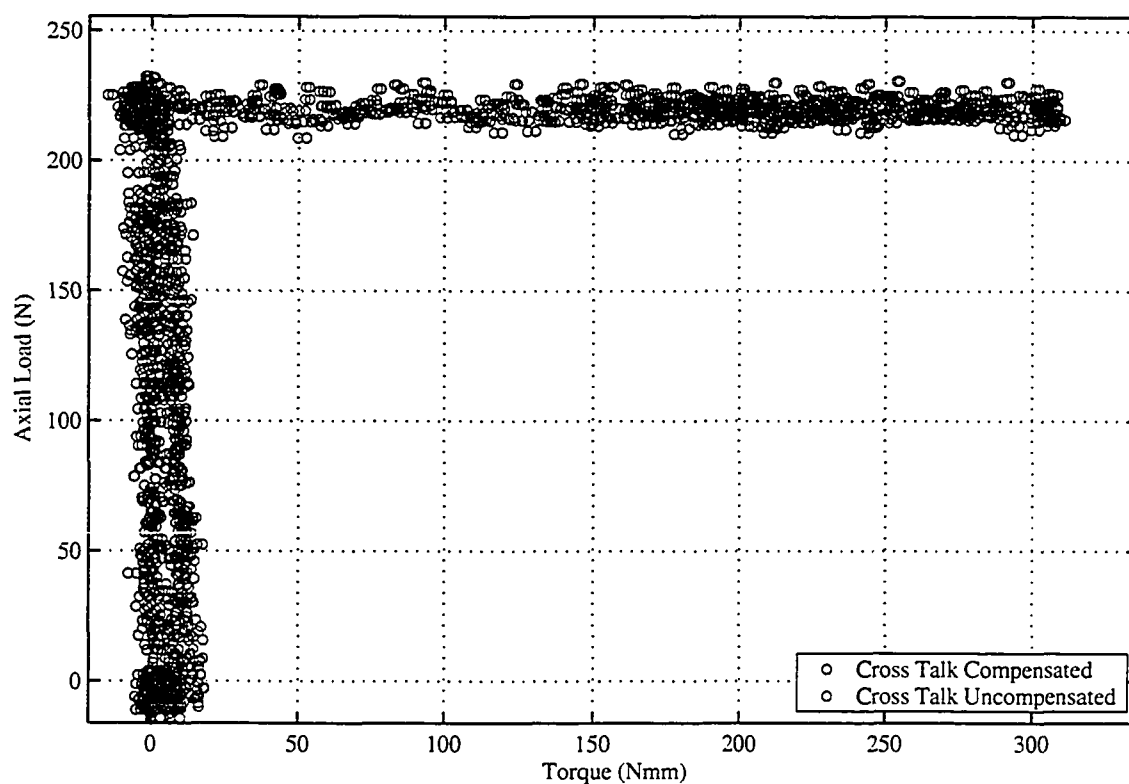


Figure C.17: Sample 1, Test 1: Combined Axial-Torsional Loading (115 MPa Axial Preload) - Experimental axial stress and torque

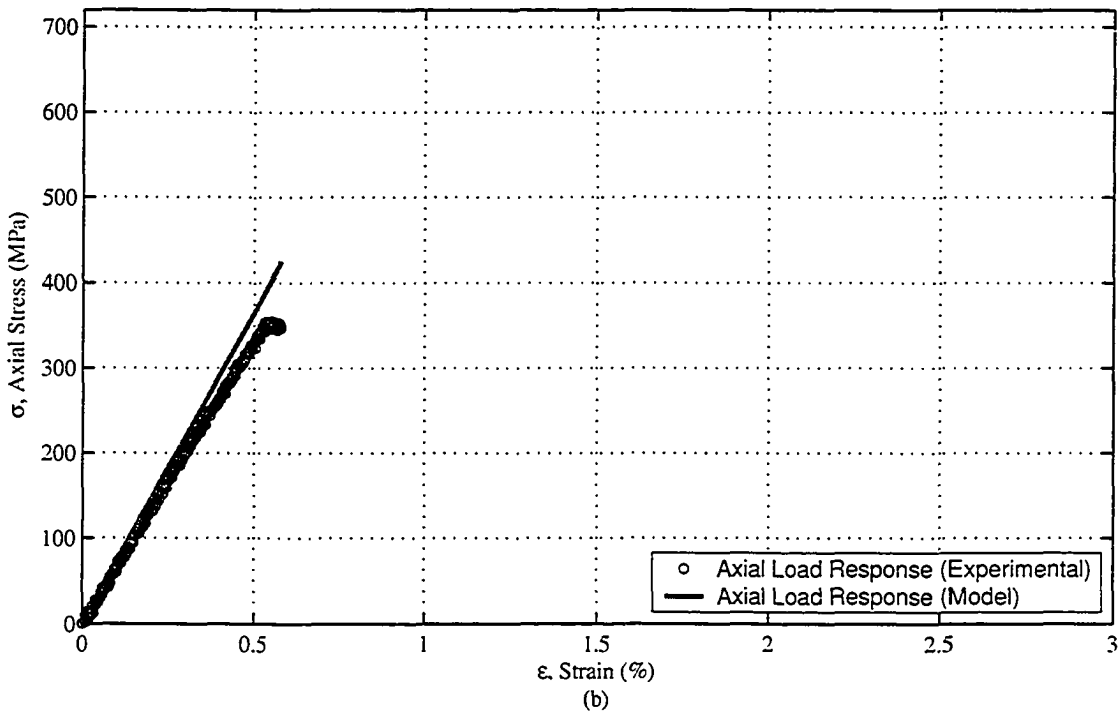
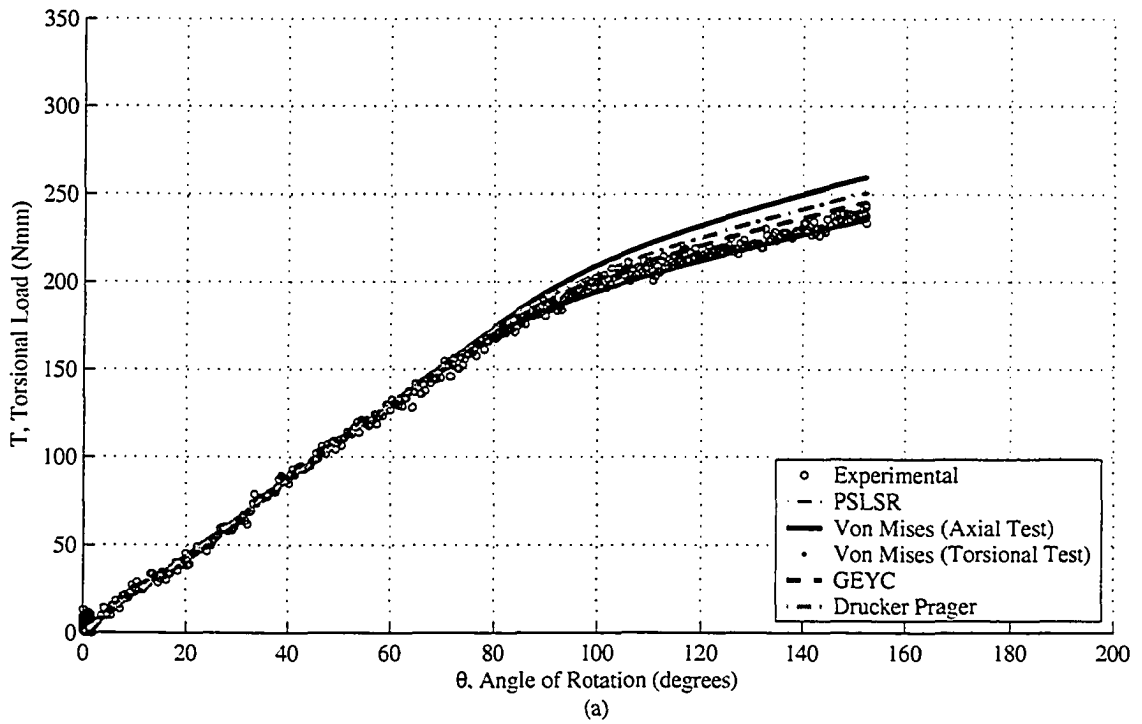


Figure C.18: Sample 1, Test 1: Combined Axial-Torsional Loading (350 MPa Axial Preload) Theoretical Prediction

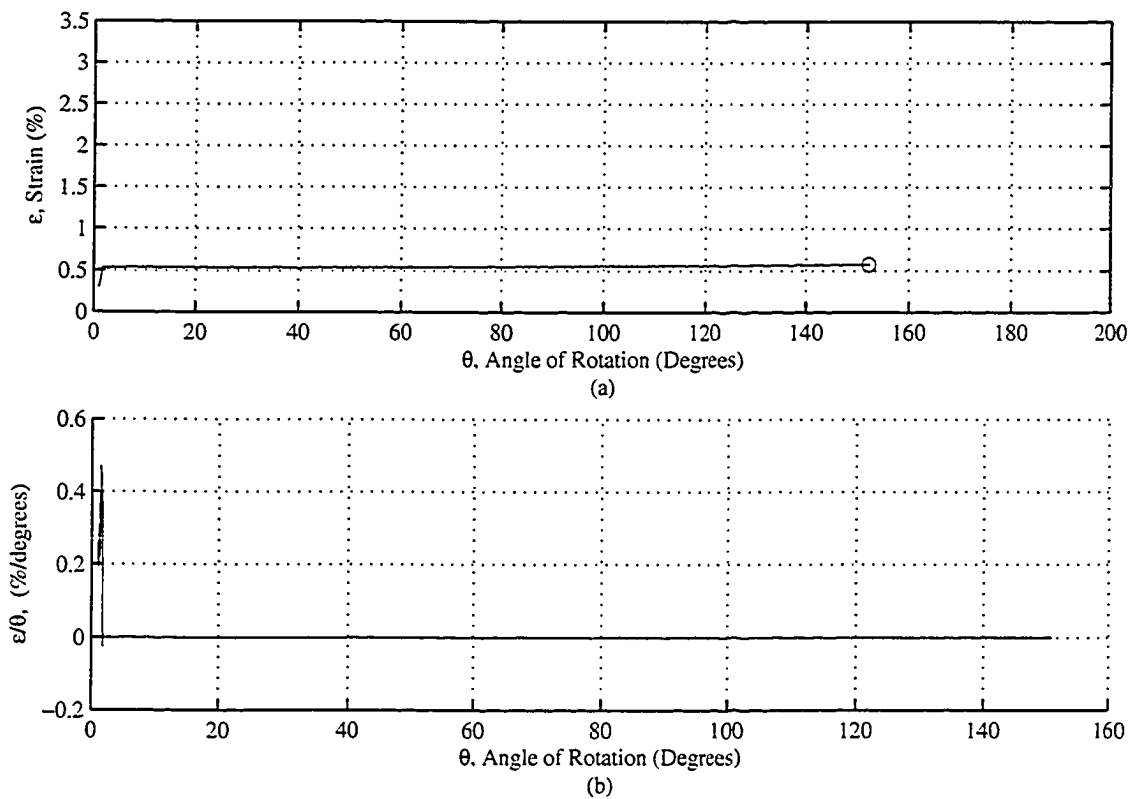


Figure C.19: Sample 1, Test 1: Combined Axial-Torsional Loading (350 MPa Axial Preload) - Experimental axial strain and torsional rotation

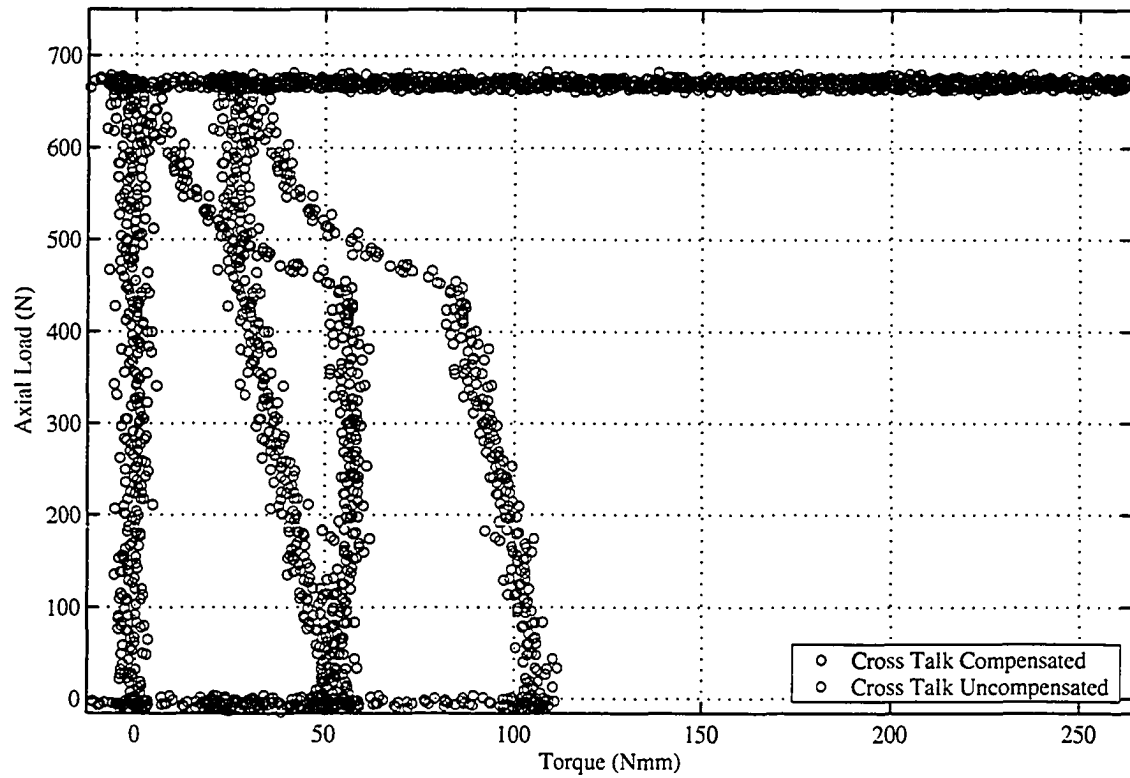


Figure C.20: Sample 1, Test 1: Combined Axial-Torsional Loading (350 MPa Axial Preload) - Experimental axial stress and torque

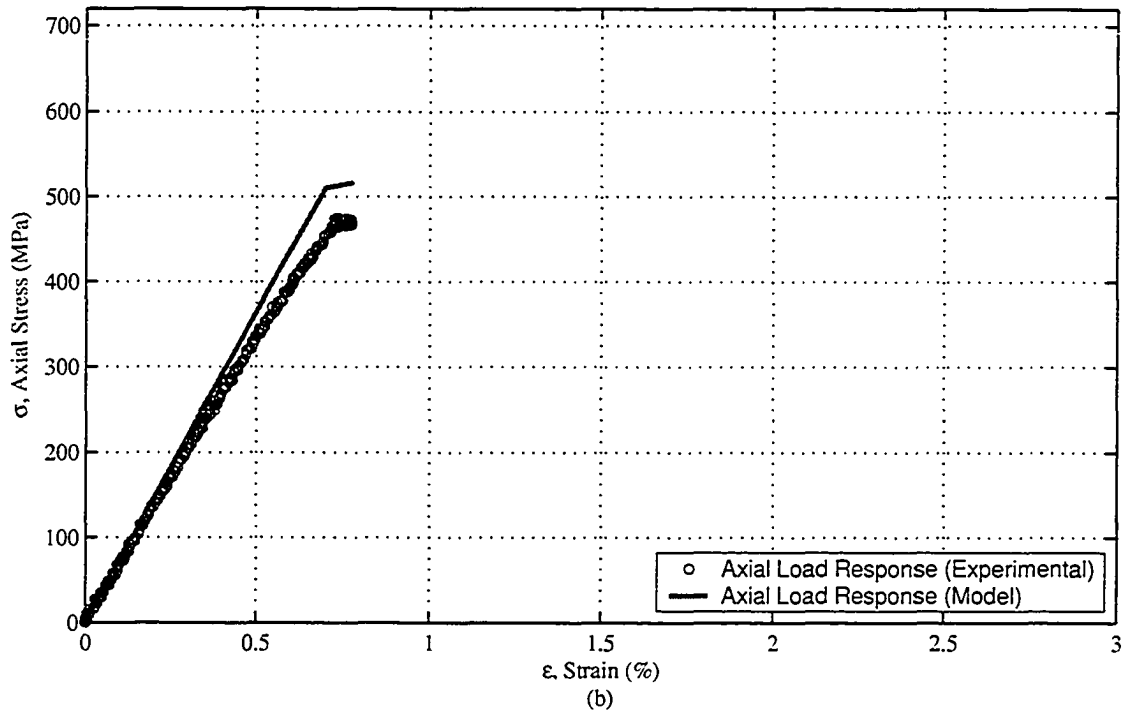
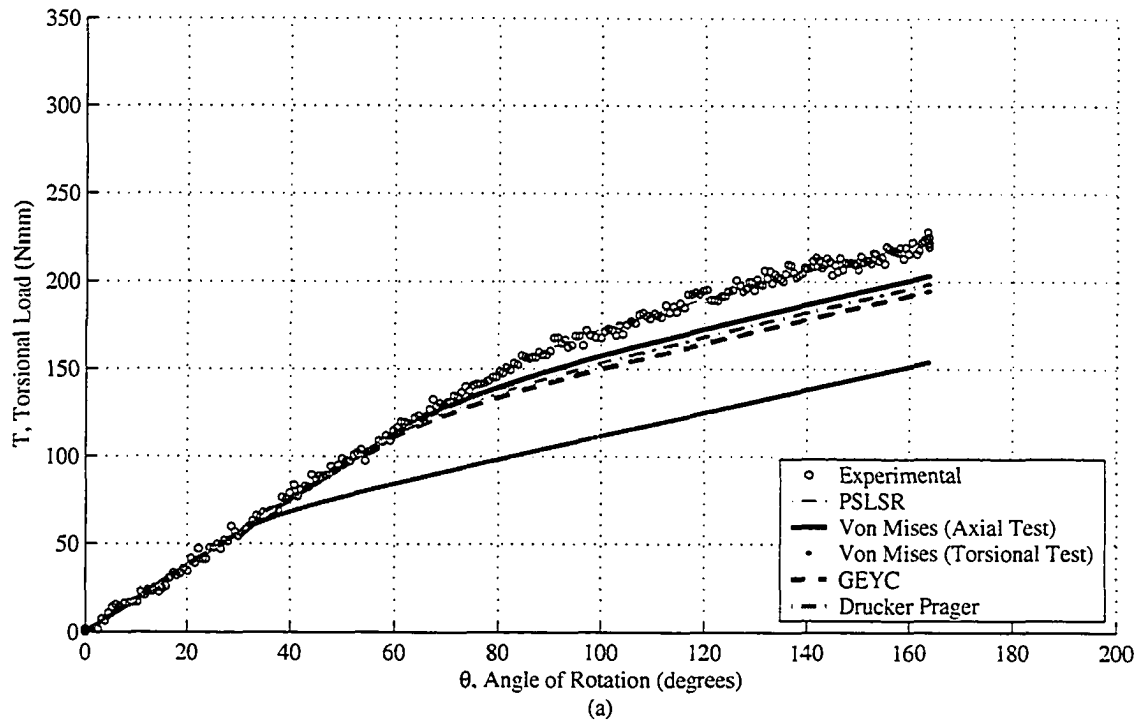


Figure C.21: Sample 1, Test 1: Combined Axial-Torsional Loading (470 MPa Axial Preload) Theoretical Prediction

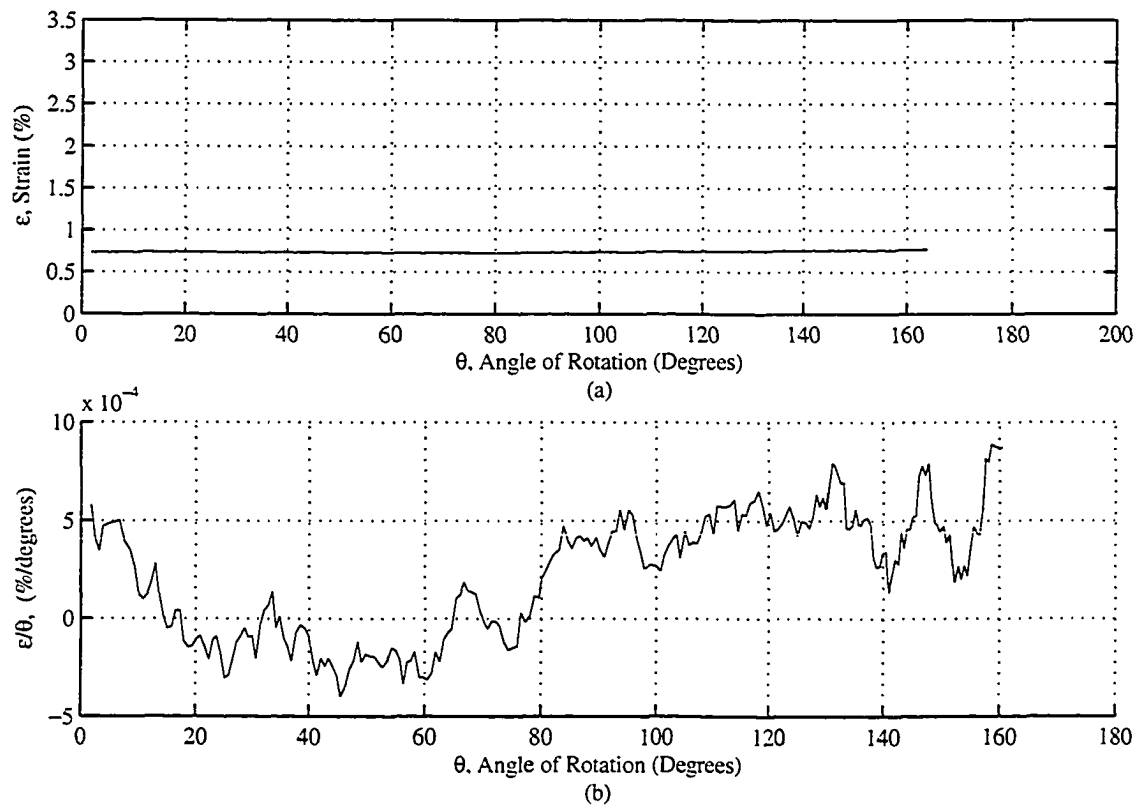


Figure C.22: Sample 1, Test 1: Combined Axial-Torsional Loading (470 MPa Axial Preload) - Experimental axial strain and torsional rotation

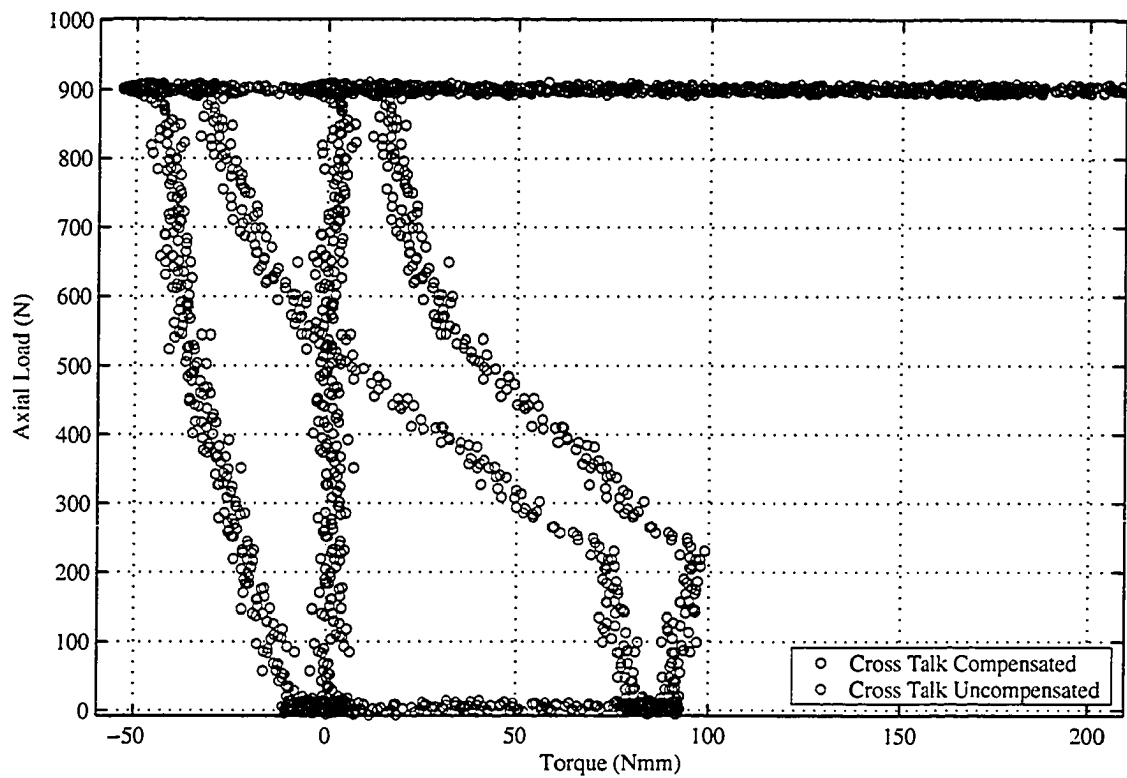


Figure C.23: Sample 1, Test 1: Combined Axial-Torsional Loading (470 MPa Axial Preload) - Experimental axial stress and torque

C.1 Sample Testing Summary

APPENDIX C. EXPERIMENTAL COMBINED LOAD TESTS

Combined Axial and Torsional Loading
Properties determined from the experimental load response

Table with 15 columns: Axial Preload (Nominal), Sample Number, Initial Wire Length, Mean Axial Preload, Mean Axial Stress, Initial Strain, Maximum Strain, Mean Strain, Min Strain, Max Strain, Max Rotation Angle, Max Torsion, Mean Slope, Min Slope. Contains multiple rows of data for various samples and load conditions.

APPENDIX C. EXPERIMENTAL COMBINED LOAD TESTS

Combined Axial and Torsional Loading
 Properties determined from the experimental load response

Axial Preload (Nominal)	Sample Number	Max Slope	Yield Torque Nmm	Yield Shear Stress MPa	Predicted YS (Von Mises Axial) MPa	Predicted YS (Von Mises Torsional) MPa	Predicted YS (GEYC) MPa	Predicted YS (Drucker Prager) MPa	Elastic Modulus GPa	Elastic Transform ation Modulus GPa	Elastic Shear Modulus Nmm ²	Elastic Shear Modulus MPa	Yield Slope (85% Initial Slope) Nmm ²
0	1	0	216.59108	288.72238	309.51745	280.49997	280.49998	280.48786	74.2	0	2.27704584	224.559726	1.8963827
0	1	0	210.30719	280.99444	309.51365	280.49581	280.49585	280.53948	74.2	0	2.267271	224.28084	1.9218931
0	1	0	207.23017	275.88319	309.50804	280.48959	280.49145	280.753	74.2	0	2.1775288	215.43704	2.0397398
60	1	0.001203451	231.6565	309.51957	307.5789	278.35941	278.74316	281.62665	74.2	0	2.1714832	215.66898	1.8607062
60	1	0.000750461	232.49275	310.63689	307.40659	278.169	278.58701	281.58017	74.2	0	2.2195366	215.8436	1.902394
60	1	0.001022709	228.90756	305.84567	307.70467	278.49838	278.85715	281.65663	74.2	0	2.2113578	21901.731	1.9197185
115	1	0.005713393	215.36071	287.74652	302.35409	272.57509	274.00819	278.95821	74.2	0	2.2084717	21841.067	1.8907599
115	1	0.000792862	171.25202	228.81228	302.25551	272.46573	273.91885	278.8946	74.2	0	2.2366905	22124.658	2.0600162
115	1	0.001139448	228.29673	305.03053	302.13428	272.33124	273.80898	278.816	74.2	0	2.2643117	22397.701	1.9523897
233	1	0.001035577	195.22739	260.84611	277.65565	244.89148	251.62524	259.48003	74.2	0	2.2930325	22681.055	2.0078843
233	1	0.001558187	195.97359	261.84311	277.80421	245.05991	251.75987	259.60728	74.2	0	2.2364967	22015.185	1.9683115
233	1	0.000946416	199.83696	267.00502	278.51684	245.86747	252.4057	260.2155	74.2	0	2.3085114	22837.397	1.8956097
233	1	0.002786544	183.42798	245.08075	277.07867	244.23712	251.10236	258.98658	74.2	0	2.0111232	19918.055	1.8513436
350	1	0.46977036	187.73995	250.89547	242.2573	203.88178	219.54551	228.09213	74.2	0	2.1712904	21478.762	1.7467267
350	1	0.000757434	173.66543	232.03687	233.28897	193.13965	211.41797	219.92042	74.2	0	2.2400893	22162.999	2.0727988
350	1	0.000710284	155.64778	207.96323	234.38898	194.4669	212.41485	220.92579	74.2	0	2.1303546	20977.24	1.9113326
470	1	0.000890092	123.7014	165.27921	148.9826	21.078762	134.546	141.31883	74.2	0	1.8829671	14630.357	1.7631936
470	1	0.001361972	157.8328	210.86926	150.17185	73.693717	136.09313	142.50959	74.2	0	1.9385316	19182.81	1.6618519
470	1	0.001093451	215.35694	287.74148	151.99414	77.339497	137.74458	144.22613	74.2	0	1.7429001	17246.435	1.7041188
565	1	0	-3.079026	-4.119331	10	10	10	10	74.674033	7.8218816	0	0	40
565	1	0.68562451	0.2681339	0.3582575	12.45183	10	11.284462	11.85356	73.915288	7.5033806	0	0	40
565	1	0.4281257	1.5570348	2.0803764	34.433228	10	31.205089	32.77466	74.192968	8.355745	0	0	40
0	2	0	233.79172	312.37246	309.51572	280.49806	280.49841	280.59589	74.2	0	2.450802	244.9673	2.0013507
0	2	0	217.2004	290.20455	309.51701	280.49948	280.49957	280.44877	74.2	0	2.4223082	24213.346	2.0138718
0	2	0	206.29221	275.62998	309.51527	280.49757	280.498	280.60714	74.2	0	2.4029819	24070.679	2.0482077
60	2	0.001021794	199.65739	266.76531	307.84791	278.65662	278.98695	281.68619	74.2	0	2.239376	22823.736	1.8953372
60	2	0.00513146	168.42552	225.03574	307.75257	278.55129	278.90055	281.66708	74.2	0	2.118016	21168.72	1.9731244
60	2	0.000831979	203.38856	271.75036	307.90735	278.72522	279.041	281.69693	74.2	0	2.5150595	2536.585	1.9369976
115	2	0.000556633	205.35065	274.63916	301.51512	271.64416	273.24787	278.40841	74.2	0	2.4350608	24239.269	1.9002349
115	2	0.002416307	201.26359	266.91117	302.35117	272.57185	274.00554	278.95633	74.2	0	2.3300151	23886.657	1.9001586
115	2	0.000670281	153.00757	204.4356	302.13551	272.3326	273.8101	278.8168	74.2	0	2.1950421	21943.267	2.099083
233	2	0.59331417	181.8402	242.96945	279.01835	245.43542	252.86018	260.64264	74.2	0	2.3162858	23149.416	1.917555
233	2	0.003794051	277.78918	371.15809	279.41143	246.68039	253.21641	260.97691	74.2	0	2.2784955	22776.043	2.0950822
233	2	0.000681099	154.38343	206.27391	278.58952	245.9499	252.47164	260.27553	74.2	0	2.6073359	26062.06	2.0776738
233	2	0.003191223	174.36001	232.96449	274.31629	241.09875	248.59895	256.61071	74.2	0	0.4416891	4414.8338	1.7892926
350	2	0.000510764	146.16485	195.29296	234.49328	194.59259	212.50937	221.02107	74.2	0	2.0879339	20867.223	1.8265946
350	2	0.000607378	157.26685	210.12649	233.27505	193.12283	211.40535	219.90769	74.2	0	2.2507356	22497.56	1.7924999
470	2	0.018000936	100.78964	134.66648	152.872	79.050796	133.54014	145.05284	74.2	0	1.9046185	19034.647	1.7869422
470	2	0.01931754	113.61554	151.80335	153.15319	79.593216	138.79497	145.31762	74.2	0	1.7057518	17051.849	1.4997558
470	2	0.020983633	143.00018	191.06459	151.50838	76.382407	137.30527	143.78956	74.2	0	2.0974269	20967.095	1.8256758
565	2	0	-0.181806	-0.242914	34.630074	10	31.383481	32.961969	73.506797	8.4776176	0	0	40
565	2	0	-0.301689	-0.403092	69.236093	10	62.745161	65.871112	73.891205	8.6372719	0	0	40
565	2	0.44224784	3.6870947	4.9263799	52.868767	10	47.912283	50.31208	75.130957	7.8801334	0	0	40
0	3	0	185.93756	248.43383	309.51669	280.49913	280.49928	280.56477	74.2	0	2.4807216	24853.728	1.9835482
0	3	0	175.44491	234.41445	309.51284	280.49488	280.4958	280.33066	74.2	0	2.2711222	22755.591	2.0726553
0	3	0	237.0941	316.78482	309.51191	280.49386	280.49495	280.31981	74.2	0	2.4279122	24323.525	1.8740062
60	3	0.000837376	242.49276	323.95805	308.07619	278.9088	279.19384	281.72166	74.2	0	2.5068001	25139.67	2.1046583
60	3	0.00126214	218.81289	292.35903	307.8667	278.67738	279.00388	281.68968	74.2	0	2.1932627	21992.688	1.9505941
60	3	0.000851888	211.46416	282.54029	307.94005	278.75841	279.07045	281.70236	74.2	0	2.2471622	22532.917	1.7400444
115	3	0.000722914	209.32129	279.67717	302.2123	272.4178	273.87969	278.86664	74.2	0	2.1671343	21730.413	1.9665954
115	3	0.000972847	220.04603	294.00665	303.16297	273.47205	274.74123	279.46888	74.2	0	1.8447009	18499.315	1.7592816
115	3	0.000829367	218.315	291.6938	302.69166	272.94949	274.31411	279.17385	74.2	0	2.0500172	20555.185	1.731973
115	3	0.000861721	203.4617	271.84808	302.33934	272.55872	273.99482	278.94871	74.2	0	2.2522022	22583.609	1.9451774
233	3	0.014613565	167.69946	224.06565	279.37634	246.84067	253.18461	260.94709	74.2	0	2.2222007	22266.613	2.0447206
233	3	0.000765689	206.54555	275.96846	279.06834	246.49203	252.90549	260.68518	74.2	0	2.1175575	21220.799	1.7964807
233	3	0.000665474	198.8166	265.6417	278.5397	245.89336	252.42641	260.23499	74.2	0	2.4099652	24144.254	2.0135438
350	3	0.03043181	172.51511	230.4999	236.77302	197.33384	214.57539	223.1019	74.2	0	2.1758518	21802.598	1.8069618
350	3	0.00056939	163.41593	218.34236	233.93349	193.91765	212.00206	220.50958	74.2	0	2.2823349	22872.786	1.943042
350	3	0.000670808	166.78442	222.84305	236.11654	196.54565	213.98945	222.50306	74.2	0	2.3182797	23230.376	1.8943443
470	3	0.48514732	127.20188	169.95625	154.18618	81.563223	139.73112	146.29021	74.2	0	1.8802265	18841.923	1.6758829
470	3	0.0009916	101.2562	135.28986	153.6734	80.589667	138.26641	145.80744	74.2	0	1.4808494	14842.456	1.6137132
470	3	0.001556447	96.661891	129.15134	161.59449	94.825947	146.4449	153.25974	74.2	0	1.6738277	1678.24	1.5665532
565	3	0	1.3549122	1.8103175	10	10	10	10	72.675909	7.2124071	0	0	40
565	3	0.68336717	0.3786737	0.5059513	10	10	10	10	74.625918	7.0192069	0	0	40
565	3	0	2.4322854	3.2498113	10	10	10	10	73.627241	6.5178336	0	0	40

APPENDIX C. EXPERIMENTAL COMBINED LOAD TESTS

Combined Axial and Torsional Loading
 Properties determined from the experimental load response

Axial Preload (Nominal)	Sample Number	Yield	Yield	Elastic	Elastic	Transform	Transform
		Torque (PSLSR)	Stress (PSLSR)	Modulus (PSLSR)	Modulus (PSLSR)	ation Shear Modulus (PSLSR)	ation Shear Modulus (PSLSR)
		Nmm	MPa	Nmm ²	MPa	G	L/G TR
0	1	195.45108	261.14498	2.2704584	22459.726	0.42	9433.0848
0	1	215.10719	287.40779	2.267271	22428.84	0.39	8747.2477
0	1	223.55017	298.68858	2.1778288	21543.704	0.39	8402.0444
60	1	195.4565	262.48834	2.2174832	21956.898	0.43	9445.756
60	1	196.49275	262.53678	2.2195366	21984.346	0.46	10112.799
60	1	193.38756	258.38789	2.2113578	21901.731	0.49	10731.848
115	1	191.68071	256.10734	2.2084717	21841.067	0.36	7862.7842
115	1	184.69202	246.76965	2.2366905	22124.658	0.41	9071.1097
115	1	171.33673	228.92546	2.2643117	22397.701	0.43	9631.0113
233	1	157.94739	211.03577	2.2930325	22681.055	0.44	9979.6642
233	1	158.53359	211.81899	2.3364967	23115.185	0.38	8783.7703
233	1	161.75696	216.12579	2.3085114	22837.397	0.4	9134.9587
233	1	223.26798	298.31155	2.0111232	19918.055	0.07	1394.2639
350	1	156.89995	209.63626	2.1712904	21478.762	0.28	6014.0533
350	1	164.06543	219.21017	2.2400893	22162.999	0.29	6427.2697
350	1	169.72778	226.77572	2.1203646	20977.24	0.21	4405.2204
470	1	135.7014	181.31258	1.8828871	18630.337	0.35	6320.6181
470	1	93.032799	124.32245	1.9385316	19182.81	0.55	10550.545
470	1	98.956935	132.21778	1.7429001	17246.435	0.63	10865.254
565	1	0	0	0	0	0	0
565	1	0	0	0	0	0	0
565	1	0	0	0	0	0	0
0	2	185.79172	248.23898	2.450802	24496.873	0.45	11023.593
0	2	193.0404	257.92403	2.4223082	24213.346	0.45	10896.006
0	2	190.45221	254.46593	2.4029819	24020.679	0.44	10569.099
60	2	211.33739	282.37091	2.329376	23283.736	0.29	6752.2834
60	2	220.42552	294.51369	2.118016	21168.72	0.26	5503.8671
60	2	176.34856	235.62183	2.5150959	25136.585	0.4	10054.634
115	2	173.55065	231.8835	2.4250608	24239.269	0.42	10180.493
115	2	178.22359	238.12709	2.3900151	23886.657	0.37	8838.063
115	2	205.80757	274.88243	2.1652421	21943.297	0.31	6802.4231
233	2	181.20032	242.10434	2.3162858	23149.416	0.29	6713.3307
233	2	204.66918	273.46142	2.2784955	22776.043	0.06	1366.5626
233	2	165.10343	220.59705	2.6073358	26062.06	0.35	9121.7212
233	2	31.231204	41.728458	0.4416891	4414.8338	1	4414.8338
350	2	157.84485	210.89877	2.0879339	20867.223	0.25	5216.8057
350	2	164.14685	219.31896	2.2507356	22497.56	0.26	5849.3656
470	2	142.70964	190.67639	1.9046185	19034.647	0.26	4949.0081
470	2	127.05554	169.76073	1.7057518	17051.849	0.36	6138.6658
470	2	110.52018	147.6676	2.0874269	20967.998	0.4	8327.120
565	2	0	0	0	0	0	0
565	2	0	0	0	0	0	0
565	2	0	0	0	0	0	0
0	3	203.85756	272.3177	2.4807216	24853.728	0.34	8450.2677
0	3	221.84491	295.34126	2.2711228	22755.691	0.31	7854.2331
0	3	188.2141	264.6367	2.4279122	24323.525	0.38	9242.9396
60	3	183.45276	245.11386	2.5068001	25139.67	0.4	10055.868
60	3	206.33289	275.68432	2.1932627	21992.688	0.33	7257.5872
60	3	200.42416	267.78959	2.2471622	22532.917	0.37	8337.1793
115	3	203.08129	271.33982	2.1671343	21730.413	0.33	7171.0361
115	3	257.16603	343.60322	1.8447009	18499.315	0.26	4809.8219
115	3	222.955	297.89337	2.0500172	20555.185	0.24	4933.2445
115	3	201.8617	269.7103	2.2522022	22583.609	0.36	8130.0993
233	3	210.89946	281.78579	2.2223007	22266.613	0.15	3339.9919
233	3	220.14555	294.13962	2.1175575	21220.799	0.11	2334.2879
233	3	200.7366	268.20704	2.4095652	24144.254	0.25	6036.0635
350	3	186.75511	249.52617	2.1758518	21802.598	0.1	2180.2598
350	3	176.53593	235.87218	2.2823349	22872.786	0.15	3430.9178
350	3	165.82442	221.56038	2.3182797	23230.376	0.21	4878.379
470	3	133.60188	178.56738	1.8832265	18841.923	0.33	6217.8346
470	3	157.4162	210.32604	1.4808494	14842.456	0.39	5788.5579
470	3	123.661	165.22523	1.6738277	16778.24	0.53	8892.4674
565	3	0	0	0	0	0	0
565	3	0	0	0	0	0	0
565	3	0	0	0	0	0	0